Preorganised halogen bonding host systems for anion recognition

Grace Turner

Lincoln College, Oxford



A thesis submitted for the degree of Doctor of Philosophy

Inorganic Chemistry Laboratory

University of Oxford

Michaelmas Term 2018

Preorganised halogen bonding host systems for anion recognition

Grace Turner, Lincoln College, University of Oxford

Abstract of thesis submitted for the degree of D. Phil., Michaelmas Term 2018

This thesis describes the preparation of acyclic, macrocyclic, mechanically interlocked host molecules and cryptand-like structures exploiting halogen bonding for the recognition of anionic guests.

Chapter One introduces the field of anion supramolecular chemistry. Non-covalent interactions for anion recognition are outlined, and the synthesis of mechanically interlocked molecules described, with an emphasis on halogen bonding-based receptors.

Chapter Two discusses the preparation of novel halogen bonding and hydrogen bonding acyclic, macrocyclic and interlocked imidazolium–triazole and -iodotriazole based systems. Investigations into their anion recognition properties are undertaken, with a focus on determining the nature of interaction between host and guest.

Chapter Three expands on the work of Chapter Two and details the incorporation of the novel bis(triazole)–imidazolium and bis(iodotriazole)–imidazolium motifs into [2]rotaxane structural host frameworks as axle components for anion recognition applications. The attempted synthesis of a benzimidazolium-containing system and an exotic hetero[3]rotaxane is also discussed.

Chapter Four explores for the first time, the application of the Ugi-four-component reaction for the construction of complex halogen bond donor architectures for anion recognition. An unprecedented halogen bonding cryptand is synthesised and preliminary anion binding properties realised *via* fluorescence spectroscopy.

Chapter Five provides a summary of the major conclusions of this thesis.

Chapter Six details the experimental procedures used throughout this work and details characterisation data of novel compounds.

Acknowledgements

It has been the best three years in Oxford and I am grateful to so many people for making this possible. Firstly, I would like to thank my supervisor Professor Paul Beer for giving me the opportunity to join his group and for his expertise and guidance throughout the DPhil. His tireless efforts in proofreading this thesis (multiple times!) are greatly appreciated.

My time in the Beer Group has been fantastic, wholly due to the amazing people who I have had the privilege to work alongside and who I know will be life-long friends. In particular, members of S8, both past and present, thank you for ensuring that even in the dark-depths of imidazole chemistry there was always something to laugh about. There was never a dull day and that's thanks to the dream team of Dr Tim Barendt, Dr Valentine Bunchuay, Tom Mole, Sam Sutton (chief entertainment provider) and Andrew Docker. Thanks for providing the often-questionable soundtrack to the past three years in the lab and ultimately agreeing with me that nothing beats Fleetwood Mac. I must also thank you all for invaluable discussions and synthetic guidance and (the very soon to be Dr!) Harry Klein, Tom and Tim for stepping up to the unenviable task of proofreading this thesis, I have really appreciated all your help and advice. Lastly, thanks to my fellow fourth year Harry for keeping me sane during the writing process and ensuring there was always time for coffee!

Outside of the lab, I am so fortunate to have the support of great friends, who thankfully never want to hear about the wonders of halogen bonding, but instead provided welcome distraction, often accompanied with a G&T. Especially to the friendships I first formed in St Andrews, thank you for helping me through this journey. A special mention must go to a dear friend Hannah Meikle, whose reassurance and wise words have been a constant source of inspiration.

Finally, I am eternally grateful to my family, for your unwavering love, support and encouragement. Without you all by my side, none of this would not have been possible – thank you.

This thesis is dedicated to the loving memory of my auntie, Anne Starkie (1949–2017), who I wish I could have shared this with.

Grace Turner

3rd December 2018

Abbreviations

Δδ	change in chemical shift relative to free host
λ	wavelength
μ	micro
Å	Angstrom
A	hydrogen or halogen bond acceptor
aq.	Aqueous
Ar	aryl
ATP	adenosine triphosphate
Bn	benzyl
Br.	broad
Bu	butyl
^{t}Bu	tertiary butyl
c	centi
°C	degrees Celsius
cat.	catalytic
calc.	calculated
COSY	homonuclear correlation spectroscopy
CuAAC	copper(I)-catalysed azide–alkyne cycloaddition
d	deuterated
d	doublet
D	hydrogen bond donor
DBU	1,8-diazabicycloundec-7-ene
DCM	dichloromethane
dd	doublet of doublets
DIPEA	*N,N'*-diisopropylethylamine

DMF	*N,N'*-dimethylformamide
DMSO	dimethylsulfoxide
DNA	deoxyribonucleic acid
e.g.	*exempli gratia*
equiv./eq	equivalent
ESI	electrospray isonisation
Et	ethyl
g	gram
G	Gibbs free energy
Grubbs' II	Grubbs' second generation catalyst
H	enthalpy
HB	hydrogen bond
H	hour
HRESI-MS	high resolution electrospray ionisation mass spectrometry
Hz	hertz
IUPAC	International Union of Pure and Applied Chemistry
J	joule
J	coupling constant
K	kelvin
K_a	association constant
L	litre
LRESI-MS	low resolution electrospray ionisation mass spectrometry
m	metre, milli, multiplet
m	meta
M	moles per litre
Me	methyl
Mes	mesityl

MHz	megahertz
MIM	mechanically interlocked molecule
min	minute
MLCT	metal-to-ligand charge transfer
mol	mole
MS	mass spectrometry
m/z	mass/charge ratio
n	nano
nm	nanometre
neg.	negative
NMR	nuclear magnetic resonance
OAc^-	acetate anion
OTf^-	triflate anion
p	para
PBP	phosphate binding protein
Ph	phenyl
pH	$-\log_{10}[H^+]$
pK_a	$-\log_{10}K_a$
pos.	positive
Pr	propyl
Py	pyridine/pyridinium
q	quartet
quint	quintet
R	aryl or alkyl substituent
RCM	ring-closing metathesis
R_f	retention factor
ROESY	rotating-frame nuclear Overhauser effect correlation spectroscopy

r.t.	room temperature
s	singlet
S	entropy
sat.	saturated
SBP	sulfate binding protein
t	triplet
t, tert	tertiary
TBA	tetrabutylammonium cation
TBTA	ter[(1-benzyl-1,2,3-triazol-4-yl)methyl]amine
TFA	trifluoroacetic acid
THF	tetrahydrofuran
TLC	thin layer chromatography
TMS	trimethylsilyl
tosyl	4-toluenesulfonyl
UV	ultraviolet
wt.	weight
X	halogen atom
XB	halogen bond

Table of Contents

1 Introduction 1
1.1 Anion supramolecular chemistry 3
1.1.1 The Importance of Anions 4
1.1.2 The Challenges of Anion Recognition 5
1.1.3 Biotic anion receptors 8
1.2 Design of synthetic anion receptors 10
1.2.1 Design principles 10
1.2.2 Traditional non-covalent interactions 13
1.3 Synthetic receptors for anion recognition 16
1.3.1 Cationic receptors 16
1.3.2 Neutral anion receptors 21
1.4 Halogen Bonding 26
1.4.1 Principles of halogen bonding 26
1.4.2 Halogen bonding for anion recognition 28
1.5 Synthesis and applications of mechanically interlocked molecules 35
1.5.1 The mechanical bond 35
1.5.2 Synthesis of interlocked molecules 36
1.5.3 Template-directed synthesis of interlocked molecules 38
1.5.4 Applications of interlocked molecules 48
1.6 Project Aims 53
1.7 References 54
2 Imidazole–triazole and –iodotriazole based systems for anion recognition 65
2.1 Introduction 67
2.1.1 Chapter aims 71
2.2 Acyclic receptors 71
2.2.1 Synthesis of imidazolium–triazole and –iodotriazole acyclic receptors 71
2.2.2 Synthesis of imidazole–triazole transition metal complexes 74
2.2.3 Preliminary anion binding properties of acyclic receptors 76
2.3 Macrocyclic systems 80
2.3.1 Synthesis 80
2.3.2 Attempted active metal-template synthesis of HB and XB[2]rotaxanes 83

2.3.3 Synthesis of cationic macrocycle 86
2.3.4 Pseudorotaxane studies 86
2.4 Incorporation of imidazolium–triazole and –iodotriazole into an axle 88
2.4.1 Synthesis of HB and XB axles 88
2.4.2 Synthesis of dicationic axle 92
2.4.3 Alternative route to HB axle 94
2.5 Incorporation into a [2]rotaxane 95
2.5.1 Synthesis of imidazolium–triazole and –iodotriazole [2]rotaxanes 95
2.5.2 Preliminary anion binding studies 98
2.5.3 Summary 100
2.6 2-Methylimidazolium–triazole motif 101
2.6.1 Synthesis of acyclic receptor 101
2.6.2 Anion binding studies 102
2.7 Conclusions 104
2.8 Future work 106
2.9 References 107
3 Bis(triazole)–imidazolium and –benzimidazolium based systems for anion recognition 109
3.1 Introduction 111
3.2 Chapter aims 113
3.3 Bis(triazole)– and bis(iodotriazole)–imidazolium containing [2]rotaxanes 114
3.3.1 Synthesis of imidazolium–alkyne axle precursor 114
3.3.2 Attempted active–metal template synthesis of [2]rotaxane 116
3.3.3 Synthesis of HB and XB axles 118
3.3.4 Incorporation into a [2]rotaxane 121
3.3.5 Anion binding studies 123
3.4 Attempted synthesis of hetero[3]rotaxane utilising active–metal and anion–template methods 126
3.4.1 Pseudorotaxane investigation 127
3.4.2 Attempted hetero[3]rotaxane synthesis 128
3.5 Towards bis(triazole)–benzimidazolium containing [2]rotaxanes 129
3.5.1 Synthesis of benzimidazolium axle 130

3.5.2 Towards the incorporation of bis(iodotriazole)–benzimidazolium axle into a [2]rotaxane....135
3.6 Incorporation of bis(triazole)–imidazolium motif into the macrocycle component of interlocked structures....137
3.6.1 Attempted synthesis of macrocycle....137
3.7 Conclusions....141
3.8 Future Work....142
3.9 References....143
4 Halogen bonding supramolecular architectures utilising Ugi multicomponent macrocyclisations....145
4.1 Introduction....147
4.1.1 Multicomponent reactions....147
4.1.2 Ugi-four-component reaction....148
4.1.3 Ugi-4CR for the construction of macrocycles and cages....149
4.2 Chapter aims....153
4.3 Preliminary Ugi reactions....153
4.3.1 XB Acyclic test system....153
4.3.2 XB Macrocycle synthesis *via* Ugi-4CR....155
4.4 Halogen bonding cryptand *via* Ugi-4CR....157
4.4.1 Synthesis of XB cryptand precursors....158
4.4.2 Synthesis of XB cryptand....167
4.4.3 Fluorescence spectroscopy anion titration studies....169
4.5 Towards the synthesis of soluble XB cryptands....170
4.6 Conclusions....172
4.7 Future work....174
4.8 References....176
5 Conclusions....177
6 Experimental....183
6.1 General considerations....185
6.1.1 Solvents and reagents....185
6.1.2 Characterisation and instrumentation....185
6.1.3 Titration protocols....186
6.2 Synthetic procedures....187

6.2.1 Synthesis of novel compounds from Chapter 2 187
6.2.2 Synthesis of novel compounds from Chapter 3 221
6.2.3 Synthesis of novel compounds from Chapter 4 235
6.3 References 253

Chapter One

Introduction

1.1 Anion supramolecular chemistry

Supramolecular chemistry, often described as "*chemistry beyond the molecule*" takes inspiration from the complex assemblies found in Nature and explores the use of non-covalent intermolecular interactions for the construction of molecular architectures.[5] The field can be divided into two branches: host–guest interactions and self-assembly, the spontaneous assembly of small substrates into higher order molecular architectures. Host–guest chemistry refers to the association of a smaller guest substrate *via* intermolecular interactions with a larger receptor host molecule. Its origins are found in the pioneering work of Pedersen,[1] Lehn[2] and Cram[3] and who were jointly awarded the Nobel Prize in Chemistry in 1987 for "*their development and use of molecules with structure-specific interactions of high selectivity*". Pedersen's seminal work on complexation of alkali metal cations with crown ethers, stimulated the rapid expansion of the field which led to reports from Lehn and Cram of three-dimensional cryptands and rigid spherands for selective group I metal cation recognition, respectively (Figure 1.1a-c). Less than a year after Pedersen's cation binding crown ethers, the first abiotic anion receptors were reported by Park and Simmons, utilising protonated macrobicyclic amine structures to encapsulate halide anions in acidic aqueous media (Figure 1.1d).[4]

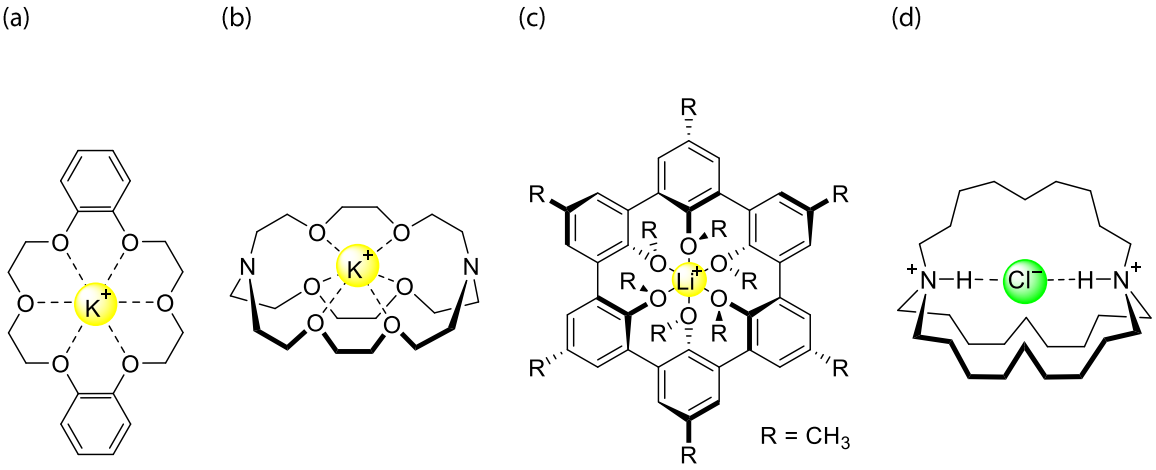


Figure 1.1: *Representative examples of (a) Pedersen's crown ethers,[1] (b) Lehn's [2,2,2] cryptands,[2] (c) Cram's spherands,[3] and (d) Park and Simmons' macrobicyclic anion receptor[4]*

Juxtapose to cation coordination, anion supramolecular chemistry has historically remained overlooked; however, over recent decades a rapid expansion of the field has occurred with research focusing on anion recognition and template-directed self-assembly.

This chapter will introduce the area of anion supramolecular chemistry and underline the importance of the field. The principles and interactions most commonly utilised in the design of receptors for anion recognition will be discussed, with an overview of abiotic host systems given. Attention will then turn to the template-directed synthesis of interlocked anion host systems, whose properties and applications will be outlined.

1.1.1 The Importance of Anions

Anions are omnipresent in the biosphere and are essential in many biological, chemical, medical and environmental processes. The role of anions in physiology is fundamental: the genetic instructions used in the growth, development, functioning and reproduction of all known living organisms are carried out by DNA and RNA, both of which are polyanions, containing a phosphate-ester backbone.[6] Indeed, phosphate is the most abundant intracellular anion, vital for a range of processes including transfer and storage of energy in ATP, muscle contraction and nerve impulses, as well as acting as a buffer. It is therefore not surprising that approximately 70% of all enzymatic co-factors and substrates are negatively charged.[7] Chloride on the other hand, is the most abundant extracellular anion, acting to maintain osmotic balance and electrical neutrality in intra- and extracellular fluid.[8] Mis-regulation of chloride transmembrane transport processes gives rise to a number of diseases such as cystic fibrosis, Dent's disease and epilepsy.[9–11] Of the other halides, iodide is essential for the biosynthesis of metabolism regulating hormones in the thyroid gland,[12] and fluoride has been shown to be beneficial in drinking water to prevent skeletal and dental problems.[13]

Environmentally, nitrates and phosphate are abundant in agricultural fertilisers; however, their overuse in arable farming has led to a plethora of environmental concerns, due to

their ability to permeate soil and enter groundwater. Eutrophication occurs when an excess of nutrients and minerals (nitrates and phosphates) induce excessive algae growth, resulting in oxygen depletion and subsequent disruption of the natural aquatic ecosystem.[14] Furthermore, the presence of nitrate and nitrite in drinking water is a public health problem;[15,16] nitrite in the blood can combine with haemoglobin giving rise to methemoglobin (blue-baby syndrome), especially in new-born infants, whereas an excess of nitrate has been linked to hypertension, increased infant mortality and changes to the immune system.[13]

Anthropogenic industrial anionic pollutants are also a major concern. For example, sulfide, a toxic, corrosive and odorous anion is present in effluent waste from petroleum refinery, paper mills and textiles industries;[17,18] cyanide is used extensively in electroplating and mining industries and poses a significant health risk due to its inherent toxicity;[19] and pertechnetate is a radioactive anion and by-product of the nuclear fuels industry.[20]

1.1.2 The Challenges of Anion Recognition

The prevalence of anions in the environment highlights their inherent importance to humans and emphasises the need for extending the frontiers of knowledge in the area of anion recognition. The field is still relatively underdeveloped when compared to cation receptors, attributed, in part, to the intrinsic properties of anionic species that pose arduous challenges in the design of selective host systems, outlined below.

Size: Anions are larger than their isoelectronic cations because of a lower effective nuclear charge, demonstrated by the effective ionic radii outlined in Table 1.1. This results in a lower charge to radius ratio and so electrostatic binding interactions with the host are comparatively less effective.

Table 1.1: *Effective ionic radii and free energies of hydration of selected isoelectronic cations and anions*

Cation	Ionic radius (Å)[21]	$\Delta G_{hydration}$ (kJ mol^{-1})[5]	Anion	Ionic radius (Å)[21]	$\Delta G_{hydration}$ (kJ mol^{-1})[5]
Na^+	1.16	−365	F^-	1.19	−465
K^+	1.52	−295	Cl^-	1.67	−340
Rb^+	1.66	-	Br^-	1.82	−315
Cs^+	1.81	−250	I^-	2.06	−275

Geometry: A wide range of geometries are exhibited by anions (Figure 1.2) including spherical (halides), linear (cyanide, cyanate, azide), trigonal planar (acetate, nitrate), tetrahedral (sulfate, phosphate), octahedral (hexafluorophosphate) and more complex structures (ATP, DNA, etc.). Whilst this offers potential advantages in selectivity, it consequently also requires a higher degree of host design to ensure complementarity between host and guest.

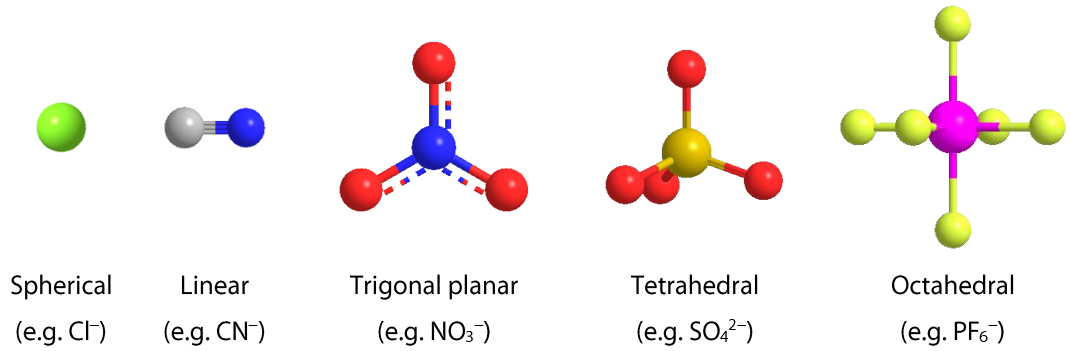


Figure 1.2: *Selected examples of difference anion geometries*

pH Dependence: At low pH, many anions undergo protonation leading to a loss of negative charge, impeding the use of electrostatic interactions for anion binding.[22] Many hosts also exhibit pH dependence; for example, positively charged polyammonium-based systems are deprotonated at high pH.[23] It is imperative for anion binding that both host and guest maintain their charges, and as a consequence many systems can only operate within a limited "pH-window". Furthermore, strongly basic anions can deprotonate acidic sites on the receptor; a

property that has been utilised for the colorimetric detection of fluoride and acetate.[24,25]

Solvation: Strength and selectivity of anion binding is perturbed considerably by solvent effects. Compared to their isoelectronic cations, anions generally exhibit a higher degree of solvation, due to their ability to form hydrogen bonds with the solvent.[26] For an anion receptor to function it must therefore overcome the desolvation energy barrier and effectively compete with the solvent environment. Polar solvents with high dielectric constants are able to interact effectively with charged species, and thus significantly weaken ion-pairing interactions. Furthermore, the extent to which an anion is hydrated in protic solvents such as water is reflected in the Hofmeister series of anion hydrophobicity which was established through studies on the effects of anions on the solubilities of proteins (Figure 1.3).[27] Larger anions such as iodide, tend to be more hydrophobic and less solvated, whereas smaller anions like fluoride, are more hydrophilic and solvated; hence, hydrophobic anions tend to be more strongly bound by a receptor with a hydrophobic cavity than hydrophilic anions in aqueous and aqueous–organic solvent mixtures. To achieve anti-Hofmeister selectivity for well-solvated anions, the receptor must therefore compete effectively with the solvent.

Hydrophilic *Hydrophobic*

$SO_4^{2-} \approx F^- > H_2PO_4^- > AcO^- > Cl^- > Br^- > NO_3^- > I^- > ClO_4^- > SCN^-$

Strongly hydrated *Weakly hydrated*

Figure 1.3: *The Hofmeister series*[27]

1.1.3 Biotic anion receptors

Despite the inherent challenges of anion recognition, Nature provides a multitude of elegant and impressive examples that provide inspiration to the synthetic chemist. The elucidation of X-ray crystal structures of biological anion receptors, such as DNA helicase RepA sulfate complex,[28] haloalkane dehalogenase chloride complex,[29,30] ClC (chloride-conducting) chloride channel[31] and the sulfate-[32,33] and phosphate-binding proteins[34] have allowed for direct visualisation of anion recognition sites in biological systems. A combination of non-covalent interactions, mainly hydrogen bonding and favourable coulombic cation–anion electrostatic interactions, are employed in well-defined complementary arrangements to produce a high degree of selectivity. For example, Dijkstra and co-workers reported a 2.4 Å-resolution X-ray structure showing a chloride anion bound to the active site of haloalkane dehalogenase from *Xanthobacter autotrophicus* GJ10 (Figure 1.4a),[29,30] providing important evidence to help elucidate the mechanism that converts 1-haloalkanes into the corresponding primary alcohols and a halide ion *via* hydrolytic cleavage of carbon-halogen bonds.

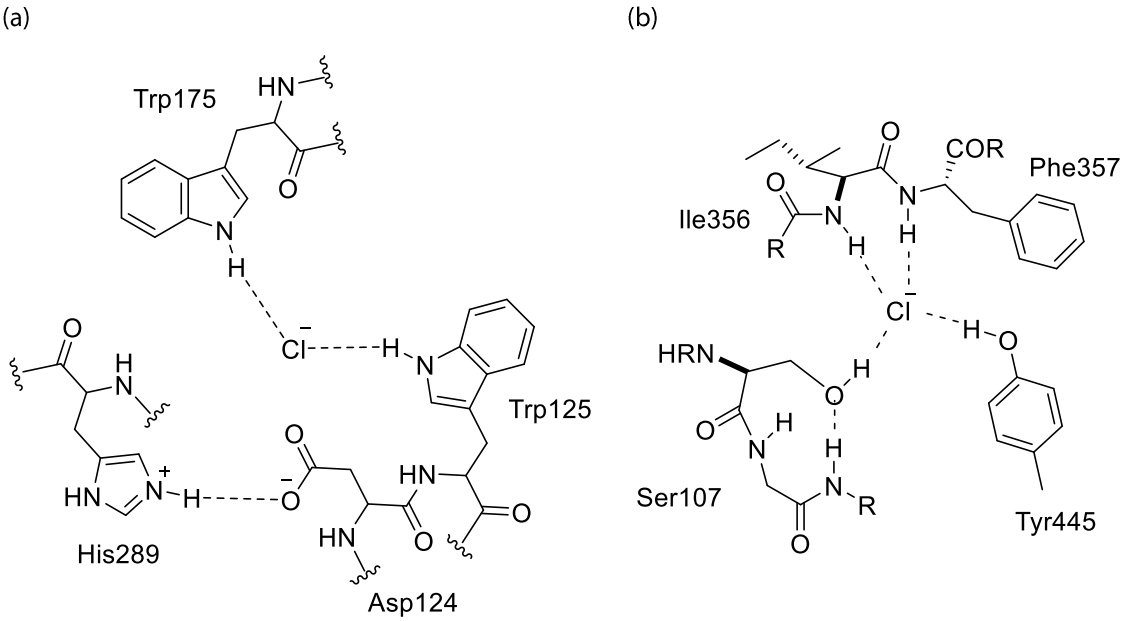


Figure 1.4: *(a) Enzymatic active site of haloalkane dehalogenase revealing the presence of a bound chloride anion,[29] and (b) structure of the chloride site in the ClC chloride anion channel[31]*

The ClC chloride channels catalyse the selective flow of Cl^- ions across cell membranes. In 2002, the 3 Å-resolution X-ray structure of the ClC chloride channel was solved, revealing a homodimer-derived channel with a negatively charged glutamate side chain just above the channel entrance acting as an anion-regulating gate; when open, Cl^- ions enter the channel pore and are directed towards the constricted neutral centre of the channel by a surface rich in positively polarised residues (Figure 1.4b).[31] The elegance of the structure is apparent, yet, understanding of biological anion transport is still extremely limited.

Further sophisticated examples of biotic anion hosts are the phosphate binding protein (PBP)[34] and sulfate binding protein (SBP)[32,33] (Figure 1.5), utilised for active transport. Together they demonstrate the ability of biological systems to discriminate structurally similar tetrahedrally shaped oxoanions through the precise arrangement of hydrogen bond donors and acceptors. The PBP (Figure 1.5a) is structurally distinct from the SBP and cannot recognise other inorganic oxoanions, with sulfate bound at least five orders of magnitude less tightly than hydrogen phosphate. The protein is comprised of two separate similarly folded globular domains, with a deep cleft between domains containing the bound phosphate, in the dehydrated state, ~ 8 Å below the protein surface. The phosphate species is held tightly by 12 hydrogen bonds from a combination of charged and neutral peptide residues including a salt bridge involving the guanidinium group of Arg-135. The pairing of all polar groups and the total involvement of donatable protons in the binding region gives rise to an extensive and precise array of hydrogen bonds. The Asp-56 residue plays a pivotal role in the selectivity of the PBP, being the only residue to fully discriminate between sulfate and hydrogen phosphate: sulfate is repulsed by the negatively charged side arm through unfavourable electrostatic interactions, whereas for hydrogen phosphate it acts as a hydrogen bond acceptor. The major difference between the PBP and SBP is the absence of a carboxylate side chain in the SBP recognition site (Figure 1.5); sulfate is bound through seven hydrogen bonding interactions with exclusively neutral peptide residues, in a similar cleft to the PBP.

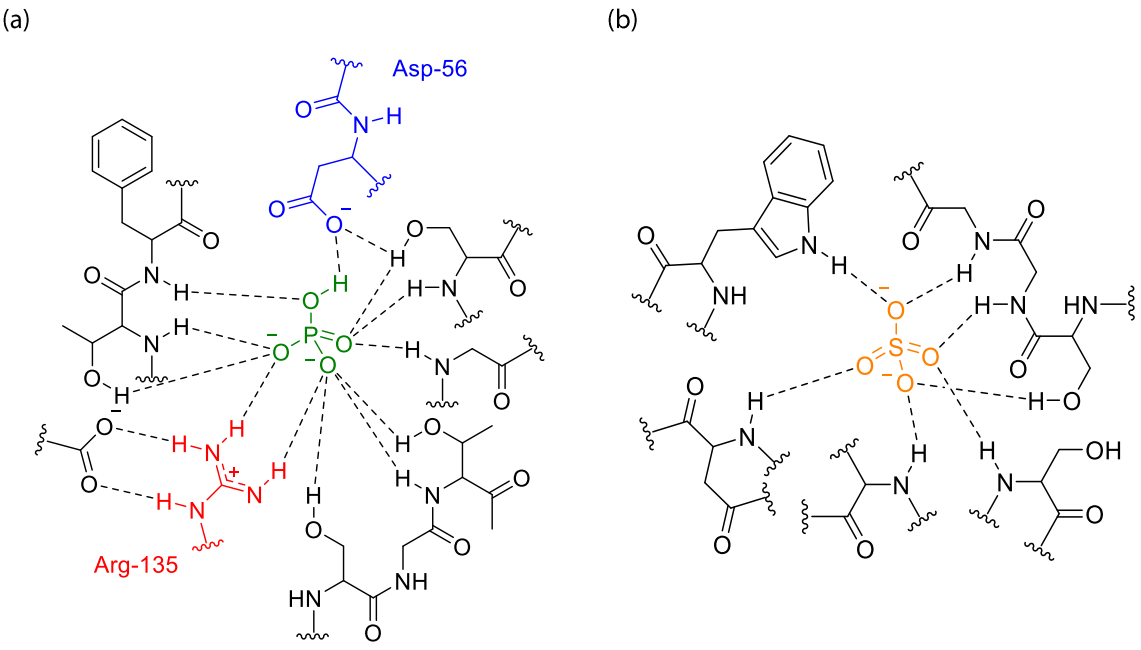


Figure 1.5: *Two-dimensional projection of binding cavities of truncated biological protein structures: (a) phosphate binding protein (PBP),[34] and (b) sulfate binding protein (SBP)[33]*

1.2 Design of synthetic anion receptors

1.2.1 Design principles

Nature's ability to recognise species, such as anions, is unparalleled, exemplified by the highly-selective binding of substrates to enzymes as described above. The strategies adopted by biotic host structures such as structural rigidity and well-defined three-dimensional binding cavities provide guiding design principles for the construction of synthetic receptors.

Complementarity

The most fundamental of supramolecular host-guest chemistry principles is complementarity, which states that the interaction of two or more chemical entities is maximised when they are geometrically matched. This concept was introduced by Fischer in 1894, who proposed the "lock and key" model describing the binding of a substrate, the

key, to the active site of an enzyme, the key hole of the lock, to explain the specific action of an enzyme with a single substrate through defined complementary geometric shapes.[35] More recently, the "induced fit" model has been postulated by Koshland,[36,37] which also takes into account subtle conformational changes in the enzyme host upon binding, leading to enhancement in recognition and selectivity. An elegant example of anion host-guest complementarity in synthetic receptors was demonstrated by Lehn's polyammonium macrocycles (Figure 1.6), which displayed selective binding in aqueous solution for dicarboxylate guests of complementary size to their cavities.[38] The strongest complexes of the smaller host macrocycle (n = 7) are with the shorter dicarboxylates (x = 2, 3) and likewise the strongest complexes of the larger host (n = 10) are seen with the longer dicationic guests (x = 5,6).

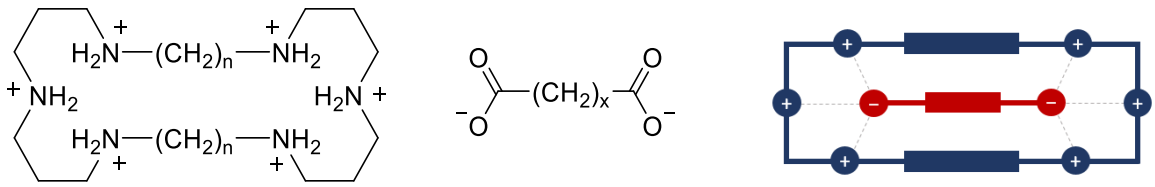


Figure 1.6: *Lehn's polyammonium macrocyclic hosts and dicarboxylate guests[38] and cartoon representation of the host–guest complex*

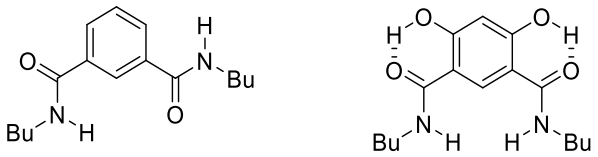
Preorganisation and the macrocyclic effect

The concept of preorganisation was introduced by Cram in the 1980s.[39] He stated:

"the more highly hosts and guests are organised for binding and low solvation prior to their complexation, the more stable will be their complexes".[39]

Through careful design, a receptor can utilise the effects of preorganisation by adopting the conformation of the complexed species to maximise association strength. This was illustrated by two acyclic isophthalamide derivatives reported by Quesada *et al.* (Figure 1.7).[40] Intramolecular hydrogen bonding interactions between hydroxyl and carbonyl

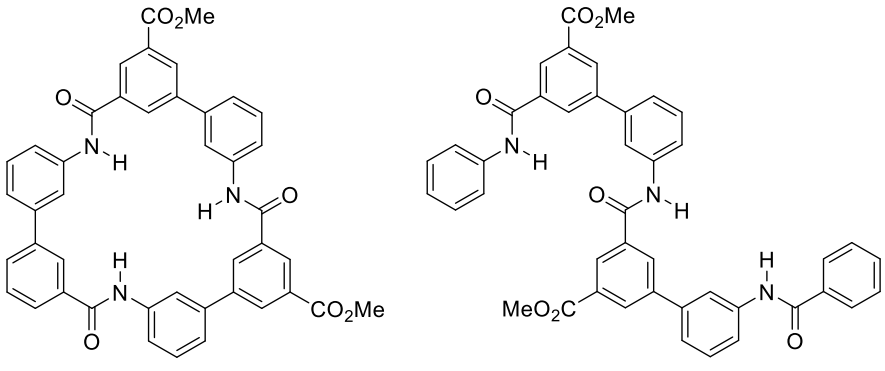
groups, result in the formation of preorganised convergent amide N-H bond donors. An impressive enhancement of chloride binding in CD_3CN was observed for the preorganised receptor compared to the non-preorganised host.



K (Cl^-) / M^{-1} (CD_3CN)	195	5230

Figure 1.7: *Preorganisation of an isophthalamide receptor and associated enhancement of anion binding*[40]

Preorganisation also contributes to the *macrocyclic effect*, which describes the phenomenon of a cyclic structure often displaying enhanced affinity for guests when compared to acyclic analogues.[41] This effect has both enthalpic and entropic contributions:[42] a favourable entropic term arises from losing fewer degrees of freedom upon complexation due to the greater rigidity; whereas, enhanced size and shape complementarity produces favourable enthalpic contributions. In addition, the relatively lower solvation of macrocycles, results in a smaller enthalpic penalty from desolvation prior to guest binding. For example, Hamilton and co-workers showed that their macrocyclic triamide host bound iodide over 100 times more strongly than the acyclic analogue (Figure 1.8).[43]



K (I^-) / M^{-1} (2% DMSO-d_6/ $CDCl_3$)	1.3×10^5	120

Figure 1.8: *Demonstration of the macrocyclic effect – Hamilton's macrocycle and acyclic analogue*[43]

1.2.2 Traditional non-covalent interactions

Alongside complementarity and preorganisation, the utilisation of non-covalent interactions is fundamental to supramolecular host-guest chemical research. Individually, these intermolecular forces are normally much weaker than conventional covalent bonds, but when acting in concert can produce strong and selective binding affinities, exemplified by the naturally occurring phosphate and sulfate binding proteins (Section 1.1.3). The following section describes the non-covalent interactions most commonly employed in anion recognition in greater detail.

Coulombic interactions

Owing to their inherent negative charge, anions undergo attractive electrostatic interactions with both positively charged (ion–ion) and positively-polarised moieties (ion–dipole) (Figure 1.9). Attractive ion-ion interactions have strengths approaching those of covalent bonds, allowing for anion binding in highly competitive protic solvent media; however, the isotropic nature of the interactions results in non-directionality and unselective binding.[44] Ion–dipole interactions although weaker in magnitude, are anisotropic and exhibit enhanced directionality. The strength is maximised according to the relative orientation of the dipole, hence improved selectivity of anionic guests can be achieved by means of its defined geometry. Due to their complementary nature, ion–ion and ion–dipole interactions are often used in unison.

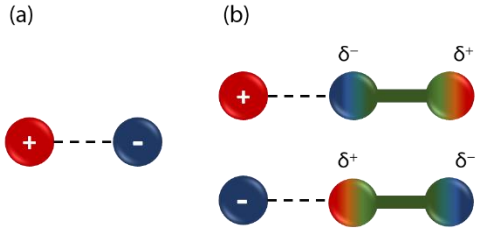


Figure 1.9: *Coulombic interactions with anions: (a) ion–ion, and (b) ion–dipole*

Hydrogen bonding

Hydrogen bonds are essential in Nature, the most renowned example being DNA base-pair recognition and stabilisation of the DNA double helical structure (Figure 1.10).[45] Hydrogen bonding is primarily electrostatic in character with strengths ranging from 4-170 kJ mol^{-1}.[46] It is a special case of dipole-dipole or ion-dipole interactions, arising from the interaction of a hydrogen atom attached to a more electronegative atom (e.g. O, N or C) with an anion or neighbouring dipole. The strength of these interactions are maximised when the *donor*–H···acceptor angle is near linearity, with strength decreasing rapidly with deviations from 180°. Strong hydrogen bonds tend to exhibit a higher degree of linearity, with weak ones displaying a large range of possible R–H···B bond angles.[46] Halogen bonding, defined as R–X···B, where X is a halogen atom, is closely related to the analogous hydrogen bonding, and will be discussed in detail in Section 1.4.

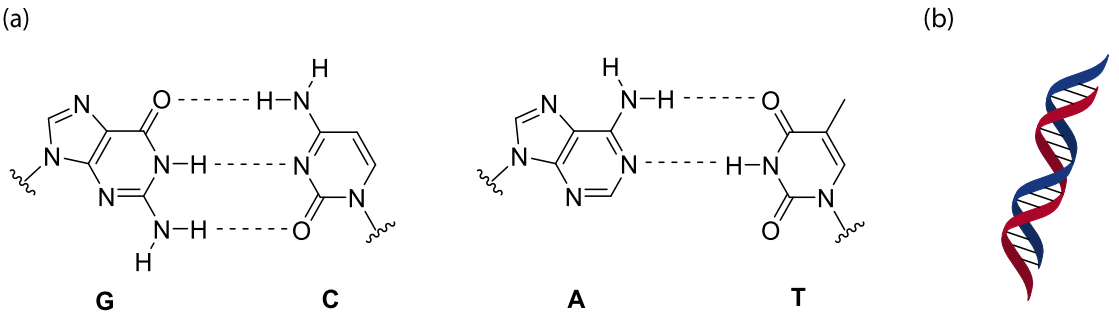


Figure 1.10: *(a) pairing of DNA base pairs via hydrogen bonding, and (b) the resulting double helical structure of DNA*

Anion–π interactions

Attractive interactions between aromatic π-systems and charged substrates such as the cation–π interaction are well-established (Figure 1.11a).[47–50] More recently anion–π interactions, arising from the interaction between an anionic species and an electron-deficient aromatic system have been observed theoretically[51,52] and experimentally in the solid state[53] and in solution.[54] The interaction of π–acidic naphthalenediimide with halide

anions has been exploited by Saha *et al.* in a molecular tweezer selective for fluoride (Figure 1.11b)[55] and by Matile *et al.* in an 'anion–π slide' displaying selective chloride transport across lipid bilayer membranes (Figure 1.11c).[56]

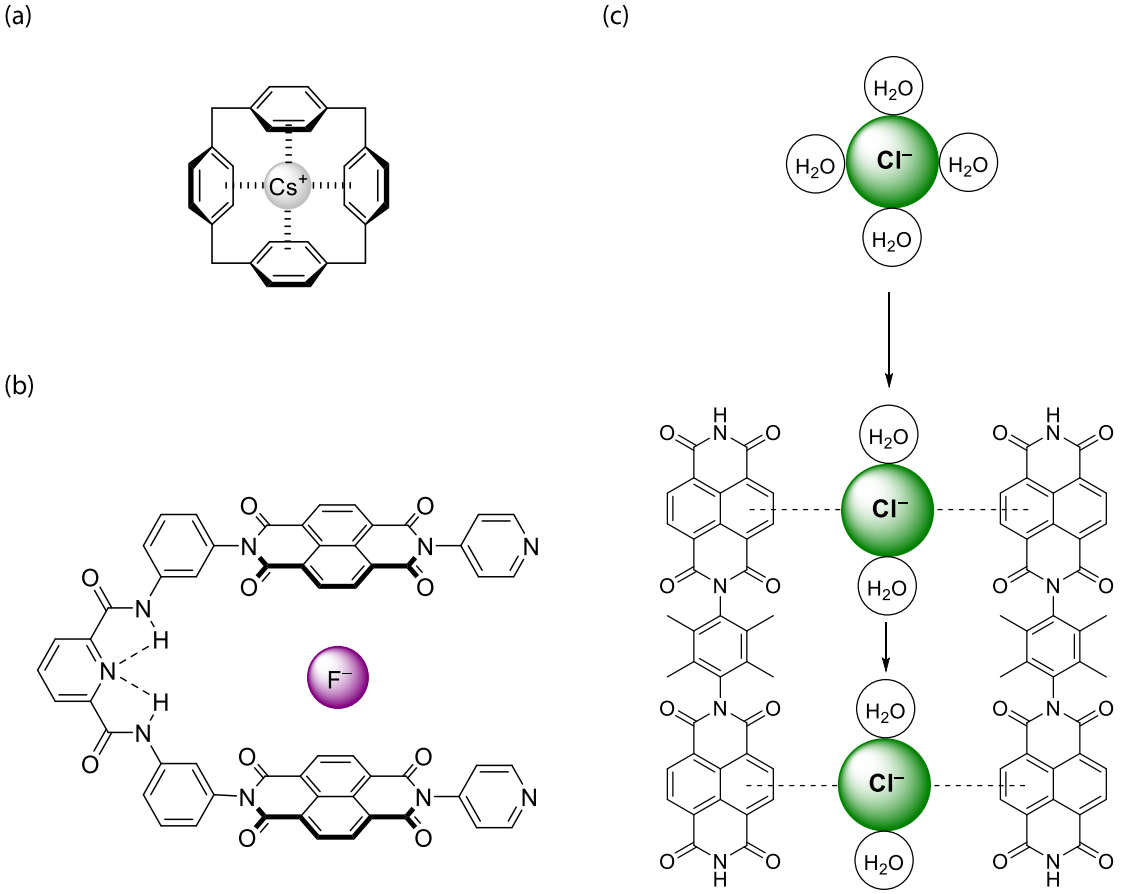


Figure 1.11: *Examples of ion–π interactions: (a) cation–π interaction[48] (b) molecular tweezer incorporating the NDI motif for anion–π interactions,[55] and (c) Matile's anion–π slides for transmembrane transport[56]*

Coordinate bond

The interaction between a Lewis acid and base such as an anion often involves a significant degree of orbital overlap and is therefore not strictly non-covalent; it is, however, still widely used in anion recognition chemistry. Common neutral and cationic Lewis acid motifs include main group elements such as boron,[57,58] antimony,[59] tin[60,61] and silicon[62,63] and transition metal cations in general, such as Zn^{2+},[64] Ni^{2+} and Cu^{2+}.[65]

Solvophobic interactions

Preferential aggregation of non-polar molecules in polar solvents occurs to minimise the total energy of the system and is termed the hydrophobic effect in water.[66,67] The "classical" hydrophobic effect is mainly driven by entropy through the release of water molecules in the hydration shells of the host and guest during their association.[66,68] In contrast, the "non-classical" hydrophobic effect is dominated by an enthalpic contribution, owing to the liberation of high energy water molecules, from the hydrophobic cavity of a macrocycle for instance, now free to form a hydrogen bonding network with the bulk water.[69] This phenomenon is still poorly understood but plays pivotal roles in biomolecular interactions[70] and has recently gained interest in anion recognition in water.[69]

1.3 Synthetic receptors for anion recognition

Employing the design principles and non-covalent interactions outlined above, a wealth of synthetic anion receptors have been reported. Frequently, hydrogen bonding is exploited in both neutral and cationic host systems using a wide variety of anion-coordinating motifs. This section will explore and discuss commonly applied motifs in anion receptor design.

1.3.1 Cationic receptors

Positively charged motifs utilising strong electrostatic ion–ion interactions are designed when integrated into an anion host structural framework to function in highly competitive polar, protic solvent media, such as methanol and water. They are, however, isotropic in nature, which can result in poor selectivity between anions and are therefore often augmented by other more directional non-covalent interactions, most commonly hydrogen bonding.

Protonated amine-, quaternary ammonium- and guanidinium-based receptors

Park and Simmons' seminal report in 1968 of a series of macrobicyclic receptors, pioneered modern anion receptor chemistry (Figure 1.1d).[4] These receptors, referred to as katapinands utilised two protonated tertiary ammonium groups at its bridgeheads, and bound halides in aqueous trifluoroacetic acid solution through a combination of electrostatic and hydrogen bonding interactions. Building on this, Lehn and co-workers developed a range of macrocyclic and macrobicyclic polyammonium hosts based on bis-tren azacryptands capable of selectively recognising anions in aqueous media through size complementarity between the host binding cavity and guest. In particular, the receptor shown in Figure 1.12a, containing an ellipsoidal cavity, exhibited selectivity for azide anions ($\log K_a = 4.6$ in H_2O),[71,72] whereas the smaller host (Figure 1.12b) was selective for fluoride ($\log K_a = 10.6$ in H_2O).[73–75] More recently, Bencini and co-workers reported receptors containing two 1,4,7-triazacyclononane macrocycles (Figure 1.12c), with selectivity preferences for mono-, di- and tri-phosphate species dependent on the spacer unit present between the two positively-charged rings.[76]

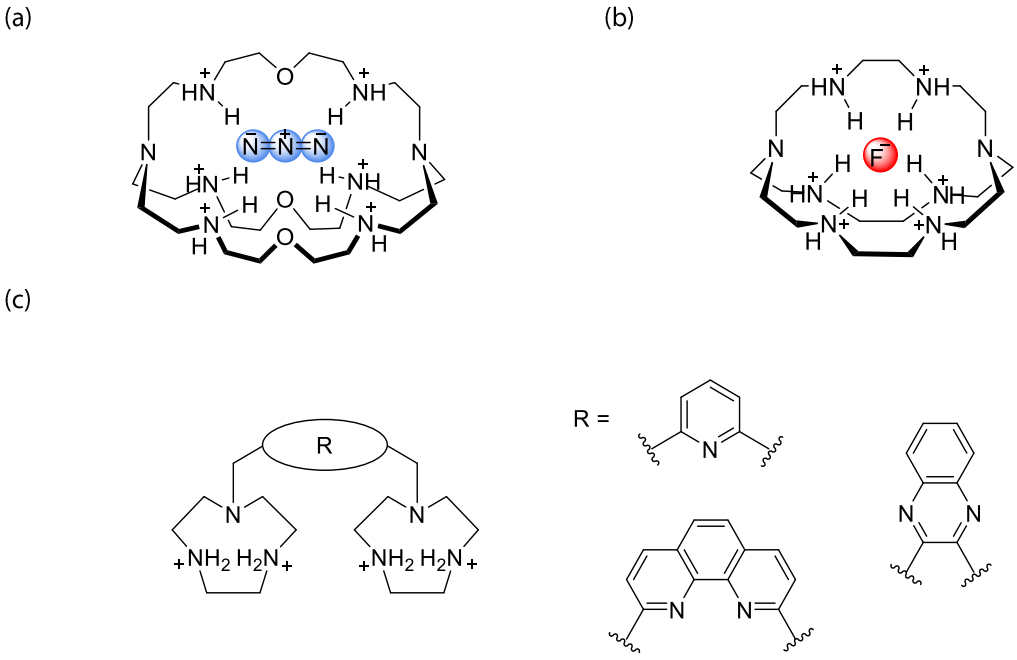


Figure 1.12: *Ammonium receptors: (a) Lehn's azide-selective ellipsoidal receptor[71,72] (b) Lehn's fluoride-selective octaazacryptand receptor,[73–75] and (c) Bencini's triazacyclononane-based receptor[76]*

These protonated polyammonium-based receptors are capable of operating in highly competitive aqueous solvent mixtures; however, a low or moderate pH is a necessary requirement. Inspired by the arginine side-chain of the phosphate binding protein (Figure 1.5a), the guanidinium moiety has been incorporated into a variety of synthetic anion receptors. Advantageously, its highly basic nature (pK_a ~ 13.5)[77] means it remains protonated over a much wider pH range compared to ammonium groups and its ability to form two strong parallel hydrogen bonds is a geometric match for binding oxoanions such as carboxylates and phosphates. Khrustalev *et al.* have recently reported new guanidinium based receptors demonstrating high selectivity; orthophosphate was bound with an affinity at least three orders of magnitude higher than other inorganic anions in a 1:1 methanol/buffer mixture (Figure 1.13).[78]

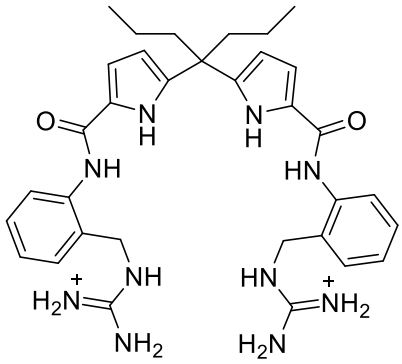


Figure 1.13: *Khrustalev's guanidinium based receptor*[78]

Employing the quaternary ammonium moiety removes hydrogen bond donors and results in a purely electrostatic interaction that inevitably leads to a lower anion binding affinity; however, importantly, the overall charge of the host is not dependent on pH. Schmidtchen *et al.* developed a series of tetrahedral macrotricyclic cage-like compounds that are able to encapsulate a range of halide and oxoanionic guests in water, through a combination of electrostatics and the hydrophobic effect (Figure 1.14a).[79–81] Inevitably, with any cationic host, such as quaternary ammonium systems, counter-anions are present that can compete with any favourable complexation of target anionic guests. To

overcome this, relatively non-coordinating counter anions are used, such as hexafluorophosphate, perchlorate or nitrate. An alternative approach, demonstrated by Schmidtchen *et al.* was to prepare electroneutral zwitterionic quaternary ammonium cages, with rigid substituents extending radially to the periphery carrying negatively charged groups (Figure 1.14b); this receptor demonstrated enhanced halide binding in water over the cationic analogue.[82]

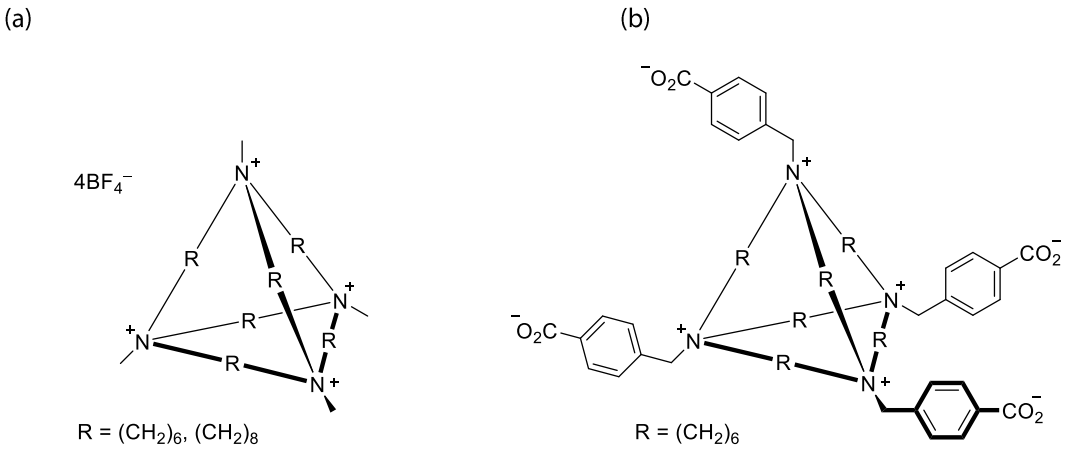


Figure 1.14: *Quaternary ammonium cage receptors: (a) Schmidtchen's tetrahedral macrotricyclic cages,[79–81] and (b) the zwitterionic analogue[82]*

Imidazolium-based receptors

The imidazolium moiety is capable of strong interactions with anions through charge assisted hydrogen bonding.[83] A seminal report by Sato *et al.* in 1999 described the first example of C–H···A⁻ hydrogen bonding interactions of imidazolium in host–guest chemistry; a tripodal receptor containing three imidazolium groups, preorganised for anion binding demonstrated high affinity for halide anions in CD_3CN.[84] Through the incorporation of a nitro-imidazolium moiety to further polarise the C–H hydrogen bond donor, Sato *et al.* went on to describe a tripodal receptor capable of strong and selective binding of Cl^- (K_a = 1.1 × 10^6 M^{-1}) and an affinity for $H_2PO_4^-$ (Figure 1.15a).[83] Contemporaneously, in 1999 Alcalde *et al.* reported a family of 'imidazoliophane' macrocycles (Figure 1.15b), shown to bind a variety of anions in the order $H_2PO_4^-$ > F^- >

CH_3COO^- > CN^- > Cl^- in d_6-DMSO.[85] More recently, Steed *et al.* developed a ditopic tetrapodal imidazolium-based receptor utilising a 1,3-alternate calix[4]arene scaffold, resulting in a 1:2 host:guest binding stoichiometry in CD_3CN (Figure 1.15c).[86] Interestingly, an allosteric enhancement of the binding of a second anion is observed with Cl^-, but not observed with other anions (Br^- and I^-).

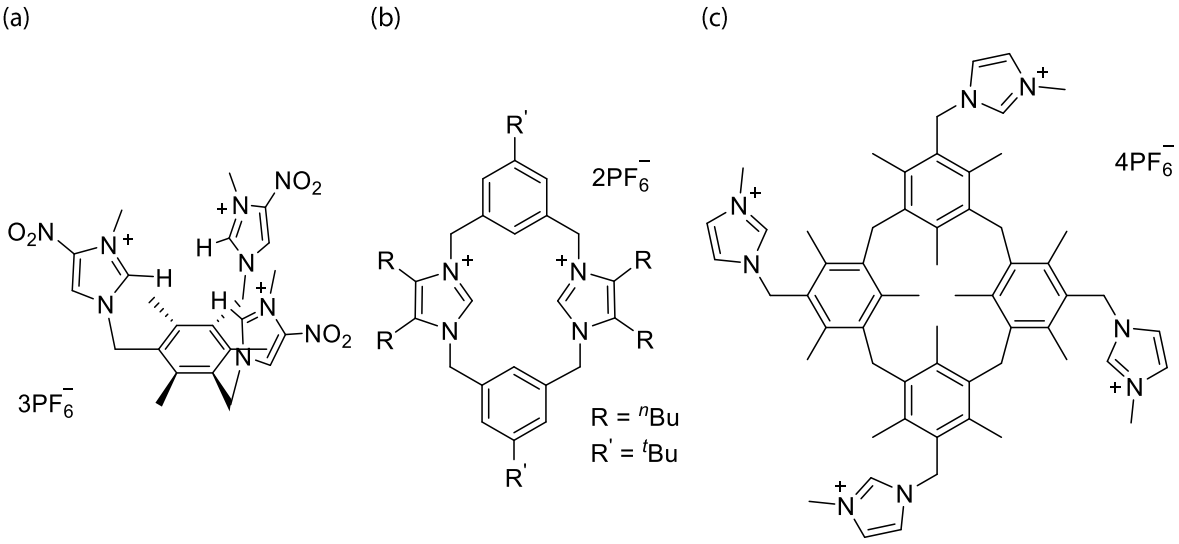


Figure 1.15: *Imidazolium host systems: (a) Sato's tripodal imidazolium receptor,[83] (b) Alcalde's macrocyclic host[85] and (c) Steed's tetrapodal receptor[86]*

Triazolium-based receptors

The triazolium motif is able to bind anions through charge-assisted C-H hydrogen bonding in a similar manner to imidazolium. A formal positive charge and polarisation of the C^5-H bond is achieved through alkylation at the N^3 position of the triazole. The first report of a triazolium-based receptor was by Pandey *et al.*, who demonstrated the ability of a bis-triazolium functionalised steroid to bind $H_2PO_4^-$ selectively over halides and acetate in $CDCl_3$ (Figure 1.16a).[87] More recently, many examples of triazolium receptors have been reported, including by Schubert *et al.* who synthesised an acyclic bis-triazolium benzene receptor which forms a 2:1 host:guest complex with sulfate[88] and Sessler *et al.* who described a triazolium-phane with high affinities for oxoanions (HSO_4^-, $H_2PO_4^-$, $HP_2O_7^{3-}$) in CD_3OD (Figure 1.16b).[89]

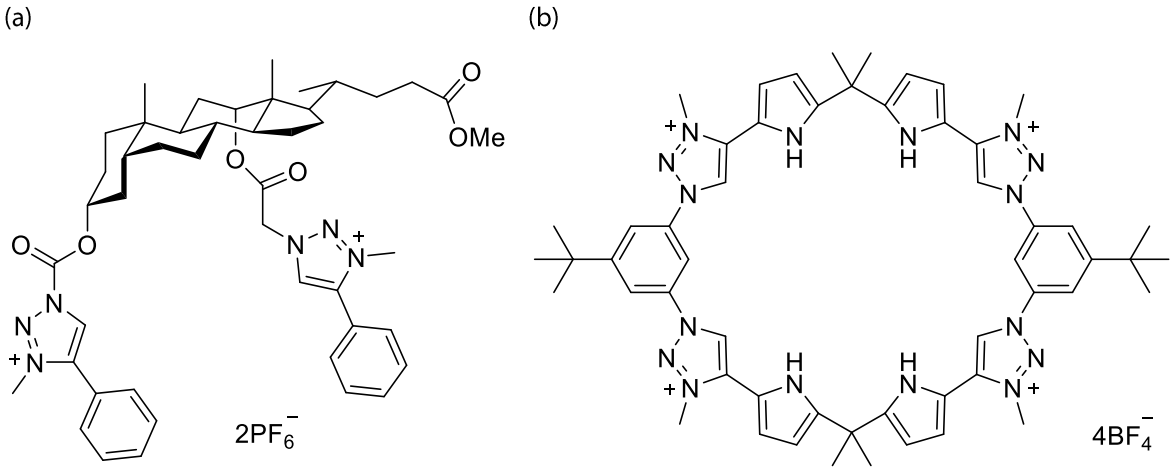


Figure 1.16: *Triazolium-based receptors: (a) Pandey's steroid-based bis-triazolium receptor,[87] and (b) Sessler's triazolium-phane receptor[89]*

1.3.2 Neutral anion receptors

Neutral anion receptors are designed to function in aprotic organic solvent media, and employ weak intermolecular interactions, the most highly exploited being hydrogen bonding. Common neutral hydrogen bonding motifs incorporated into anion receptors include amides,[90] ureas and thioureas,[91,92] pyrroles[93] and triazoles.[94–96]

Amide-based receptors

Amides are abundant in peptide frameworks and extensively present in biotic anion receptors. Consequently, due to their synthetic accessibility many abiotic host systems utilise the amide moiety, most commonly in a preorganised fashion within a convergent molecular architecture. The first report of an amide-based neutral receptor was by Pascal *et al.* in 1986, who described a cryptand containing three convergent amide hydrogen-bond donors able to bind fluoride in DMSO-d_6.[97] Over a decade later, Crabtree *et al.* demonstrated the ability of the isophthalamide motif to complex anions, in particular halides, through simple non-preorganised acyclic receptors.[98] Jurczak *et al.* reported a similar 2,6-bis-amide pyridine motif for anion recognition in 2005, utilising the preorganisation of the system *via* intramolecular hydrogen bonding between the amides and pyridine-nitrogen in a *syn-syn* conformation.[99,100] Bowman-James *et al.* reported

cryptands containing 2,6-bis-amide isophthalamide and pyridine motifs, with both displaying selectivity for fluoride over other halides and a range of oxoanions in DMSO-d_6 (Figure 1.17a).[101–103] Due to the charge neutrality of the amide group, the majority of receptors only function effectively in aprotic organic solvents. However, pioneering work by Kubik and co-workers demonstrated the ability of bis-cyclopeptides to bind anions in aqueous media *via* a combination of the hydrophobic effect and hydrogen bonding interactions.[104,105] In particular, a receptor comprising two covalently liked cyclic hexapeptide rings showed remarkable binding of iodide and sulfate in 95:5 D_2O/CD_3OD (log K_a = 3.70 and 3.96 respectively) (Figure 1.17b).[106]

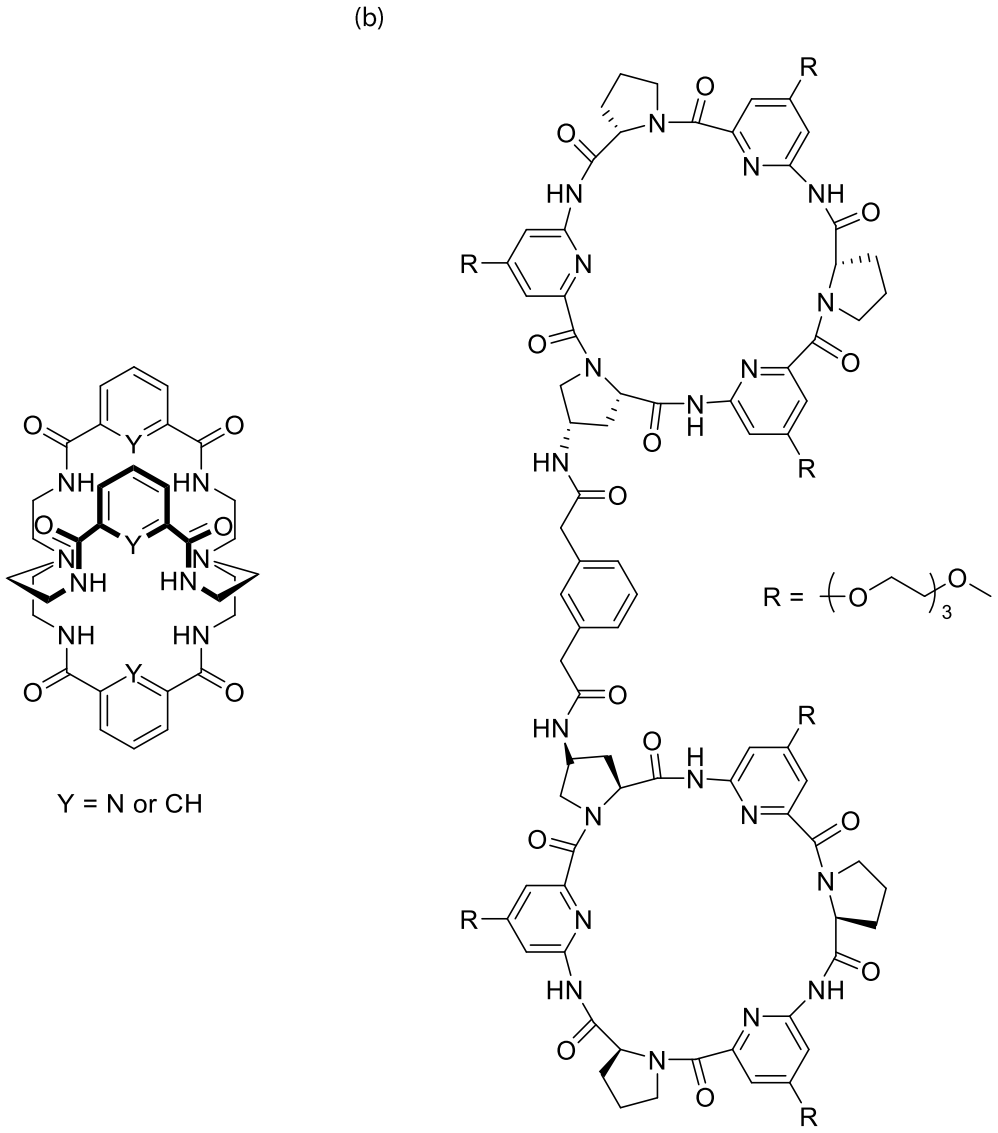
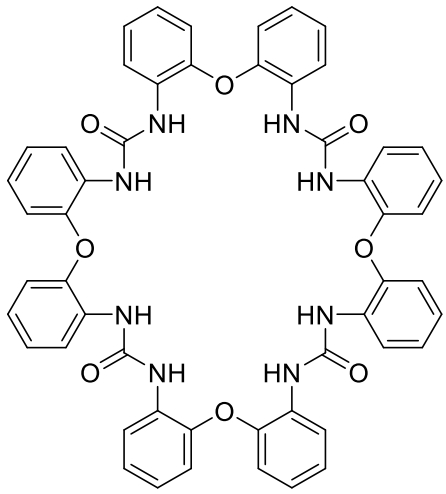


Figure 1.17: *Examples of amide-based receptors: (a) Bowman-James' cryptand,[102,103] and (b) Kubik's bis-cyclopeptide receptor[106]*

Urea- and thiourea-based receptors

Analogous to the cationic guanidinium motif, neutral urea and thiourea moieties provide two parallel N–H hydrogen bond donors, ideal for recognition of oxoanions such as carboxylates and phosphates. For example, Böhmer and co-workers reported a tetrameric urea macrocyclic host system (Figure 1.18a), capable of binding acetate and dihydrogen phosphate in a 1:1 binding stoichiometry in 3:1 THF/MeCN (log K_a = 5.2 and 5.8, respectively).[107] Thioureas are more acidic than ureas, however, this also results in a greater ease of deprotonation.[108] Boyle *et al.* reported 'molecular cleft-like' hosts utilising Troger's base as a rigid scaffold for two thiourea groups. The receptor shown in Figure 1.18b demonstrates strong binding for acetate (1:2 host/guest stoichiometry) and dihydrogen phosphate (1:1 host/guest stoichiometry) in DMSO, concomitant with dramatic changes in the UV-Vis absorption spectra allowing for colorimetric sensing. Furthermore, no binding of sulfate was observed and deprotonation occurred at high concentrations of fluoride.[109]

(a)



(b)

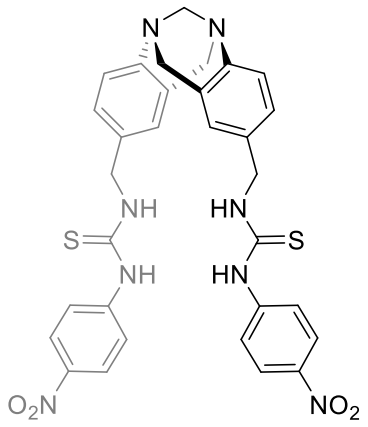


Figure 1.18: *Examples of urea and thiourea-based receptors: (a) Böhmer's tetrameric macrocycle,[107] and (b) Boyle's 'molecular cleft-like' host[109]*

Pyrrole-based receptors

Pyrroles are an attractive choice of neutral hydrogen bond donors, as unlike other moieties such as ureas and amides, the pyrrole moiety does not contain hydrogen bond acceptors. Further to this, they are neither particularly basic or acidic and can therefore function over a wide range of pH conditions. The most notable advancement of pyrrole-based receptors for anion recognition is the pioneering work of Sessler *et al.* in the development of calix[4]pyrroles: macrocycles containing four pyrrole units arranged with the N–H hydrogen bond donors directed towards the central cavity (Figure 1.19a). The parent calix[4]pyrrole displays superior binding of fluoride over chloride in CD_2Cl_2 (K_a = 17170 and 350, respectively) due to size-match complementarity of fluoride and the calix-cavity of four pyrrolic N–H protons.[110] Through the incorporation of a strap containing a C–H hydrogen bond donor an order of magnitude increase in affinity for chloride was observed (measured *via* ITC in CH_3CN $K_a = 2.2 \times 10^5$ and 2.2×10^6, for unstrapped and strapped respectively) attributed to the better size matching between the chloride ion and the binding site by the presence of the strap (Figure 1.19b).[111] Additionally, through tuning of the strap to include a pyrrolic N–H hydrogen bond donor (Figure 1.19c), a further increase of another order of magnitude was observed for chloride ($K_a = 1.8 \times 10^7$ in CH_3CN).[112]

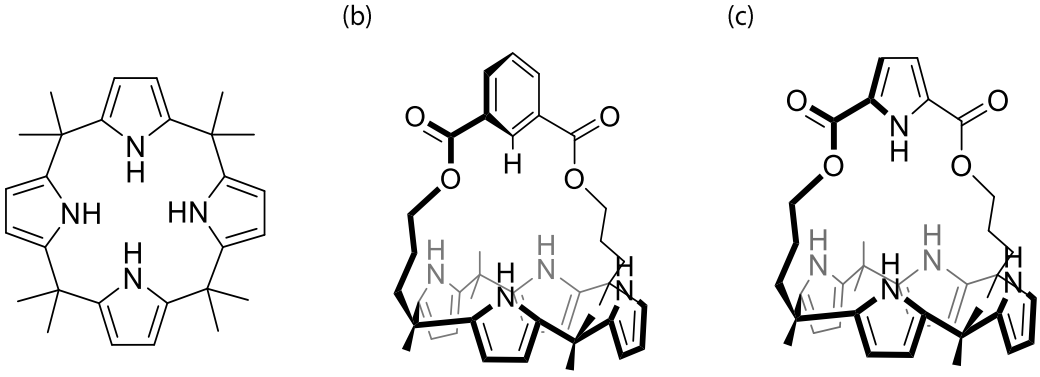


Figure 1.19: *Examples of Sessler's calix[4]pyrrole based systems: (a) calix[4]pyrrole[110] (b) benzene-strapped calix[4]pyrrole,[111] and (c) pyrrole-strapped calix[4]pyrrole[112]*

Triazole-based receptors

The 1,2,3-triazole moiety is a source of neutral C–H hydrogen bond donors, which has emerged over recent years as a potent anion binding motif.[113–115] In 2008, two seminal publications emerged: Flood *et al.* reported a shape persistent preorganised macrocycle (Figure 1.20a),[116] which showed strong affinity for chloride in CD_2Cl_2 ($K_a = 1.1 \times 10^7$) due to its ideal cavity size and the cumulative effects of multiple C–H hydrogen bonds and Craig *et al.* reported a oligotriazole foldamer, which in the presence of chloride resulted in anion-induced folding (Figure 1.20b).[95]

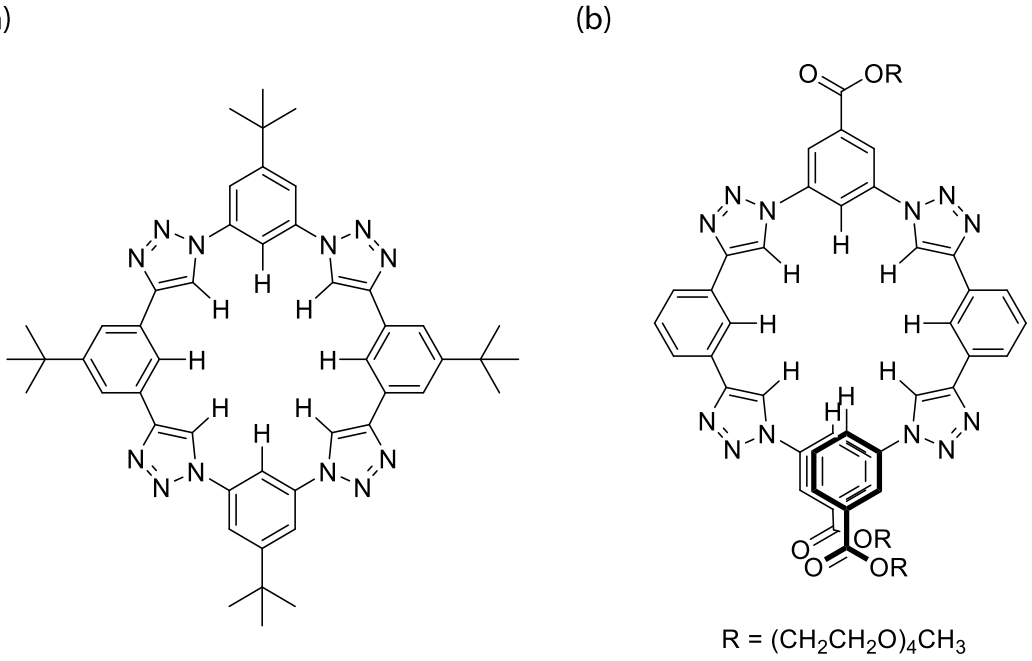


Figure 1.20: *Examples of triazole-based receptors: (a) Flood's tetratriazole macrocycle,[116] and (b) Craig's tetratriazole foldamer[95]*

1.4 Halogen Bonding

Traditional non-covalent interactions, such as electrostatics and hydrogen bonding have proven to be effective for anion receptor design (Section 1.3). A more recent addition, halogen bonding has also been exploited for anion recognition applications and is gaining attention as a superior alternative to hydrogen bonding.

1.4.1 Principles of halogen bonding

The interaction between an electrophilic halogen atom and a nucleophilic region was first reported by Guthrie in 1863,[117] and demonstrated crystallographically by Hassel *et al.* in 1954.[118] However, it was Dumas *et al.* in 1983[119] who first coined the term halogen bonding for such an interaction. Recently defined by IUPAC, a "halogen bond" is said to occur when:

> *"there is evidence of a net attractive interaction between an electrophilic region associated with a halogen atom in a molecular entity and a nucleophilic region in another, or the same, molecular entity."*[120]

Halogen bonding can be represented as R–X···B, showing the non-covalent interaction between the electrophilic halogen atom (X, XB donor) covalently attached to an electron-withdrawing group (R) and the nucleophilic Lewis base (B, XB acceptor).[121,122] Whilst counterintuitive that a halogen atom would possess an electrophilic region, when bound to an electron-withdrawing R-group, the halogen atom becomes polarised and results in the formation of a σ-hole; a region of reduced electron density, and increased positive charge at the terminus of the halogen atom. This is surrounded by an equatorial ring of negative potential, resulting in the amphoteric ability of halogen atoms to interact with electrophiles approaching orthogonally to the R–X bond (Figure 1.21).[123] The anisotropic distribution of electron density results in an interaction with a highly directional nature between the σ-hole and an electron-rich region on another atom or functional group, producing an attractive force of near linearity R–X···B.[122,124]

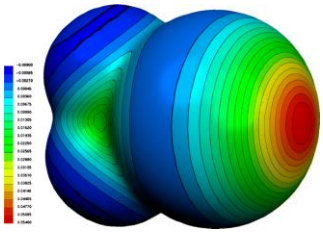


Figure 1.21: *The molecular electrostatic potential showing the σ-hole as the region of positive potential (red) in Hartrees, at the 0.001 electrons Bohr^{-3} isodensity surface of CF_3I*[123]

Interaction energies of halogen bonds are in the range of 10-200 kJ mol^{-1}, broadly similar to the range observed for hydrogen bonds.[125] The strength of the XB interaction increases with: heavier halogens due to decreasing electronegativity and an increase in polarisability (XB donor ability increases R–F << R–Cl < R–Br < R–I);[126,127] the increased electron-withdrawing ability of the substituent R, resulting in enhanced polarisation of the halogen atom, and the degree of *sp*-hybridisation being reduced for R, in the order C(sp^3)–X < C(sp^2)–X < C(*sp*)–X, leading to an increase in donor ability.[128] It should be noted that although the σ-hole concept, introduced by Politzer[123] elegantly accounts for the majority of observed interactions, there are examples of XB interactions that cannot be explained purely by the σ-hole,[129,130] but through a combination of interactions including electrostatics, charge-transfer and dispersion.[131] The nature of the halogen bond is therefore being investigated theoretically[132] but it is still the subject of heated debate.

Halogen bonding has been exploited extensively in the solid-state in crystal engineering[128,133] and has led to applications in solid-state functional materials;[131,134,135] however, only recently has the potential of solution-phase halogen bonding applications been explored with seminal reports in catalysis,[136–138] self-assembly,[139–141] gelation[142,143] and medicinal chemistry.[144]

1.4.2 Halogen bonding for anion recognition

The highly directional nature of the halogen bond, coupled with the ability to tune the strength of the interactions provides an exciting alternative to traditional non-covalent interactions for the design of supramolecular host systems. The incorporation of XB donor groups into anion receptors is still in its infancy compared to their HB counterparts; however, a rapid expansion has been observed over the last decade. As outlined in section 1.4.1, the XB interaction increases with increasing polarizability of the halogen, due to the formation of a more electrophilic σ-hole; bromine and iodine are therefore most commonly exploited in XB recognition systems. To date, the vast majority of the receptors developed have incorporated either haloperfluoroarene, halotriazole/halotriazolium or haloimidazolium motifs (Figure 1.22). Used in a multivalent manner and/or in concert with other non-covalent interactions such as HB, this section will outline the use of such motifs for anion recognition. In particular, the elegant ability of XB to enhance the strength and selectivity of anion binding affinities will be demonstrated through comparison of XB receptors with the analogous HB host systems.

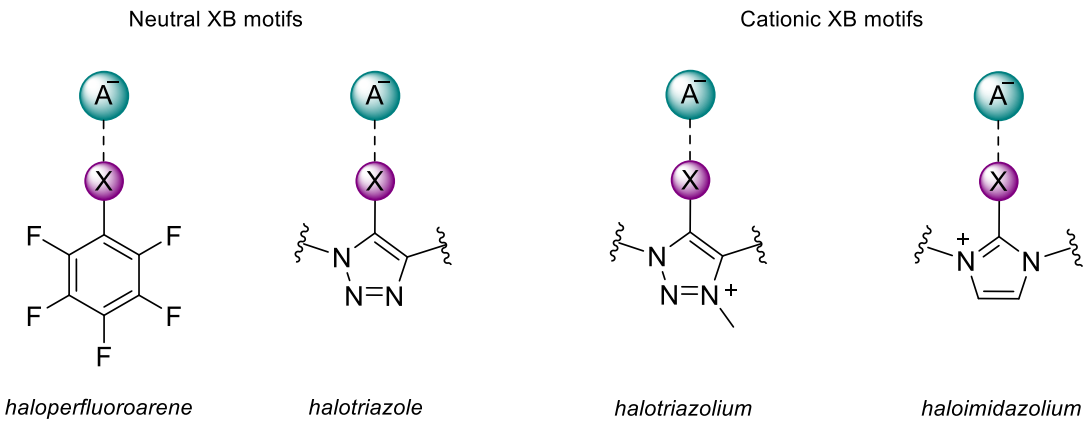


Figure 1.22: *Common neutral and cationic XB-donor motifs for anion recognition (X = Br/I)*

Neutral halogen bonding receptors

The emergence of XB interactions for anion recognition in the solution-phase was through a seminal publication by Resnati *et al.* in 2005, where an iodoperfluoroarene heteroditopic tripodal receptor with recognition sites for both alkali metal cation and counter-anion was shown to bind the NaI ion pair in $CDCl_3$ 20 times more strongly than the pentaperfluoroarene analogue (Figure 1.23a).[145] Haloperfluoroarenes are well documented in XB systems, attributed to their ease of functionalisation at any position with Br or I, thus allowing for tuning of anion coordination geometries at will. The nature of Resnati's receptor prevented cooperative interactions of all three XB donors; Taylor *et al.* utilised convergent halogen bonds through functionalisation at the 2-position of the perfluoroarene with the XB donor, reporting a tripodal host system which displayed good selectivity for halides over oxoanions in d_6-acetone (Figure 1.23b).[146] These preliminary results suggested a preference of XB to interact with 'softer' halides compared with 'harder' oxoanions.

(a) (b)

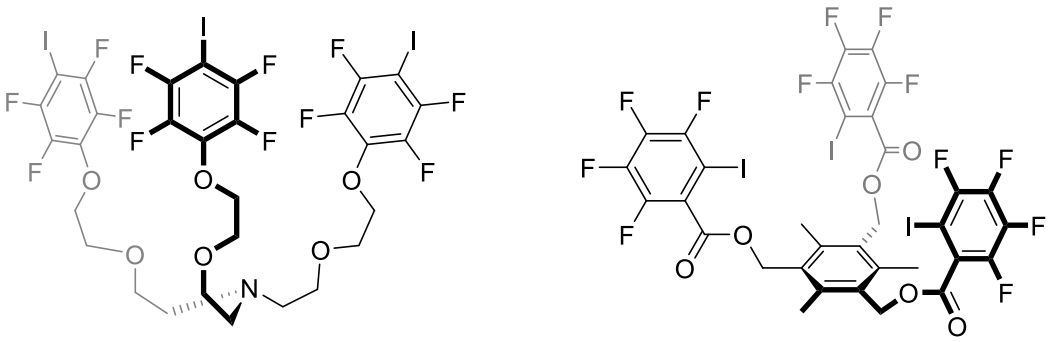


Figure 1.23: *Iodoperfluoroarene containing XB anion receptors: (a) Resnati's receptor,[145] and (b) Taylor's receptor[146]*

Halotriazoles, in particular iodotriazoles, have been effectively incorporated into anion receptor design utilising convergent donors and/or preorganisation. Owing to their synthetic accessibility *via* Cu^I catalysed azide-alkyne cycloaddition (CuAAC) 'click'

reactions using terminal azides and haloalkynes,[147,148] the iodotriazole motif in particular has gained considerable interest. For example, Schubert *et al.* designed a bidentate receptor, containing a carbazole spacer between two iodotriazole motifs.[149] The chloride and bromide binding affinities were determined for the carbazole and the phenol functionalised carbazole receptors (Figure 1.24) *via* isothermal calorimetry titration experiments (ITC) in THF; a binding mode of 2:1 host/guest was determined for both anions and enhanced affinities were observed for the hydroxy-functionalised receptor. It was postulated that the augmented binding was due to intramolecular hydrogen bonding interactions between the hydroxyl -OH and N atom of the iodotriazole groups acting to preorganise the system and so minimise the entropic penalty of conformational reorganisation upon binding.

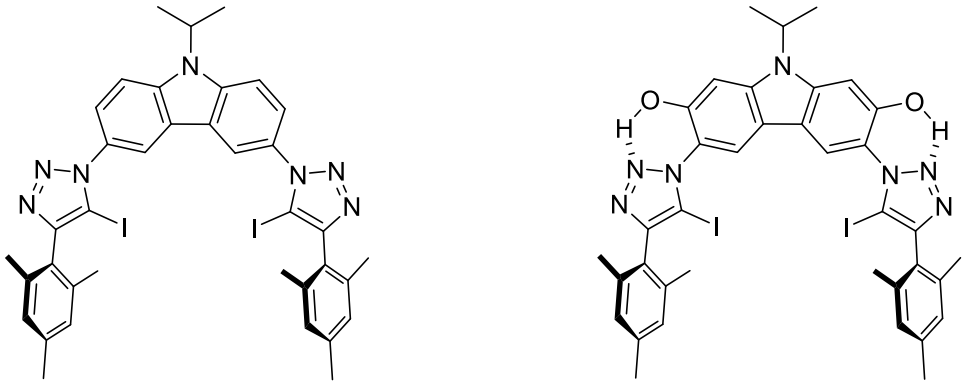


Figure 1.24: *Schubert's bidentate XB carbazole receptors*[149]

Beer *et al.* have recently reported the first examples of neutral tetradentate XB donor foldamers using the iodotriazole motif (Figure 1.25);[150] the potency of this system for anion binding was displayed in iodide selectivity over the lighter halide, carboxylate and dihydrogen phosphate anions in $CDCl_3$. Additionally, an enhancement in affinities was observed compared to their hydrogen bonding analogues.

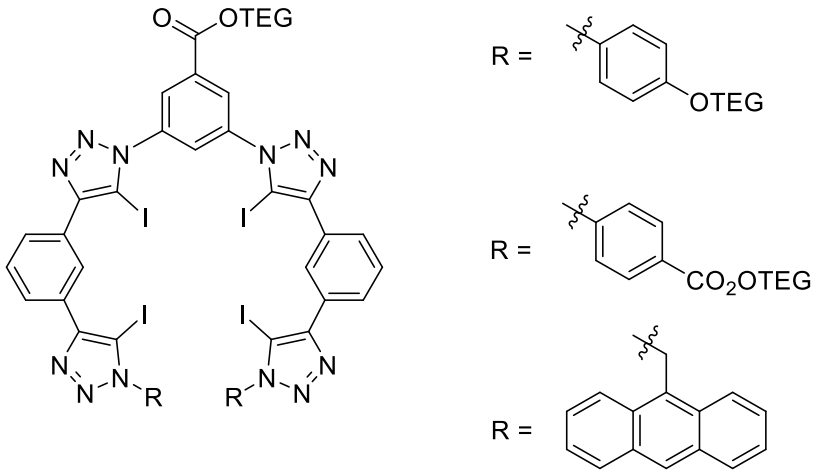


Figure 1.25: *Beer's tetradentate XB donor foldamers*[150]

Cationic halogen bonding receptors

The cationic halotriazolium motif has been shown to be a more potent XB donor than the charge neutral iodotriazole analogue,[152–154] through a combined effect of greater C–X bond polarisation and charge assistance. The increased potency has enabled the recognition of environmentally and biologically relevant anions, such as pyrophosphate and allows for binding in highly competitive protic solvent systems. An elegant example has been reported by Beer *et al.* using the bis-iodotriazolium motif and incorporating tetraethylene glycol substituents to render the receptors water soluble (Figure 1.26).[151] Anion selectivity in D_2O followed the Hofmeister bias ($I^- > Br^- > Cl^-$) due to the greater ease of desolvation of the heavier halides. Remarkably, the XB receptor exhibited superior perrhenate (ReO_4^-) recognition (K_a = 44 M^{-1}), with the HB analogue displaying no appreciable binding affinity: perrhenate was used as an analogue for the environmentally relevant radioactive nuclear waste by-product pertechnetate anion, due to their comparable physical properties.[155–157] Furthermore, they demonstrated that the XB receptor is capable of sensing perrhenate in water *via* a fluorescent response, the first example of its kind.

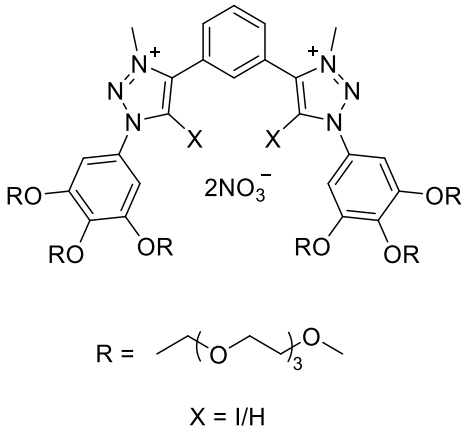


Figure 1.26: *Beer's bis-iodotriazolium water soluble receptor*[151]

Another example of a XB fluorescent sensor is the pyrene-functionalised bis-halotriazolium receptor that has been described by Molina *et al.* (Figure 1.27),[158] which demonstrated a selective enhancement in the emission intensity of the pyrene excimer band in acetone for the pyrophosphate anion, which from computational modelling, was attributed to a conformational rearrangement upon anion complexation. Interestingly, they also investigated the influence of the number and strength of halogen bond donors on the association strength: the mixed halogen- and hydrogen-bonding receptor demonstrated an association constant for $HP_2O_7^{3-}$ of K_a = 1734 M^{-1}; upon introducing another halogen bond donor to produce the bis-iodotriazolium system, the association constant increased over five-fold. Furthermore, the bis-bromotriazolium (a weaker XB donor) receptor exhibited an association constant for $HP_2O_7^{3-}$ of K_a = 3032 M^{-1}, almost twice that of the mixed receptor, but significantly lower than the iodo analogue. This confirmed that the integration of halogen bond donors significantly improves the anion recognition affinity, which in turn can be augmented further through increasing the XB donor strength.

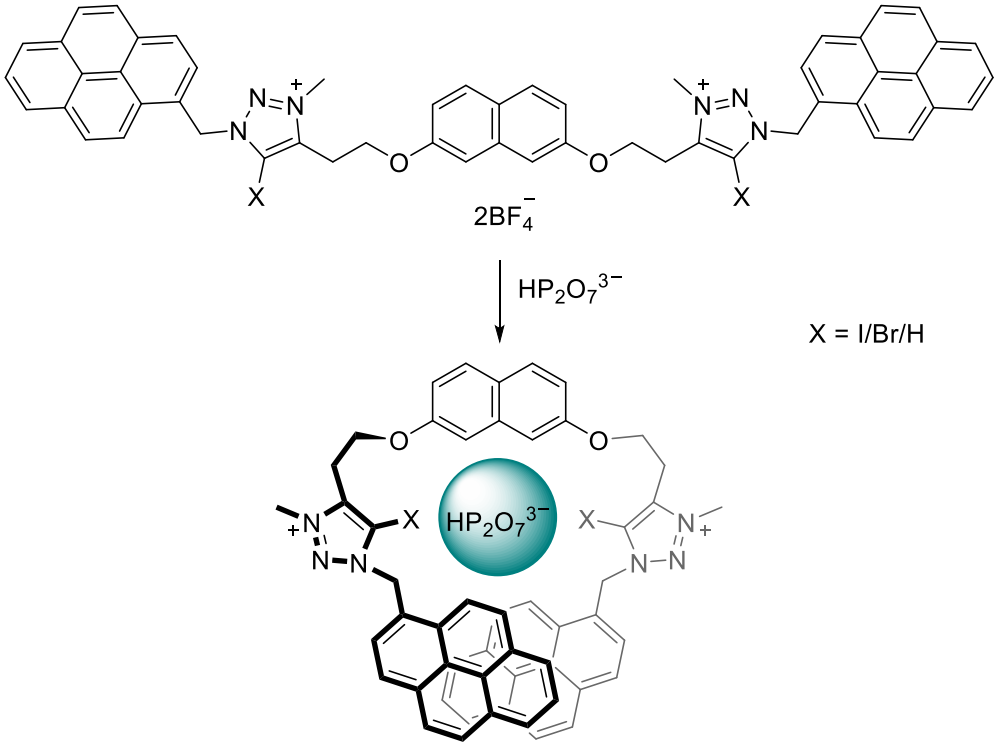


Figure 1.27: *Molina's pyrene-functionalised bis-halotriazolium receptor*[158]

The employment of imidazolium derivatives as charge assisted C–H hydrogen bond donors in anion recognition processes is well documented (Section 1.3.1). More recently, the potential of 2-haloimidazolium derivatives for analogous XB anion receptors has been investigated. Resnati *et al.* reported a simple 2-iodoimidazolium receptor bearing an anthracenyl substituent, showing selective binding of $H_2PO_4^-$ in d_6–DMSO (Figure 1.28a);[159] the protic analogue in comparison exhibited weak, unselective binding of the anions investigated. Interestingly, from solid state structures obtained of the Cl^-, Br^- and I^- complexes, strong linear XB interactions were observed for all three halide complexes. Furthermore, haloimidazolium motifs have been incorporated into a variety of structures, such as: the seminal report of a bidentate bromoimidazoliophane by Beer *et al.* displaying selective binding of bromide in a 9:1 mixture of CD_3OD and D_2O (Figure 1.28b),[160] through cooperativity of two preorganised XB bromine donor atoms; a tripodal 2-iodoimidazolium receptor by Ghosh *et al.* impressively demonstrating selective removal of bromide from a solution of competitive anions through crystallisation (Figure 1.28c);[161] and, an organocatalyst reported by Minakata *et al.* exploiting a 2-iodoimidazolium salt for

XB interactions to catalyse an aza-Diels–Alder reaction achieving an 85% yield, with no product observed with the HB analogue (Figure 1.28d).[162]

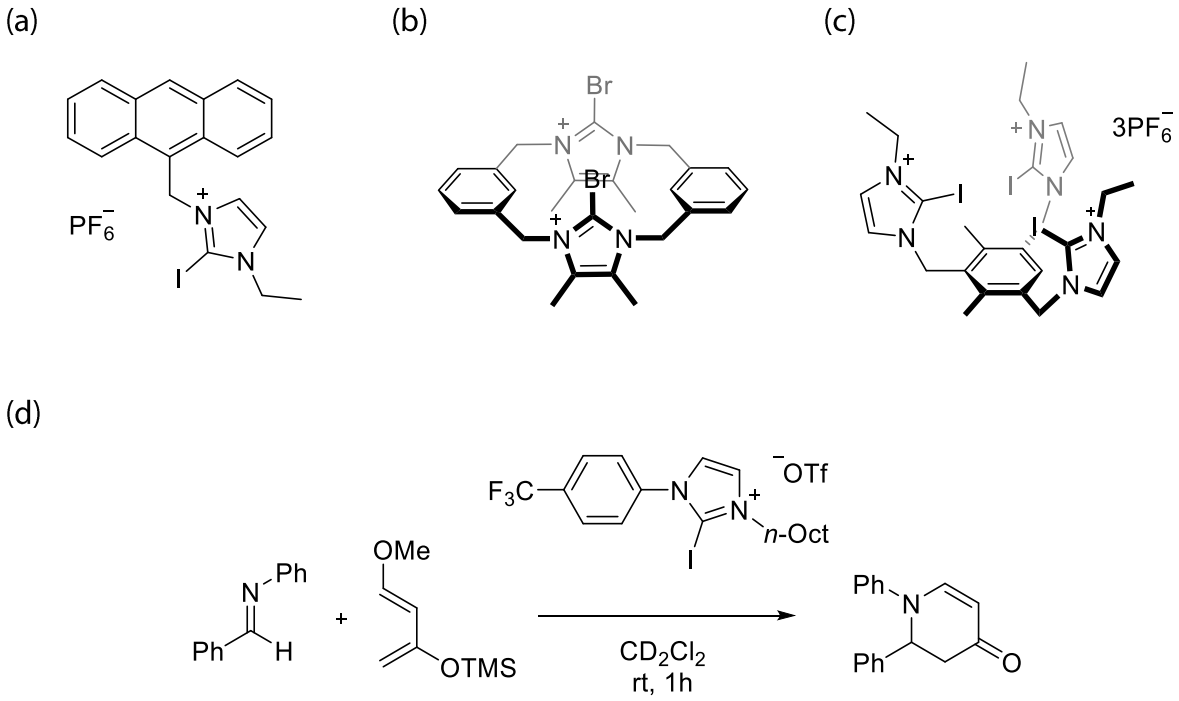


Figure 1.28: *Examples of haloimidazolium XB donor systems: (a) Resnati's iodoimidazolium-based receptor,[159] (b) Beer's bidentate bromoimidazolium macrocyclic receptor,[160] (c) Ghosh's tripodal iodoimidazolium receptor,[161] and (d) reaction scheme for the aza-Diels–Alder reaction utilising Minakata's iodoimidazolium XB organocatalyst[162]*

1.5 Synthesis and applications of mechanically interlocked molecules

1.5.1 The mechanical bond

Mechanically interlocked molecules (MIMs) consist of two or more molecules held together by mechanical rather than covalent bonds, such that they cannot be separated without cleavage of a covalent bond, despite the components not being covalently linked themselves. Since the first report of the synthesis of a catenane[163] in 1960 and a rotaxane[164] in 1967, MIMs have captured the imagination of synthetic chemists due to their aesthetic appeal and inherent challenge associated with their construction. More recently, investigations into MIMs are being driven by the realisation of a wealth of potential applications, such as in molecular machinery,[165] nanomedicine,[166] nanotechnology[167] and most relevant to this thesis, recognition and sensing of charged species.[168] In the context of anion recognition, interlocked molecules have been shown to function as highly selective receptors (Section 1.5.4); their complex topologies mimic Nature to generate three-dimensional pre-organised binding pockets, often shielded from solvent and the close proximity of molecular components results in reduced degrees of freedom and augmented non-covalent interactions.[169]

The most common MIMs are [*n*]rotaxanes and [*n*]catenanes, where *n* indicates the number of molecular components within the structure (Figure 1.29). A rotaxane consists of one or more linear molecules, known as axles, threaded through one or more macrocyclic molecules with bulky stopper groups attached to both ends of the axle components to prevent dethreading (Figure 1.29a). Catenanes, however, are species consisting of two or more discrete interlocked macrocyclic molecules (Figure 1.29b). A related class are [*n*]pseudorotaxanes, described as an interpenetrated rather than an interlocked assembly, whereby the bulky stopper groups are absent, hence the axle and macrocyclic components exist in an equilibrium between the threaded and dethreaded states. Pseudorotaxanes are commonly employed as precursors to rotaxanes and

catenanes. More complex interlocked structures are also known such as Solomon knots, Borromean rings and trefoil knots.[170]

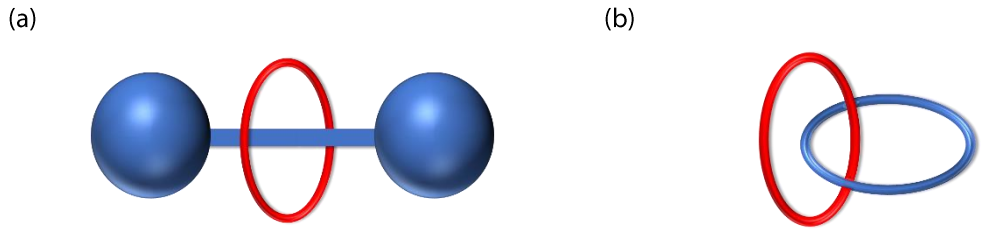


Figure 1.29: *Cartoon representations of (a) [2]rotaxane, and (b) [2]catenane*

1.5.2 Synthesis of interlocked molecules

The two most common strategies for rotaxane synthesis are *clipping* and *stoppering*, although more exotic methods such as *slippage*,[171] *snapping*,[172,173] *swelling*[174] and *shrinkage*[175] exist. Clipping involves the ring-closing of an acyclic macrocyclic precursor around a stoppered axle component of sufficient size to inhibit dethreading; whereas, stoppering involves appending bulky stopper groups to a pseudorotaxane assembly (Figure 1.30).[176] Of the more esoteric methods: slippage refers to the coaxing of a macrocycle over the stopper groups under thermodynamically forcing conditions, to form a rotaxane that under ambient conditions is stable; snapping is the joining of two half-axle components within a macrocycle; swelling involves the formation of a pseudorotaxane with an axle containing small stoppers, which under thermal or photochemical stimuli, can swell to larger, bulky stoppers capable of holding the macrocycle in place; and conversely, a large macrocycle can undergo shrinkage after slipping onto a stoppered axle.

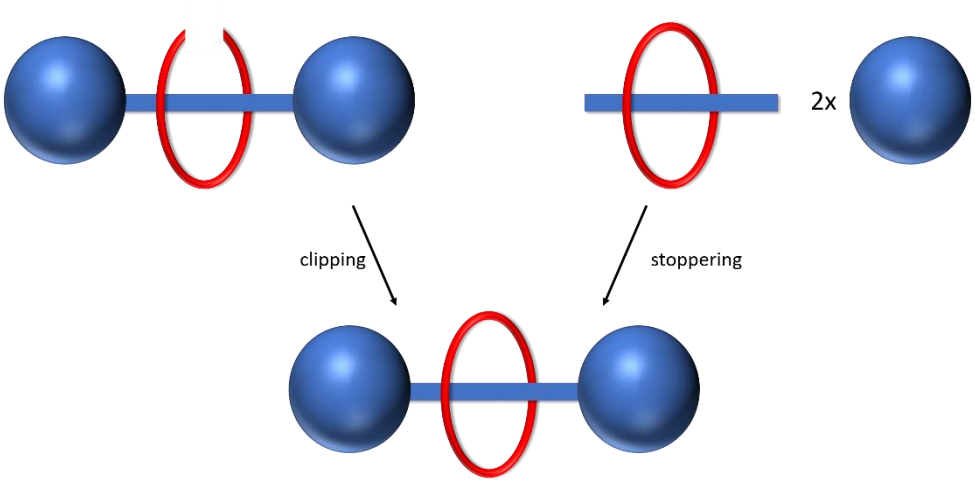


Figure 1.30: *Cartoon representation of methods to prepare a [2]rotaxane*

Strategies towards the synthesis of catenanes are less varied. The two main routes, employ a *clipping* strategy, whereby either cyclisation is carried out on the thread component of a pseudorotaxane assembly, or, a double cyclisation of two macrocyclic precursors held in an orthogonal geometry is used (Figure 1.31).[177]

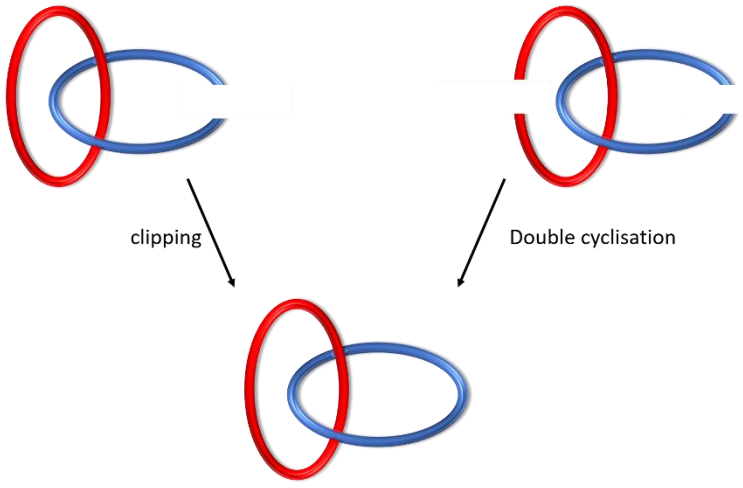


Figure 1.31: *Cartoon representation of methods to prepare a [2]catenane*

1.5.3 Template-directed synthesis of interlocked molecules

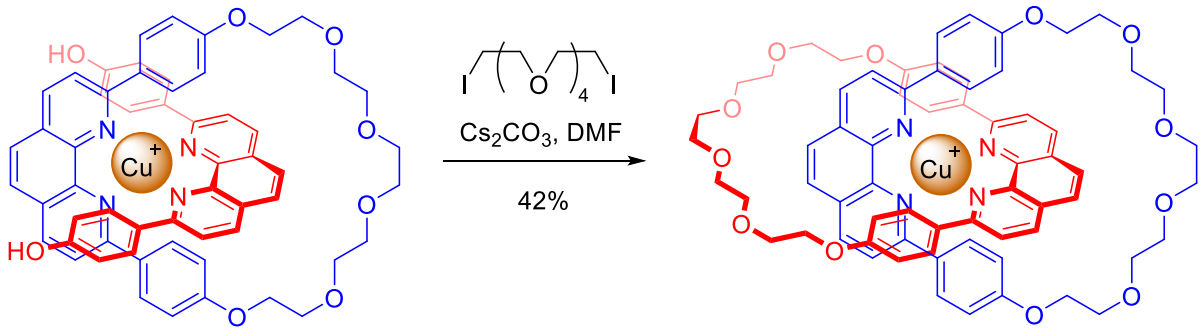
Of the utmost importance to the synthesis of interlocked structures, is the driving force used to bring together the molecular entities. Early approaches employed towards interlocked molecules relied on low yielding statistical methods;[163,178–180] for example, the first reported synthesis of a [2]catenane by Wasserman utilising statistical threading obtained a yield of less than 1%.[163] Although an impressive feat, and unprecedented at the time, the resulting poor yield inspired the development of template-directed methods. By holding the required components together in a favourable conformation through attractive interactions, a dramatic increase in yield of MIMs can be achieved. The chemical template was first defined by Busch as an entity which:

> *"organises an assembly of atoms with respect to one or more geometric loci, in order to achieve a particular linking of atoms".*[181]

Many templated strategies have been employed including the use of discrete species such as cations and anions, as well as mutual interactions between the components of the system, with examples including hydrogen bonding, π–π stacking and the hydrophobic effect.[182,183]

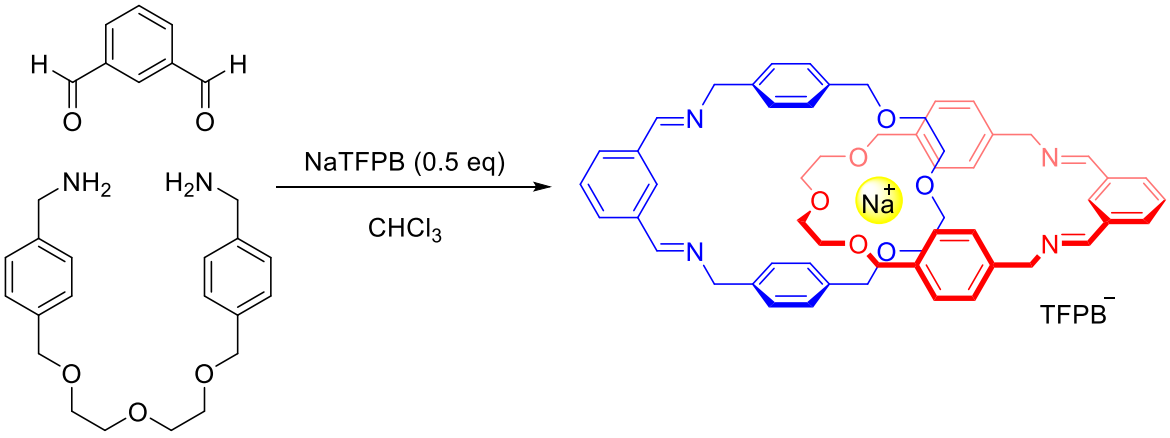
Cation templated synthesis

The seminal report by Sauvage *et al.* in 1983 of a [2]catenane synthesised *via* a Cu^{I} template was ground-breaking and paved the way for cation-templated synthesis of MIMs.[170,184,185] Exploiting the tetrahedral geometric preference of Cu^{I}, the synthesis relied on the orthogonal arrangement of two functionalised phenanthroline heterocycles, held together by a central Cu^{I} ion, which, upon a clipping reaction, produced the metallo-catenane in 42% yield (Scheme 1.1).[184] Subsequently, Cu^{I} decomplexation was achieved using KCN, to obtained the free [2]catenane.[185]



Scheme 1.1: *Sauvage's Cu^{I} passive metal templated [2]catenane*[184]

There have since been a plethora of reports of both rotaxane and catenane syntheses employing a range of transition metal template coordination geometries including octahedral (e.g. Cd^{II}, Ru^{II}, Ni^{II}, Co^{III}, Fe^{II}),[186–189] linear (e.g. Au^{I}),[190] square planar (e.g. Pd^{II})[191,192] and trigonal bipyramidal (e.g. Cu^{II}, Zn^{II}).[193] Furthermore, the versatility of this approach is reflected in the range of complicated and higher-order structures that have been achieved, such as Stoddart's Zn^{II}-templated Borromean rings,[194] Leigh's Fe^{II}-templated 'Star of David' [2]catenane, consisting of two interlocked triply-intertwined macrocycles,[195] Sauvage's Cu^{I}-templated porphyrin-containing [4]rotaxane[196] and Nitschke's Fe^{II}-templated [3]catenane.[197] As well as transition metals, MIMS can also be templated by alkali metals (e.g. Li^{+}, Na^{+}, K^{+}),[198–201] alkaline earth metals (e.g. Ca^{2+}, Ba^{2+})[202,203] and lanthanides.[204,205] Generally, these metal cations do not possess stringent stereochemical geometries and templated-assemblies instead rely on 'hard–hard' interactions, for example, with the oxygens in crown ethers. Chiu *et al.* have demonstrated the ability of Na^{+} to template the synthesis of a [2]catenane, using the interactions of the metal ion with ethylene glycol units of the two molecular components to form an orthogonal complex and cyclised *via* a Schiff base condensation reaction (Scheme 1.2).[201] Importantly, the sodium salt used contained a weakly coordinating tetrakis(3,5-trifluoromethylphenyl)borate (TFPB) counter-anion to maximise the templating effect.



Scheme 1.2: *Chiu's sodium cation templated [2]catenane*[201]

The examples of cation templated synthesis of MIMs described thus far use the metal in a purely organisational role by arranging the components favourably and do not take part in the MIM-forming reaction themselves, hence they are described as 'passive metal-template' processes. However, as well as a defined coordination geometry utilised in passive-templated routes, transition metals can be exploited further for their ability to catalyse reactions, and therefore also play an active role in the formation of the MIM. In 2006 Leigh *et al.* reported pioneering work on the synthesis of interlocked structures *via* an 'active metal-template' (AMT) strategy, employing both the catalytic and geometric properties of the metal (Figure 1.32a). In particular, they described a Cu^{I} coordinating endotopic-binding macrocycle, which allowed for favourable spatial positioning of suitable stopper appended azide and alkyne components. This allowed the Cu^{I} catalysed azide-alkyne cycloaddition (CuAAC) 'click' reaction to occur through the cavity of the macrocycle, resulting in high-yielding rotaxane formation *via* a snapping strategy (Figure 1.32b).[206] Importantly, an 'active metal-template' strategy, unlike the 'passive metal-template' approach can use substoichiometric amounts of metal cations, as permanent recognition sites are not necessary.

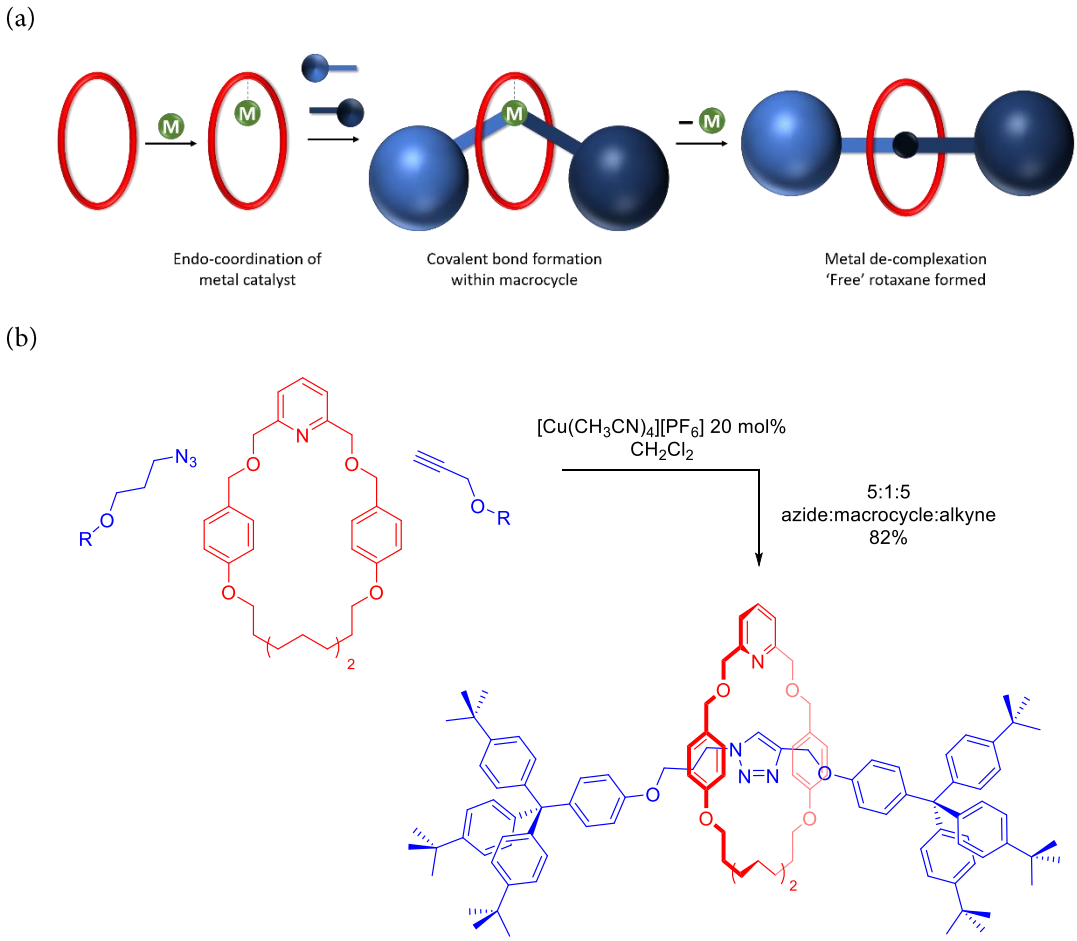
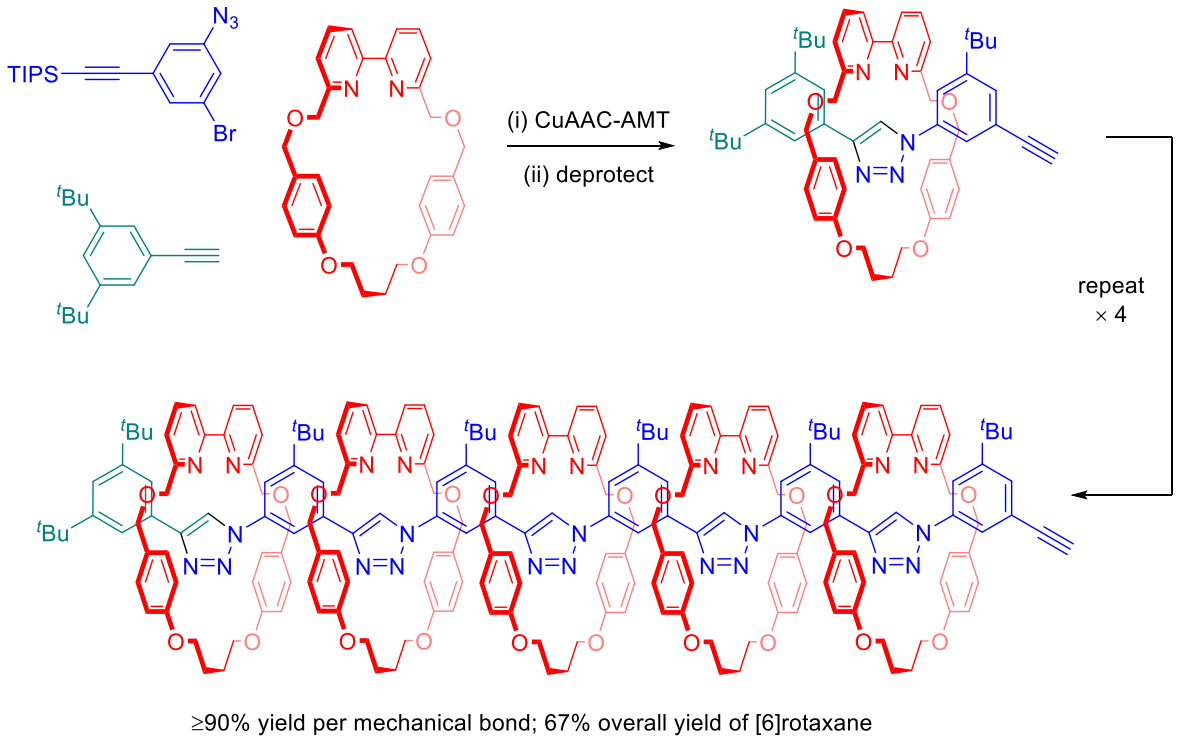


Figure 1.32: *Active metal template synthesis of MIMs: (a) schematic illustration of AMT strategy, and (b) reaction scheme for Leigh's CuAAC-AMT route to [2]rotaxane*[206]

Since this seminal report, exploitation of the CuAAC 'click' reaction for AMT synthesis of MIMs is arguably the most prevalent.[206–211] For example, Goldup *et al.* conducted a study into the efficacy of the CuAAC-AMT reaction with respect to the size of the macrocyclic cavity. Perhaps surprisingly, the smallest macrocycle investigated gave a quantitative yield using an equimolar mixture of macrocycle and half-axle precursor components.[209] Building on these results, an iterative coupling strategy for the synthesis of oligomeric [*n*]rotaxanes, whereby macrocycles are sequentially added to the growing axle was employed. Impressively, Goldup successfully demonstrated the ability to precisely control the composition of the oligo[*n*]rotaxanes by synthesising a hetero[4]rotaxane with three

different macrocycles on the axle, the order of which are reflected in the order the coupling reactions were carried out; analogously the structure of the axle can be controlled through varying the nature of the half-axle precursor components. Furthermore, Goldup *et al.* report the synthesis of a homo[6]rotaxane with a remarkable yield of ≥ 90% per mechanical bond and an overall yield of 67% (Scheme 1.3).[212] Subsequently, a range of transition metal catalysed reactions have been employed for MIM synthesis, including: Cu^{I}- and Pd^{II}-catalysed alkyne homocouplings,[213–216] Pd^{II}-mediated Michael addition,[217] Ni^{II} C(sp^3)–C(sp^3) homocoupling,[218] and Zn^{II}-catalysed Diels-Alder reaction.[219]

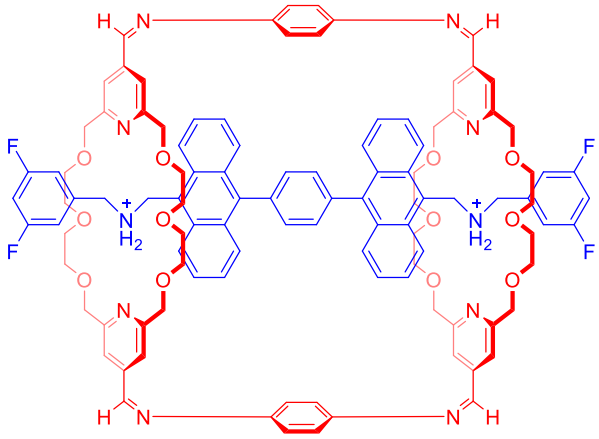


Scheme 1.3: *Goldup's iterative synthesis of homo[6]rotaxane utilising CuAAC-AMT reaction*[212]

Organic cations have also been shown to act as templates for the construction of MIMs. Protonated ammonium species have been exploited for their favourable association with polyether macrocycles to assemble [*n*]pseudorotaxanes,[220] [*n*]rotaxanes[221,222] and [*n*]catenanes.[223–225] Stoddart *et al.* employed this strategy to prepare a [20]rotaxane[226] and

a new class of interlocked molecule, a suit[2]ane (Figure 1.33a)[227,228] and Loeb *et al.* reported a 1,2-bis(4,4'-dipyridinium)ethane-derived [3]rotaxane (Figure 1.33b).[229] The ammonium motif has the advantage of possessing a protonation equilibrium, opening up the potential of pH-dependent molecular-machine-like behaviour.

(a)



(b)

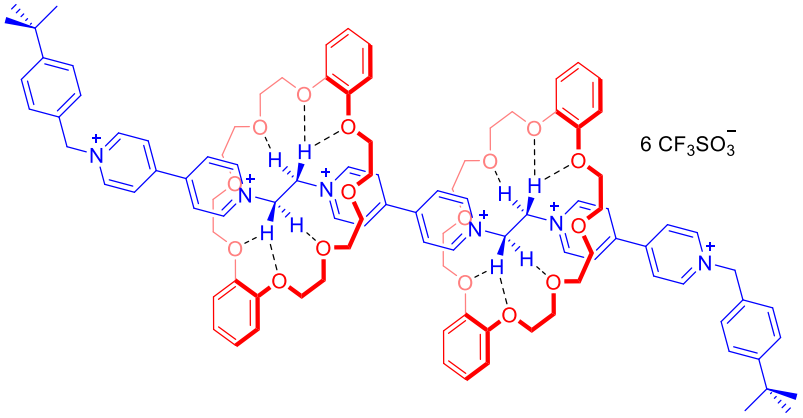


Figure 1.33: *(a) Stoddart's suit[2]ane,[228] and (b) Loeb's dipyridinium [3]rotaxane[229]*

Anion templated synthesis

Examples of anion templated synthesis of interlocked structures was slow to develop and examples are still fairly limited. This can be ascribed to the absence of predictable strongly directing coordination geometries, presenting challenges in successfully arranging the components of an interlocked structure in the desired orientation.[230] The first report came as recently as 1999 by Vögtle *et al.* who used a bulky phenoxide 'half-axle', held within the cavity of a bis-isophthalamide macrocycle *via* hydrogen bonds, before subsequently undergoing a S_N2 reaction with another alkyl bromide 'half-axle' to form the [2]rotaxane in 95% yield (Figure 1.34a).[173] A more recent example by Flood *et al.* reported the dipropargylphosphate anion templated formation of a [3]rotaxane. Exploiting the ability of his oxoanion-binding 'cyanostar' macrocycles to form 2:1 'sandwich' complexes with

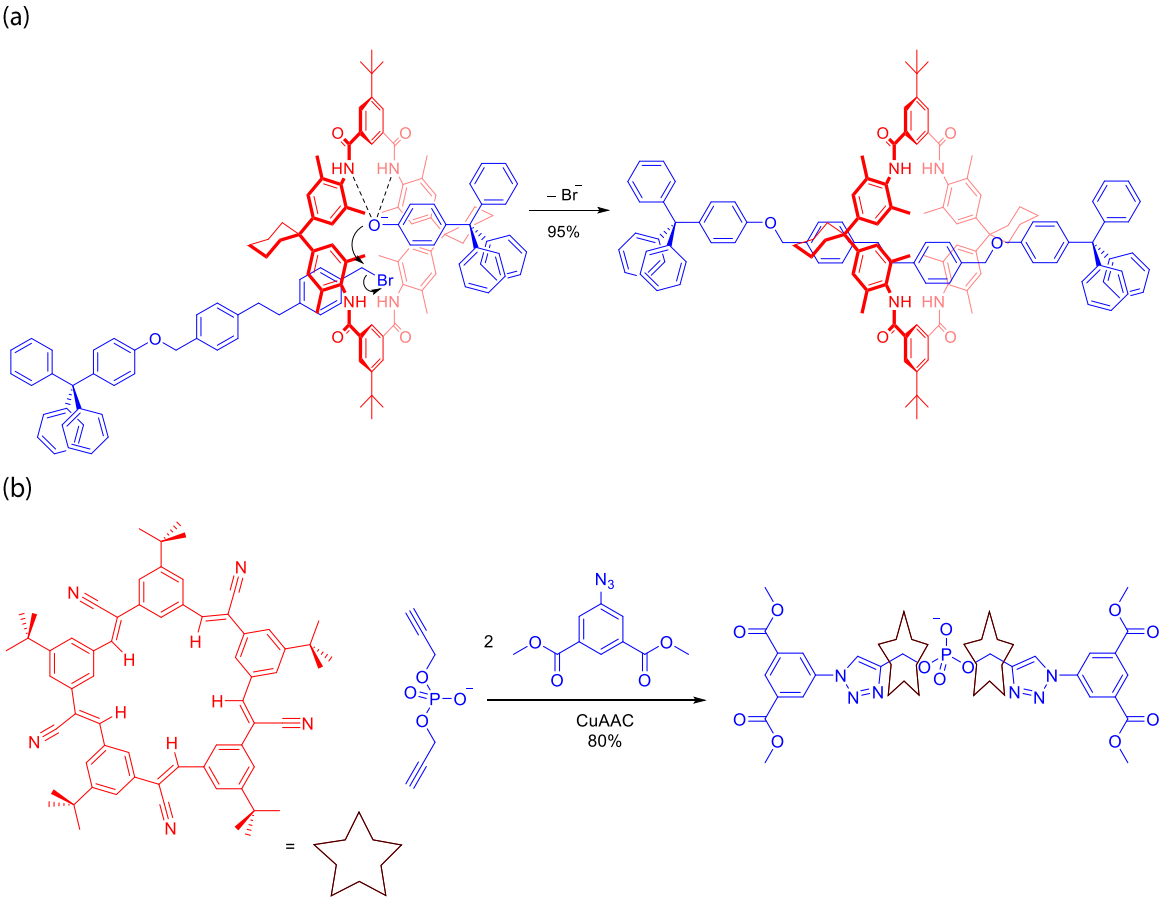


Figure 1.34: *Examples of anion-templated interlocked structures: (a) proposed reaction mechanism to form Vögtle's [2]rotaxane,[173] and (b) Flood's dialkyl-phosphate-templated [3]rotaxane[231]*

oxoanions, an interpenetrative assembly with two 'cyanostar' macrocycles and the alkyl-phosphate anion template was formed, followed by a subsequent CuAAC-stoppering reaction with a suitable azide-functionalised stopper to afford the target [3]rotaxane in yields as high as 80% (Figure 1.34b).[231,232]

Beer *et al.* have pioneered the use of a *discrete* anion template to assemble interpenetrated and interlocked architectures. In a seminal report from 2001 they describe the formation of a pseudorotaxane through the "sharing" of a templating halide anion between two components; in particular, that chloride can template the formation of an orthogonal complex between a 3,5-bis-amide pyridinium compound and a neutral isophthalamide derivative (Figure 1.35a).[233] Additionally, the assembly is stabilised through donor–acceptor aromatic stacking interactions between the two electron-rich hydroquinone groups of the macrocycle and the electron-deficient pyridinium motif and *N*-methyl-pyridinium···polyether hydrogen bonding. Inspired by the success of this approach, Beer *et al.* utilised the strategy to construct interlocked structures, by first forming the pseudorotaxane assembly, followed by either clipping or stoppering reactions to product the target MIM. Utilising ring-closing metathesis (RCM) methodology, a bis-vinyl appended macrocycle precursor was cyclised around a terphenyl-stoppered pyridinium chloride axle component to afford a [2]rotaxane (Figure 1.35b).[234] Importantly, once the MIM has been formed, post-synthetic removal of the templating halide anion produced a unique interlocked three-dimensional cavity capable of binding anions.

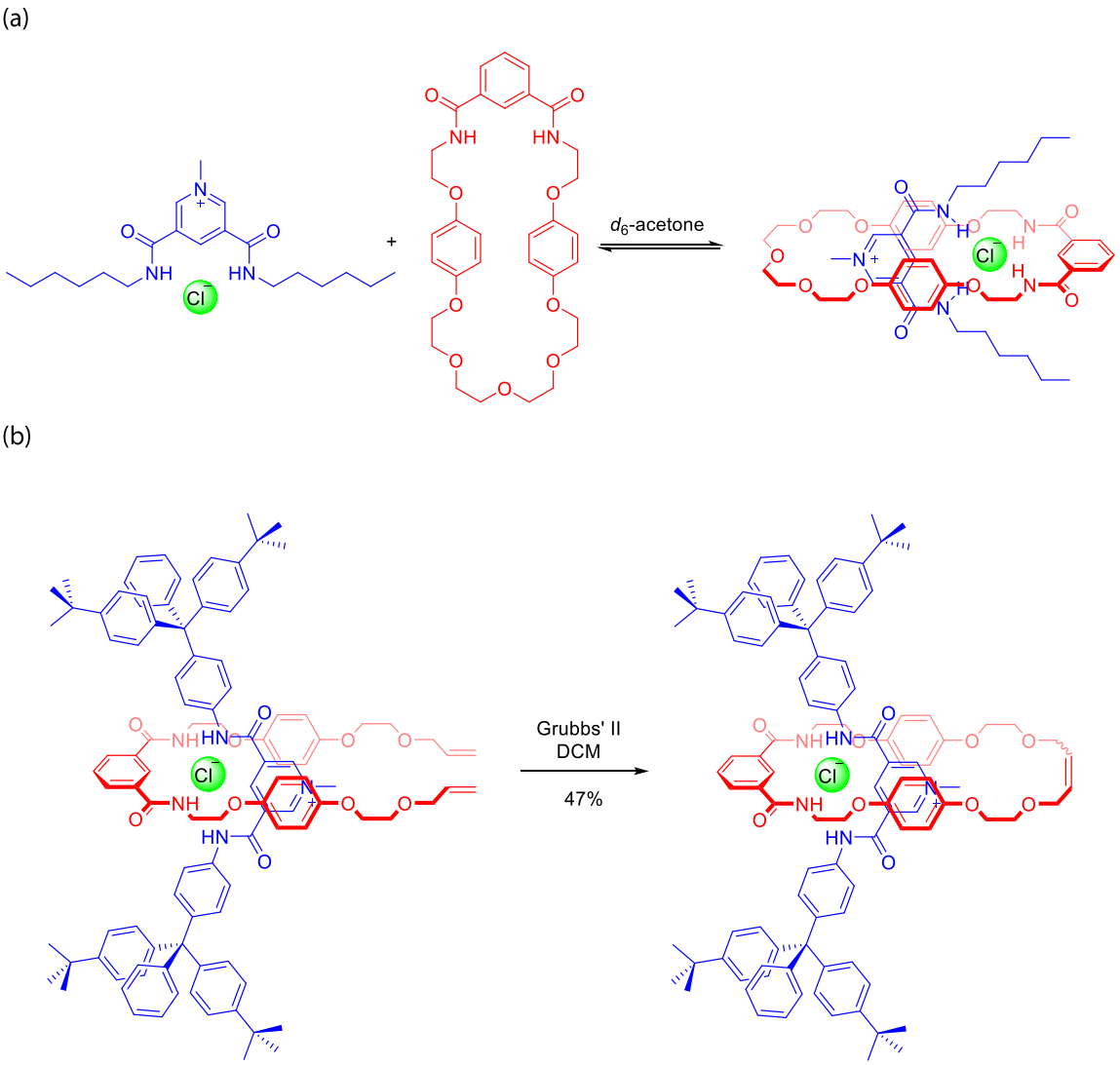


Figure 1.35: (a) *Beer's chloride-templated psuedorotaxane assembly,*[233] *and (b) Beer's seminal chloride-templated [2]rotaxane via ring closing metathesis*[234]

Further reports have shown the breadth of applications of the isophthalamide motif for chloride templated MIMs including [2]-[235,236] and [3] rotaxanes,[237,238] [2]catenanes,[239,240] a 'Janus' rotaxane[241] and a handcuff catenane.[242] A variety of anion coordinating groups have also been reported such as prototriazolium,[243] imidazolium[244] and indolocarbazole.[245] For example, Jeong *et al.* published an indolocarbazole-based homo[2]catenane prepared *via* a chloride template (Figure 1.36)[246] and anions such as bromide,[247] nitrate[248] and nitrite[249] have also been used.

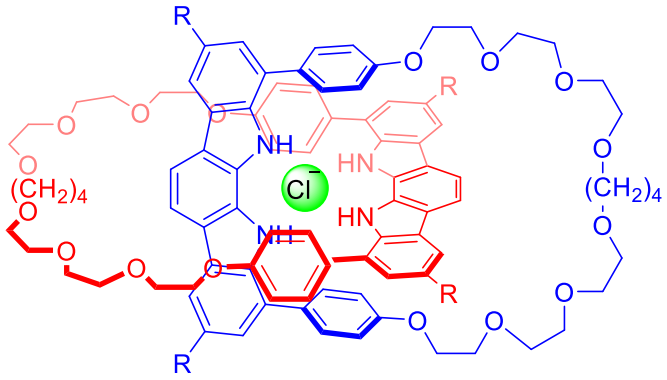


Figure 1.36: *Jeong's chloride-templated indolocarbazole [2]catenane*[246]

More recently XB has been utilised as a templating interaction. Exploiting the linearity of XB to enhance the strength of association, Beer *et al.* in a seminal report in 2010 demonstrated the bromide-templated formation of a [2]rotaxane containing a 5-iodotriazolium axle component (Figure 1.37).[250] Further examples from Beer *et al.* include a bis-bromoimidazolium [2]catenane[251] and an all-XB [2]rotaxane.[252]

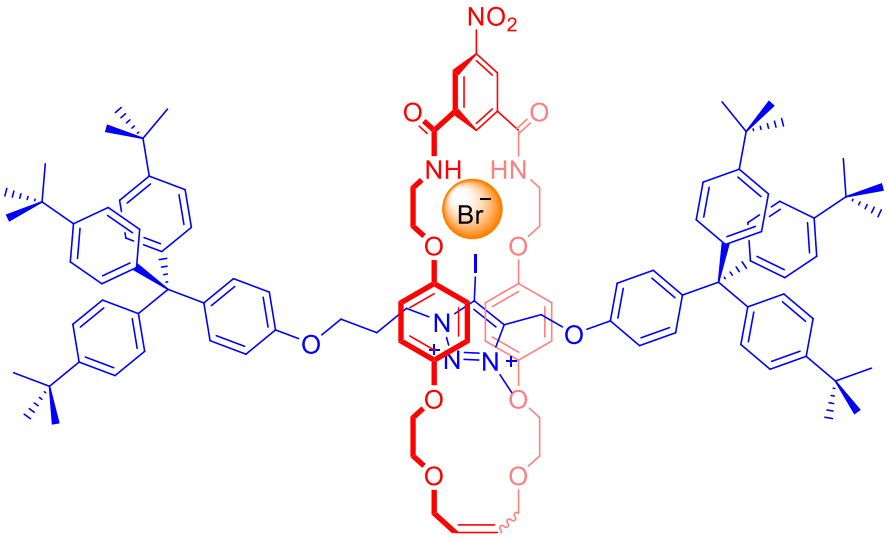


Figure 1.37: *Beer's halogen bond bromide-templated [2]rotaxane*[250]

1.5.4 Applications of interlocked molecules

The strategies outlined in Section 1.5.3 have provided viable high yielding synthetic routes towards MIMs. This in turn has led to a plethora of applications in a wide range of fields, exploiting the unique properties the mechanical bond imparts (Section 1.5.1). This section will briefly outline a few recent developments, in this rapidly expanding area.

Recognition of charged species

The unique three-dimensional preorganised cavity present between the components of MIMs allows for effective and selective encapsulation of guests, in particular charged species, when compared to acyclic systems.[253] For example, Hiratani *et al.* demonstrated the binding of Cs^+ between two macrocycle components of a [3]rotaxane to form a 'sandwich' complex in CH_2Cl_2/CH_3CN (Figure 1.38).[254] The cation-induced conformational change resulted in enhancement of the anthracene emission.

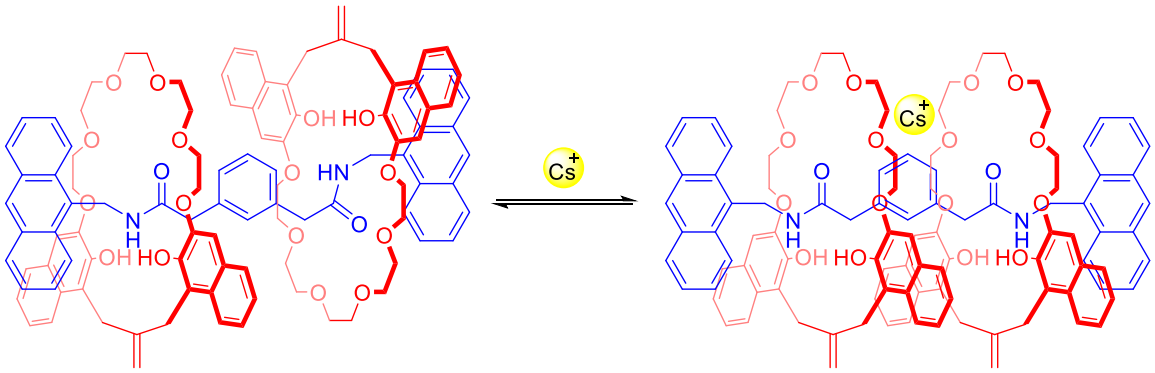


Figure 1.38: *Hiratani's Cs^+ binding [3]rotaxane*[254]

When using the discrete anion template strategy for MIM synthesis, the removal of the templating anion reveals a cavity capable of selective anion association. For example, Beer *et al.* have reported a chloride-templated [2]rotaxane (Figure 1.35b) capable of selectively binding chloride (K_a = 1130 M^{-1}) over the more basic dihydrogen phosphate (K_a = 300 M^{-1}) and acetate (K_a = 100 M^{-1}) in 1:1 $CDCl_3/CD_3OD$, through convergent hydrogen bond donors.[234] The selectivity can be attributed to the complementary size and shape of the host interlocked cavity for the halide anion, compared to the larger oxoanions.

Incorporation of XB donors has led to advancements in the strength and selectivity of anion association, culminating in the preparation by Beer *et al.* of a permethylated β-cyclodextrin-stoppered XB water-soluble [2]rotaxane (Figure 1.39), which demonstrated impressively strong and selective iodide binding (K_a = 2200 M^{-1}) in D_2O, far superior to the HB analogue (K_a = 20 M^{-1}).[255] Additionally, a dramatic two orders of magnitude enhancement was observed over the related acyclic structure.

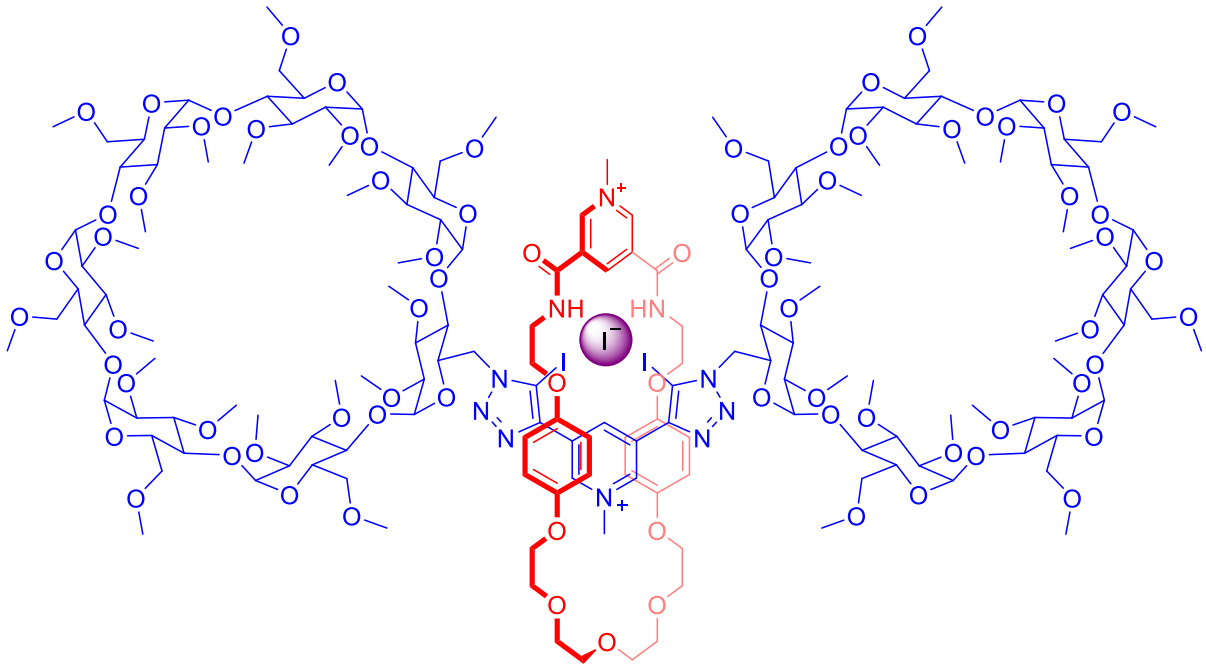


Figure 1.39: *Beer's water-soluble XB iodide selective [2]rotaxane*[255]

Nanotechnology

The dynamic nature of the components in a mechanical bond has been exploited for the design of molecular machines; a stimuli-responsive conformational change can result in a task being performed on the nanoscale.[165] In [2]catenanes, rotational movement is observed, whereas for [2]rotaxanes both rotational movement and shuttling are present. Seminal work from Stoddart *et al.* in 1991 reporting the first molecular shuttle demonstrated the large-amplitude translational motion of a macrocycle between two identical stations (binding sites) on the axle, and paved the way for rapid growth of

machine-like systems in the following years. Building on this, through incorporation of two different stations Stoddart *et al.* demonstrated the ability to control the motion between the two stations using an external stimulus, such as a change in pH or *via* electrochemical oxidation.[257] Since these seminal publications, systems of increasing complexity have been reported, such as: molecular muscles,[258,259] molecular elevators,[260,261] macroscopic transport of a liquid droplet against gravity by a light-driven molecular machine,[262] and a sequence-specific oligopeptide synthesising [2]rotaxane (Figure 1.40).[167] Furthermore, in 2018 Loeb *et al.* reported a new dynamic process, demonstrating for the first time ring-through-ring shuttling in a saturated [3]rotaxane, by utilising two different sized macrocycles to allow them to slip through each other (Figure 1.41).[256] This opens up possible applications for molecular-level weaving and the writing and rewriting of encoded information by an external stimuli.[263]

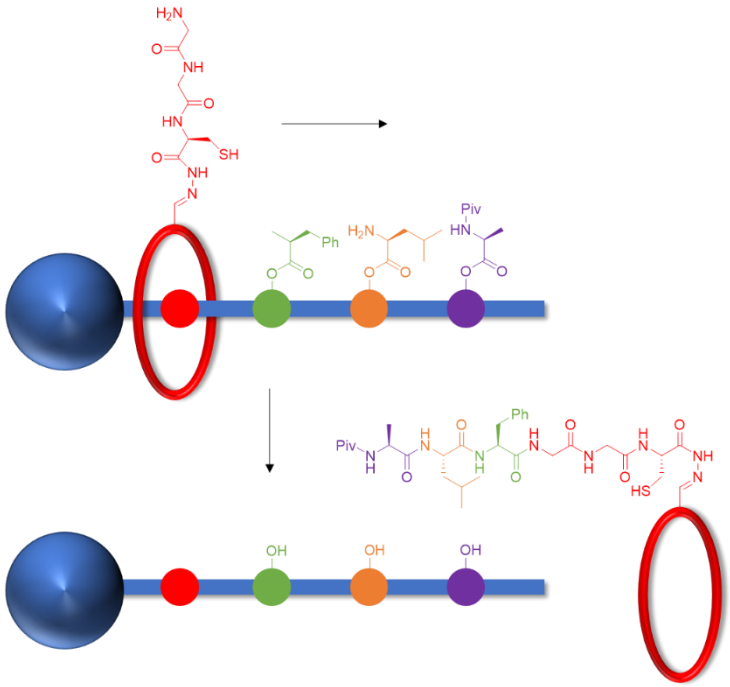


Figure 1.40: *Leigh's peptide-synthesising [2]rotaxane*[167]

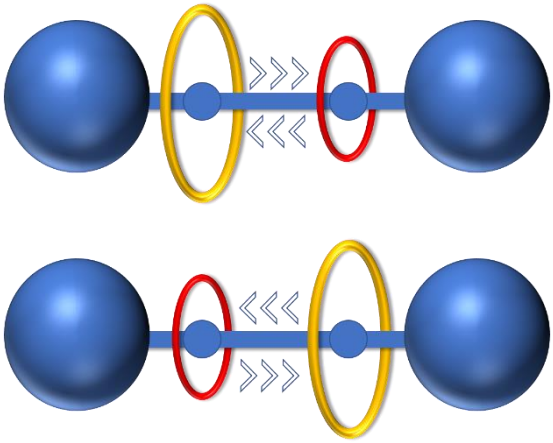
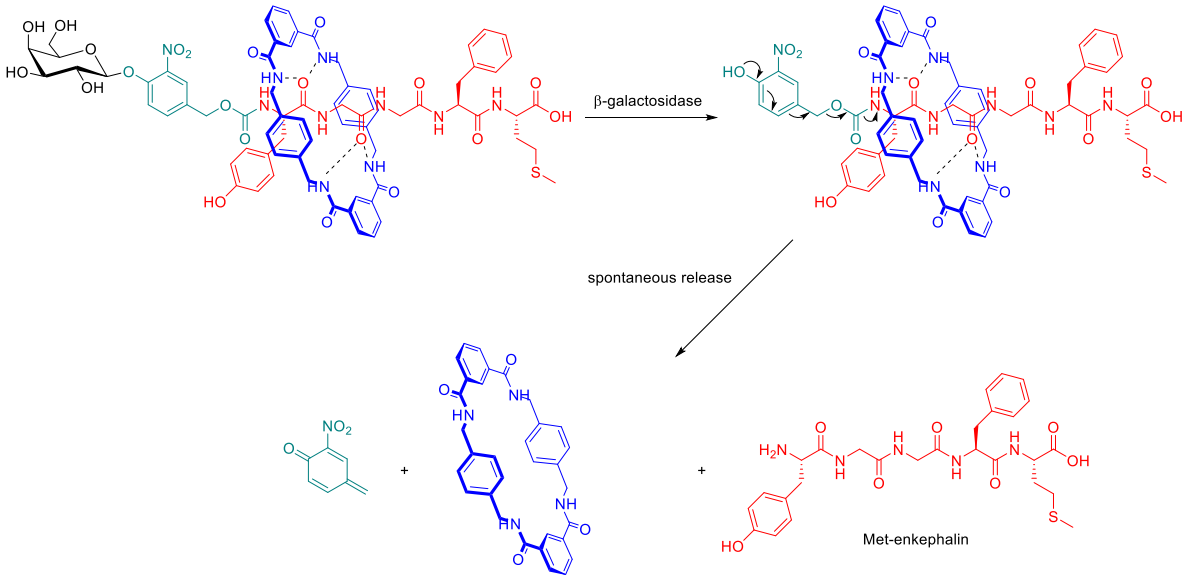


Figure 1.41: *Loeb's ring-through-ring shuttling in a saturated [3]rotaxane*[256]

Nanomedicine

The application of MIMs in medicinal chemistry utilises the enhanced stability of the mechanically-bonded components compared to the free molecules and the three-dimensional cavity to encapsulate substrates for delivery of prodrugs or drugs, which are usually unstable *in vivo*. For example, the groups of Leigh and Papot prepared a [2]rotaxane containing the bioactive peptide Met-encephalin,[264] which demonstrated the ability of the macrocycle component of the interlocked structure to protect the oligopeptide from degradation by peptidases and enzymes present in human plasma. Release of the peptide is achieved by β-galactosidase enzyme-mediated hydrolysis to cleave the carbohydrate unit and thus allow for dethreading (Scheme 1.4). More recently, Leigh and Papot have reported the incorporation of the anticancer prodrug paclitaxel into the axle of a rotaxane, where it is protected from esterase-mediated hydrolysis, with release of the prodrug triggered by a β-galactosidase-responsive self-opening macrocycle.[166]



Scheme 1.4: *Enzyme-triggered release of Met-enkephalin by Leigh's [2]rotaxane*[264]

Catalysis

MIMs have also been exploited in catalysis by incorporating catalytically active metals or organocatalytic functionality into the structure. For example, Leigh *et al.* reported a switchable [2]rotaxane asymmetric catalyst for Michael addition, by shuttling of the macrocycle to reveal or conceal the catalytic site in response to changes in pH.[265] Furthermore, Goldup *et al.* have recently produced the first example of a rotaxane-based metal complex with stimuli responsive catalytic activity;[266] a conformational change upon Cu(I)-cofactor binding results in the switching on of the Au catalyst resulting in excellent activity and selectivity in the Ohe-Uemura cyclopropanation reaction (Figure 1.42).

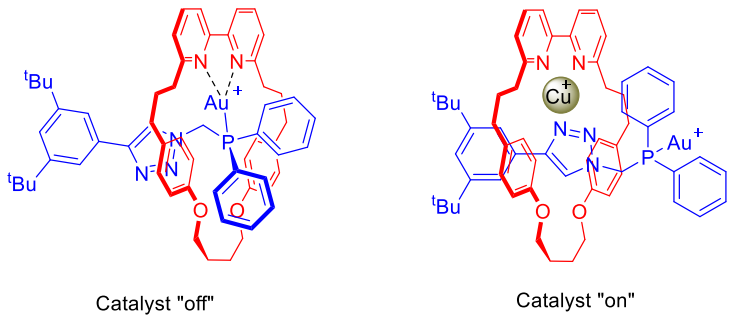


Figure 1.42: *Goldup's Cu(I)-switchable Au(I)-[2]rotaxane catalyst*[266]

1.6 Project Aims

The use of halogen bonding interactions for solution phase anion recognition is still in its infancy. This thesis aims to further explore these interactions through the preparation of acyclic, macrocyclic, interlocked and complex supramolecular architectures for the recognition of anions in competitive organic and aqueous solvent media. In particular, the potency of the halogen bonding 5-iodo-1,2,3-triazole motif compared to the hydrogen bonding prototriazole analogue for anion binding strength and selectivity is investigated *via* its incorporation into various novel motifs.

Chapter Two concerns the synthesis of acyclic, macrocyclic and interlocked receptors containing novel unsymmetric imidazolium–triazole and –iodotriazole motifs. Comparison of anion selectivity trends between acyclic and interlocked systems as well as between halogen and hydrogen bonding systems will be discussed.

Chapter Three focuses on the incorporation of symmetric halogen bonding bis(iodotriazole)–imidazolium and corresponding hydrogen bonding motifs into interlocked structures and their anion binding properties determined. Attempts to construct analogous benzimidazolium containing receptor systems and a hetero[3]rotaxane are also outlined.

Chapter Four discusses the use of multicomponent reactions for the unprecedented synthesis of halogen bonding cryptands. The Ugi-four-component reaction (Ugi-4CR) is employed for the synthesis of halogen bonding macrocycles and cryptands utilising the iodotriazole motif. Preliminary investigations into the anion binding properties are undertaken using fluorescence spectroscopy.

1.7 References

1 C. J. Pedersen, *Angew. Chem. Int. Ed. English*, 1988, **27**, 1021–1027.

2 J.-M. Lehn, *Angew. Chem. Int. Ed. English*, 1988, **27**, 89–112.

3 D. J. Cram, *Angew. Chem. Int. Ed. English*, 1988, **27**, 1009–1020.

4 C. H. Park and H. E. Simmons, *J. Am. Chem. Soc.*, 1968, **90**, 2431–2432.

5 J. W. Steed and J. L. Atwood, *Supramolecular chemistry*, Wiley, 2009.

6 D. Dalkara, G. Zuber and J.-P. Behr, *Mol. Ther.*, 2004, **9**, 964–969.

7 P. Chakrabarti, *J. Mol. Biol.*, 1993, **234**, 463–482.

8 J. L. Sessler, P. Gale, W.-S. Cho, J. L. Sessler, P. Gale and W.-S. Cho, *Anion Receptor Chemistry*, Royal Society of Chemistry, Cambridge, 2006.

9 O. Devuyst, P. T. Christie, P. J. Courtoy, R. Beauwens and R. V. Thakker, *Hum. Mol. Genet.*, 1999, **8**, 247–257.

10 J. Rommens, M. Iannuzzi, B. Kerem, M. Drumm, G. Melmer, M. Dean, R. Rozmahel, J. Cole, D. Kennedy and N. Hidaka, *Science*, 1989, **245**, 1059–1065.

11 M. I. González, *Neurosci. Lett.*, 2016, **628**, 213–8.

12 F. Delange, *Thyroid*, 1994, **4**, 107–128.

13 P. F. Lito, J. P. S. Aniceto and C. M. Silva, *Water, Air, Soil Pollut.*, 2012, **223**, 6133–6155.

14 B. Moss, *Philos. Trans. R. Soc. Lond. B. Biol. Sci.*, 2008, **363**, 659–66.

15 J. B. de Heredia, J. R. Domínguez, Y. Cano and I. Jiménez, *Appl. Surf. Sci.*, 2006, **252**, 6031–6035.

16 Ö. Neşe and K. T. Ennil, *Desalination*, 2008, **223**, 174–179.

17 M. Chanda and G. L. Rempel, *React. Polym.*, 1995, **24**, 203–212.

18 P. K. Dutta, K. Rabaey, Z. Yuan, R. A. Rozendal and J. Keller, *Water Res.*, 2010, **44**, 2563–2571.

19 R. R. Dash, A. Gaur and C. Balomajumder, *J. Hazard. Mater.*, 2009, **163**, 1–11.

20 K. Yoshihara, *Technetium in the Environment*, Springer, Berlin, Heidelberg, 1996, pp. 17–35.

21 R. D. Shannon, *Acta Crystallogr. Sect. A*, 1976, **32**, 751–767.

22 C. Caltagirone, G. W. Bates, P. A. Gale and M. E. Light, *Chem. Commun.*, 2008, **0**, 61–63.

23 J. W. Steed, D. R. Turner and K. J. Wallace, *Core concepts in supramolecular chemistry and nanochemistry*, John Wiley, 2007.

24 M. Kigga and D. R. Trivedi, *J. Fluor. Chem.*, 2014, **160**, 1–7.

25 M. A. Kaloo and J. Sankar, *Analyst*, 2013, **138**, 4760.

26 S. Goldman and R. G. Bates, *J. Am. Chem. Soc.*, 1972, **94**, 1476–1484.

27 F. Hofmeister, *Arch. für Exp. Pathol. und Pharmakologie*, 1888, **24**, 247–260.

28 H. Xu, N. Sträter, W. Schröder, C. Böttcher, K. Ludwig and W. Saenger, *Acta Crystallogr. D. Biol. Crystallogr.*, 2003, **59**, 815–22.

29 K. H. G. Verschueren, S. M. Franken, H. J. Rozeboom, K. H. Kalk and B. W. Dijkstra, *J. Mol. Biol.*, 1993, **232**, 856–872.

30 K. H. G. Verschueren, F. Seljée, H. J. Rozeboom, K. H. Kalk and B. W. Dijkstra, *Nature*, 1993, **363**, 693–698.

31 R. Dutzler, E. B. Campbell, M. Cadene, B. T. Chait and R. MacKinnon, *Nature*, 2002, **415**, 287–294.

32 J. W. Pflugrath and F. A. Quiocho, *Nature*, 1985, **314**, 257–260.

33 J. W. Pflugrath and F. A. Quiocho, *J. Mol. Biol.*, 1988, **200**, 163–180.

34 H. Luecke and F. A. Quiocho, *Nature*, 1990, **347**, 402–406.

35 E. Fischer, *Berichte der Dtsch. Chem. Gesellschaft*, 1894, **27**, 2985–2993.

36 D. E. Koshland, *Angew. Chem. Int. Ed. English*, 1995, **33**, 2375–2378.

37 D. E. Koshland and Jr., *Proc. Natl. Acad. Sci. U. S. A.*, 1958, **44**, 98–104.

38 M. W. Hosseini and J. M. Lehn, *J. Am. Chem. Soc.*, 1982, **104**, 3525–3527.

39 D. J. Cram, *Angew. Chem. Int. Ed. English*, 1988, **27**, 1009–1020.

40 P. V. Santacroce, J. T. Davis, M. E. Light, P. A. Gale, J. C. Iglesias-Sánchez, P. Prados and R. Quesada, *J. Am. Chem. Soc.*, 2007, **129**, 1886-1887.

41 D. K. Cabbiness and D. W. Margerum, *J. Am. Chem. Soc.*, 1969, **91**, 6540–6541.

42 A. E. Martell, R. D. Hancock and R. J. Motekaitis, *Coord. Chem. Rev.*, 1994, **133**, 39–65.

43 K. Choi and A. D. Hamilton, *J. Am. Chem. Soc.*, 2003, **125**, 10241–10249.

44 H.-J. Schneider, *Angew. Chem. Int. Ed.*, 2009, **48**, 3924–3977.

45 J. D. Watson and F. H. C. Crick, *Nature*, 1953, **171**, 737–738.

46 G. A. Jeffrey, *An introduction to hydrogen bonding*, Oxford University Press, 1997.

47 L. M. Salonen, M. Ellermann and F. Diederich, *Angew. Chem. Int. Ed.*, 2011, **50**, 4808–4842.

48 F. Inokuchi, Y. Miyahara, T. Inazu and S. Shinkai, *Angew. Chem. Int. Ed. English*, 1995, **34**, 1364–1366.

49 L. M. Salonen, C. Bucher, D. W. Banner, W. Haap, J.-L. Mary, J. Benz, O. Kuster, P. Seiler, W. B. Schweizer and F. Diederich, *Angew. Chem. Int. Ed.*, 2009, **48**, 811–814.

50 J. C. Ma and and D. A. Dougherty, *Chem. Rev.*,1997, **97**, 1303-1324

51 M. Mascal, A. Armstrong and M. D. Bartberger, *J. Am. Chem. Soc.*, 2002, **124**, 6274-6276.

52 D. Quiñonero, C. Garau, C. Rotger, A. Frontera, P. Ballester, A. Costa and P. M. Deyà, *Angew.*

Chem. Int. Ed., 2002, **41**, 3389–3392.

53 T. J. Mooibroek, C. A. Black, P. Gamez and J. Reedijk, *Cryst. Growth Des.*, 2008, **8**, 1082–1093.

54 G. Gil-Ramírez, E. C. Escudero-Adán, J. Benet-Buchholz and P. Ballester, *Angew. Chem. Int. Ed.*, 2008, **47**, 4114–4118.

55 S. Guha and S. Saha, *J. Am. Chem. Soc.*, 2010, **132**, 17674–17677.

56 J. Mareda and S. Matile, *Chem. Eur. J.*, 2009, **15**, 28–37.

57 M. J. Kelly, A. E. J. Broomsgrove, I. R. Morgan, I. Siewert, P. Fitzpatrick, J. Smart, D. Vidovic and S. Aldridge, *Organometallics*, 2013, **32**, 2674–2684.

58 H. Zhao, L. A. Leamer and F. P. Gabbaï, *Dalt. Trans.*, 2013, **42**, 8164.

59 J. S. Jones and F. P. Gabbaï, *Acc. Chem. Res.*, 2016, **49**, 857–867.

60 M. Newcomb and M. T. Blanda, *Tetrahedron Lett.*, 1988, **29**, 4261–4264.

61 M. Newcomb, J. H. Horner and M. T. Blanda, *J. Am. Chem. Soc.*, 1987, **109**, 7878–7879.

62 K. Tamao, T. Hayashi, Y. Ito and M. Shiro, *J. Am. Chem. Soc.*, 1990, **112**, 2422–2424.

63 K. Tamao, T. Hayashi and Y. Ito, *J. Organomet. Chem.*, 1996, **506**, 85–91.

64 H. T. Ngo, X. Liu and K. A. Jolliffe, *Chem. Soc. Rev.*, 2012, **41**, 4928.

65 T. Zhang, N. Y. Edwards, M. Bonizzoni and E. V. Anslyn, *J. Am. Chem. Soc.*, 2009, **131**, 11976–11984.

66 M. S. Cubberley and and B. L. Iverson, *J. Am. Chem. Soc.,* 2001, **123**, 7560-7563.

67 W. Blokzijl and J. B. F. N. Engberts, *Angew. Chem. Int. Ed. English*, 1993, **32**, 1545–1579.

68 F. Biedermann, W. M. Nau and H.-J. Schneider, *Angew. Chem. Int. Ed.*, 2014, **53**, 11158–11171.

69 M. J. Langton, C. J. Serpell and P. D. Beer, *Angew. Chem. Int. Ed.*, 2016, **55**, 1974–1987.

70 J. M. Sturtevant, J. Mecinović, D. T. Moustakas, S. W. Thomas, M. Harder, E. T. Mack, M. R. Lockett, A. Héroux, W. Sherman and G. M. Whitesides, *Proc. Natl. Acad. Sci.*, 1977, **74**, 2236–2240.

71 B. Dietrich, J. Guilhem, J.-M. Lehn, C. Pascard and E. Sonveaux, *Helv. Chim. Acta*, 1984, **67**, 91–104.

72 J. M. Lehn, E. Sonveaux and A. K. Willard, *J. Am. Chem. Soc.*, 1978, **100**, 4914–4916.

73 S. D. Reilly, G. R. K. Khalsa, D. K. Ford, J. R. Brainard, B. P. Hay and P. H. Smith, *Inorg. Chem.*, 1995, **34**, 569–575.

74 B. Dietrich, B. Dilworth, J.-M. Lehn, J.-P. Souchez, M. Cesario, J. Guilhem and C. Pascard, *Helv. Chim. Acta*, 1996, **79**, 569–587.

75 B. Dietrich, J.-M. Lehn, J. Guilhem and C. Pascard, *Tetrahedron Lett.*, 1989, **30**, 4125–4128.

76 C. Bazzicalupi, A. Bencini, C. Giorgi, B. Valtancoli, V. Lippolis and A. Perra, *Inorg. Chem.*, 2011, **50**, 7202–7216.

77 T. H. Wirth and N. Davidson, *J. Am. Chem. Soc.*, 1964, **86**, 4325–4329.

78 E. A. Kataev, C. Müller, G. V. Kolesnikov and V. N. Khrustalev, *Eur. J. Org. Chem.*, 2014, 2747–2753.

79 F. P. Schmidtchen and G. Müller, *J. Chem. Soc., Chem. Commun.*, 1984, **0**, 1115–1116.

80 F. P. Schmidtchen, *Chem. Ber.*, 1981, **114**, 597–607.

81 F. P. Schmidtchen, *Angew. Chemie Int. Ed. English*, 1977, **16**, 720–721.

82 K. Worm and F. P. Schmidtchen, *Angew. Chem. Int. Ed. English*, 1995, **34**, 65–66.

83 H. Ihm, S. Yun, H. G. Kim, J. K. Kim and K. S. Kim, *Org. Lett.*, 2002, **4**, 2897-2900.

84 K. Sato, S. Arai and T. Yamagishi, *Tetrahedron Lett.*, 1999, **40**, 5219–5222.

85 E. Alcalde, N. Mesquida, L. Pérez-García, C. Alvarez-Rúa, S. García-Granda and E. García-Rodriguez, *Chem. Commun.*, 1999, **0**, 295–296.

86 C. E. Willans, K. M. Anderson, L. C. Potts and J. W. Steed, *Org. Biomol. Chem.*, 2009, **7**, 2756–2760.

87 A. Kumar and and P. S. Pandey, *Org. Lett.*, 2008, **10**, 165-168.

88 B. Schulze, C. Friebe, M. D. Hager, W. Günther, U. Köhn, B. O. Jahn, H. Görls and U. S. Schubert, *Org. Lett.*, 2010, **12**, 2710–2713.

89 J. Cai, B. P. Hay, N. J. Young, X. Yang and J. L. Sessler, *Chem. Sci.*, 2013, **4**, 1560–1567.

90 C. R. Bondy and S. J. Loeb, *Coord. Chem. Rev.*, 2003, **240**, 77–99.

91 A.-F. Li, J.-H. Wang, F. Wang and Y.-B. Jiang, *Chem. Soc. Rev.*, 2010, **39**, 3729–3745.

92 V. Amendola, L. Fabbrizzi and L. Mosca, *Chem. Soc. Rev.*, 2010, **39**, 3889–2915.

93 J. L. Sessler, S. Camiolo and P. A. Gale, *Coord. Chem. Rev.*, 2003, **240**, 17–55.

94 Y. Hua and A. H. Flood, *Chem. Soc. Rev.*, 2010, **39**, 1262–1271.

95 H. Juwarker, J. M. Lenhardt, D. M. Pham and S. L. Craig, *Angew. Chem. Int. Ed.*, 2008, **47**, 3740–3743.

96 Y. Li and A. H. Flood, *Angew. Chem. Int. Ed.*, 2008, **47**, 2649–2652.

97 R. A. Pascal, J. Spergel and D. Van Engen, *Tetrahedron Lett.*, 1986, **27**, 4099–4102.

98 K. Kavallieratos, S. R. de Gala, D. J. Austin and R. H. Crabtree, *J. Am. Chem. Soc.*, 1997, **119**, 2325–2326.

99 M. J. Chmielewski and J. Jurczak, *Chem. Eur. J.*, 2006, **12**, 7652–7667.

100 M. J. Chmielewski and J. Jurczak, *Chem. Eur. J.*, 2005, **11**, 6080–6094.

101 S. O. Kang, V. W. Day and K. Bowman-James, *Org. Lett.*, 2009, **11**, 3654–3657.

102 S. O. Kang, D. VanderVelde, D. Powell and K. Bowman-James, *J. Am. Chem. Soc.*, 2004, **126**, 12272–12273.

103 S. O. Kang, J. M. Llinares, D. Powell, D. VanderVelde and K. Bowman-James, *J. Am. Chem. Soc.*, 2003, **125**, 10152–10153.

104 S. Kubik and R. Goddard, *Proc. Natl. Acad. Sci.*, 2002, **99**, 5127–5132.

105 S. Kubik, R. Kirchner, D. Nolting and J. Seidel, *J. Am. Chem. Soc.*, 2002, **124**, 12752–12760.

106 F. Sommer and S. Kubik, *Org. Biomol. Chem.*, 2014, **12**, 8851–8860.

107 D. Meshcheryakov, F. Arnaud-Neu, V. Böhmer, M. Bolte, J. Cavaleri, V. Hubscher-Bruder, I. Thondorf and S. Werner, *Org. Biomol. Chem.*, 2008, **6**, 3244.

108 D. E. Gómez, L. Fabbrizzi, M. Licchelli and E. Monzani, *Org. Biomol. Chem.*, 2005, **3**, 1495–1500.

109 E. M. Boyle, S. Comby, J. K. Molloy and T. Gunnlaugsson, *J. Org. Chem.*, 2013, **78**, 8312–8319.

110 P. A. Gale, J. L. Sessler,V. Král and V. Lynch, *J. Am. Chem. Soc.*, 1996, **118**, 5140–5141.

111 D.-W. Yoon, H. Hwang and C.-H. Lee, *Angew. Chem. Int. Ed.*, 2002, **41**, 1757–1759.

112 D.-W. Yoon, D. E. Gross, V. M. Lynch, J. L. Sessler, B. P. Hay and C.-H. Lee, *Angew. Chem. Int. Ed.*, 2008, **47**, 5038–5042.

113 V. Haridas, S. Sahu, P. P. Praveen Kumar and A. R. Sapala, *RSC Adv.*, 2012, **2**, 12594.

114 Y. Hua and A. H. Flood, *Chem. Soc. Rev.*, 2010, **39**, 1262–1271.

115 B. Schulze and U. S. Schubert, *Chem. Soc. Rev.*, 2014, **43**, 2522–71.

116 Y. Li and A. H. Flood, *Angew. Chem. Int. Ed.*, 2008, **47**, 2649–2652.

117 F. Guthrie, *J. Chem. Soc.*, 1863, **16**, 239–244.

118 O. Hassel, J. Hvoslef, E. H. Vihovde and N. A. Sörensen, *Acta Chem. Scand.*, 1954, **8**, 873–873.

119 J.-M. Dumas, M. Gomel and M. Guerin, in *Halides, Pseudo-Halides and Azides: Part 2 (1983)*, John Wiley & Sons, Ltd., Chichester, UK, pp. 985–1020.

120 G. R. Desiraju, P. S. Ho, L. Kloo, A. C. Legon, R. Marquardt, P. Metrangolo, P. Politzer, G. Resnati and K. Rissanen, *Pure Appl. Chem.*, 2013, **85**, 1711–1713.

121 B. K. Saha, A. Nangia and M. Jaskólski, *CrystEngComm*, 2005, **7**, 355–358.

122 P. Politzer, P. Lane, M. C. Concha, Y. Ma and J. S. Murray, *J. Mol. Model.*, 2007, **13**, 305–311.

123 T. Clark, M. Hennemann, J. S. Murray and P. Politzer, *J. Mol. Model.*, 2007, **13**, 291–296.

124 O. Hassel, *Science*, 1970, **170**, 497–502.

125 B. K. Saha, A. Nangia and M. Jaskólski, *CrystEngComm*, 2005, **7**, 355–358.

126 M. T. Messina, P. Metrangolo, W. Panzeri, E. Ragg and G. Resnati, *Tetrahedron Lett.*, 1998, **39**, 9069–9072.

127 K. Eskandari and M. Lesani, *Chem. Eur. J.*, 2015, **21**, 4739–4746.

128 P. Metrangolo, F. Meyer, T. Pilati, G. Resnati and G. Terraneo, *Angew. Chem. Int. Ed.*, 2008, **47**,

6114–6127.

129 S. V Rosokha and M. K. Vinakos, *Cryst. Growth Des.*, 2012, **12**, 4149–4156.

130 S. M. Huber, E. Jimenez-Izal, J. M. Ugalde and I. Infante, *Chem. Commun.*, 2012, **48**, 7708–7710.

131 G. Cavallo, P. Metrangolo, R. Milani, T. Pilati, A. Priimagi, G. Resnati and G. Terraneo, *Chem. Rev.*, 2016, **116**, 2478–2601.

132 L. P. Wolters, P. Schyman, M. J. Pavan, W. L. Jorgensen, F. M. Bickelhaupt and S. Kozuch, *Wiley Interdiscip. Rev. Comput. Mol. Sci.*, 2014, **4**, 523–540.

133 P. Metrangolo, Hannes Neukirch, Tullio Pilati and Giuseppe Resnati, *Acc. Chem. Res.*, 2005, **38**, 386–395.

134 G. Berger, J. Soubhye and F. Meyer, *Polym. Chem.*, 2015, **6**, 3559–3580.

135 A. Priimagi, G. Cavallo, P. Metrangolo and G. Resnati, *Acc. Chem. Res.*, 2013, **46**, 2686–2695.

136 J.-P. Gliese, S. H. Jungbauer and S. M. Huber, *Chem. Commun.*, 2017, **53**, 12052–12055.

137 S. Jungbauer, S. Schindler, F. Kniep, S. Walter, L. Rout and S. Huber, *Synlett*, 2013, **24**, 2624–2628.

138 F. Kniep, S. H. Jungbauer, Q. Zhang, S. M. Walter, S. Schindler, I. Schnapperelle, E. Herdtweck and S. M. Huber, *Angew. Chem. Int. Ed.*, 2013, **52**, 7028–7032.

139 T. M. Beale, M. G. Chudzinski, M. G. Sarwar and M. S. Taylor, *Chem. Soc. Rev.*, 2013, **42**, 1667–1680.

140 N. Houbenov, R. Milani, M. Poutanen, J. Haataja, V. Dichiarante, J. Sainio, J. Ruokolainen, G. Resnati, P. Metrangolo and O. Ikkala, *Nat. Commun.*, 2014, **5**, 4043.

141 A. Priimagi, G. Cavallo, A. Forni, M. Gorynsztejn-Leben, M. Kaivola, P. Metrangolo, R. Milani, A. Shishido, T. Pilati, G. Resnati and G. Terraneo, *Adv. Funct. Mater.*, 2012, **22**, 2572–2579.

142 A. Bertolani, L. Pirrie, L. Stefan, N. Houbenov, J. S. Haataja, L. Catalano, G. Terraneo, G. Giancane, L. Valli, R. Milani, O. Ikkala, G. Resnati and P. Metrangolo, *Nat. Commun.*, 2015, **6**, 7574.

143 L. Meazza, J. A. Foster, K. Fucke, P. Metrangolo, G. Resnati and J. W. Steed, *Nat. Chem.*, 2013, **5**, 42–47.

144 R. Wilcken, M. O. Zimmermann, A. Lange, A. C. Joerger and F. M. Boeckler, *J. Med. Chem.*, 2013, **56**, 1363–1388.

145 A. Mele, P. Metrangolo, H. Neukirch, T. Pilati and G. Resnati, *J. Am. Chem. Soc.*, 2005, **127**, 14972–14973.

146 M. G. Sarwar, B. Dragisic, S. Sagoo and M. S. Taylor, *Angew. Chem. Int. Ed.*, 2010, **49**, 1674–1677.

147 W. S. Brotherton, R. J. Clark and L. Zhu, *J. Org. Chem.*, 2012, **77**, 6443–6455.

148 J. E. Hein, J. C. Tripp, L. B. Krasnova, K. B. Sharpless and V. V. Fokin, *Angew. Chem. Int. Ed.*, 2009, **48**, 8018–8021.

149 R. Tepper, B. Schulze, H. Görls, P. Bellstedt, M. Jäger and U. S. Schubert, *Org. Lett.*, 2015, **17**, 5740–5743.

150 A. Borissov, J. Y. C. Lim, A. Brown, K. E. Christensen, A. L. Thompson, M. D. Smith and P. D. Beer, *Chem. Commun.*, 2017, **53**, 2483–2486.

151 J. Y. C. Lim and P. D. Beer, *Chem. Commun.*, 2015, **51**, 3686–3688.

152 B. Nepal and S. Scheiner, *J. Phys. Chem. A*, 2015, **119**, 13064–13073.

153 R. Tepper, B. Schulze, M. Jäger, C. Friebe, D. H. Scharf, H. Görls and U. S. Schubert, *J. Org. Chem.*, 2015, **80**, 3139–3150.

154 B. Nepal and S. Scheiner, *Chem. Eur. J.*, 2015, **21**, 13330–13335.

155 V. Amendola, G. Bergamaschi, M. Boiocchi, R. Alberto and H. Braband, *Chem. Sci.*, 2014, **5**, 1820–1826.

156 R. Alberto, G. Bergamaschi, H. Braband, T. Fox and V. Amendola, *Angew. Chem. Int. Ed.*, 2012, **51**, 9772–9776.

157 E. A. Katayev, G. V. Kolesnikov and J. L. Sessler, *Chem. Soc. Rev.*, 2009, **38**, 1572–1586.

158 F. Zapata, A. Caballero, P. Molina, I. Alkorta and J. Elguero, *J. Org. Chem.*, 2014, **79**, 6959–6969.

159 M. Cametti, K. Raatikainen, P. Metrangolo, T. Pilati, G. Terraneo and G. Resnati, *Org. Biomol. Chem*, 2012, **10**, 1329–1333.

160 A. Caballero, N. G. White and P. D. Beer, *Angew. Chem. Int. Ed.*, 2011, **50**, 1845–1848.

161 S. Chakraborty, R. Dutta and P. Ghosh, *Chem. Commun.*, 2015, **51**, 14793–14796.

162 Y. Takeda, D. Hisakuni, C.-H. Lin and S. Minakata, *Org. Lett.*, 2015, **17**, 318–321.

163 E. Wasserman, *J. Am. Chem. Soc.*, 1960, **82**, 4433–4434.

164 I. T. Harrison and S. Harrison, *J. Am. Chem. Soc.*, 1967, **89**, 5723–5724.

165 E. R. Kay and D. A. Leigh, *Angew. Chem. Int. Ed.*, 2015, **54**, 10080–10088.

166 R. Barat, T. Legigan, I. Tranoy-Opalinski, B. Renoux, E. Péraudeau, J. Clarhaut, P. Poinot, A. E. Fernandes, V. Aucagne, D. A. Leigh and S. Papot, *Chem. Sci.*, 2015, **6**, 2608–2613.

167 B. Lewandowski, G. De Bo, J. W. Ward, M. Papmeyer, S. Kuschel, M. J. Aldegunde, P. M. E. Gramlich, D. Heckmann, S. M. Goldup, D. M. D'Souza, A. E. Fernandes and D. A. Leigh, *Science*, 2013, **339**, 189–193.

168 N. H. Evans and P. D. Beer, *Angew. Chem. Int. Ed.*, 2014, **53**, 11716–11754.

169 H. Lahlali, K. Jobe, M. Watkinson and S. M. Goldup, *Angew. Chem. Int. Ed.*, 2011, **50**, 4151–4155.

170 J. F. Stoddart, *Chem. Soc. Rev.*, 2009, **38**, 1802–1820.

171 P. R. Ashton, M. Bělohradský, D. Philp and J. F. Stoddart, *J. Chem. Soc., Chem. Commun.*, 1993, **0**, 1269–1274.

172 V.Aucagne, J Berná, J. D. Crowley, S. M. Goldup, K. D. Hänni, D. A. Leigh, P. J. Lusby, V. E. Ronaldson, A. M. Z. Slawin, A. Viterisi and D. B. Walker, *J. Am. Chem. Soc.*, 2007, **129**, 11950–11963.

173 G. M. Hübner, J. Gläser, C. Seel and F. Vögtle, *Angew. Chem. Int. Ed.*, 1999, **38**, 383–386.

174 C.-W. Chiu, C.-C. Lai and Sheng-Hsien Chiu, *J. Am. Chem. Soc.*, 2007, **129**, 3500–3501.

175 I. Yoon, M. Narita, T. Shimizu and M. Asakawa, *J. Am. Chem. Soc.*, 2004, **126**, 16740–16741.

176 P. L. Anelli, P. R. Ashton, R. Ballardini, V. Balzani, M. Delgado, M. T. Gandolfi, T. T. Goodnow, A. E. Kaifer and D. Philp, *J. Am. Chem. Soc.*, 1992, **114**, 193–218.

177 C. O. Dietrich-Buchecker and J. P. Sauvage, *Chem. Rev.*, 1987, **87**, 795–810.

178 G. Agam and A. Zilkha, *J. Am. Chem. Soc.*, 1976, **98**, 5214–5216.

179 G. Agam, D. Graiver and A. Zilkha, *J. Am. Chem. Soc.*, 1976, **98**, 5206–5214.

180 I. T. Harrison and S. Harrison, *J. Am. Chem. Soc.*, 1967, **89**, 5723–5724.

181 D. H. Busch, *J. Incl. Phenom. Mol. Recognit. Chem.*, 1992, **12**, 389–395.

182 G. Gil-Ramírez, D. A. Leigh and A. J. Stephens, *Angew. Chem. Int. Ed.*, 2015, **54**, 6110–6150.

183 M. Xue, Y. Yang, X. Chi, X. Yan and F. Huang, *Chem. Rev.*, 2015, **115**, 7398–7501.

184 C. . Dietrich-Buchecker, J. . Sauvage and J. . Kintzinger, *Tetrahedron Lett.*, 1983, **24**, 5095–5098.

185 C. O. Dietrich-Buchecker, J. P. Sauvage and J. M. Kern, *J. Am. Chem. Soc.*, 1984, **106**, 3043–3045.

186 D. Pomeranc, D. Jouvenot, J.-C. Chambron, J.-P. Collin, V. Heitz and J.-P. Sauvage, *Chem. Eur. J.*, 2003, **9**, 4247–4254.

187 A. I. Prikhod'ko and J.-P. Sauvage, *J. Am. Chem. Soc.*, 2009, **131**, 6794–6807.

188 L. Hogg, D. A. Leigh, P. J. Lusby, A. Morelli, S. Parsons and J. K. Y. Wong, *Angew. Chem. Int. Ed.*, 2004, **43**, 1218–1221.

189 D. A. Leigh, P. J. Lusby, R. T. McBurney, A. Morelli, A. M. Z. Slawin, A. R. Thomson and D. B. Walker, *J. Am. Chem. Soc.*, 2009, **131**, 3762–3771.

190 S. M. Goldup, D. A. Leigh, P. J. Lusby, R. T. McBurney and A. M. Z. Slawin, *Angew. Chem. Int. Ed.*, 2008, **47**, 6999–7003.

191 A.-M. Fuller, D. A. Leigh, P. J. Lusby, I. D. H. Oswald, S. Parsons and D. B. Walker, *Angew. Chem. Int. Ed.*, 2004, **43**, 3914–3918.

192 J. D. Crowley, D. A. Leigh, P. J. Lusby, R. T. McBurney, L.-E Perret-Aebi, C. Petzold, A. M. Z. Slawin and M. D. Symes, *J. Am. Chem. Soc.*, 2007, **129**, 15085–15090.

193 C. Hamann, J.-M. Kern and J.-P. Sauvage, *Inorg. Chem.*, 2003, **42**, 1877–1883.

194 K. S. Chichak, S. J. Cantrill, A. R. Pease, S.-H. Chiu, G. W. V Cave, J. L. Atwood and J. F. Stoddart, *Science*, 2004, **304**, 1308–1312.

195 D. A. Leigh, R. G. Pritchard and A. J. Stephens, *Nat. Chem.*, 2014, **6**, 978–982.

196 J.-P. Collin, F. Durola, J. Frey, V. Heitz, F. Reviriego, J.-P. Sauvage, Y. Trolez and K. Rissanen, *J. Am. Chem. Soc.*, 2010, **132**, 6840–6850.

197 C. S. Wood, T. K. Ronson, A. M. Belenguer, J. J. Holstein and J. R. Nitschke, *Nat. Chem.*, 2015, **7**, 354–358.

198 T. Han and C.-F. Chen, *J. Org. Chem.*, 2008, **73**, 7735–7742.

199 G. Kaiser, T. Jarrosson, S. Otto, Y.-F. Ng, A. D. Bond and J. K. M. Sanders, *Angew. Chem. Int. Ed.*, 2004, **43**, 1959–1962.

200 T.-H. Ho, C.-C. Lai, Y.-H. Liu, S.-M. Peng and S.-H. Chiu, *Chem. Eur. J.*, 2014, **20**, 4563–4567.

201 S.-T. Tung, C.-C. Lai, Y.-H. Liu, S.-M. Peng and S.-H. Chiu, *Angew. Chem. Int. Ed.*, 2013, **52**, 13269–13272.

202 L. M. Hancock and P. D. Beer, *Chem. Commun.*, 2011, **47**, 6012.

203 R. Mitra, M. Thiele, F. Octa-Smolin, M. C. Letzel and J. Niemeyer, *Chem. Commun.*, 2016, **52**, 5977–5980.

204 C. Lincheneau, B. Jean-Denis and T. Gunnlaugsson, *Chem. Commun.*, 2014, **50**, 2857.

205 F. Zapata, O. A. Blackburn, M. J. Langton, S. Faulkner and P. D. Beer, *Chem. Commun.*, 2013, **49**, 8157.

206 V. Aucagne, K. D. Hänni, D. A. Leigh, Paul J. Lusby and D. B. Walker, *J. Am. Chem. Soc.*, 2006, **128**, 2186–2187.

207 A. Brown, T. Lang, K. M. Mullen and P. D. Beer, *Org. Biomol. Chem.*, 2017, **15**, 4587–4594.

208 J. Winn, A. Pinczewska and S. M. Goldup, *J. Am. Chem. Soc.*, 2013, **135**, 13318–13321.

209 H. Lahlali, K. Jobe, M. Watkinson and S. M. Goldup, *Angew. Chem. Int. Ed.*, 2011, **50**, 4151–4155.

210 S. M. Goldup, D. A. Leigh, P. R. McGonigal, V. E. Ronaldson and A. M. Z. Slawin, *J. Am. Chem. Soc.*, 2010, **132**, 315–320.

211 V Aucagne, J. Berná, James D. Crowley, Stephen M. Goldup, Kevin D. Hänni, D. A. Leigh, P. J. Lusby, V. E. Ronaldson, A. M. Z. Slawin, A Viterisi and D. B. Walker, *J. Am. Chem. Soc.*, 2007, **129**, 11950–11963.

212 J. E. M. Lewis, J. Winn, L. Cera and S. M. Goldup, *J. Am. Chem. Soc.*, 2016, **138**, 16329–16336.

213 Y. Sato, R. Yamasaki and S. Saito, *Angew. Chem. Int. Ed.*, 2009, **48**, 504–507.

214 S. M. Goldup, D. A. Leigh, P. R. McGonigal, V. E. Ronaldson and A. M. Z. Slawin, *J. Am. Chem. Soc.*, 2010, **132**, 315–320.

215 J. Berná, S. M. Goldup, A.-L. Lee, D. A. Leigh, M. D. Symes, G. Teobaldi and F. Zerbetto, *Angew. Chem. Int. Ed.*, 2008, **47**, 4392–4396.

216 J. Berná, J. D. Crowley, S. M. Goldup, K. D. Hänni, A.-L. Lee and D. A. Leigh, *Angew. Chem. Int. Ed.*, 2007, **46**, 5709–5713.

217 S. M. Goldup, D. A. Leigh, P. J. Lusby, R. T. McBurney and A. M. Z. Slawin, *Angew. Chem. Int. Ed.*, 2008, **47**, 3381–3384.

218 S. M. Goldup, D. A. Leigh, R. T. McBurney, P. R. McGonigal and A. Plant, *Chem. Sci.*, 2010, **1**, 383–

386.

219 J. D. Crowley, K. D. Hänni, D. A. Leigh and A. M. Z. Slawin, *J. Am. Chem. Soc.*, 2010, **132**, 5309–5314.

220 W. Jiang, D. Sattler, K. Rissanen and C. A. Schalley, *Org. Lett.*, 2011, **13**, 4502–4505.

221 M.-V. Martínez-Díaz, N. Spencer and J. F. Stoddart, *Angew. Chem. Int. Ed. English*, 1997, **36**, 1904–1907.

222 S.-Y. Hsueh, K.-W. Cheng, C.-C. Lai and S.-H. Chiu, *Angew. Chem. Int. Ed.*, 2008, **47**, 4436–4439.

223 M. C. T. Fyfe and and J. F. Stoddart, *Acc. Chem. Res.,* 1997, **30**, 393–341.

224 P. R. Ashton, P. J. Campbell, P. T. Glink, D. Philp, N. Spencer, J. F. Stoddart, E. J. T. Chrystal, S. Menzer, D. J. Williams and P. A. Tasker, *Angew. Chem Int. Ed. English*, 1995, **34**, 1865–1869.

225 Erin N. Guidry, S. J. Cantrill, J. F. Stoddart and R. H. Grubbs, *Org. Lett.,* 2005, **7**, 2129–2132.

226 M. E. Belowich, C. Valente, R. A. Smaldone, D. C. Friedman, J. Thiel, L. Cronin and J. F. Stoddart, *J. Am. Chem. Soc.*, 2012, **134**, 5243–5261.

227 B. H. Northrop, F. Aricó, N. Tangchiavang, J. D. Badjić and J. F. Stoddart, *Org. Lett.,* 2006, **8**, 3899–3902.

228 A. R. Williams, B. H. Northrop, T. Chang, J. F. Stoddart, A. J. P. White and D. J. Williams, *Angew. Chem. Int. Ed.*, 2006, **45**, 6665–6669.

229 D. J. Mercer, S. J. Vella, L. Guertin, N. D. Suhan, J. Tiburcio, V. N. Vukotic, J. A. Wisner and S. J. Loeb, *Eur. J. Org. Chem.*, 2011, **2011**, 1763–1770.

230 G. Gil-Ramírez, D. A. Leigh and A. J. Stephens, *Angew. Chem. Int. Ed.*, 2015, **54**, 6110–6150.

231 B. Qiao, Y. Liu, S. Lee, M. Pink and A. H. Flood, *Chem. Commun.*, 2016, **52**, 13675–13678.

232 S. Lee, C.-H. Chen and A. H. Flood, *Nat. Chem.*, 2013, **5**, 704–710.

233 J. A. Wisner, P. D. Beer and M. G. B. Drew, *Angew. Chem. Int. Ed.*, 2001, **40**, 3606.

234 J. A. Wisner, P. D. Beer, M. G. B. Drew and M. R. Sambrook, *J. Am. Chem. Soc.*, 2002, **124**, 12469–12476.

235 N. H. Evans, C. J. Serpell, N. G. White and P. D. Beer, *Chem. Eur. J.*, 2011, **17**, 12347–12354.

236 J. M. Mercurio, F. Tyrrell, J. Cookson and P. D. Beer, *Chem. Commun.*, 2013, **49**, 10793.

237 M. J. Langton and P. D. Beer, *Chem. Eur. J.*, 2012, **18**, 14406–14412.

238 N. H. Evans, C. J. Serpell and P. D. Beer, *Chem. Commun.*, 2011, **47**, 8775.

239 M. R. Sambrook, P. D. Beer, J. A. Wisner, R. L. Paul and A. R. Cowley, *J. Am. Chem. Soc.*, 2004, **126**, 15364–15365.

240 N. H. Evans, H. Rahman, A. V. Leontiev, N. D. Greenham, G. A. Orlowski, Q. Zeng, R. M. J. Jacobs, C. J. Serpell, N. L. Kilah, J. J. Davis and P. D. Beer, *Chem. Sci.*, 2012, **3**, 1080–1089.

241 N. H. Evans and P. D. Beer, *Chem. Eur. J.*, 2011, **17**, 10542–10546.

242 N. H. Evans, C. J. Serpell and P. D. Beer, *Angew. Chem. Int. Ed.*, 2011, **50**, 2507–2510.

243 N. G. White, H. G. Lovett and P. D. Beer, *RSC Adv.*, 2014, **4**, 12133–12147.

244 G. T. Spence, N. G. White and P. D. Beer, *Org. Biomol. Chem.*, 2012, **10**, 7282–7291.

245 A. Brown, K. M. Mullen, J. Ryu, M. J. Chmielewski, S. M. Santos, V. Felix, A. L. Thompson, J. E. Warren, S. I. Pascu and P. D. Beer, *J. Am. Chem. Soc.*, 2009, **131**, 4937–4952.

246 M. K. Chae, J. Suk and K.-S. Jeong, *Tetrahedron Lett.*, 2010, **51**, 4240–4242.

247 K. M. Mullen, J. Mercurio, C. J. Serpell and P. D. Beer, *Angew. Chem. Int. Ed.*, 2009, **48**, 4781–4784.

248 M. J. Langton and P. D. Beer, *Chem. Commun.*, 2014, **50**, 8124–8127.

249 M. J. Langton, O. A. Blackburn, T. Lang, S. Faulkner and P. D. Beer, *Angew. Chem. Int. Ed.*, 2014, **53**, 11463–11466.

250 N. L. Kilah, M. D. Wise, C. J. Serpell, A. L. Thompson, N. G. White, K. E. Christensen and P. D. Beer, *J. Am. Chem. Soc.*, 2010, **132**, 11893–11895.

251 A. Caballero, F. Zapata, N. G. White, P. J. Costa, V. Félix and P. D. Beer, *Angew. Chem. Int. Ed.*, 2012, **51**, 1876–1880.

252 B. R. Mullaney, A. L. Thompson and P. D. Beer, *Angew. Chem. Int. Ed.*, 2014, **53**, 11458–11462.

253 A. Caballero, F. Zapata and P. D. Beer, *Coord. Chem. Rev.*, 2013, **257**, 2434–2455.

254 Y. Nagawa, J. Suga, K. Hiratani, E. Koyama and M. Kanesato, *Chem. Commun.*, 2005, **0**, 749–751.

255 M. J. Langton, S. W. Robinson, I. Marques, V. Félix and P. D. Beer, *Nat. Chem.*, 2014, **6**, 1039–1043.

256 K. Zhu, G. Baggi and S. J. Loeb, *Nat. Chem.*, 2018, **10**, 625–630.

257 R. A. Bissell, E. Córdova, A. E. Kaifer and J. F. Stoddart, *Nature*, 1994, **369**, 133–137.

258 C. J. Bruns and J. F. Stoddart, *Acc. Chem. Res.*, 2014, **47**, 2186–2199.

259 F. Niess, V. Duplan, C. S. Diercks and J.-P. Sauvage, *Chem. Eur. J.*, 2015, **21**, 14393–14400.

260 J. D. Badjic, V. Balzani, A. Credi, S. Silvi and J. F. Stoddart, *Science*, 2004, **303**, 1845–1849.

261 J. D. Badjic, C. M. Ronconi, J. F. Stoddart, V. Balzani, S. Silvi and Alberto Credi, *J. Am. Chem. Soc.*, 2006, **128**, 1489–1499.

262 J. Berná, D. A. Leigh, M. Lubomska, S. M. Mendoza, E. M. Pérez, P. Rudolf, G. Teobaldi and F. Zerbetto, *Nat. Mater.*, 2005, **4**, 704–710.

263 S. Goldup, *Nature*, 2018, **557**, 39–40.

264 A. Fernandes, A. Viterisi, F. Coutrot, S. Potok, D. A. Leigh, V. Aucagne and S. Papot, *Angew. Chem. Int. Ed.*, 2009, **48**, 6443–6447.

265 V. Blanco, D. A. Leigh, V. Marcos, J. A. Morales-Serna and A. L. Nussbaumer, *J. Am. Chem. Soc.*, 2014, **136**, 4905–4908.

266 M. Galli, J. E. M. Lewis and S. M. Goldup, *Angew. Chem. Int. Ed.*, 2015, **54**, 13545–13549.

Chapter Two

Imidazole–triazole and –iodotriazole based systems for anion recognition

2.1 Introduction

The imidazolium motif has been exploited extensively in many diverse areas of chemistry. For example, an enormous variety of 1,3-dialkylimidazolium salts have received much attention as ionic liquids due to the ability to control their physical and chemical properties.[1–3] In particular, their low vapour pressure and capacity to be recycled and customised has led to a rapid increase in use as 'green' solvents.[4–6] Furthermore, they have found applications as liquid crystal materials,[7] and as highly effective surfactant-like stabilisers for metal nanoparticles.[8,9] In organometallic chemistry imidazolium salts are utilised as precursors to *N*-heterocyclic carbenes (NHCs).[10]

Of most importance to this chapter, imidazolium derivatives are effective charge-assisted C–H hydrogen bond (HB) donors, and their capability to act as potent anion receptors is well documented (Section 1.3.1). To maximise the strength of interaction with anions, receptors are often designed to incorporate several imidazolium groups acting in a convergent manner in a preorganised macrocyclic scaffold, exemplified by a report by Kim *et al.* of a tetrakis-imidazolium system displaying a strong preference for fluoride (K_a = 28,900 M^{-1} in DMSO) (Figure 2.1).[11]

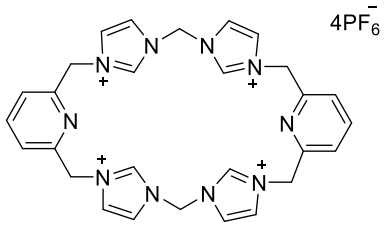


Figure 2.1: *Kim's tetra-imidazolium macrocycle*[11]

Beer *et al.* reported the incorporation of an imidazolium motif into the axle component of a [2]rotaxane (Figure 2.2).[12] Synthesised *via* a chloride-templated ring-closing metathesis (RCM) 'clipping' reaction, the rotaxane exhibited a preference for halides over oxoanions, determined *via* ^{1}H NMR spectroscopy titration studies in 1:1 $CDCl_3/CD_3OD$. The reversal

in selectivity compared to the acyclic analogue was attributed to oxoanions being too large to penetrate the rotaxane binding pocket.

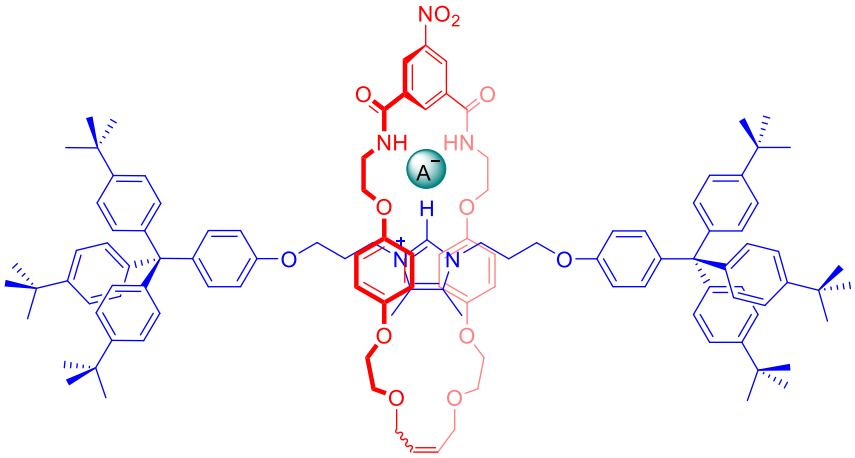


Figure 2.2: *Beer's 4,5-dimethylimidazolium rotaxane*[12]

With the aim of achieving selectivity between halides, the imidazolium motif has also been utilised for halogen bonding (XB), with the first XB catenane reported by Beer *et al.* incorporating the 2-bromoimidazolium moiety (Figure 2.3).[13] Owing to the naphthalene reporter group, the anion recognition properties of the XB catenane were determined by fluorescence spectroscopy, and displayed a strong preference for chloride and bromide, with no response observed for iodide and various oxoanions in acetonitrile solution. This demonstrated the potential for XB imidazolium motifs to facilitate selectivity in a preorganised 3D cavity.

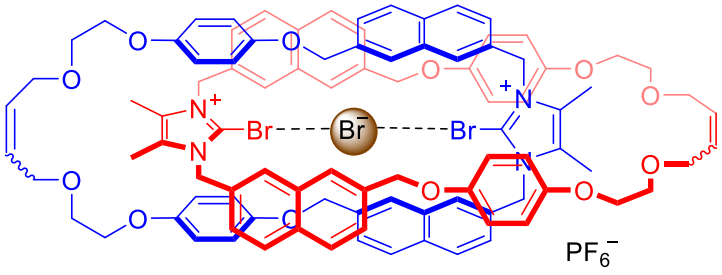


Figure 2.3: *Beer's XB 2-bromoimidazolium catenane*[13]

The imidazolium motif has also been integrated into systems containing luminescent transition metal complexes, which when placed in close proximity to the anion binding site, can allow for detection through an optical response. Beer *et al.* reported an imidazolium functionalised ruthenium(II) bipyridyl receptor, which displayed selective binding of chloride in 9:1 CH_3CN/H_2O (Figure 2.4). A hypsochromic (blue) shift and enhancement of the MLCT emission band of the Ru(II) centre was observed upon halide binding.[14]

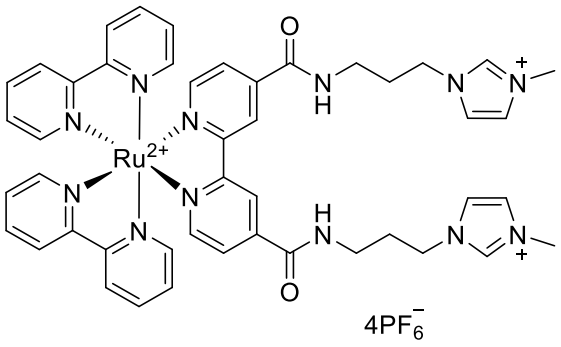


Figure 2.4: *Beer's bis-imidazolium Ru(bipy)$_3$ receptor*[14]

The imidazole motif has also been used as a ligand in transition metal complexes. Ye *et al.* described a 2,2'-bis-imidazole-like ligand complexed to a Ru(II)-bipyridine moiety (Figure 2.5).[15] Upon addition of basic anions, naked eye colour changes were observed. For example, from yellow to orange brown for acetate and from yellow to violet with fluoride in acetonitrile solution.

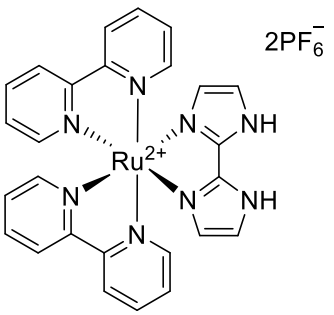


Figure 2.5: *Ye's Ru(II) based 2,2'-bisimidazole containing receptor*[15]

The attraction of incorporating an imidazolium motif into a system beyond its anion binding capability, is the potential for further functionalisation or modification. For example, a preformed imidazolium anion receptor could be subsequently used to stabilise metal nanoparticles. Johnson *et al.* utilised the facile nature of the copper(I)-catalysed azide-alkyne cycloaddition (CuAAC) 'click' reaction to form an adjacent triazole moiety and append a solubilising poly(ethylene glycol) group onto an imidazolium motif. This was then converted to the NHC before being reduced to form PEGylated NHC stabilised gold nanoparticles, compatible with biologically relevant conditions (Figure 2.6).[16]

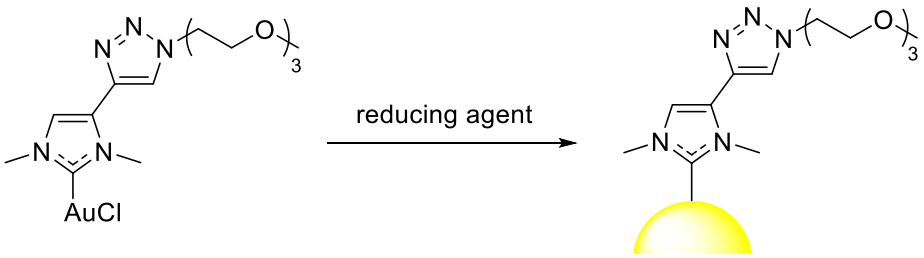


Figure 2.6: *Johnson's Au-NHC and corresponding PEGylated NHC stabilised gold nanoparticles*[16]

The combination of the triazole and imidazolium moieties, as shown in the work by Johnson *et al.* has great appeal for applications in anion binding. Both motifs have separately emerged as potent C–H HB donors (Sections 1.3.1 and 1.3.2) but have yet to be used in conjunction; this will form the theme of this chapter. Importantly, the impact of an XB donor can also be assessed through the incorporation of the corresponding iodotriazole motif.

2.1.1 Chapter aims

The work described in this chapter aims to exploit covalently linked imidazolium–triazole (Figure 2.7a) and transition metal complexed imidazole–triazole (Figure 2.7b) XB and HB receptors for anion recognition and sensing applications. Through incorporation into acyclic, macrocyclic and interlocked [2]rotaxane host structural frameworks and subsequent alkylation, novel imidazolium–triazole containing receptors with convergent XB/HB donors are produced. The anion recognition properties of the receptors are ascertained and discussed with particular focus on the direct comparison of anion binding strength and selectivity of the halogen bonding receptor with its hydrogen bonding analogue.

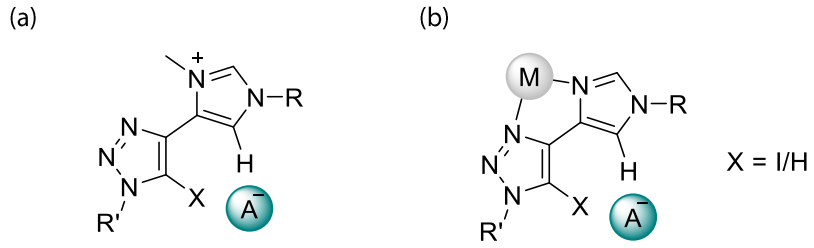


Figure 2.7: *(a) Target imidazolium–triazole and –iodotriazole motifs, and (b) transition metal coordinated imidazole–triazole and –iodotriazole motifs*

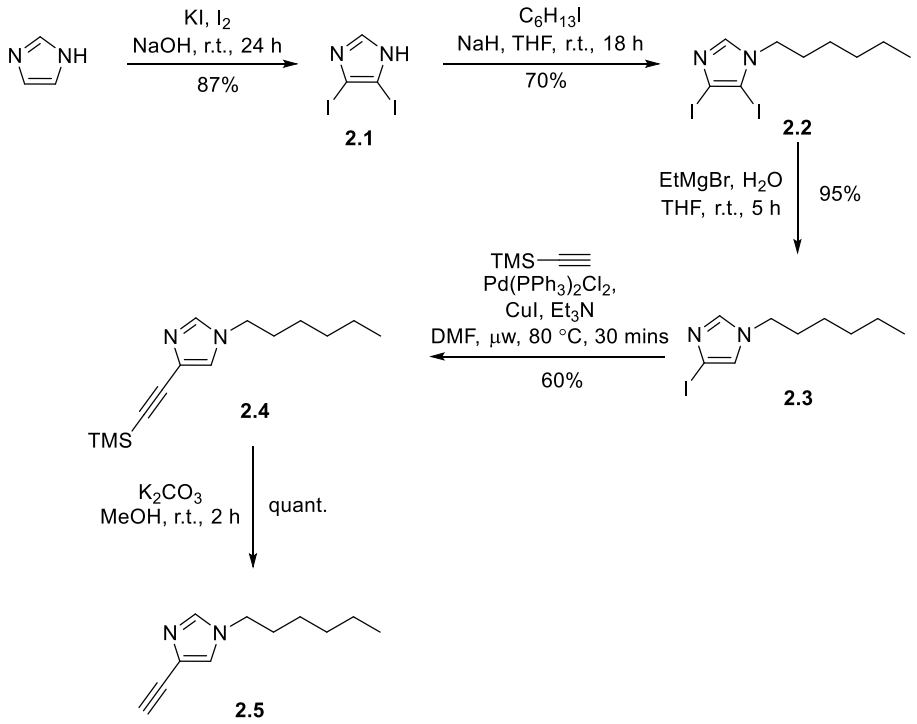
2.2 Acyclic receptors

Initial work focused on the synthesis of an imidazole–triazole acyclic system, which upon alkylation or transition metal coordination produced receptors suitable for their anion recognition properties to be determined.

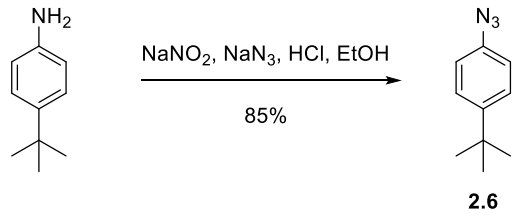
2.2.1 Synthesis of imidazolium–triazole and –iodotriazole acyclic receptors

Synthesis of the novel imidazole–triazole motif was carried out, starting from 4,5-diiodoimidazole **2.1**, prepared *via* a literature procedure.[17] *N*-alkylation at the N^1-position with iodohexane produced **2.2**, and subsequent selective dehalogenation with ethylmagnesium bromide and quenching with water afforded 4-iodoimidazole **2.3**.[18]

Palladium-catalysed Sonogashira coupling[19] between **2.3** and trimethylsilyl acetylene produced the desired trimethylsilyl-protected alkyne **2.4** in 30% yield; however, a significant increase in yield to 60% was obtained by performing the coupling reaction under microwave irradiation. Basic deprotection of the trimethylsilyl group using potassium carbonate in methanol produced the desired alkyne **2.5** in a quantitative yield (Scheme 2.1). Meanwhile, aryl azide **2.6** was synthesised from *tert*-butyl aniline in 85% yield (Scheme 2.2).

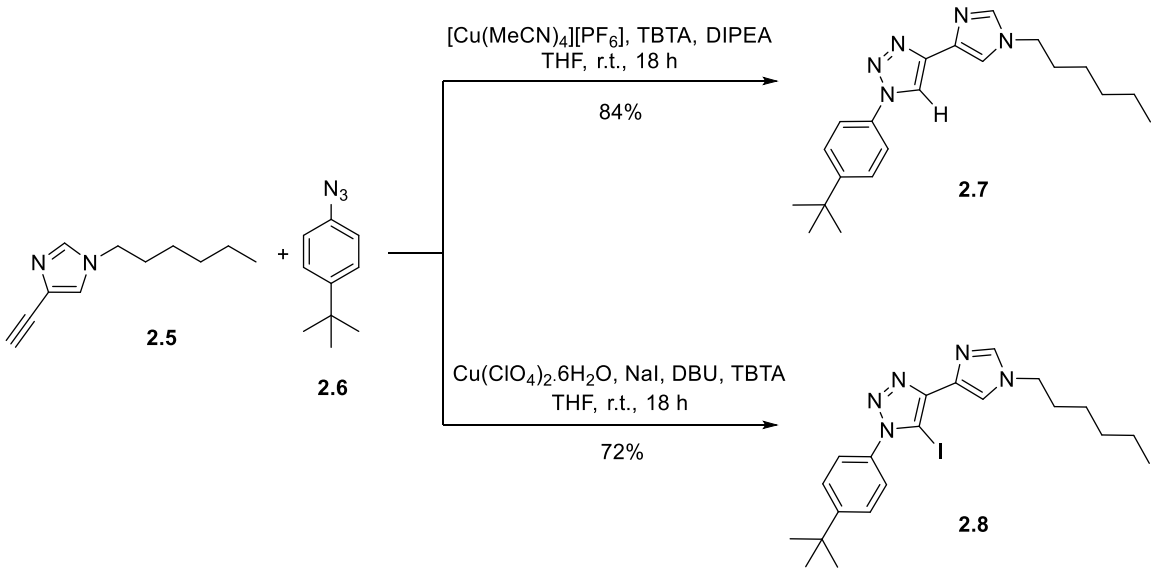


Scheme 2.1: *Synthetic route to prepare imidazole–alkyne* ***2.5***



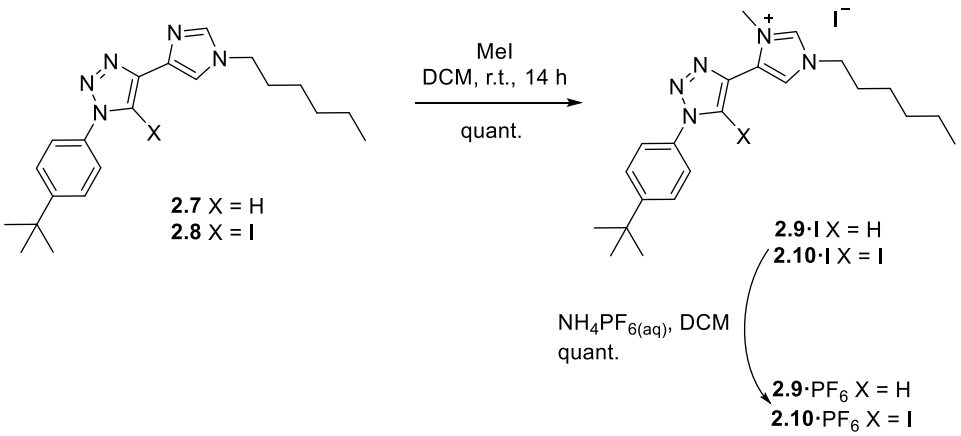
Scheme 2.2: *Synthesis of azide* ***2.6***

Utilising the CuAAC 'click' reaction between imidazole–alkyne **2.5** and azide **2.6,** acyclic HB receptor **2.7** was formed in 84% yield. The 5-iodotriazole analogue XB receptor **2.8** was synthesised in 72% yield using the 'one-pot iodo-click' procedure reported by Brotherton *et al*[20] (Scheme 2.3).



Scheme 2.3: *Synthetic routes to HB imidazole–triazole receptor **2.7** and XB imidazole–iodotriazole receptor **2.8***

The neutral acyclic receptor precursors were alkylated using methyl iodide, to afford **2.9**·I and **2.10**·I in quantitative yield. The iodide salts were anion exchanged to the non-coordinating hexafluorophosphate salt by successive washing with $NH_4PF_{6(aq)}$, to afford receptors **2.9**·PF_6 and **2.10**·PF_6 (Scheme 2.4), for subsequent anion binding studies.

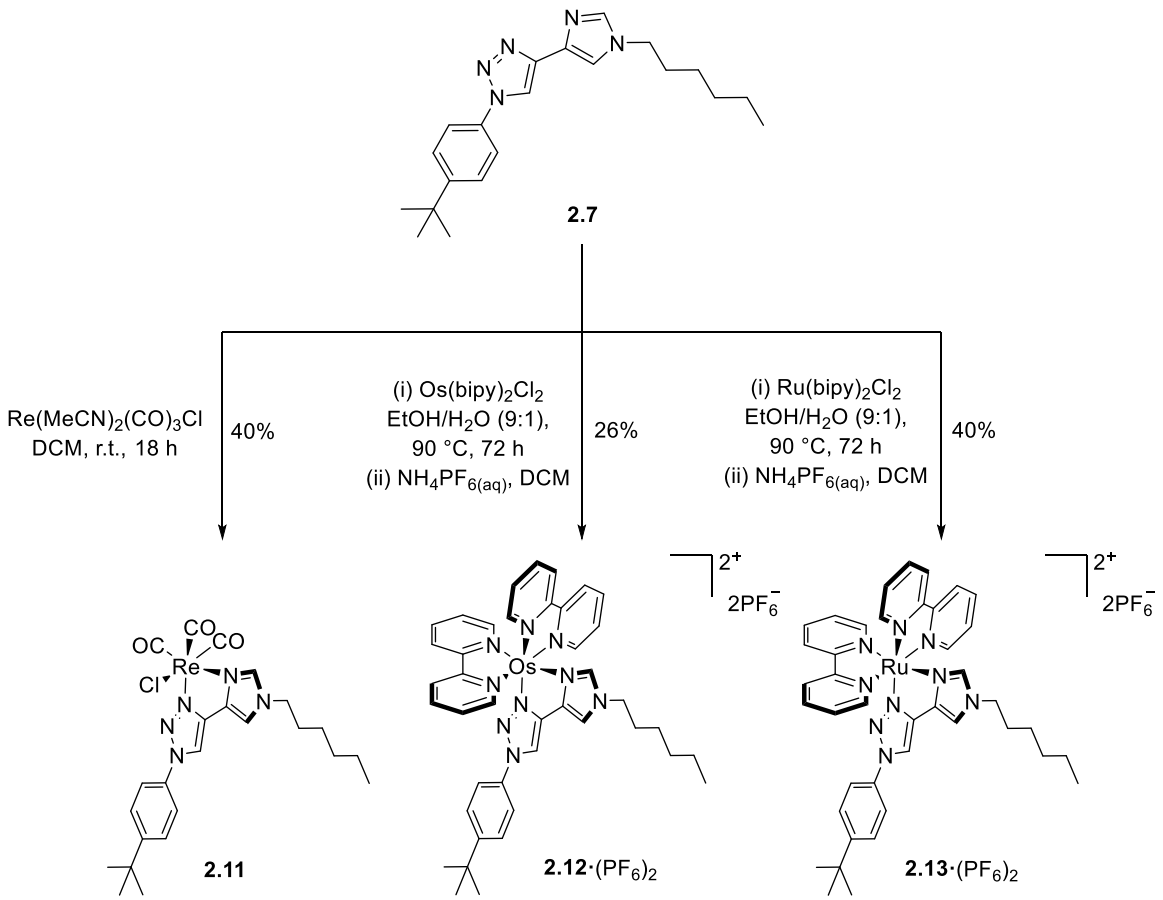


Scheme 2.4: *Synthesis of cationic HB imidazolium–triazole receptor* ***2.9***·PF_6 *and XB imidazolium–iodotriazole receptor* ***2.10***·PF_6

2.2.2 Synthesis of imidazole–triazole transition metal complexes

An alternative to alkylation for generating a potential anion receptor was metal chelation. Rhenium(I) was an appealing choice for metal complex formation due to its photophysical properties, which have been exploited previously in anion sensing.[21,22] An initial complexation reaction was carried out between rhenium pentacarbonyl chloride and imidazole–triazole **2.7**; however, the reaction failed to produce the target neutral receptor, with a species identified as [**2.7**·$Re(CO)_4$]Cl being isolated. To circumvent this, the more reactive [$Re(MeCN)_2(CO)_3Cl$] was synthesised by refluxing [$Re(CO)_5Cl$] in acetonitrile and subsequently reacted with **2.7** to afford target neutral rhenium complex **2.11**, which was isolated in 40% yield (Scheme 2.5).

The formation of charged osmium (II) and ruthenium (II) containing receptors was also undertaken. The osmium(II) complex **2.12**·$(PF_6)_2$ was synthesised by refluxing **2.7** with $Os(bipy)_2Cl_2$ in an ethanol/water (9:1) mixture followed by purification by preparative TLC and after anion exchange with $NH_4PF_{6(aq)}$ isolated as the PF_6^- salt in 26% yield. The corresponding ruthenium(II) complex **2.13**·$(PF_6)_2$ was produced using an analogous procedure with $Ru(bipy)_2Cl_2$ in 40% yield (Scheme 2.5).



Scheme 2.5: *Synthetic route to Re receptor* ***2.11****, Os receptor* ***2.12****·(PF$_6$)$_2$ and Ru receptor* ***2.13****·(PF$_6$)$_2$*

Analogous metal complexation reactions were attempted using the imidazole–iodotriazole ligand analogue **2.8**; however, in all cases only the corresponding HB metal complexes were isolated, which suggested the metal bound iodotriazole C–I bond was unstable under the metal complexation reaction conditions employed.

2.2.3 Preliminary anion binding properties of acyclic receptors

Initially, the anion binding properties of HB receptor **2.9**·PF_6 were investigated *via* ^{1}H NMR spectroscopy titration experiments with TBA·Cl in $CDCl_3$. Upon addition of chloride a significant downfield shift in the resonance of the imidazolium C^2–proton *a* was observed ($\Delta\delta$ ppm = 2.18 after 15 equivalents of TBA·Cl). The imidazolium proton *b* and triazole proton *c* also displayed notable downfield perturbations upon addition of the halide (Figure 2.8). WinEQNMR2[23] analysis of the titration data following either proton *a*, *b* or *c* determined a stoichiometric 1:1 (host/guest) association constant of $K = >10^4$ M^{-1}. An analogous ^{1}H NMR spectroscopy titration experiment with XB receptor **2.10**·PF_6 also determined an association constant of $K = >10^4$ M^{-1}. In order to obtain comparable quantitative data, the titration experiments were repeated in a more competitive solvent mixture of $CDCl_3/CD_3OD/D_2O$ (45:45:10). WinEQNMR2[23] analysis of the titration data generated binding isotherms (Figure 2.9) revealed a 1:2 (host/guest) binding stoichiometry (Table 2.1). K_1 values were over two orders of magnitude greater than K_2, suggesting the second anion binding event was not significant. Both HB and XB acyclic receptors bound chloride strongly in the aqueous–organic solvent mixture, with XB receptor **2.10**·PF_6 forming only a slightly stronger strength of association. This indicated the iodotriazole motif of the XB receptor may not be involved in the primary halide binding event (vide infra).

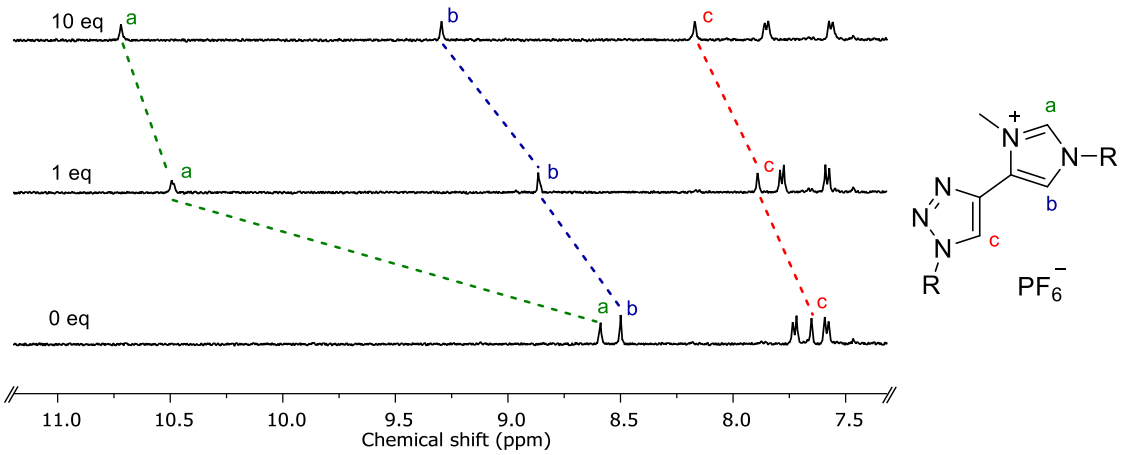


Figure 2.8: *Truncated ^{1}H NMR spectra of receptor **2.9**•PF_6 with increasing equivalents of TBA•Cl ($CDCl_3$, 500 mHz, 298 K)*

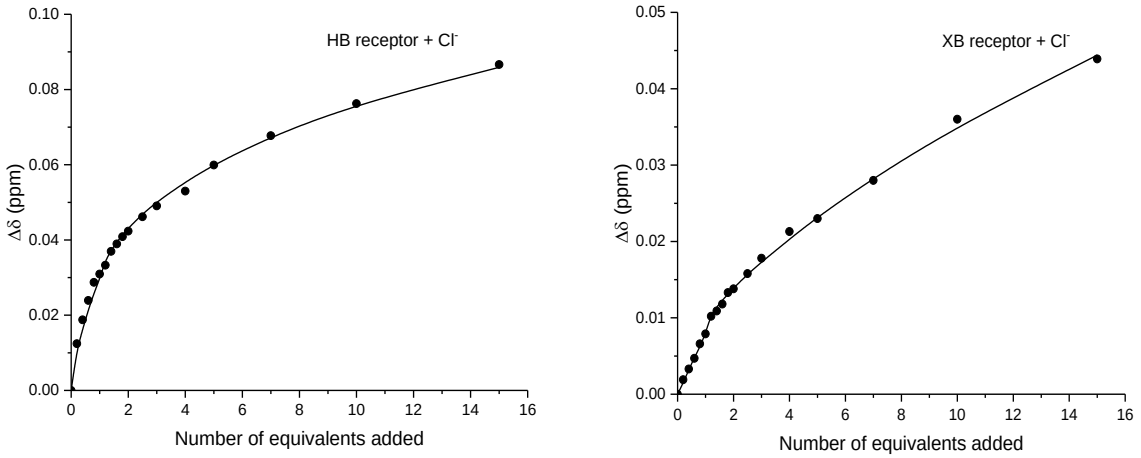


Figure 2.9: *Experimental titration data (points) and calculated 1:2 binding isotherms (lines) for the addition of TBA•Cl to HB receptor **2.9**•PF_6 and XB receptor **2.10**•PF_6, monitoring proton a ($CDCl_3$/CD_3OD/D_2O 45:45:10, 298 K, 500 MHz)*

Table 2.1: *Chloride anion association constants of receptors* ***2.9***·PF_6 *and* ***2.10***·PF_6

Association constants calculated using WinEQNMR2,[23] chloride added as the TBA salt, estimated standard errors given in parentheses, 500 MHz, 298 K

Receptor	Solvent system	K_1 (M^{-1})	K_2 (M^{-1})
2.9·PF_6 (HB)	$CDCl_3$	$> 10^4$	-
2.10·PF_6 (XB)		$> 10^4$	-
2.9·PF_6 (HB)	$CDCl_3/CD_3OD/D_2O$ 45:45:10	3729 (167)	9
2.10·PF_6 (XB)		4342 (94)	26

The chloride binding affinity of metal complexes **2.11**, **2.12**·$(PF_6)_2$ and **2.13**·$(PF_6)_2$ was also determined *via* ^{1}H NMR titration experiments with TBA·Cl in $CDCl_3$ quantitatively. The titration data shown in Figure 2.10 indicated strong chloride binding by both Os and Ru receptors **2.12**·$(PF_6)_2$ and **2.13**·$(PF_6)_2$, with weaker binding shown by Re receptor **2.11**. This was to be expected when taking into consideration the overall dicationic charge on the Os and Ru complexes compared to the neutral Re complex. Unfortunately, the titration data could not be fitted to either a 1:1, 1:2 or 2:1 host/guest stoichiometric binding model using WinEQNMR2[23] analysis, suggesting complex equilibria present.

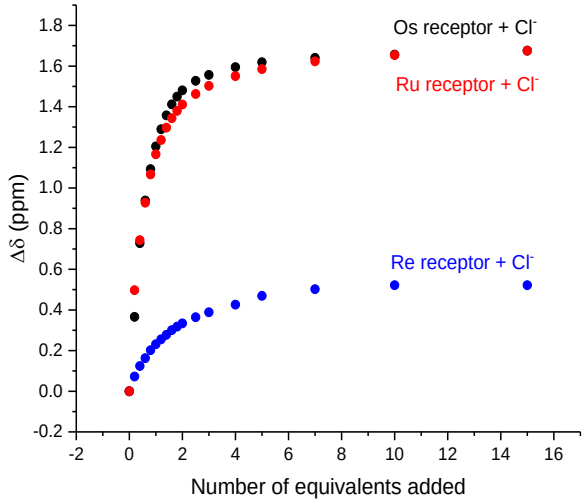


Figure 2.10: *Experimental titration data (points) for the addition of TBA·Cl to Re complex* ***2.11***, *Os complex* ***2.12***·$(PF_6)_2$ *and Ru complex* ***2.13***·$(PF_6)_2$ *monitoring proton a ($CDCl_3$, 298 K, 500 MHz)*

The ability of receptors **2.12**·$(PF_6)_2$ and **2.13**·$(PF_6)_2$ to sense anions was then investigated using luminescence spectroscopy. The observed excitation and emission wavelengths were typical for the MLCT transition of osmium(II) and ruthenium(II) bipy poly-pyridyl complexes (Table 2.2).[24,25] The Re receptor **2.11** was found to not be photo-active. Preliminary titration experiments were carried out with receptors **2.12**·$(PF_6)_2$ and **2.13**·$(PF_6)_2$; upon addition of 50 equivalents of TBA·Cl luminescence quenching was observed (Figure 2.11).

Table 2.2: *Luminescent properties of osmium(II) receptor* ***2.12***·*$(PF_6)_2$ and ruthenium(II) receptor* ***2.13***·*$(PF_6)_2$ (MeCN, [5 x 10^{-5} M], 298 K)*

	$\lambda_{excit,\ max}$ (nm)	$\lambda_{emission,\ max}$ (nm)
Os(II) **2.12**·$(PF_6)_2$	460	780
Ru(II) **2.13**·$(PF_6)_2$	510	640

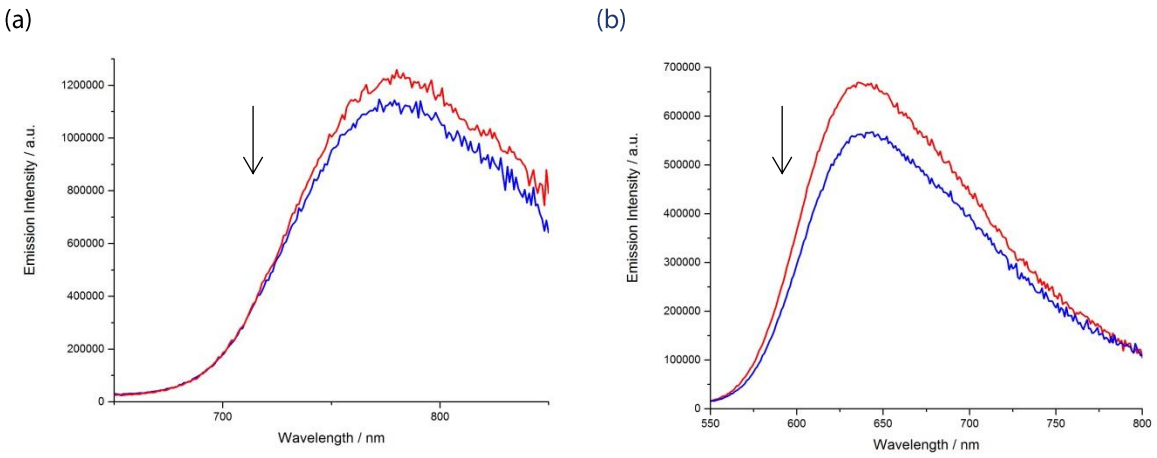


Figure 2.11: *Changes in luminescence emission intensity upon addition of 50 equivalents of chloride (as TBA·Cl) (a) Os(II) receptor* ***2.12***·*$(PF_6)_2$, MeCN, [5 x 10^{-5} M], λ_{ex} = 460 nm, and (b) Ru(II) receptor* ***2.13***·*$(PF_6)_2$, MeCN, [5 x 10^{-5} M], λ_{ex} = 510 nm*

The preliminary photophysical studies performed with TBA·Cl showed promise for the HB Os and Ru receptors **2.12**·$(PF_6)_2$ and **2.13**·$(PF_6)_2$ to act as anion sensors. However, taking into account that quantitative association constants could not be ascertained from

the ^{1}H NMR spectroscopy titration data for the receptors and the corresponding XB metal complexes could not be isolated, efforts were focused toward investigations into the more promising imidazolium–triazole and –iodotriazole motifs.

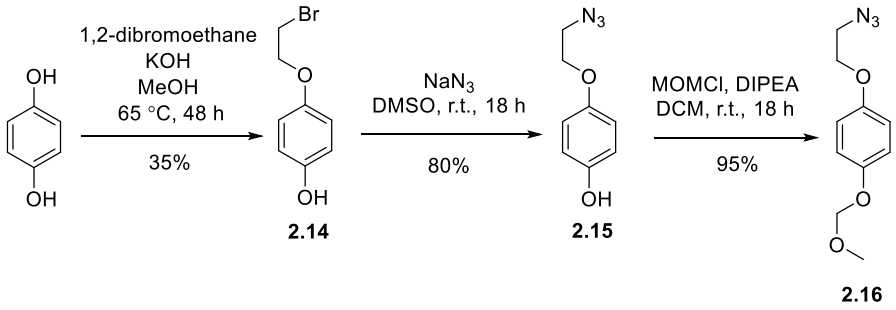
2.3 Macrocyclic systems

Having demonstrated that the acyclic imidazolium–triazole and –iodotriazole receptors function as potent anion recognition motifs, attention was turned to their incorporation into preorganised architectures, with macrocycles initially targeted.

2.3.1 Synthesis

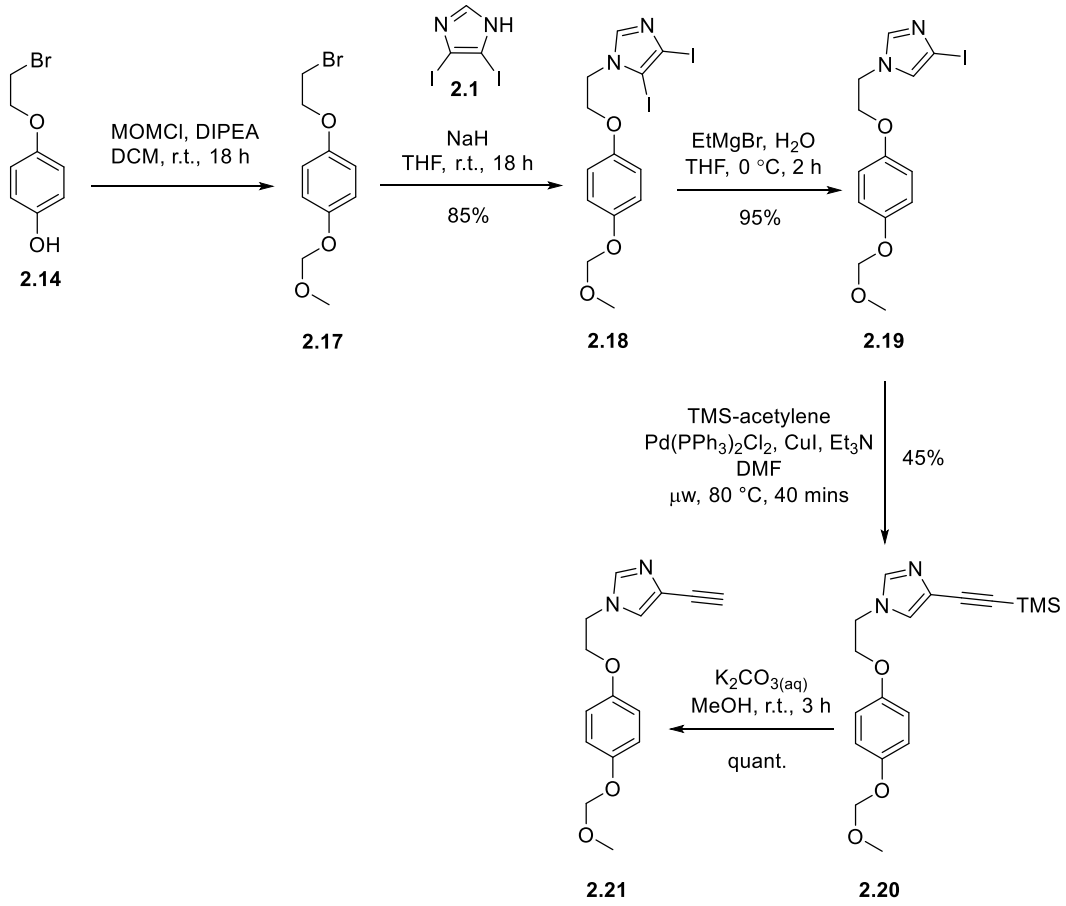
The synthetic strategy employed for the preparation of the unsymmetric macrocycle was a CuAAC 'click' reaction between an appropriate imidazole–alkyne and azide to form an imidazole–triazole bis-phenolic macrocyclic precursor. A subsequent ring closing reaction with triethylene glycol bis-tosylate under basic conditions was envisaged to produce the target macrocycles.

Initially, hydroquinone was alkylated with 1,2-dibromoethane in a statistical reaction to form mono substituted hydroquinone **2.14**. A S_N2 substitution reaction with sodium azide and subsequent reaction with chloromethyl methyl ether produced the desired methoxymethyl protected azide **2.16** in two steps, in an overall yield of 76% (Scheme 2.6).[26]



Scheme 2.6: *Synthetic route to azide* ***2.16***

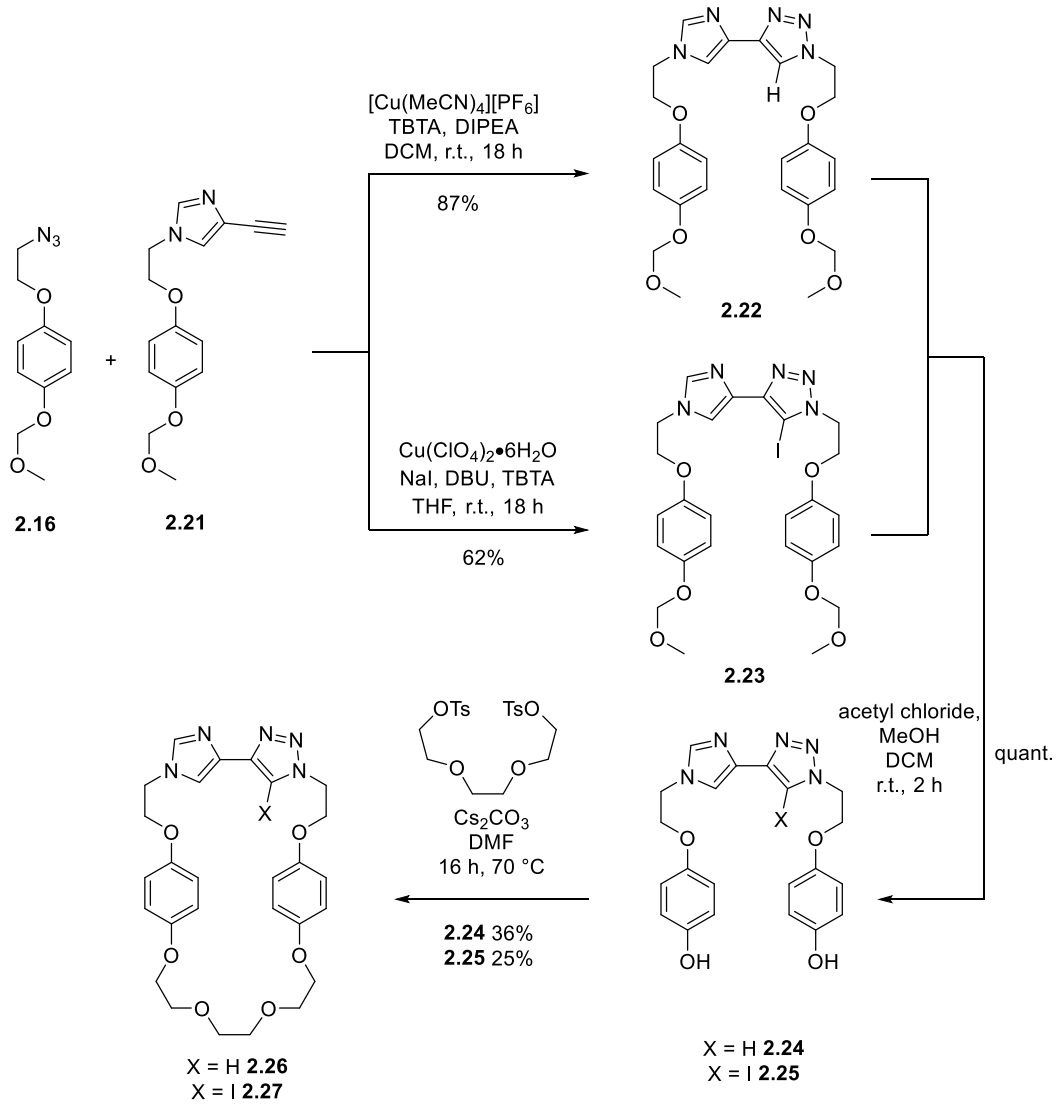
The hydroquinone compound **2.14** was protected with chloromethyl methyl ether, before reaction with 4,5-diiodoimidazole **2.1** in the presence of NaH to give derivative **2.18** in 85% yield. Subsequent dehalogenation with ethylmagnesium bromide, Sonogashira coupling with trimethylsilyl acetylene and deprotection under standard conditions produced the desired imidazole–alkyne **2.21** in an overall 43% yield (Scheme 2.7).



Scheme 2.7: *Synthetic route to imidazole–alkyne* ***2.21***

The CuAAC 'click' reaction between imidazole–alkyne **2.21** and azide **2.16** formed the imidazole–triazole macrocycle precursor **2.22** in 87% yield; employing the 'one-pot iodo-click' conditions afforded the corresponding iodotriazole species **2.23** in 62% yield. Following removal of the methoxymethyl protecting group, bis-phenols **2.24** and **2.25** were reacted with triethylene glycol bistosylate and an excess of anhydrous caesium

carbonate in dry DMF at 70 °C to afford macrocycles **2.26** and **2.27** in yields of 36% and 25% respectively (Scheme 2.8).

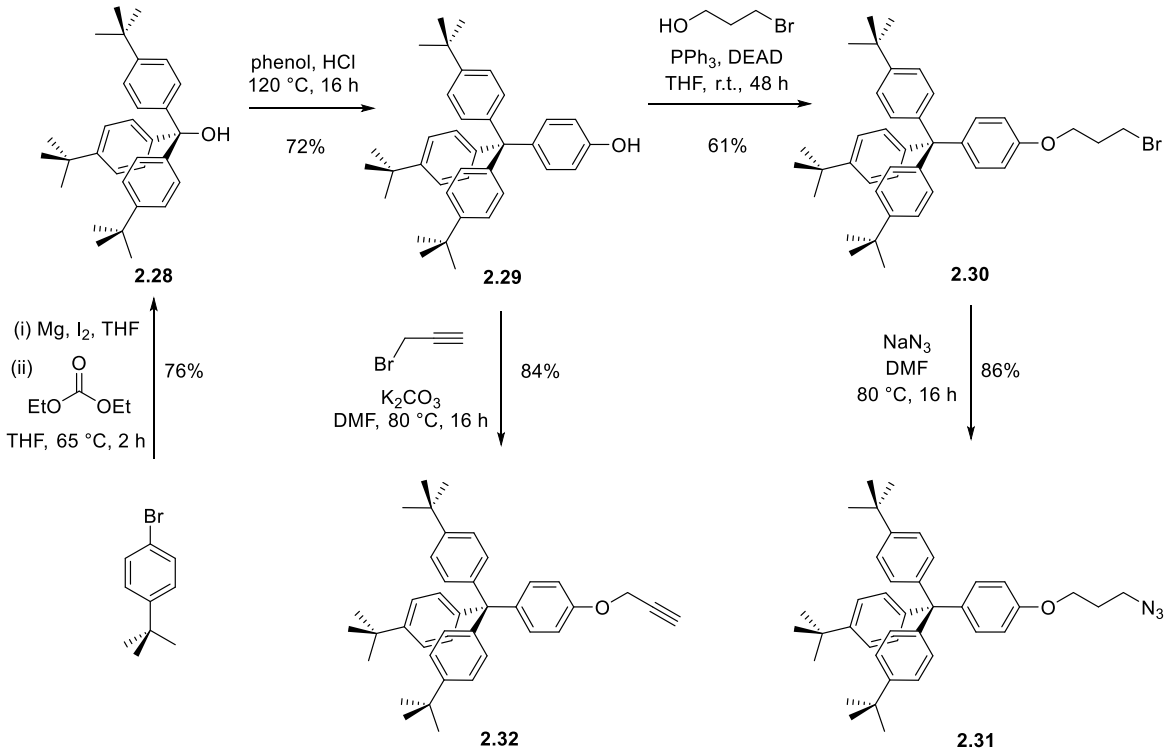


Scheme 2.8: *Synthetic route to HB macrocycle **2.26** and XB macrocycle **2.27***

2.3.2 Attempted active metal-template synthesis of HB and XB[2]rotaxanes

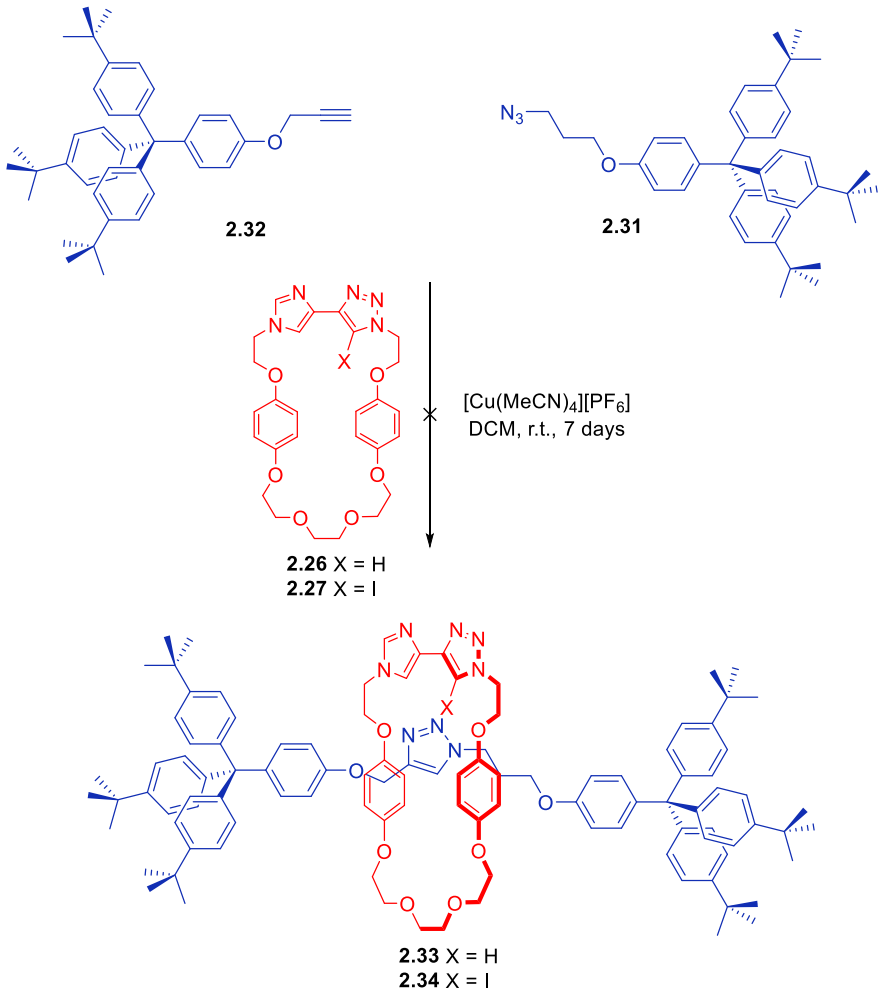
Beer and co-workers have recently demonstrated that the 'active-metal template' synthetic protocol (Section 1.5.3) can be exploited for the synthesis of [2]rotaxanes *via* an endotopic copper(I) cation coordination mode to a bis(triazole)-containing macrocycle.[26] Subsequent CuAAC 'click' reaction between alkyne and azide stopper derivatives occurs with a high level of positional integrity at the bis-triazole coordinated copper(I) centre resulting in the formation of an interlocked [2]rotaxane.

Therefore, the active metal-template synthesis of a [2]rotaxane was investigated using HB imidazole–triazole macrocycle **2.26**. Initially, the preparation of stopper azide **2.31** and alkyne **2.32** was required, synthesised *via* previously reported synthetic procedures[27] (Scheme 2.9). Reaction of 1-bromo-4-*tert*-butylbenzene with magnesium turnings in the presence of a catalytic amount of iodine generated the Grignard reagent, which was reacted with diethylcarbonate to give alcohol **2.28** in 76% yield. A S_N1 substitution reaction with phenol was carried out to form stopper alcohol **2.29** in 72% yield and a subsequent Mitsunobu reaction with 3-bromo-propan-1-ol afforded stopper-bromide **2.30** in 61% yield. Reaction of **2.30** with NaN_3 gave the target stopper azide **2.31**. A stopper bearing an alkyne group, **2.32**, was prepared by appending propargyl bromide to alcohol **2.29** in 84% yield.



Scheme 2.9: *Synthetic route to propyl-azide stopper* ***2.31*** *and alkyne stopper* ***2.32***

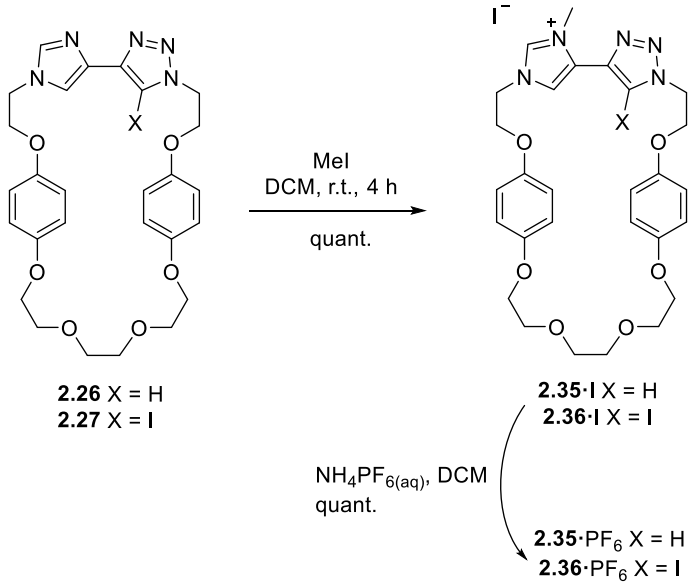
Subsequently, the synthesis of [2]rotaxanes **2.33** and **2.34** *via* an 'active-metal template' approach was targeted. Macrocycle **2.26** was dissolved in degassed dry DCM with a stoichiometric quantity of $[Cu(MeCN)_4][PF_6]$, before an excess of stopper azide **2.31** and alkyne **2.32** were added (Scheme 2.10). No evidence was observed for the formation of [2]rotaxane **2.33** by either TLC or ESI mass spectrometry of the crude reaction mixture, with axle and macrocycle isolated separately after preparative TLC. An analogous reaction was attempted with the XB macrocycle **2.27**; again, only the individual rotaxane components were isolated. The results from these AMT attempts suggested that the copper(I) catalyst was coordinating exotopically to the macrocycle instead of the endotopic arrangement required for successful formation of an interlocked structure.



Scheme 2.10: *Attempted active metal-templated synthesis of rotaxanes* ***2.33*** *and* ***2.34***

2.3.3 Synthesis of cationic macrocycle

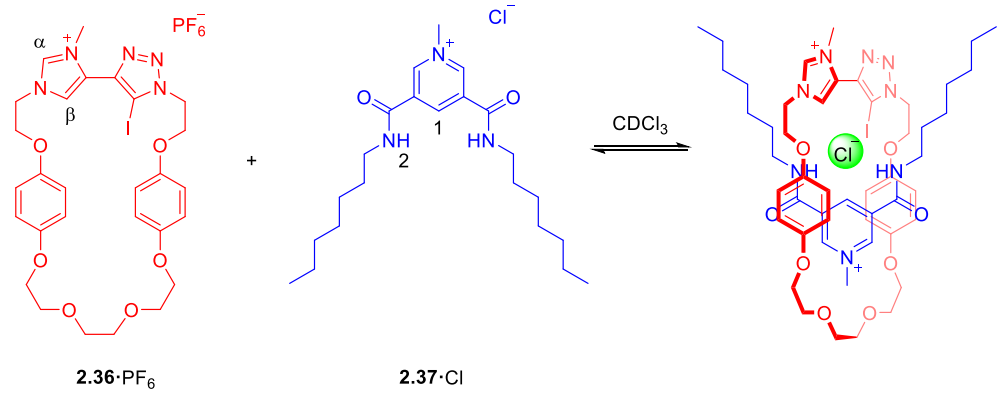
Attention then turned to the possibility of employing an anion-template methodology for the synthesis of a [2]rotaxane. Macrocycles **2.26** and **2.27** were alkylated with an excess of methyl iodide to produce **2.35**·I and **2.36**·I in quantitative yield and anion exchanged to the corresponding hexafluorophosphate salts *via* successive washing with aqueous NH_4PF_6 (0.1 M) to afford cationic macrocycles **2.35**·PF_6 and **2.36**·PF_6 (Scheme 2.11).



Scheme 2.11: *Synthesis of cationic HB macrocycle* ***2.35***·PF_6 *and XB macrocycle* ***2.36***·PF_6

2.3.4 Pseudorotaxane studies

The ability of XB macrocycle **2.36**·PF_6 to participate in anion–templated rotaxane formation was investigated initially through a qualitative ^{1}H NMR spectroscopy pseudorotaxane assembly experiment (Scheme 2.12). The ^{1}H NMR spectrum of an equimolar mixture of XB macrocycle **2.36**·PF_6 and 3,5-bis-amide pyridinium chloride thread **2.37**·Cl in $CDCl_3$ was recorded and compared to the spectrum of each individual component (Figure 2.12).



Scheme 2.12: *Pseudorotaxane formation between XB macrocycle* ***2.36***·PF_6 *and thread* ***2.37***·*Cl*

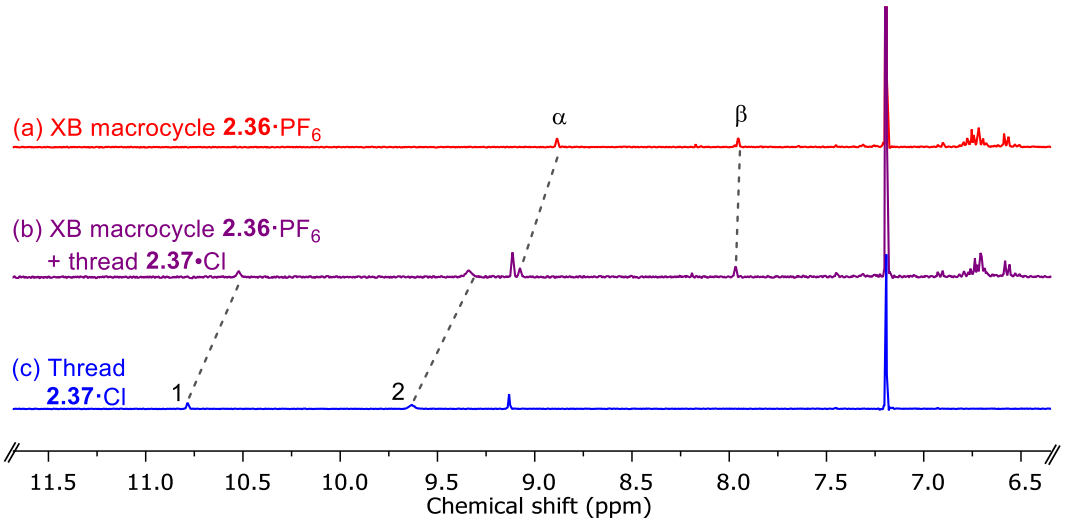


Figure 2.12: *truncated* ^{1}*H NMR spectra of (a) XB macrocycle* ***2.36***·PF_6*, (b) an equimolar mixture of XB macrocycle* ***2.36***·PF_6 *and thread* ***2.37***·*Cl, and (c) thread* ***2.37***·*Cl (*$CDCl_3$*, 298 K, 400 MHz)*

Tentative evidence for pseudorotaxane formation can be ascertained from the significant downfield shift of imidazolium proton *α* and a very slight downfield shift of imidazolium proton *β*, concomitant with the upfield shift of protons *1* and *2* of the pyridinium thread. Typically, the diagnostic observation for the formation of a pseudorotaxane is the splitting and shift of the hydroquinone resonances of the macrocycle, an effect arising from the desymmetrisation of these proton environments and favourable aromatic donor-acceptor stacking interactions between the electron rich hydroquinone rings of the macrocycle and the electron-deficient pyridinium of the threading component. In this system, macrocycle

2.36·PF_6 is inherently unsymmetric, giving a complex multiplet pattern of the hydroquinone proton resonances. Therefore, evidence of interpenetrated assembly formation from the splitting of the resonances was challenging to ascertain. Furthermore, no noticeable shift in the hydroquinone resonances was observed whilst the greatest perturbation for the macrocycle was seen for the external imidazolium proton. Taken together, these observations suggested that a pseudorotaxane assembly had not formed, but instead the templating chloride anion had directed the thread to be positioned on the periphery of the macrocycle. Therefore, further investigations into chloride-template rotaxane formation were not undertaken.

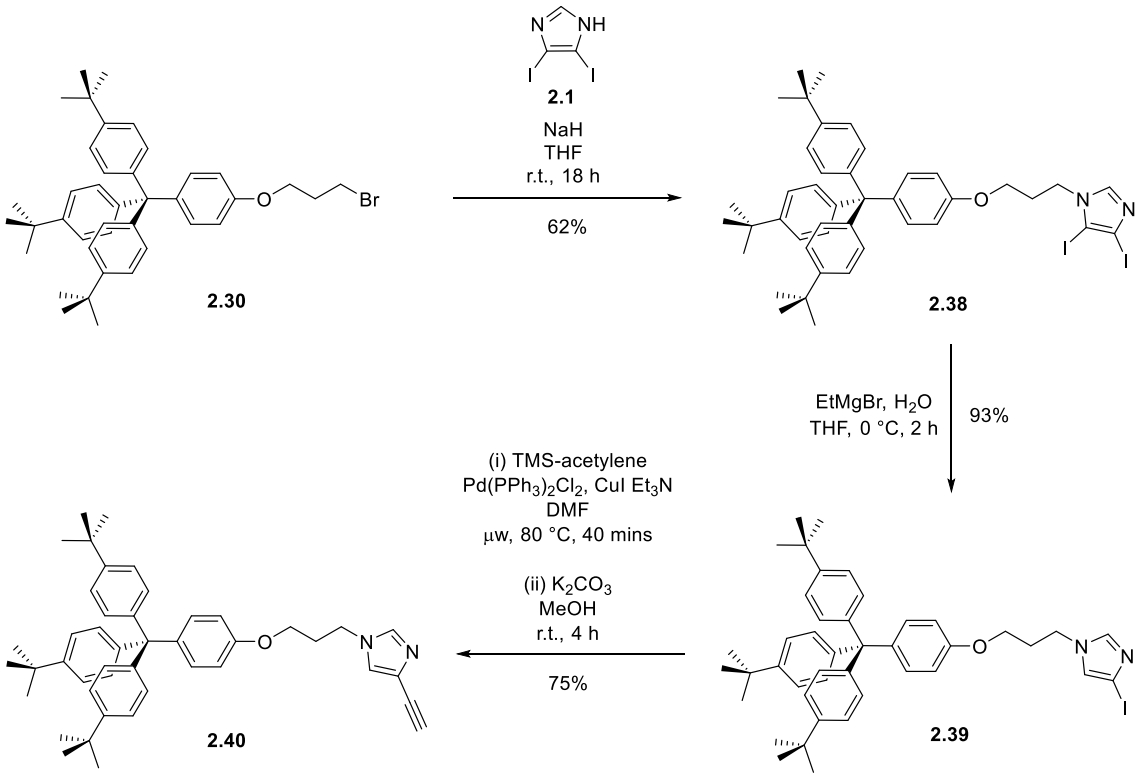
2.4 Incorporation of imidazolium–triazole and –iodotriazole into an axle

Incorporating the imidazolium–triazole and –iodotriazole motifs into the macrocyclic component of an interlocked structure proved unsuccessful *via* both active–metal template and anion template methods. Additionally, the unsymmetric nature of the macrocycle resulted in a challenging synthetic route, requiring numerous steps and produced a non-trivial ^{1}H NMR spectrum. An alternative chloride-template 'clipping' rotaxane synthesis was undertaken using imidazolium–triazole and –iodotriazole axle components and an isophthalamide based macrocycle precursor. This work was undertaken in conjunction with Amy Ford, a final year undergraduate Part II student.

2.4.1 Synthesis of HB and XB axles

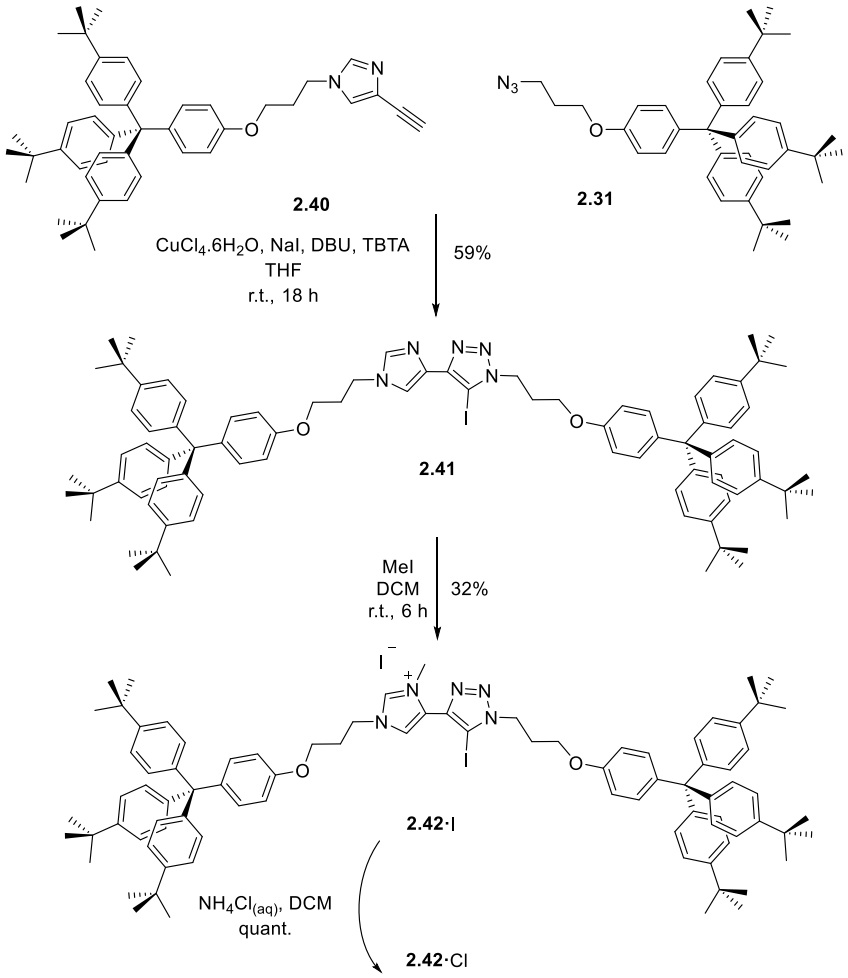
The synthetic strategy employed for the synthesis of the unsymmetric HB and XB axles was analogous to that used for the preparation of the acyclic receptor, which was achieved through coupling of stopper half axle imidazole–alkyne and azide components. For the stopper imidazole–alkyne **2.40**, *N*-alkylation at the N^1-position of 4,5-diiodoimidazole **2.1** with stopper propyl bromide **2.30** produced **2.38** in 62% yield. Selective dehalogenation with ethylmagnesium bromide and quenching with water afforded 4-iodoimidazole **2.39**

in 93% yield. Sonogashira coupling between **2.39** and trimethylsilyl acetylene and subsequent deprotection formed stopper imidazole–alkyne **2.40** in 75% yield (Scheme 2.13).



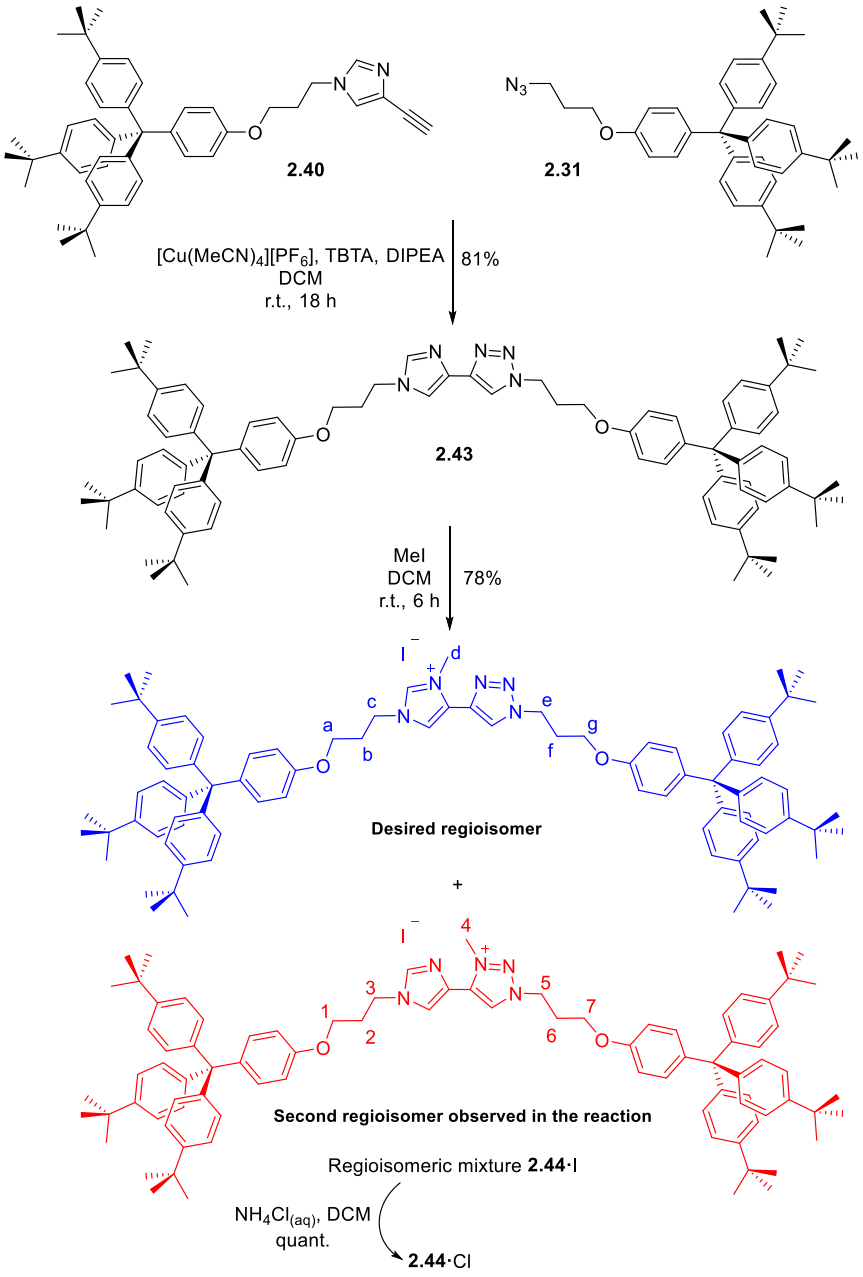
Scheme 2.13: *Synthetic route to terphenyl–stoppered imidazole–alkyne* ***2.40***

For the synthesis of the XB axle, a 'one-pot iodo-click' reaction was carried out between stopper azide **2.31** and alkyne **2.40** to give imidazole–iodotriazole axle **2.41** in 59% yield (Scheme 2.14). Alkylation of iodo-axle **2.41** was carried out with methyl iodide (20 eq) in DCM at room temperature, to produce imidazolium–iodotriazole **2.42**·Cl in 32% yield after purification and anion exchange to the chloride salt.



Scheme 2.14: *Synthetic route to imidazolium-iodotriazole axle* ***2.42****·Cl*

The synthesis of the proto-axle was carried out *via* a CuAAC 'click' reaction between stopper azide **2.31** and stopper imidazole–alkyne **2.40** to give imidazole–triazole axle **2.43** in 81% yield. Alkylation of **2.43** with methyl iodide in DCM proved unexpectedly problematic (Scheme 2.15). Several reaction conditions were attempted; however, regiospecific alkylation of the imidazole moiety could not be achieved over alkylation of the triazole. Despite numerous chromatographic attempts at purification, an inseparable mixture of both regioisomers was present, in a combined yield of 78%. Alkylation using methyl triflate at −78 °C in DCM, was also tested; however, only starting materials were seen in ESI mass spectroscopy and *via* TLC. Unfortunately, performing the reaction at room temperature resulted in a mixture of regioisomers, analogous to the methyl iodide route.



Scheme 2.15: *Synthetic route to cationic axle* ***2.44·Cl***

The presence of regioisomers **2.44·**I was confirmed by ^{1}H NMR spectroscopy, showing two discreet sets of peaks (Figure 2.13). Integration of the peaks in the ^{1}H NMR spectrum indicated a 4:1 ratio of imidazolium–triazole to imidazole–triazolium regioisomers. Anion exchange of **2.44·**I to the chloride salt, in preparation for anion-templated rotaxane formation was carried out by successive washing with $NH_4Cl_{(aq)}$ to afford cationic axle **2.44·**Cl.

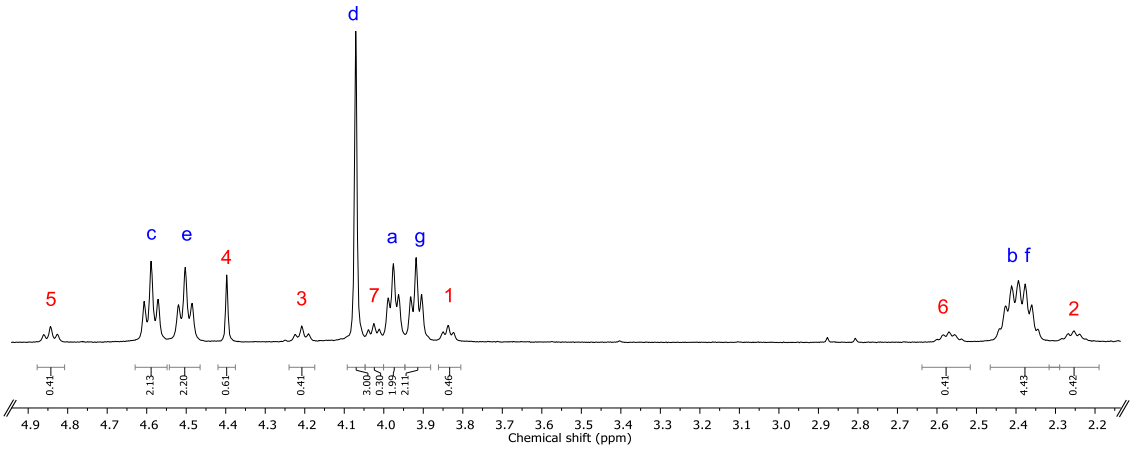


Figure 2.13: *truncated ^{1}H NMR spectrum (400 MHz, $CDCl_3$, 298 K) showing the two regioisomers present in* ***2.44·I***

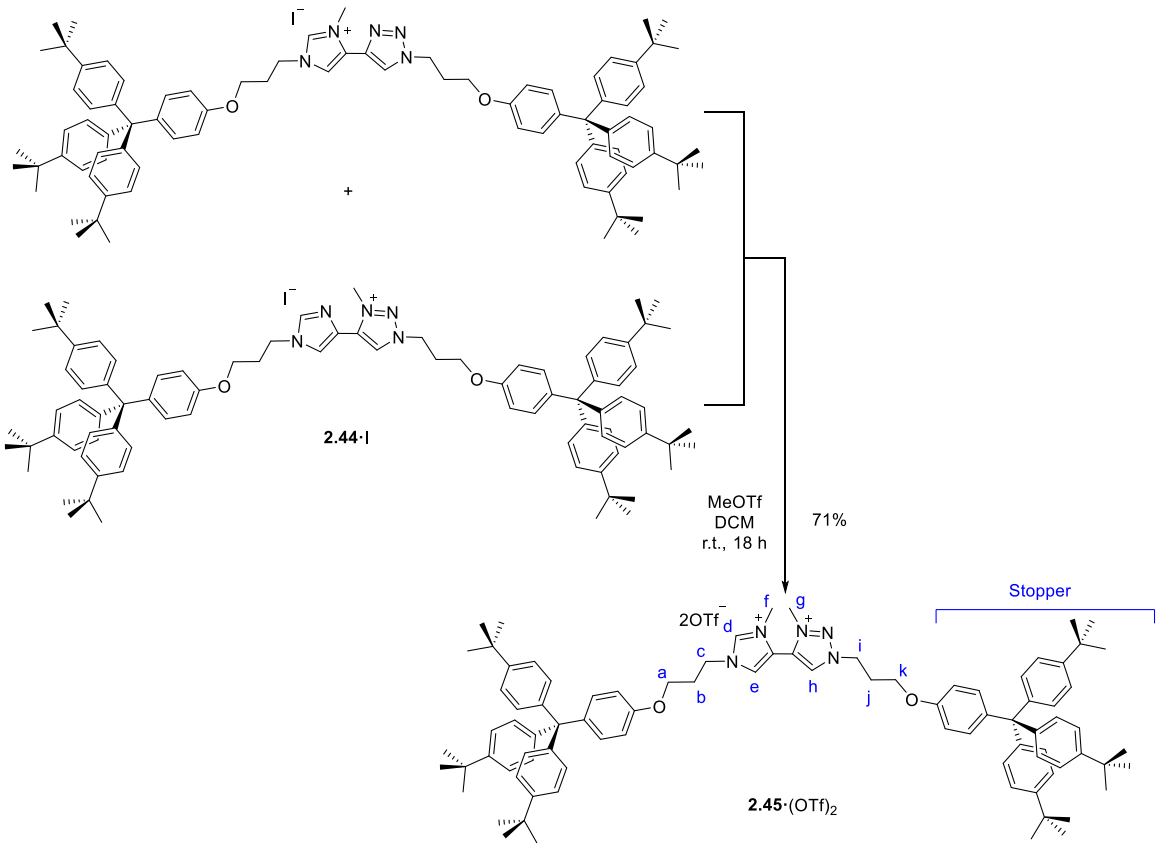
In contrast to the synthesis of cationic HB axle **2.44**·Cl, no evidence of the imidazole–iodotriazolium regioisomer was observed by ^{1}H NMR spectroscopy of the XB axle **2.42**·Cl. It was postulated that the presence of the iodine atom deactivated the triazole, and hence allowed for selective alkylation of the imidazole heterocycle.

2.4.2 Synthesis of dicationic axle

To overcome the formation of regioisomers attention then turned to the possible synthesis of the corresponding dicationic HB axle, achieved by a further alkylation reaction of the mixture of imidazole–triazolium and imidazolium–triazole axle regioisomers **2.44**·Cl. The pure dicationic axle could then be used in a novel [2]rotaxane anion host system.

Regioisomeric cationic axle **2.44**·Cl was treated with methyl iodide in DCM; however, no evidence of the desired dicationic axle was observed. An excess of methyl triflate, a more potent alkylating reagent, produced the desired dicationic axle **2.45**·$(OTf)_2$ in 71% yield (Scheme 2.16). The full conversion to imidazolium–triazolium was confirmed by the ^{1}H NMR spectrum of axle **2.45**·$(OTf)_2$, clearly showing a single species in solution (Figure 2.14). In preparation for anion-template rotaxane formation, anion exchange to the

coordinating chloride salt **2.45**·$(Cl)_2$ was achieved using a chloride-loaded Amberlite® anion-exchange resin; however, the chloride salt proved insoluble in common organic solvents, unfortunately negating any rotaxanation attempts.



Scheme 2.16: *Synthetic route to dicationic imidazolium–triazolium axle* ***2.45***·*$(OTf)_2$*

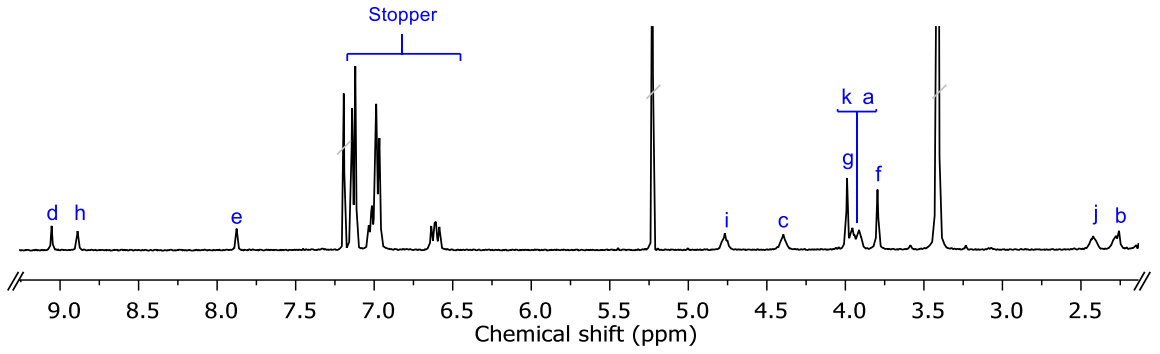
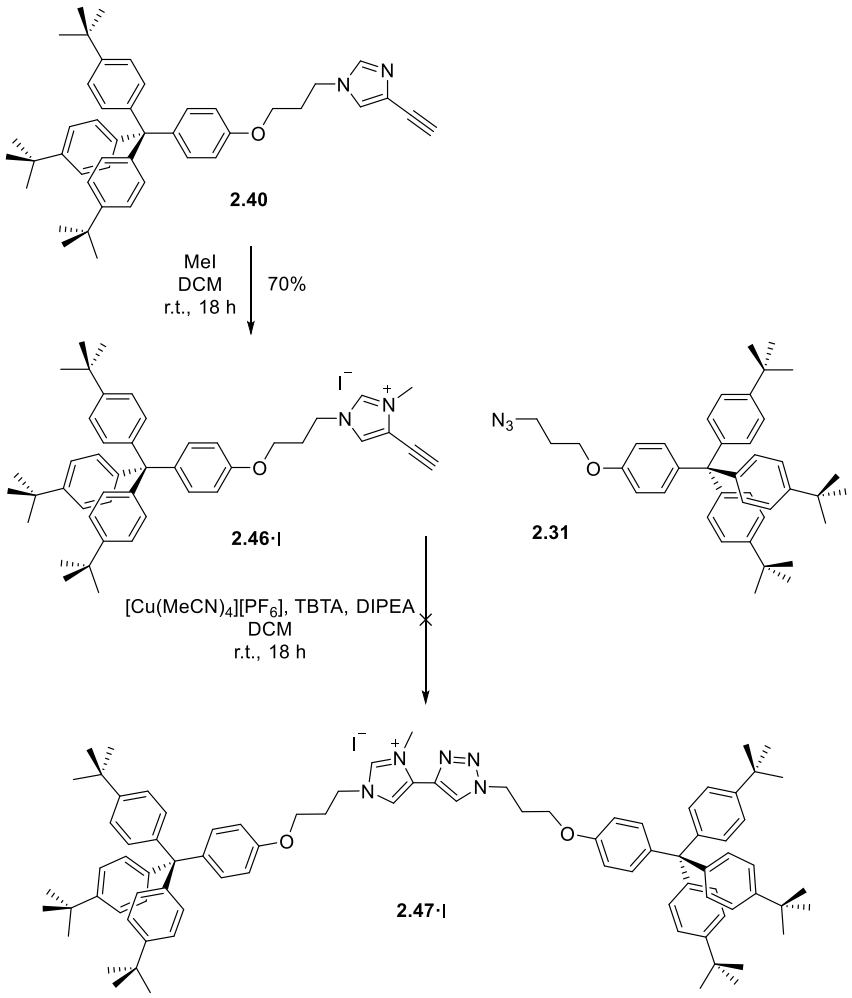


Figure 2.14: *Truncated ^{1}H NMR spectrum of dicationic imidazolium–triazolium axle* ***2.45***·*$(OTf)_2$ (400 MHz, $CDCl_3$, 298 K)*

2.4.3 Alternative route to HB axle

An alternative synthetic strategy was employed to circumvent the issues encountered with non-regiospecific alkylation; in particular, imidazole–alkyne **2.40** was alkylated prior to the CuAAC 'click' axle-forming reaction avoiding the potential alkylation of the triazole moiety. Methyl iodide was added portionwise to imidazole–alkyne **2.46**·I in DCM, purified *via* preparative TLC and isolated in 70% yield. A CuAAC 'click' reaction was carried out with cationic imidazole–alkyne **2.46**·I and stopper azide **2.31**, following a modified literature procedure (Scheme 2.17).[16] Although the target imidazolium–triazole axle **2.47**·I was observed in the ESI-MS, in spite of numerous attempts at purification *via* silica gel chromatography, the axle could not be isolated.

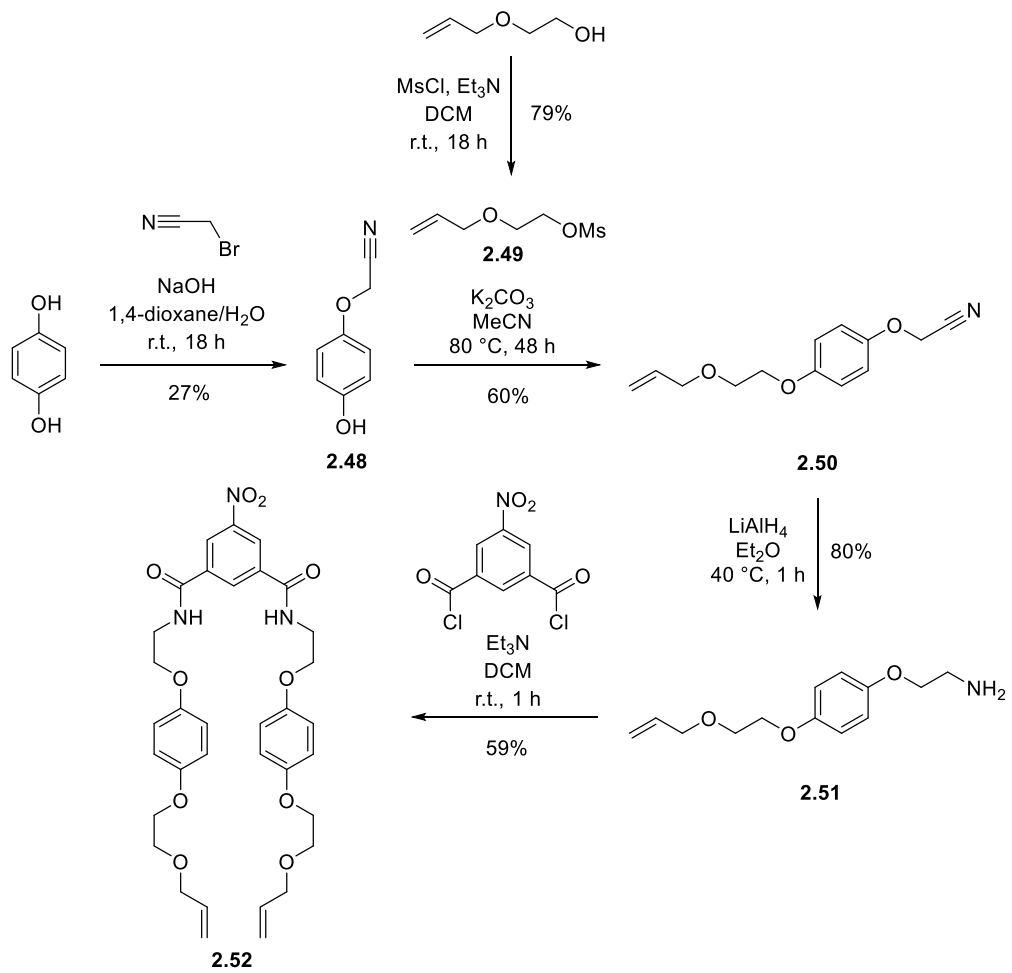


Scheme 2.17: *Attempted synthesis of cationic axle* ***2.47***·*I via imidazolium-alkyne* ***2.46***·*I*

2.5 Incorporation into a [2]rotaxane

2.5.1 Synthesis of imidazolium–triazole and –iodotriazole [2]rotaxanes

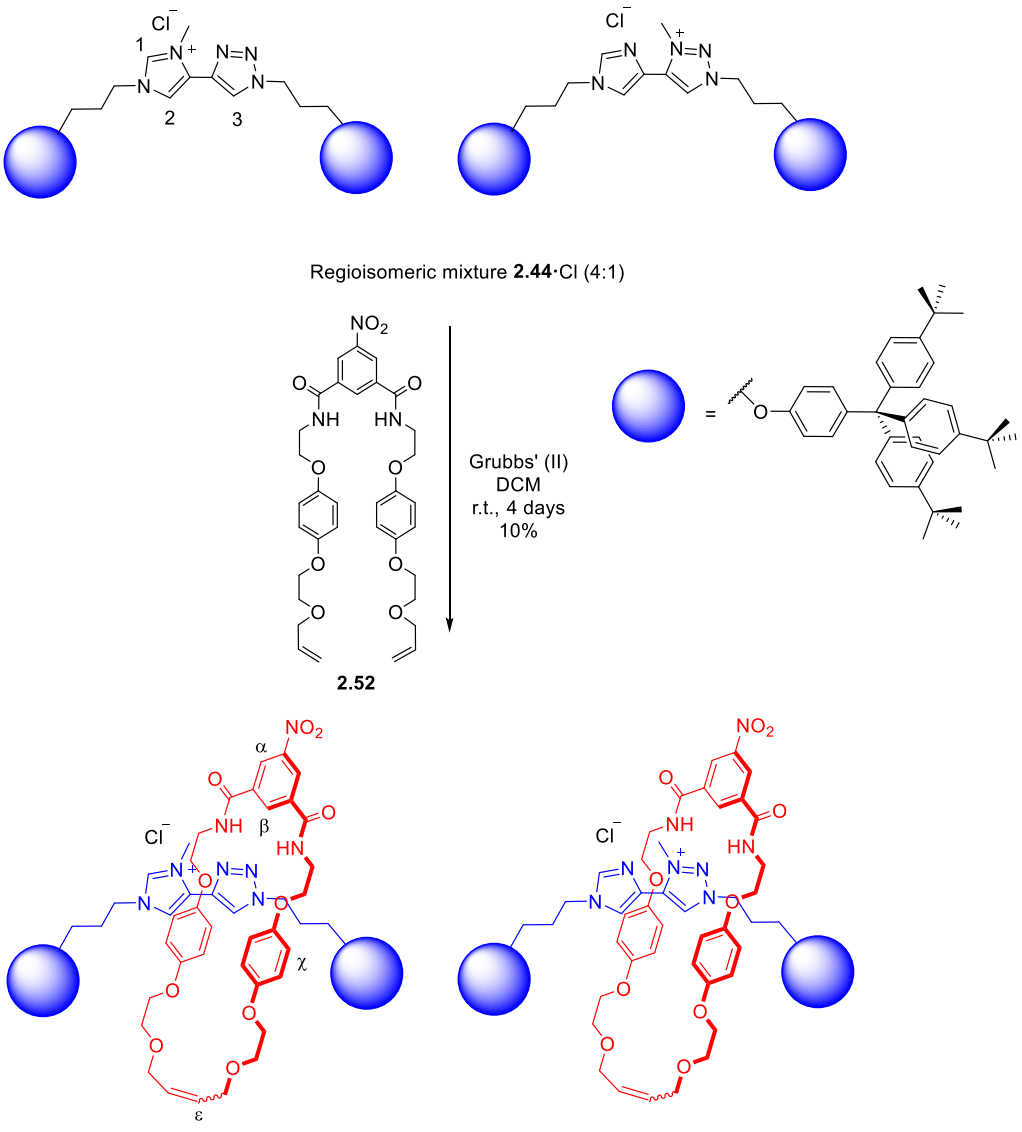
After successfully isolating axle regioisomers **2.44**·Cl, a preliminary rotaxanation reaction was carried out to ascertain if an interlocked structure could be synthesised *via* chloride–template assembly and subsequent Grubbs' II catalysed RCM reaction with a bis-vinyl appended macrocycle precursor, prepared according to literature procedures (Scheme 2.18).[28] Monofunctionalised hydroquinone **2.48** was synthesised in 27% *via* the reaction of hydroquinone and NaOH with bromoacetonitrile in 1:1 dioxane/H_2O. The reaction of **2.48** with 2-(allyloxy)ethyl methanesulfonate **2.49**,[29] prepared from the mesylation of 2-allyloxyethanol, afforded the vinyl-functionalised nitrile derivative **2.50** in 60% yield.[30]



Scheme 2.18: *Synthesis of bis-vinyl-appended isophthalamide macrocycle precursor* ***2.52***[28]

An excess of $LiAlH_4$ was used to reduce the nitrile functionality of **2.50** to form amine **2.51** in 80% yield.[30] Acid chloride condensation between 5-nitroisophthaloyl dichloride and two equivalents of **2.51**, gave macrocyclic precursor compound **2.52** in 59% yield (Scheme 2.18).[28]

For [2]rotaxane formation, a Grubbs' II catalysed ring-closing metathesis (RCM) reaction between an equimolar mixture of bis-vinyl-functionalised macrocyclic precursor **2.52** and axle **2.44**·Cl was carried out (Scheme 2.19).



Scheme 2.19: *Synthesis of HB rotaxane* ***2.53***·*Cl via chloride-templated Grubbs' (II) catalysed RCM reaction*

After purification *via* preparative TLC, HB rotaxane **2.53**·Cl was isolated in 10% yield, containing the imidazolium–triazole and imidazole–triazolium axle regioisomers, carried forward from the previous step. Anion exchange to the hexafluorophosphate salt was achieved by copious washing with $NH_4PF_{6(aq)}$. The rotaxane was characterised *via* high resolution ESI mass spectrometry. The ^{1}H NMR spectrum of rotaxane **2.53**·Cl clearly showed the splitting of macrocycle hydroquinone resonances χ indicative of aromatic donor-acceptor interactions with the axle component and the desymmetrisation of the proton environments (Figure 2.15). Furthermore, macrocycle alkene protons ε confirm that the ring closing metathesis reaction took place and a signal for the axle triazole proton 3 was also observed. ^{13}C and two-dimensional ROESY NMR spectroscopy spectra were also obtained; however, the presence of the two regioisomer axle components resulted in overlapping signals, which made full assignment of the spectra not feasible.

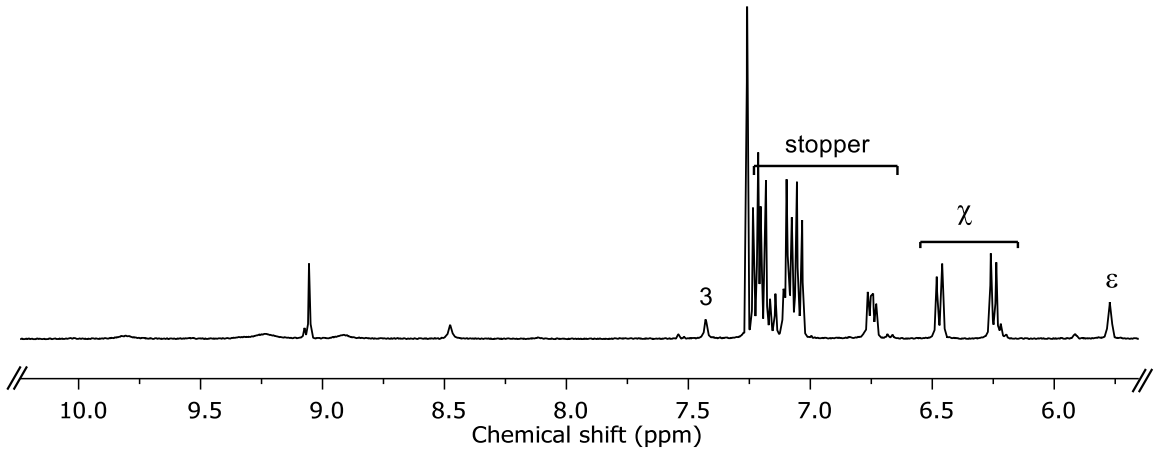
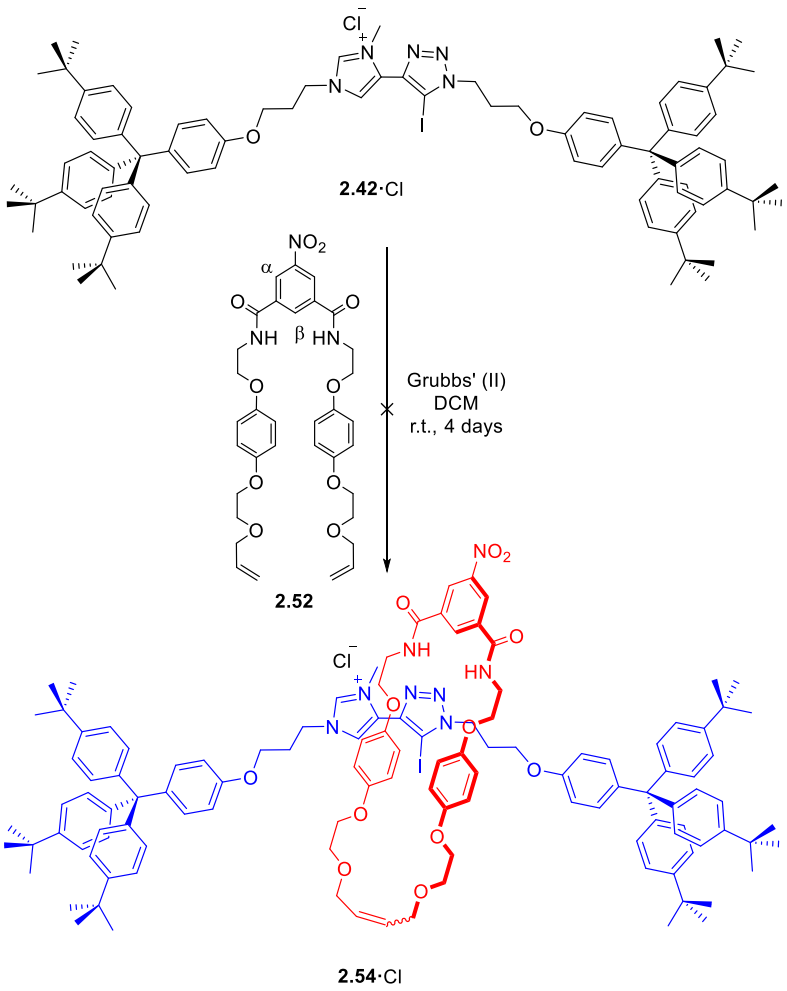


Figure 2.15: *Truncated ^{1}H NMR spectrum of regioisomeric rotaxane* ***2.53***·*Cl ($CDCl_3$, 298 K, 400 MHz)*

The synthesis of the analogous XB rotaxane **2.54**·Cl was attempted under identical conditions with XB axle **2.42**·Cl (Scheme 2.20). Formation of the XB [2]rotaxane was observed by ESI mass spectrometry of the crude reaction mixture; however, the corresponding proto-triazole-containing [2]rotaxane was also observed, indicative of decomposition of the iodotriazole moiety under the reaction conditions employed. Efforts to separate the HB rotaxane from XB rotaxane **2.54**·Cl failed because of their similar

polarity. Therefore, further investigations into the anion binding properties of the XB [2]rotaxane was not possible.



Scheme 2.20: *Attempted synthesis of XB rotaxane* ***2.54****·Cl via chloride-templated Grubbs' (II) catalysed RCM reaction*

2.5.2 Preliminary anion binding studies

Preliminary ^{1}H NMR spectroscopy anion titration studies were carried out to ascertain the binding behaviour of regioisomeric axle containing rotaxane **2.53**·PF_6 with TBAX salts (X = Cl, Br, I) in the competitive solvent mixture $CDCl_3/CD_3OD/D_2O$ (45:45:10). Upon addition of the halide anions, significant downfield shifts were observed for macrocycle proton β and axle proton 2 and 3. A slight downfield movement was also observed for macrocycle proton α. Axle imidazolium proton 1 displayed complete

broadening of the peak. Monitoring the shifts of the axle proton 2, WinEQNMR2[23] analysis of the titration data (Figure 2.16) was carried out and 1:2 (host/guest) stoichiometric association constants were determined (Table 2.3). A modest degree of selectivity was observed, which follows the trend in anion basicity, with chloride bound the strongest. When compared to the analogous acyclic system **2.9**·PF_6 (Table 2.1), the magnitude of association constant for rotaxane **2.53**·PF_6 with chloride was of similar value within error, suggesting chloride was not being bound in the rotaxane interlocked cavity.

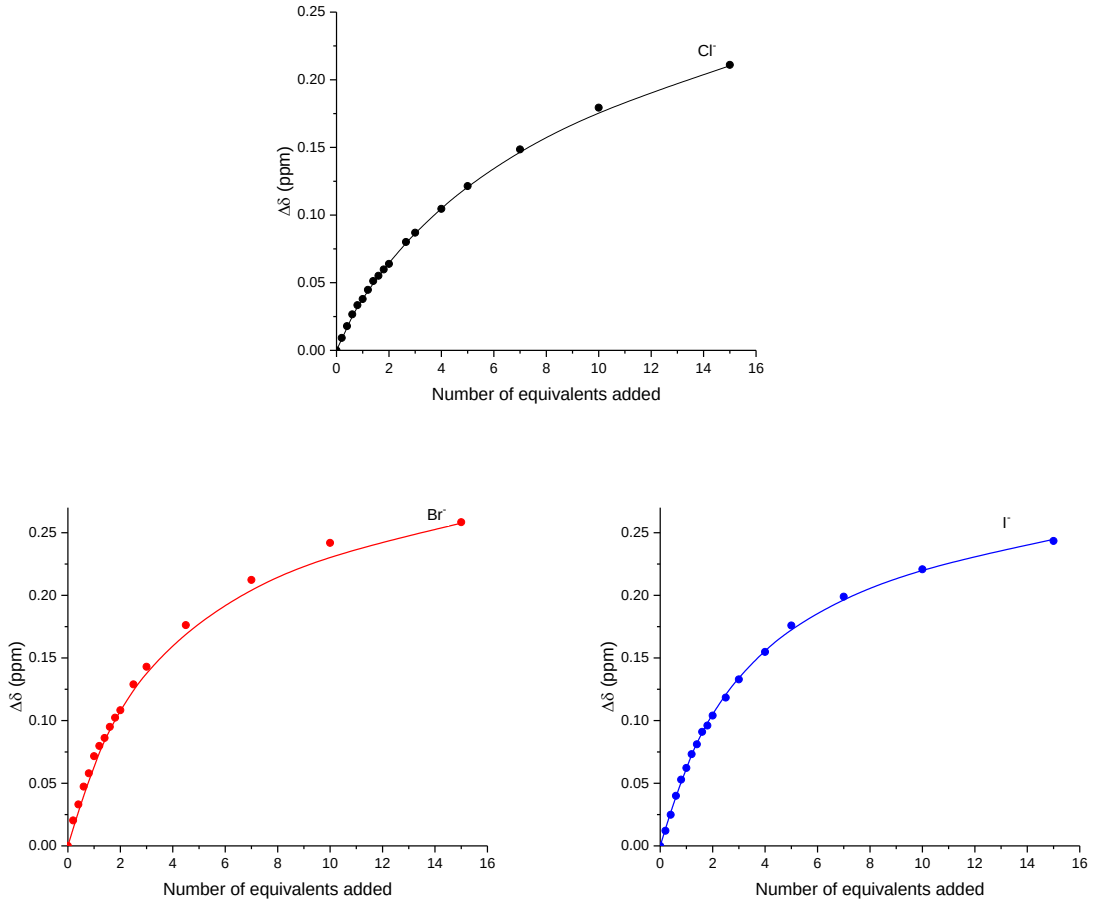


Figure 2.16: *Experimental titration data (points) and calculated 1:2 binding isotherms (lines) for the addition of halides as their TBA salts to rotaxane* ***2.53***·PF_6 *monitoring axle triazole proton ($CDCl_3$/CD_3OD/D_2O 45:45:10, 298 K, 500 MHz)*

Table 2.3: *Anion association constants of HB rotaxane* ***2.53***·PF_6 *after addition of various anions*

Association constants calculated using WinEQNMR2,[23] anions added as their TBA salt, estimated standard errors given in parentheses, 500 MHz, 298 K, solvent $CDCl_3/CD_3OD/D_2O$ (45:45:10)

Anion	K_1 (M^{-1})	K_2 (M^{-1})
Cl^-	3308 (202)	35
Br^-	2345 (224)	89
I^-	1846 (99)	92

2.5.3 Summary

The acyclic systems **2.9**·PF_6 and **2.10**·PF_6 and HB rotaxane **2.53**·PF_6 demonstrate that anion binding in imidazolium-based anion receptor systems is dominated by favourable electrostatic interactions. The strength of anion association appears to be perturbed only weakly by proximal triazole-based HB or XB donors. In all cases, a 1:2 (host/guest) binding stoichiometry is observed, suggesting two binding events are occurring. The evidence advocates that the first binding event, corresponding to K_1, is occurring at the most acidic imidazolium C^2–proton and is dominated by electrostatically driven hydrogen bonding (Figure 2.17a). The second binding event, corresponding to the much weaker K_2, can be attributed to binding utilising the HB/XB donors (Figure 2.17b). Indeed, it has been reported that anion binding to an imidazolium group at the C^2–proton can be best described as charge-*driven* HB, as opposed to the more common charge-*assisted* HB,[31] which is corroborated by these results.

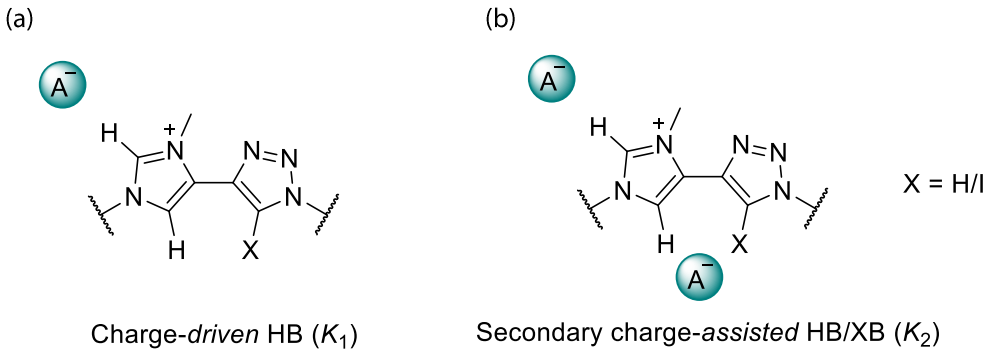


Figure 2.17: *Postulated binding sites to account for dominance of electrostatic binding and 1:2 (host/guest) binding stoichiometry*

2.6 2-Methylimidazolium–triazole motif

To further understand and elucidate the orientation of halide anion binding in the imidazolium–triazole based receptors presented in this chapter, the effect of incorporating a methyl group at the C^2-position, the charge-*driven* binding site of the imidazolium unit, was undertaken (Figure 2.18). It was postulated, that this would diminish the contribution of the electrostatically dominated charge–*driven* hydrogen bond on anion binding and thus result in a significant reduction of anion association strength, concomitant with an increase in selectivity due to the increased contribution of the charge-*assisted* HB interactions.

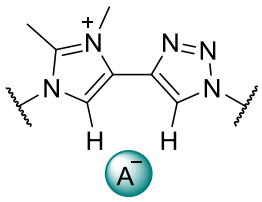
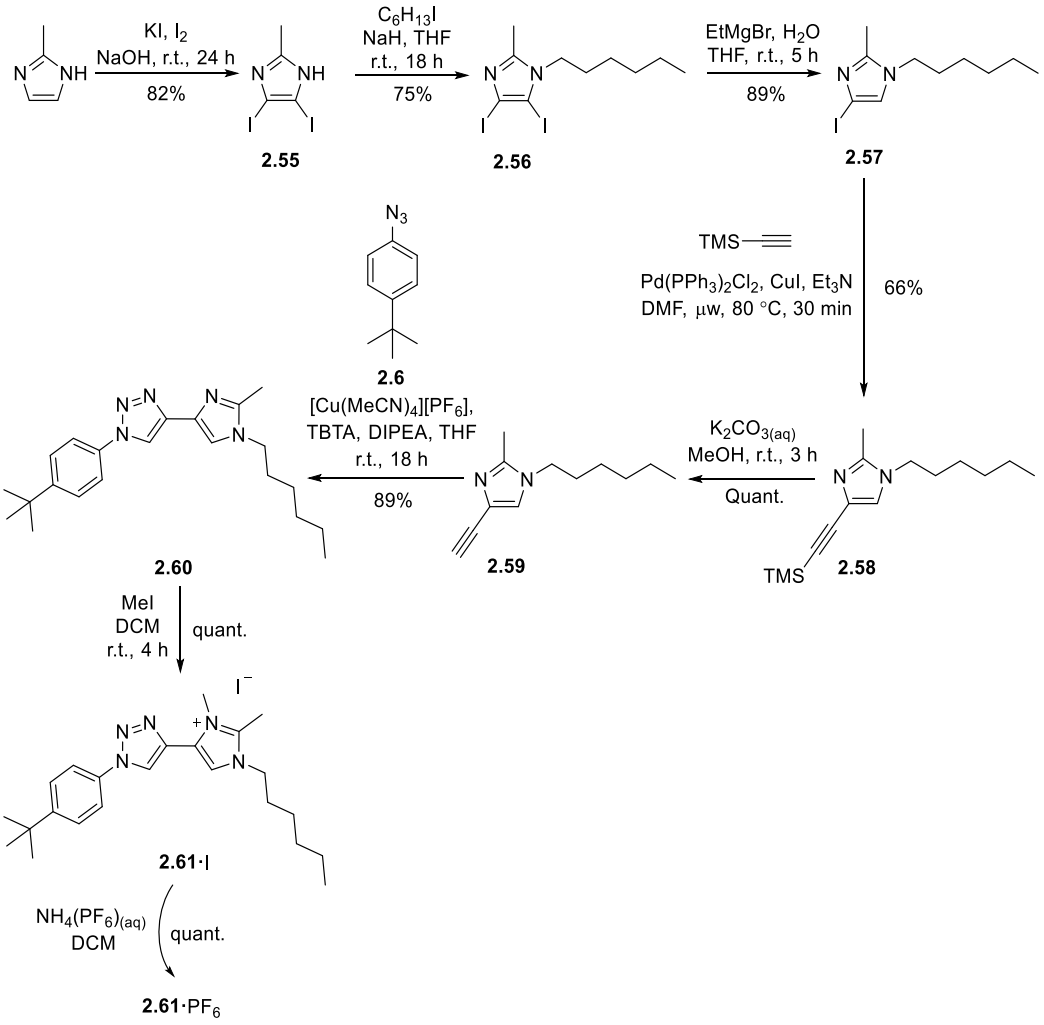


Figure 2.18: *Target 2-methylimidazolium–triazole motif*

2.6.1 Synthesis of acyclic receptor

The target 2-methylimidazolium–triazole motif was incorporated into the acyclic receptor design in an analogous fashion to that discussed in Section 2.2, to allow for direct comparison between all the receptors presented thus far. Firstly, 2-methyl-4,5-diiodoimidazole **2.55** was synthesised from 2-methylimidazole using a modified literature procedure.[17] *N*-alkylation at the N^1-position with 1-iodohexane produced **2.56** in 75% yield. Selective dehalogenation at the 5-position was achieved with ethylmagnesium bromide and quenching with water to produce 2-methyl-4-iodoimidazole **2.57** in 89% yield**.** Sonogashira coupling[17] between **2.57** and trimethylsilyl acetylene produced the trimethylsilyl-protected alkyne **2.58**, which was deprotected using aqueous potassium carbonate in methanol to produce the desired alkyne **2.59** in 66% yield over two steps (Scheme 2.21). The imidazole–triazole derivative **2.60** was formed in 89% yield by employing the CuAAC 'click' reaction between alkyne **2.59** and azide **2.6**. Alkylation

using methyl iodide, followed by anion exchange achieved *via* washing with $NH_4PF_{6(aq)}$ to afford **2.61**·PF_6 in quantitative yield (Scheme 2.21).



Scheme 2.21: *Synthetic route to imidazolium–triazole receptor* ***2.61***·*PF*$_6$

2.6.2 Anion binding studies

The anion binding properties of 2-methylimidazolium–triazole receptor **2.61**·PF_6 were investigated *via* ^{1}H NMR spectroscopy titration experiments, adding aliquots of TBA·Cl in the competitive aqueous-organic solvent mixture $CDCl_3/CD_3OD/D_2O$ (45:45:10). Monitoring the downfield shift of the imidazolium C^5-proton, the binding isotherm shown in Figure 2.19 was generated. WinEQNMR2[23] analysis of the titration data

determined a 1:1 (host/guest) binding stoichiometry with an association constant of K = 64 M^{-1}.

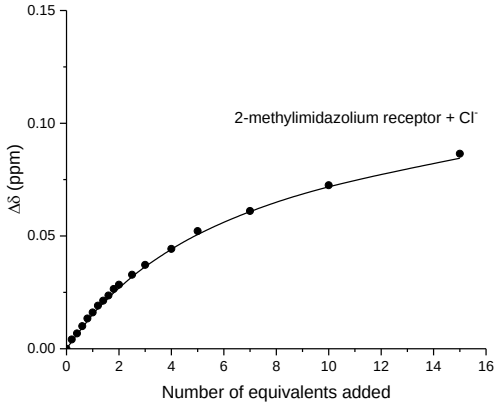
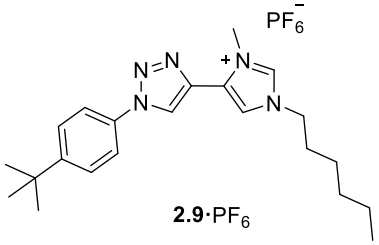
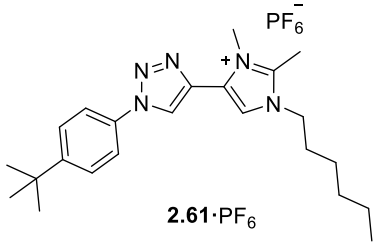


Figure 2.19: *Experimental titration data (points) and calculated 1:1 binding isotherm (line) for the addition of TBA•Cl to 2-methylimidazolium–triazole receptor* ***2.61***•PF_6

Table 2.4: *Chloride binding association constants of HB imidazolium–triazole receptor* ***2.9***•PF_6 *and HB 2-methylimidazolium–triazole receptor* ***2.61***•PF_6

Association constants calculated using WinEQNMR2,[23] chloride added as the TBA salt, estimated standard errors given in parentheses, 500 MHz, 298 K, solvent $CDCl_3/CD_3OD/D_2O$ (45:45:10)

Receptor	K_1 (M^{-1})	K_2 (M^{-1})
 **2.9**·PF_6	3729 (167)	9
 **2.61**·PF_6	64 (3)	-

By introducing a methyl group at the C^2-position on the imidazolium moiety, a drastic reduction in the chloride anion association constant was displayed, from K_1 = 3729 M^{-1} for imidazolium–triazole receptor **2.9**·PF_6 to K = 64 M^{-1} for 2-methylimidazolium–triazole receptor **2.61**·PF_6 (Table 2.4). This clearly demonstrated that the methyl group has blocked the charge-*driven* HB interactions responsible for strong halide binding observed for imidazolium receptors **2.9**·PF_6, **2.10**·PF_6 and **2.53**·PF_6 in the organic–aqueous competitive solvent mixture. Furthermore, upon incorporation of the methyl group, the binding stoichiometry changed from 1:2 (host/guest) to 1:1, confirming the exclusion of a second binding site in **2.61**·PF_6. These results corroborate the postulated anion binding sites of the imidazolium-triazole motif outlined in Figure 2.17 and the dominance of electrostatic charge–*driven* hydrogen bonding exhibited by this motif.

2.7 Conclusions

The research discussed in this chapter has investigated the new imidazolium–triazole and -iodotriazole motifs for anion recognition. Initially, acyclic HB and XB receptors **2.9**·PF_6 and **2.10**·PF_6 were synthesised. The XB receptor demonstrated a modest increase in the chloride anion association constant magnitude compared to the HB analogue in the competitive solvent mixture $CDCl_3/CD_3OD/D_2O$ (45:45:10).

The same motifs were incorporated into macrocyclic structures, **2.26** and **2.27** for [2]rotaxane construction *via* AMT. Synthesis of a [2]rotaxane was attempted using the AMT methodology. No evidence of [2]rotaxane formation was observed, which suggested exotopic coordination of copper(I) catalyst to the macrocycle. The corresponding cationic macrocycles, **2.35**·PF_6 and **2.36**·PF_6 were synthesised, with the aim of forming a [2]rotaxane *via* an anion–templated threading and subsequent stoppering reaction. A qualitative chloride–template pseudorotaxane study displayed no significant shift in the hydroquinone resonances and the greatest perturbation was observed for the external

imidazolium proton. It was concluded the formation of the pseudorotaxane assembly was not observed.

Axles containing the imidazolium–triazole and –iodotriazole motifs were prepared for subsequent chloride-template RCM 'clipping' rotaxanation reaction. The synthesis of cationic HB axle **2.39**·I resulted in the formation of imidazolium–triazole and imidazole–triazolium regioisomers, in a ratio of 4:1. Nevertheless, attempts were made to incorporate the HB and XB axles into [2]rotaxanes. The HB [2]rotaxane **2.53**·Cl was successfully isolated, however the iodotriazole in XB [2]rotaxane **2.54**·Cl decomposed and produced an inseparable mixture of HB and XB [2]rotaxanes.

The HB rotaxane **2.53**·PF_6 containing regioisomeric axle components displayed a moderate degree of selectivity between the halides, following anion basicity trends (Cl^- > Br^- > I^-) in the competitive solvent mixture $CDCl_3/CD_3OD/D_2O$ (45:45:10). The magnitude of the chloride association constant was within error of the analogous acyclic system **2.9**·PF_6, which suggested the formation of the interlocked cavity did not alter the strength of interaction and a dominance of electrostatic binding with this motif.

Finally, an analogous 2-methylimidazolium–triazole receptor **2.61**·PF_6, designed to block the imidazolium C^2-position displayed a substantial 60-fold decrease in the chloride association constant compared to imidazolium–triazole receptor **2.9**·PF_6. This clearly demonstrated the dominance of charge in the imidazolium–triazole motif in driving anion binding and explains both the low selectivity observed in the [2]rotaxane and the equivalent association constants for the acyclic and interlocked systems reported. Moreover, the 1:1 (host/guest) binding stoichiometry observed for 2-methylimidazolium–triazole receptor **2.61**·PF_6 eluded to the removal of a binding site, compared to imidazolium–triazole receptor **2.9**·PF_6.

In conclusion, it has been established that the anion binding properties of the imidazolium–triazole motif described in this chapter should be considered as an electrostatically dominated charge–*driven* hydrogen bonding interaction at the

imidazolium C^2-position with a small contribution from the HB or XB triazole donor groups.

2.8 Future work

The work presented in this chapter could be expanded by incorporating an electron-withdrawing group at the C^2-position of the imidazolium group to increase the strength of anion association; by substituting the methyl group with a nitro group, the acidity of the C^5-proton would be increased, resulting in enhanced anion binding (Figure 2.20).

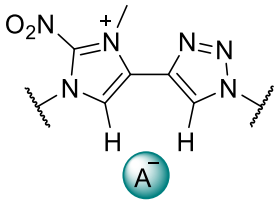


Figure 2.20: *Proposed 2-nitroimidazolium–triazole motif*

Additionally, the strong anion binding at the imidazolium C^2-position could be exploited through careful design by incorporation of other convergent HB/XB donor groups. In the following chapter this idea will be explored, with the integration of a bis(triazole)– and bis(iodotriazole)–imidazolium motif into interlocked structures.

2.9 References

1 H. Weingärtner, *Angew. Chem. Int. Ed.*, 2008, **47**, 654–670.

2 T. Welton, *Chem. Rev.,* 1999, **99**, 2071–2084.

3 M. Deetlefs, K. R. Seddon and M. Shara, *New J. Chem.*, 2006, **30**, 317–326.

4 T. Welton, *Green Chem.*, 2008, **10**, 483.

5 R. D. Rogers and K. R. Seddon, *Science*, 2003, **302**, 792–793.

6 J. Dupont and P. A. Z. Suarez, *Phys. Chem. Chem. Phys.*, 2006, **8**, 2441–2451.

7 K. Binnemans, *Chem. Rev.,* 2005, **105**, 4148–4204.

8 M.-A. Neouze, *J. Mater. Chem.*, 2010, **20**, 9593–9607.

9 J. Dupont and J. D. Scholten, *Chem. Soc. Rev.*, 2010, **39**, 1780–1804.

10 H. Jacobsen, A. Correa, A. Poater, C. Costabile and L. Cavallo, *Coord. Chem. Rev.*, 2009, **253**, 687–703.

11 K. Chellappan, N. J. Singh, I.-C. Hwang, J. W. Lee and K. S. Kim, *Angew. Chem. Int. Ed.*, 2005, **44**, 2899–2903.

12 G. T. Spence, C. J. Serpell, J. Sardinha, P. J. Costa, V. Félix and P. D. Beer, *Chem. Eur. J.*, 2011, **17**, 12955–12966.

13 A. Caballero, F. Zapata, N. G. White, P. J. Costa, V. Félix and P. D. Beer, *Angew. Chem. Int. Ed.*, 2012, **51**, 1876–1880.

14 M. S. Vickers, K. S. Martindale and P. D. Beer, *J. Mater. Chem.*, 2005, **15**, 2784–2790.

15 Y. Cui, H.-J. Mo, J.-C. Chen, Y.-L. Niu, Y.-R. Zhong, K.-C. Zheng and B.-H. Ye, *Inorg. Chem.,* 2007, **46**, 6427–6436.

16 M. J. MacLeod and J. A. Johnson, *J. Am. Chem. Soc.*, 2015, **137**, 7974–7977.

17 A. H. Sandtorv and H.-R. Bjørsvik, *Eur. J. Org. Chem.*, 2015, **2015**, 4658–4666.

18 J. Zhang, Y. Zhang, W. F. K. Schnatter and J. W. Herndon, *Organometallics*, 2006, **25**, 1279–1284.

19 K. Sonogashira, Y. Tohda and N. Hagihara, *Tetrahedron Lett.*, 1975, **16**, 4467–4470.

20 W. S. Brotherton, R. J. Clark and L. Zhu, *J. Org. Chem.*, 2012, **77**, 6443–6455.

21 T. K. Mole, W. E. Arter, I. Marques, V. Félix and P. D. Beer, *J. Organomet. Chem.*, 2015, **792**, 206–210.

22 B. R. Mullaney, A. L. Thompson and P. D. Beer, *Angew. Chem. Int. Ed.*, 2014, **53**, 11458–11462.

23 M. J. Hynes, *J. Chem. Soc. Dalton Trans.*, 1993, **0**, 311–312.

24 D. A. W. Ross, P. A. Scattergood, A. Babaei, A. Pertegás, H. J. Bolink and P. I. P. Elliott, *Dalton Trans.*, 2016, **45**, 7748–7757.

25 F. E. Lytle and D. M. Hercules, *J. Am. Chem. Soc.*, 1969, **91**, 253–257.

26 J. Y. C. Lim, T. Bunchuay and P. D. Beer, *Chem. Eur. J.*, 2017, **23**, 4700–4707.

27 V. Aucagne, K. D. Hänni, D. A. Leigh, P. J. Lusby and D. B. Walker, *J. Am. Chem. Soc.,* 2006, **128**, 2186–2187.

28 M. R. Sambrook, P. D. Beer, M. D. Lankshear, R. F. Ludlow and J. A. Wisner, *Org. Biomol. Chem.*, 2006, **4**, 1529–1538.

29 K. Bala and H. C. Hailes, *Synthesis.*, 2005, 19, 3423–3427.

30 M. D. Lankshear, N. H. Evans, S. R. Bayly and P. D. Beer, *Chem. Eur. J.*, 2007, **13**, 3861–3870.

31 G. T. Spence and P. D. Beer, *Acc. Chem. Res.*, 2013, **46**, 571–586.

Chapter Three

Bis(triazole)–imidazolium and –benzimidazolium based systems for anion recognition

3.1 Introduction

The work presented in Chapter two demonstrated the highly electrostatic nature of anion binding exhibited by the imidazolium–triazole and –iodotriazole motifs. Through modification to incorporate a methyl group at the C^2-position of the imidazolium moiety the magnitude of the anion association constants was notably diminished, demonstrating the significant contribution of charge-*driven* hydrogen bonding at this position. Indeed, Tsuzuki *et al.* determined the centre of the imidazolium positive charge to be located at the midpoint between the two nitrogen atoms and the calculated interaction energy with an anion to be inversely proportional in attraction to the distance.[1] As a consequence, charge–charge interactions dominate and are affected by the distance of the anion from the centre of the positive charge of the imidazolium moiety. Importantly, the distance from the nearest hydrogen atom is not the main factor determining the strength of the attraction.[1] This was confirmed by Beer *et al.* who investigated the effect of manipulating the orientation of the imidazolium motif with respect to potential HB for anion binding. The 4,5-dimethylimidazolium system exhibited considerably greater binding of chloride (K = 3044 M^{-1}) compared to the 2-methylimidazolium system (K = 782 M^{-1}) in $CDCl_3$, due to the smaller distance between the associated anion and the centre of the imidazolium positive charge (Figure 3.1).[2]

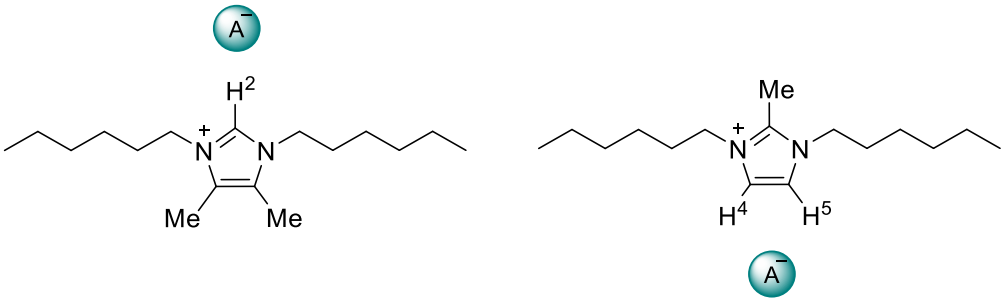


Figure 3.1: *Beer's 4,5-dimethylimidazolium and 2-methylimidazolium receptors*[2]

Therefore, it would be advantageous to incorporate the imidazolium heterocycle into a motif that is designed to exploit the strong binding at the imidazolium C^2-position with convergent XB donors. Taking a positively charged moiety and appending two convergent iodotriazoles is a strategy that has been successfully exploited in the design of anion-receptors. A well-documented example is the XB 3,5-bis-iodotriazole–pyridinium moiety, demonstrated by Beer *et al.* to display potent anion binding in competitive aqueous–organic media (Figure 3.2). Incorporated into a [2]catenane, anion recognition was notably superior in the XB derivative compared to the HB analogue, with association constants for iodide in the competitive $CDCl_3/CD_3OD/D_2O$ (45:45:10) solvent mixture of $K = >10^4$ and 510 M^{-1} respectively.[3]

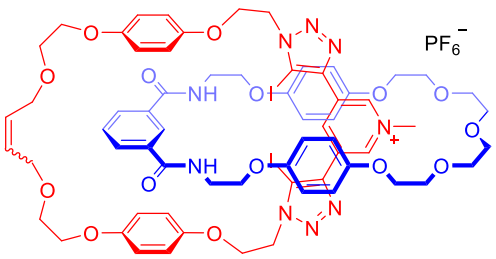


Figure 3.2: *Beer's bis-iodotriazole-pyridinium containing [2]catenane*[3]

To date, no investigations have been carried out employing the imidazolium group in an analogous system, combining the charge-*driven* HB of the imidazolium with convergent XB donors of two iodotriazole moieties.

3.2 Chapter aims

This chapter aims to build on Chapter Two by investigating the symmetric bis(triazole)–imidazolium and bis(triazole)–benzimidazolium HB moieties and their corresponding XB analogues for anion recognition applications (Figure 3.3). The anion receptor design utilises the charge–driven hydrogen bonding at the imidazolium/benzimidazolium C^2-proton in a convergent manner with appended HB and XB triazole donors. Attempts to incorporate the motifs into both the axle and the macrocycle components of interlocked structures are outlined and a comparison of anion binding properties with previous systems (Chapter Two) discussed.

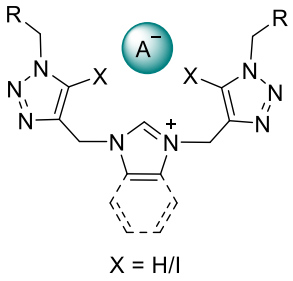


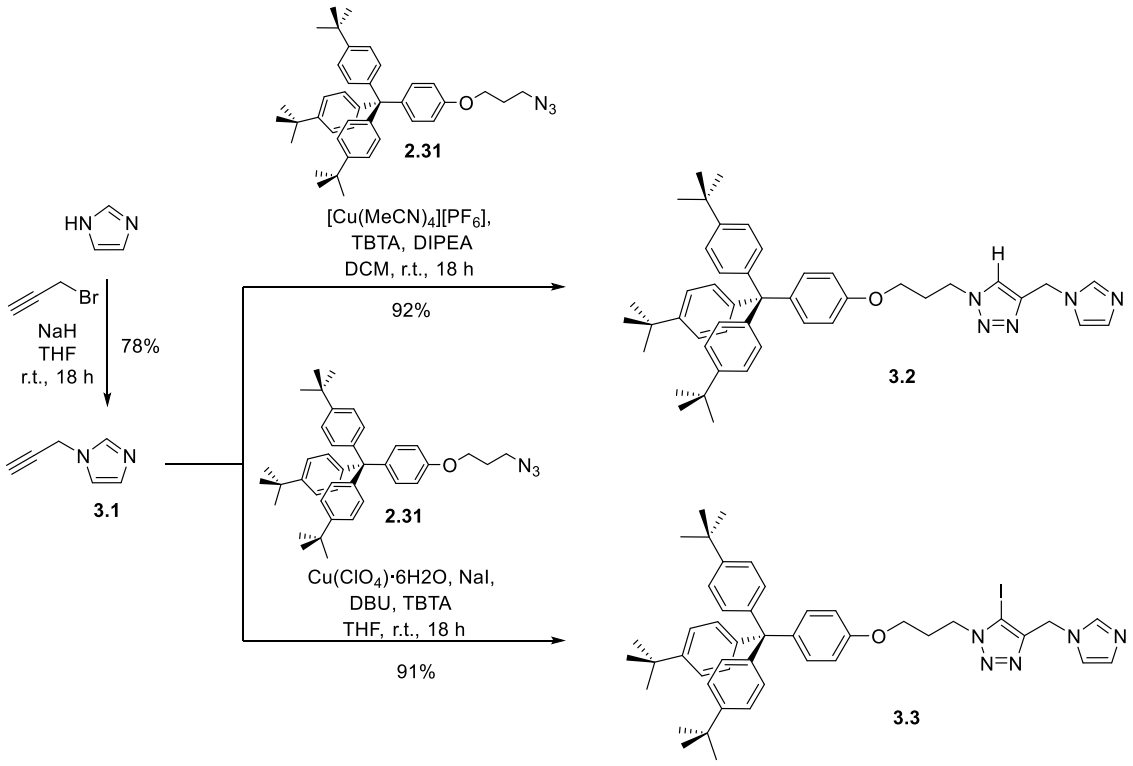
Figure 3.3: *Target symmetric bis(triazole)–imidazolium and bis(triazole)–benzimidazolium motifs and the XB analogues*

3.3 Bis(triazole)– and bis(iodotriazole)–imidazolium containing [2]rotaxanes

The initial synthetic strategy employed was to incorporate the bis(triazole)– and bis(iodotriazole)–imidazolium motif into a [2]rotaxane using the active–metal template (AMT) synthetic methodology. In particular, a stopper triazole–imidazolium–alkyne axle precursor was synthesised and subsequently used in an AMT CuAAC reaction with a suitable stopper azide axle precursor and macrocycle with the aim of forming the corresponding [2]rotaxane.

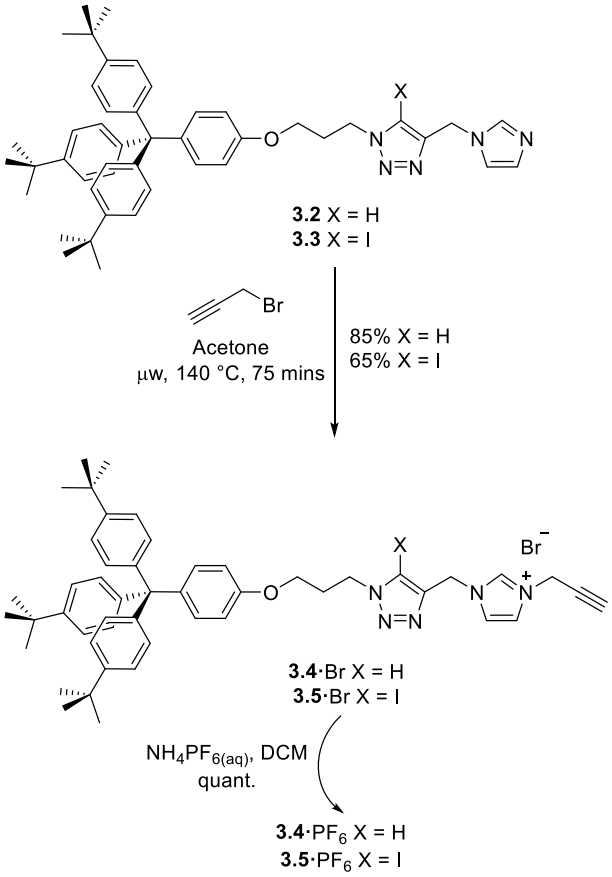
3.3.1 Synthesis of imidazolium–alkyne axle precursor

Firstly, the imidazolium–alkyne axle precursor was targeted. *N*-alkylation of imidazole at the N^1-position with propargyl bromide produced alkyne **3.1** in 78% yield and subsequent CuAAC 'click' reaction with stopper azide **2.31** afforded the proto-click product **3.2** in 92% yield (Scheme 3.1). Utilising the 'one-pot iodo-click' reaction[4] the XB iodotriazole analogue **3.3** was synthesised in 91% yield.



Scheme 3.1: *Synthesis of stoppered HB triazole–imidazole species* ***3.2*** *and corresponding XB species* ***3.3***

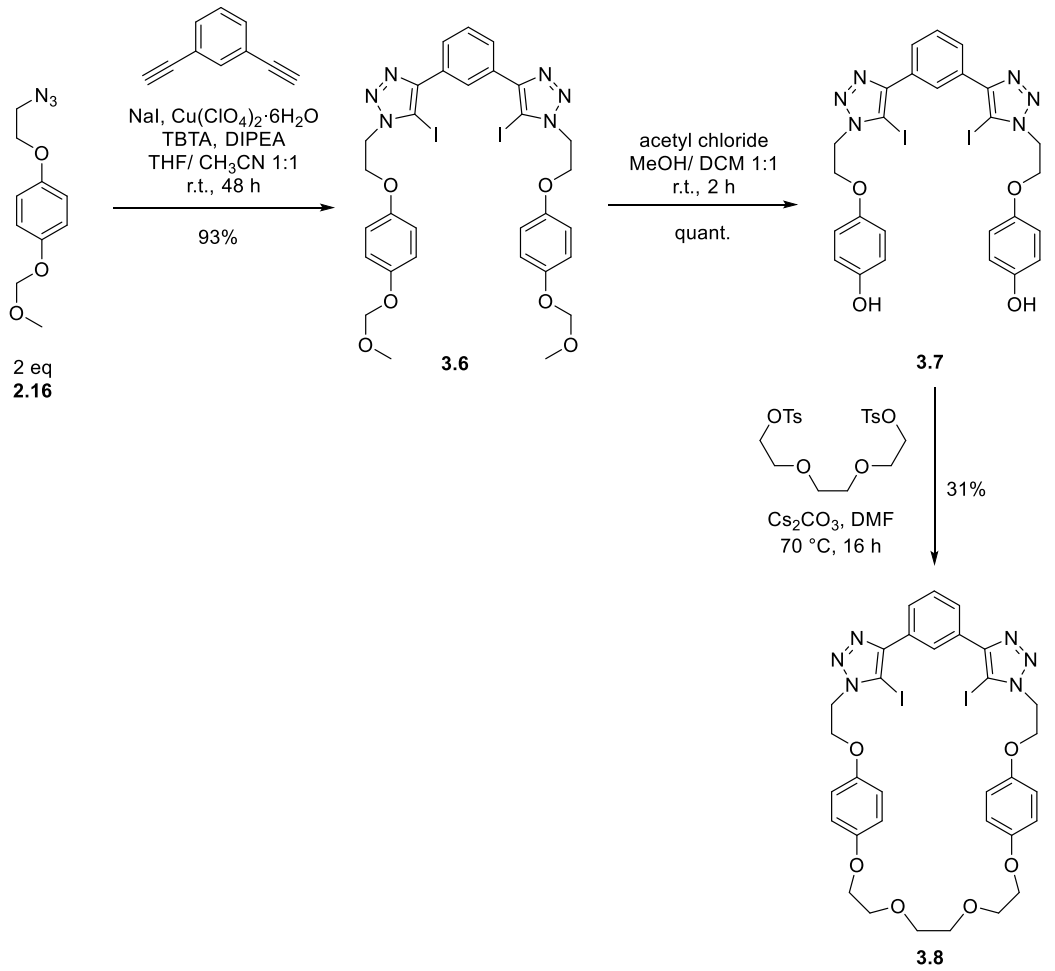
Further *N*-alkylation of **3.2** and **3.3** at the imidazole N^3-position with propargyl bromide under microwave irradiation produced imidazolium–alkyne species **3.4**·Br and **3.5**·Br, in 85% and 65% yield respectively (Scheme 3.2). No further purification was necessary, with the pure product precipitating from solution in both cases. Anion exchange to the non-coordinating hexafluorophosphate salt was carried out by copious washing with $NH_4PF_{6(aq)}$ to afford alkynes **3.4**·PF_6 and **3.5**·PF_6. This was carried out in preparation for the subsequent CuAAC 'click' reaction, to ensure the counter–anion of the imidazolium–alkyne species could not coordinate to the copper (I) catalyst employed and interfere with the reaction.



Scheme 3.2: *Synthesis of HB imidazolium–alkyne* ***3.4***·PF_6 *and XB imidazolium–alkyne* ***3.5***·PF_6

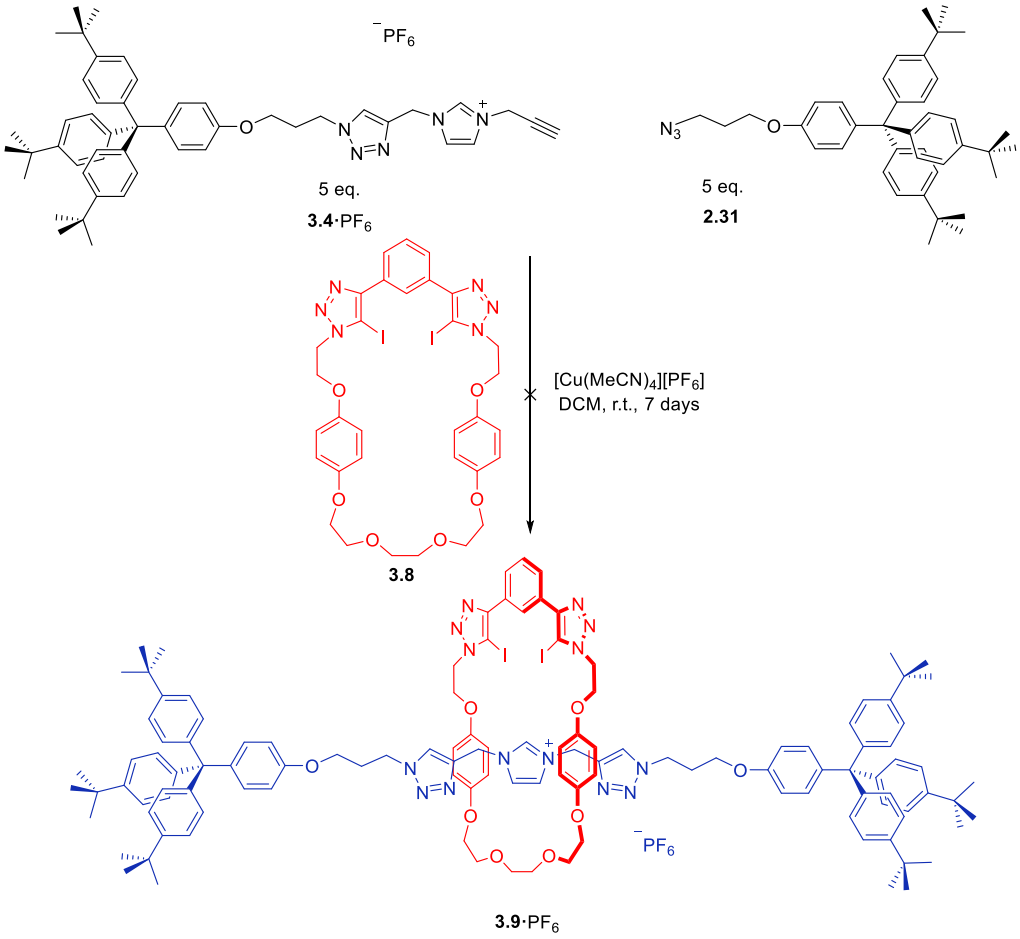
3.3.2 Attempted active–metal template synthesis of [2]rotaxane

A previously reported bis(iodotriazole) macrocycle for use in AMT reactions was synthesised *via* literature procedures.[5] Two equivalents of MOM-protected azide **2.16** was reacted with 1,3-diethynylbenzene under 'one-pot iodo-click' conditions to afford bis(iodotriazole) compound **3.6** in 93% yield (Scheme 3.3). Removal of the MOM protecting groups was achieved using *in-situ* generated hydrochloric acid from the reaction of acetyl chloride and methanol, to give bis-phenol **3.7**, quantitatively. Bis-phenol **3.7** was reacted with triethylene glycol bis-tosylate under basic conditions using an excess of caesium carbonate in DMF at high dilution to afford bis(iodotriazole) macrocycle **3.8** in 31% yield (Scheme 3.3).



Scheme 3.3: *Synthetic route to bis(iodotriazole) macrocycle* ***3.8***

Adapting a previously reported procedure,[5] the AMT reaction was carried out with bis(iodotriazole) macrocycle **3.8** and a stoichiometric quantity of $[Cu(MeCN)_4][PF_6]$, together with five equivalents of stopper azide **2.31** and stopper imidazolium–alkyne **3.4**·PF_6 (Scheme 3.4). The progress of the reaction was monitored *via* ESI mass spectrometry and after two days showed a signal corresponding to the interlocked structure (m/z = 2171), the formation of axle and the presence of unreacted imidazolium–alkyne **3.4**·PF_6. Additionally, TLC confirmed the presence of unreacted stopper azide **2.31** and imidazolium–alkyne **3.4**·PF_6. A second equivalent of $[Cu(MeCN)_4][PF_6]$ was added in an attempt to drive the reaction to completion; however, after a total of seven days, azide and alkyne were both still present, as confirmed by ESI mass spectrometry and TLC. Attempts to isolate the [2]rotaxane were carried out *via* preparative TLC using a range of eluents, but only axle and starting materials could be isolated. The presence of unreacted azide and alkyne, even after the further addition of $[Cu(MeCN)_4][PF_6]$ was postulated to be due to the cationic charge on the imidazolium–alkyne species hindering the 'click' reaction through repulsion of the copper(I) catalyst and obstruction of coordination to the alkyne. Consequently, the synthesis of a [2]rotaxane using this route could not afford a sufficient amount of interlocked product to allow for its successful isolation.

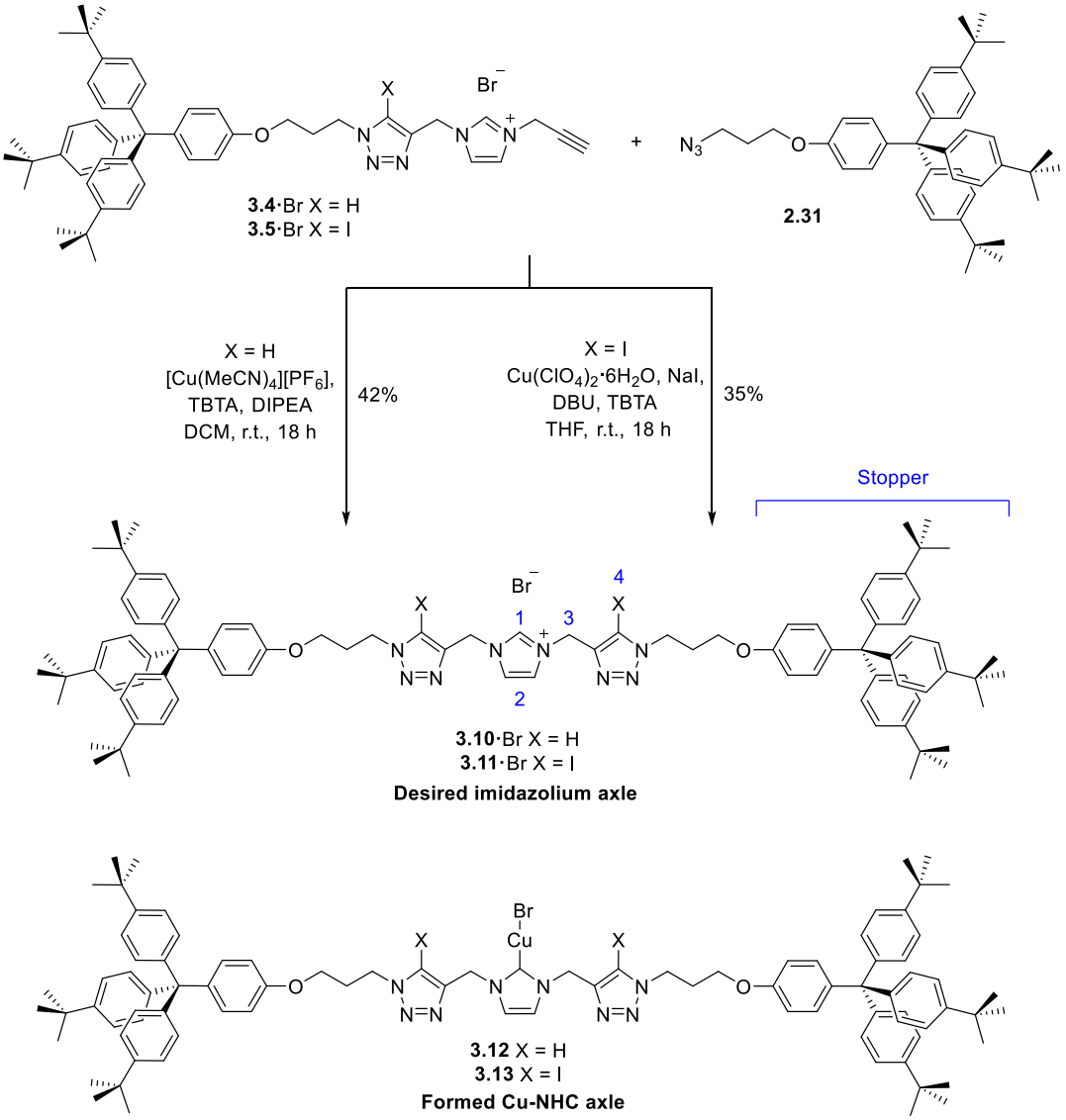


Scheme 3.4: *Attempted AMT synthesis of rotaxane* ***3.9***·PF_6

3.3.3 Synthesis of HB and XB axles

Attention turned to the incorporation of the bis(triazole)– and bis(iodotriazole)–imidazolium motifs into the axle component of a [2]rotaxane *via* a chloride-template 'clipping' strategy using the Grubbs' (II) catalysed RCM reaction with a bis-vinyl functionalised isophthalamide-based macrocycle precursor. Initially, the axle component was targeted. Imidazolium–alkyne **3.4**·Br and stopper azide **2.31** were reacted in a CuAAC 'click' reaction; the corresponding 'one-pot iodo-click' reaction was performed on XB imidazolium–alkyne **3.5**·Br (Scheme 3.5). Analysis of the ^{1}H NMR spectra of the isolated products initially suggested successful axle formation with a clear singlet observed corresponding to the methylene units, integrating to four; however, the disappearance of the imidazolium proton from the ^{1}H NMR spectrum concomitant with a greater TLC Rf value than would be expected for a cationic species was also observed (Figure 3.4a). It was postulated that in the presence of Cu(I) and base from the CuAAC 'click' reaction reagents, the imidazolium moiety had formed the Cu-NHC species **3.12** and **3.13**. To isolate the desired 'free' imidazolium axles **3.10**·PF_6 and **3.11**·PF_6, Cu-NHC axles **3.12** and **3.13** were treated with trifluoroacetic acid in DCM for ten minutes and washed with $NH_4PF_{6(aq)}$. Subsequently, a signal corresponding to the imidazolium proton was observed in the ^{1}H NMR spectra of **3.10**·PF_6 and **3.11**·PF_6 and a more typical shift of 7.4 ppm was observed for the triazole proton in the HB axle (Figure 3.4b).

Subsequent anion exchange to the chloride salt in preparation for anion-template rotaxane formation was achieved through successive washing with $NH_4Cl_{(aq)}$ to afford HB axle **3.10**·Cl and XB axle **3.11**·Cl, in overall 42% and 35% yield, respectively.



Scheme 3.5: *Attempted synthesis of HB bis(triazole)–imidazolium axle* ***3.10***·*Cl and XB bis(iodotriazole)–imidazolium axle* ***3.11***·*Cl and observed Cu-NHC axles,* ***3.12*** *and* ***3.13***

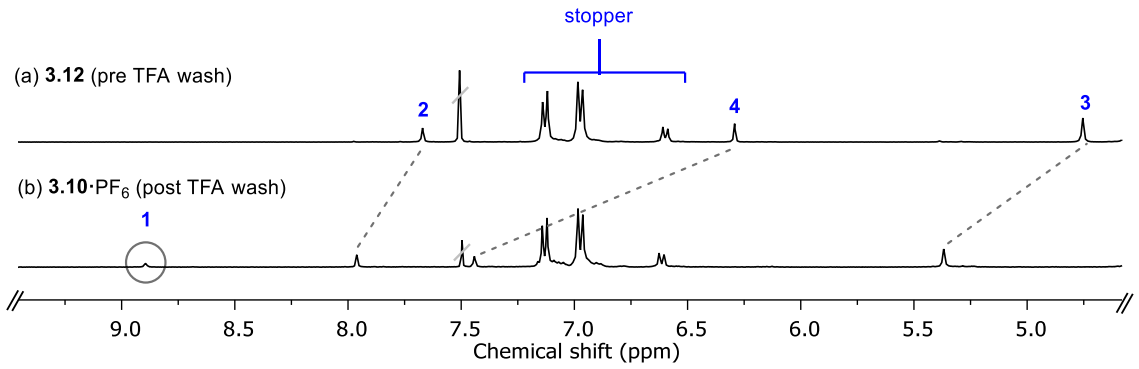
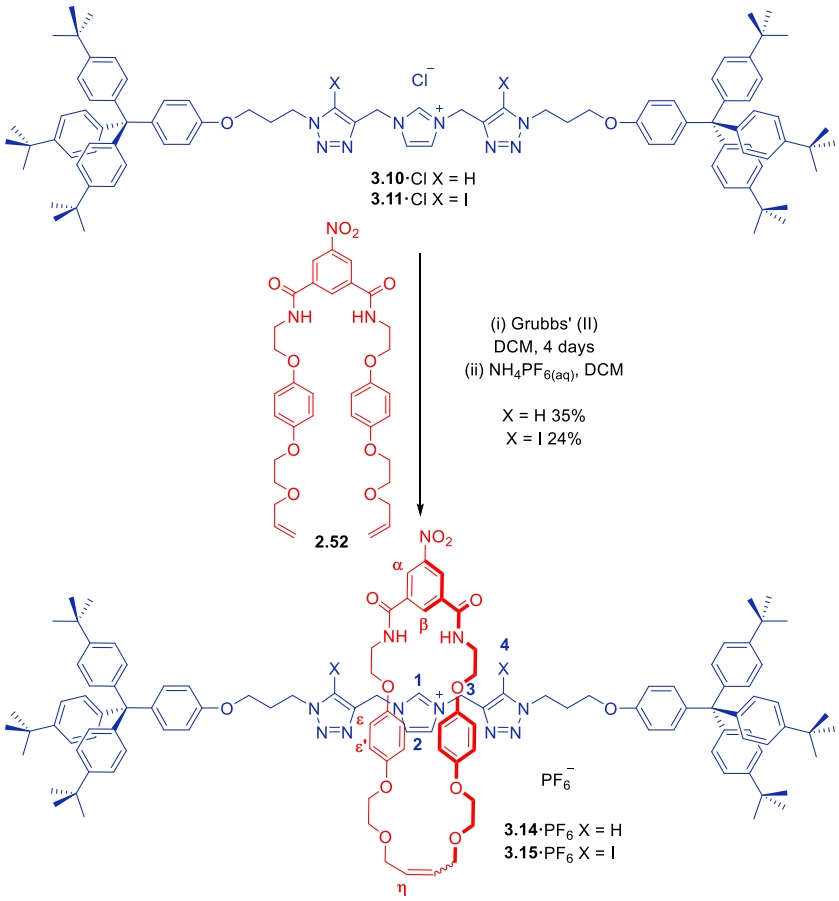


Figure 3.4: *Truncated* ^{1}*H NMR spectra of (a) axle* ***3.12*** *as isolated from the reaction, and (b) axle* ***3.10***·PF_6 *after washing with TFA and exchanging to the* PF_6^- *salt (400 MHz, 1:1* $CDCl_3/CD_3OD$*, 298 K)*

3.3.4 Incorporation into a [2]rotaxane

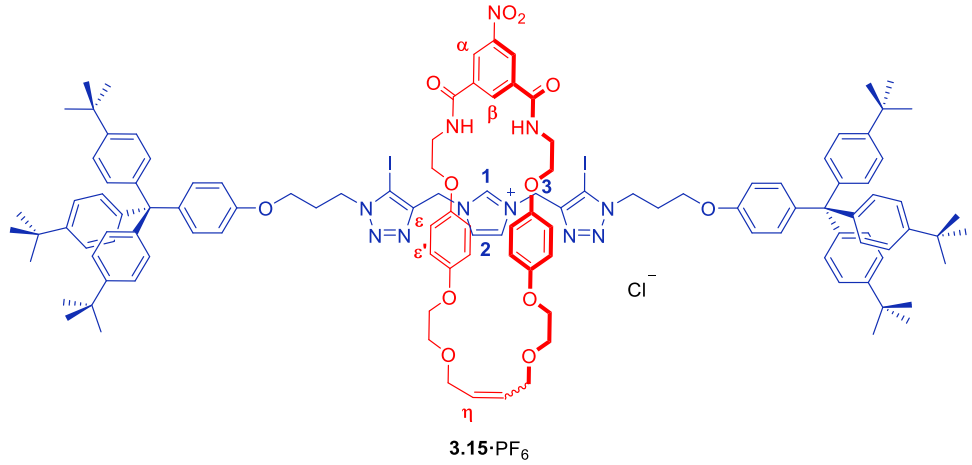
Following the successful synthesis of axles **3.10**·Cl and **3.11**·Cl, rotaxanes **3.14**·Cl and **3.15**·Cl were prepared. A chloride-template assembly was formed between an equimolar mixture in DCM of each axle and bis-vinyl functionalised macrocycle precursor **2.52**, the synthesis of which was outlined in Section 2.5.1,[5] and a subsequent Grubbs' II catalysed RCM reaction afforded XB and HB interlocked structures (Scheme 3.6). Purification was carried out by preparative TLC using 95:5 EtOAc/MeOH to remove the macrocyclic co-product species, followed by 97:3 DCM/MeOH. Anion exchange to the non-coordinating hexafluorophosphate salt for anion binding studies was achieved by copious washing with $NH_4PF_{6(aq)}$ to afford rotaxanes **3.14**·PF_6 and **3.15**· PF_6 in 35% and 24% yield, respectively. Both novel rotaxanes were characterised *via* high resolution ESI mass spectrometry and ^1H and ^{13}C NMR spectroscopy.



Scheme 3.6: *Synthesis of rotaxanes **3.14**·PF_6 and **3.15**·PF_6 via Grubbs' II ring-closing metathesis reaction with vinyl appended macrocycle precursor **2.52***

Evidence for the successful formation of XB rotaxane **3.15**·Cl was shown through comparison of ^{1}H NMR spectra of the interlocked product, the macrocycle precursor **2.52** and axle **3.11**·Cl (Figure 3.5). Upon rotaxane formation, an upfield shift of imidazolium proton *2* was observed. The signals associated with the macrocycle component hydroquinone environments (*ε*,*ε'*) split and moved significantly upfield. These diagnostic shifts were due to the favourable donor-acceptor interactions between the electron-deficient imidazolium axle and the electron-rich hydroquinone groups of the macrocycle, indicating the interlocked nature of the product. Substantial downfield shifts of the aromatic protons (*α*, *β*) of the macrocycle were also observed. Furthermore, the resonance associated with the terminal alkene protons *η* confirmed the ring-closing reaction had been successful. Similar chemical shift differences were observed in the ^{1}H NMR spectrum of HB rotaxane **3.14**·PF_6.

Further evidence for the interlocked nature of **3.15**·PF_6 was obtained by two-dimensional ROESY NMR spectroscopy, which revealed through-space interactions including those between the axle methylene spacer resonance *3* and both the internal aromatic proton *β* and hydroquinone protons *ε'* of the macrocycle component (Figure 3.6).



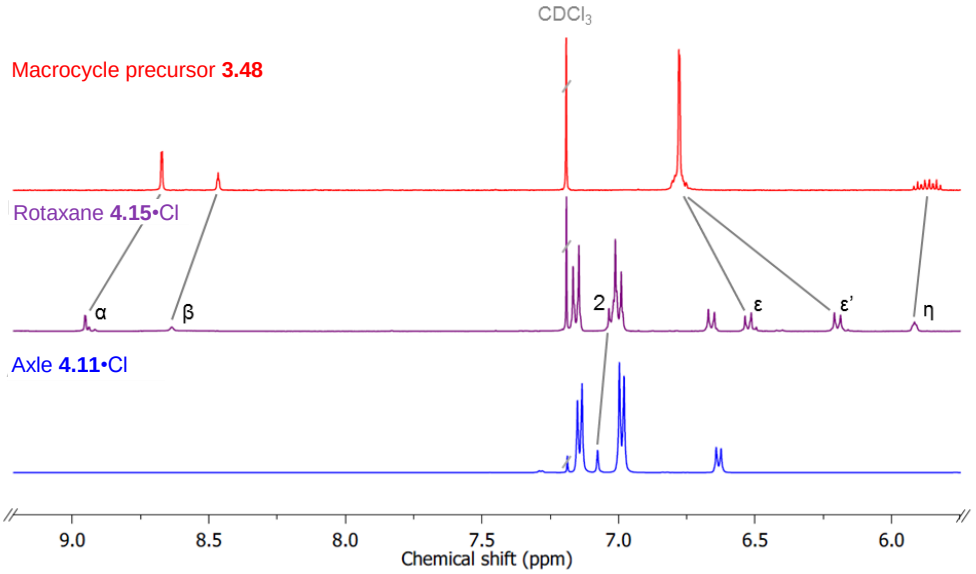


Figure 3.5: *Comparison of truncated ^{1}H NMR spectra of macrocycle precursor **2.52**, axle **3.11**•Cl and rotaxane **3.15**•Cl indicating proton shifts due to rotaxane formation ($CDCl_3$, 500 MHz, 298 K)*

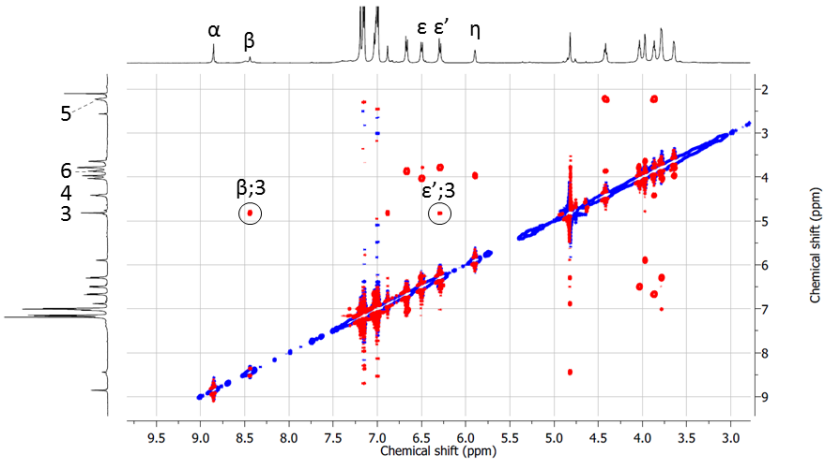


Figure 3.6: *Truncated 2D ROESY NMR spectrum of rotaxane **3.15**•PF_6 showing selected through-space ^{1}H–^{1}H correlations indicative of an interlocked assembly ($CDCl_3$, 500 MHz, 298 K)*

3.3.5 Anion binding studies

The anion binding properties of rotaxanes **3.14**·PF_6 and **3.15**·PF_6 were investigated by ^{1}H NMR titration experiments using TBA salts of a variety of anions in the competitive aqueous-organic solvent mixture $CDCl_3/CD_3OD/D_2O$ (45:45:10). Addition of chloride, bromide, iodide and sulfate resulted in significant downfield shifts of internal macrocycle proton *β* (~ 0.2-0.3 ppm) and a downfield shift of axle triazole proton *4* (~ 0.1 ppm) for HB rotaxane **3.14**·PF_6. Similarly, XB rotaxane **3.15**·PF_6 also displayed a downfield shift of internal macrocycle proton *β* (~ 0.2 ppm). Monitoring the shifts of macrocycle proton *β*, WinEQNMR2[6] analysis of the titration data (Figure 3.7) was carried out and 1:2 (host/guest) stoichiometric association constants were determined, with the K_2 values being of much smaller magnitude than K_1 (Table 3.1). Both XB and HB rotaxanes exhibited strong halide and sulfate binding in the competitive solvent mixture. It is noteworthy that the XB rotaxane **3.15**·PF_6 displayed an enhanced association constant for bromide over the HB rotaxane analogue **3.14**·PF_6. Furthermore, XB rotaxane showed a preference for the relatively smaller anions ($Cl^- = Br^- > SO_4^{2-} > I^-$), whereas HB rotaxane displayed no pronounced selectivity between Cl^-, I^- and SO_4^{2-}. This was attributed to possible steric hindrance effects on binding of larger anions imparted by the XB rotaxane's axle iodotriazole motifs. Moreover, it was postulated the imidazolium methylene spacer groups present in the axles of the rotaxanes allowed for significant flexibility both within the axle and between the components of the interlocked host, resulting in binding domains capable of accommodating a range of anionic guest species. A previously synthesised rotaxane (Chapter two, **2.53**·PF_6) utilised a more rigid covalently linked imidazolium–triazole moiety and displayed greater selectivity between halides ($Cl^- > Br^- > I^-$) following the trend in anion basicity. The flexibility introduced in rotaxanes **3.14**·PF_6 and **3.15**·PF_6 however, could prove useful for incorporation into [3]rotaxanes, allowing for the binding of larger oxoanions in the binding cavity formed between two macrocycles in a higher order interlocked structure.

(a) (b)

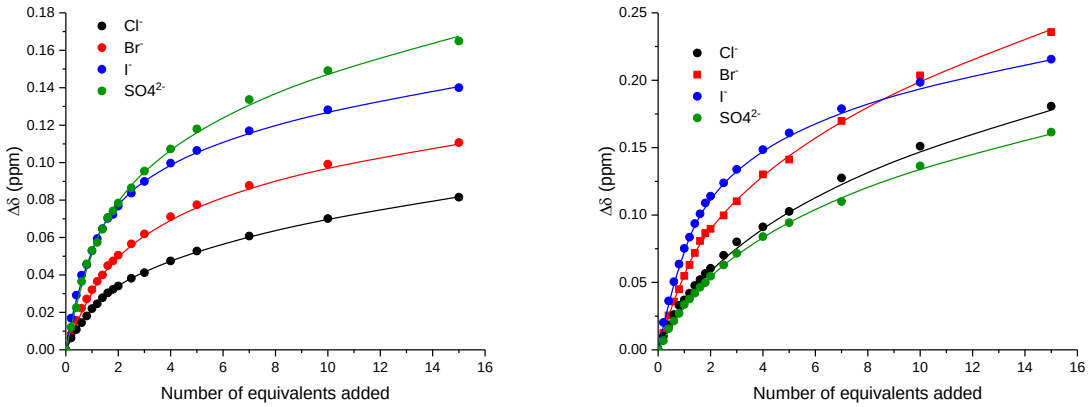


Figure 3.7: *Experimental titration data (points) and calculated 1:2 binding isotherms (lines) for the addition of anions as their TBA salts to (a) HB rotaxane* ***3.14***·PF_6*, and (b) XB rotaxane* ***3.15***·PF_6 *monitoring internal macrocycle proton β ($CDCl_3$/CD_3OD/D_2O 45:45:10, 298 K, 500 MHz)*

Table 3.1: *Association constants K_a (M^{-1}) for HB rotaxane* ***3.14***·PF_6 *and XB rotaxane* ***3.15***·PF_6 *with various anions in $CDCl_3$/CD_3OD/D_2O (45:45:10)*

Anion	**HB (3.14**·PF_6)		**XB** (**3.15**·PF_6)	
	K_1 (M^{-1})	K_2 (M^{-1})	K_1 (M^{-1})	K_2 (M^{-1})
Cl^-	2960 (83)	41	3080 (124)	51
Br^-	2110 (73)	77	3200 (132)	41
I^-	2803 (230)	72	2360 (88)	66
SO_4^{2-}	3130 (231)	67	2650 (193)	61

Calculated using WinEQNMR2,[6] estimated standard errors (in parentheses). Anions added as TBA salts. [receptor] = 1 mM, 500 MHz, 298 K

3.4 Attempted synthesis of hetero[3]rotaxane utilising active–metal and anion–template methods

The synthesis of a hetero[3]rotaxane combining both active–metal and anion–template methods was attempted. Ambitiously, it was envisaged that a chloride-template pseudorotaxane with an axle precursor containing a terminal alkyne, could subsequently be used in a AMT CuAAC 'click' reaction with stopper azide and a suitable copper(I) coordinating macrocycle to produce a hetero[3]rotaxane (Figure 3.8). It was postulated that the synthesis of a [2]rotaxane utilising AMT with a imidazolium–alkyne species was unsuccessful (Section 3.3.2) due to the positive charge of the imidazolium being in close proximity to the alkyne, resulting in the repulsion of the copper(I) catalyst. In this case, it was envisaged that through the chloride anion-template formation of a pseudorotaxane, the charge of the imidazolium would be attenuated and allow for successful CuAAC 'click' reaction at the terminal alkyne.

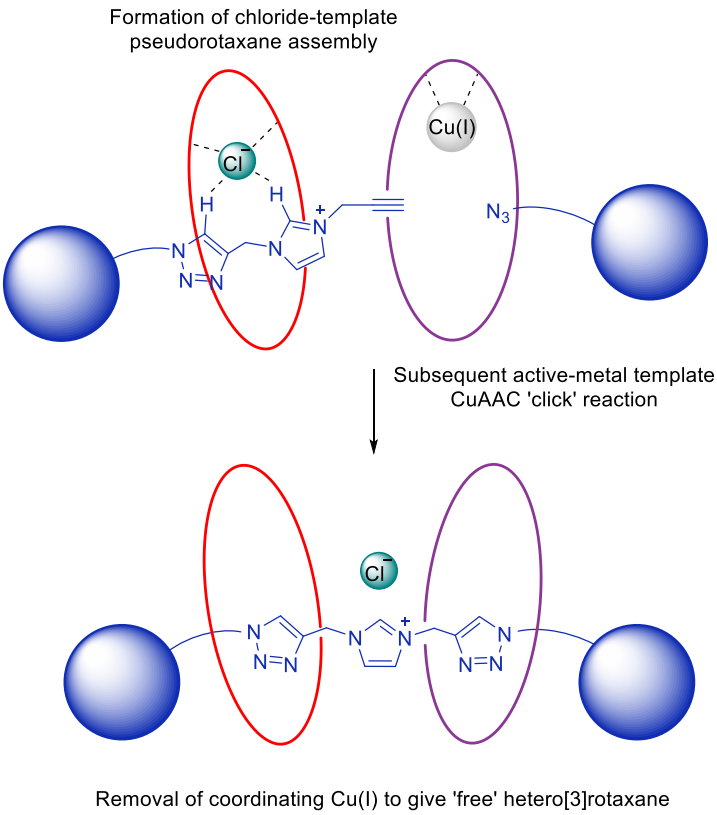
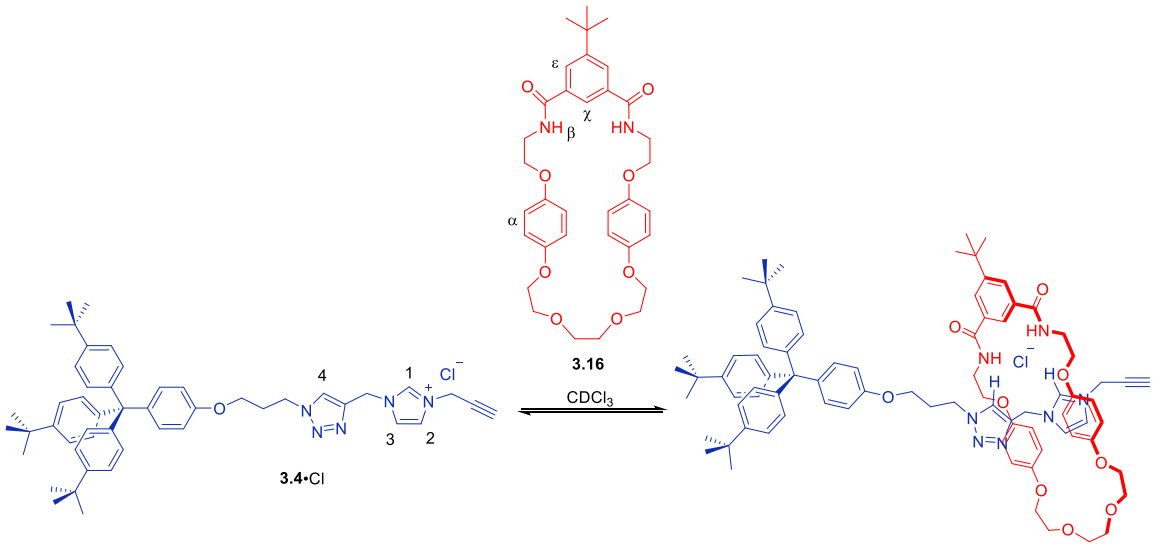


Figure 3.8: *Schematic representation of route to hetero[3]rotaxane combining chloride anion– template and active–metal template methodologies*

3.4.1 Pseudorotaxane investigation

The capability of stopper imidazolium–alkyne **3.4**·Cl to participate in anion–template pseudorotaxane assembly formation was investigated initially through a qualitative ^{1}H NMR spectroscopy experiment (Scheme 3.7). Stopper imidazolium–alkyne **3.4**·Br was converted to the chloride salt for the formation of a chloride anion–template pseudorotaxane, by successive washing with $NH_4Cl_{(aq)}$. The ^{1}H NMR spectrum of an equimolar mixture of isophthalamide macrocycle **3.16** (provided by Dr Nick White) and stopper imidazolium–alkyne **3.4**·Cl was monitored (2 mM in $CDCl_3$). Evidence of successful pseudorotaxane formation was ascertained from the upfield shift and splitting of hydroquinone protons *α* and the disappearance of imidazolium proton *1* (Figure 3.9). The splitting of the hydroquinone resonances of the macrocycle were due to *π*–*π* donor–acceptor interactions between the aromatic systems of the imidazolium thread and macrocycle.



Scheme 3.7: *Pseudorotaxane formation between imidazolium-alkyne thread* ***3.4***·*Cl and isophthalamide macrocycle* ***3.16***

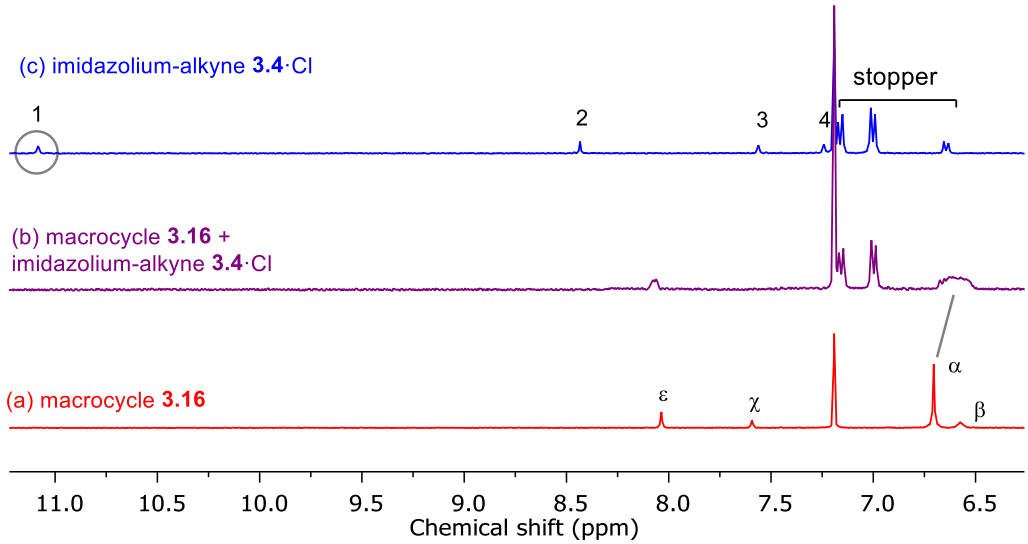
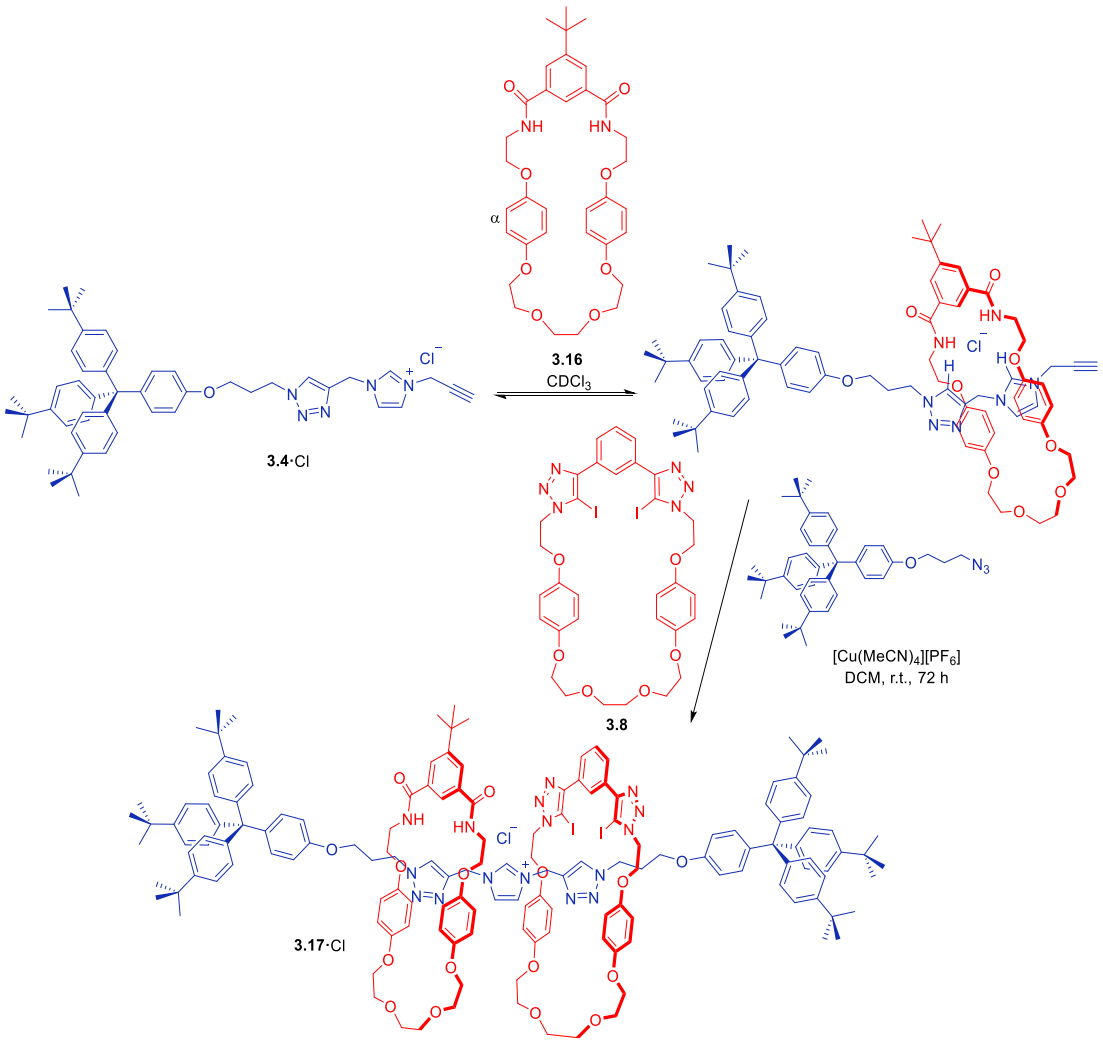


Figure 3.9: *Truncated ^{1}H NMR spectra (400 mHz, $CDCl_3$, 298 K) of (a) imidazolium-alkyne **3.4**·Cl, (b) an equimolar mixture of macrocycle **3.16** and imidazolium-alkyne **3.4**·Cl , and (c) macrocycle **3.16***

3.4.2 Attempted hetero[3]rotaxane synthesis

After the successful formation of a pseudorotaxane assembly with imidazolium–alkyne **3.4**·Cl and isophthalamide macrocycle **3.16**, the synthesis of a hetero[3]rotaxane combining active–metal and anion–template methods was then targeted (Scheme 3.8). Five equivalents of stopper imidazolium–alkyne **3.4**·Cl and isophthalamide macrocycle **3.16** were added to DCM and left to stir for 30 minutes to allow for the formation of the pseudorotaxane. Meanwhile, one equivalent of macrocycle **3.8** and $[Cu(MeCN)_4][PF_6]$ were stirred in DCM for 15 minutes in a separate flask, to which five equivalents of stopper azide **2.31** was then added. The pseudorotaxane solution was combined with the copper(I)–macrocycle solution and the reaction mixture was left to stir for three days. Analysis *via* ESI mass spectroscopy revealed the formation of axle (m/z = 1319.8), [2]rotaxane containing macrocycle **3.16** (m/z = 1927.2), [2]rotaxane with macrocycle **3.8** (m/z = 2170.9) and most importantly hetero[3]rotaxane **3.17**·Cl (m/z = 2778.1) (Figure 3.10). Attempts to isolate the interlocked products were carried out *via* preparative TLC, using a range of eluents; however, the similar polarity of the interlocked structures inhibited the isolation of the individual products. This was nonetheless a promising proof-of-principle test and demonstrated that combining active–metal and anion–template methodologies was a plausible route for the formation of a hetero[3]rotaxane.



Scheme 3.8: *Attempted synthesis of hetero[3]rotaxane **3.17**·Cl via sequential anion–templated pseudorotaxane formation and active–metal templated stoppering rotaxanation reaction*

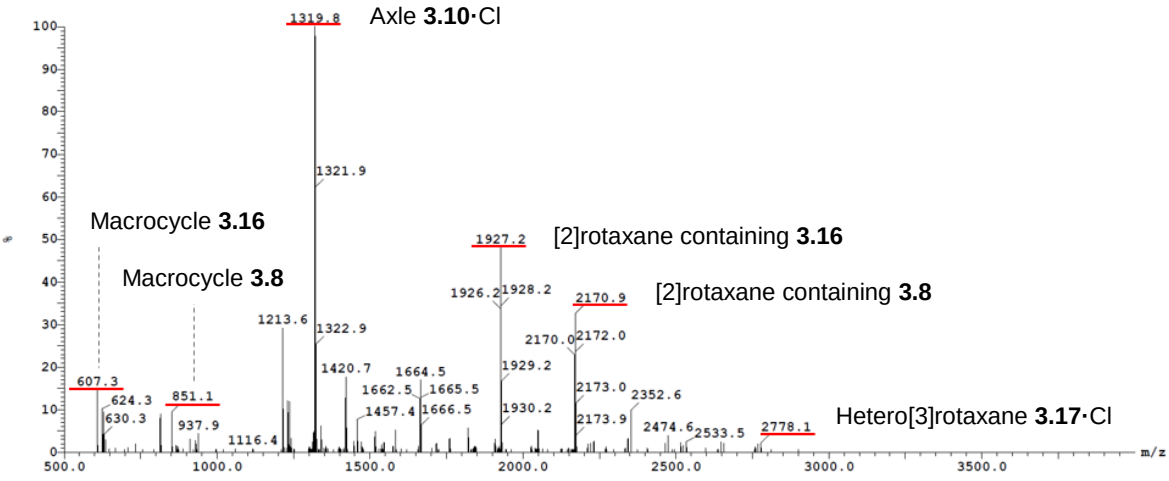


Figure 3.10: *ESI mass spectrum of crude reaction mixture showing formation of axle **3.10**·Cl, [2]rotaxane with macrocycle **3.8**, [2]rotaxane with macrocycle **3.16** and hetero[3]rotaxane **3.17**·Cl*

3.5 Towards bis(triazole)–benzimidazolium containing [2]rotaxanes

The *N*-substituted benzimidazole and benzimidazolium motifs have been incorporated into potent anion receptors and sensors.[7–9] For example, Jang *et al.* reported a novel tripodal fluorescent sensor containing the 2-aminobenzimidazole moiety, which displayed selectivity for iodide *via* fluorescence spectroscopy in buffered CH_3CN/H_2O (99:1, v,v) (Figure 3.11a).[10] Furthermore, the benzimidazolium motif has been combined with a urea group in a fluorescent receptor described by Gao *et al.*, which displayed high affinity for fluoride, acetate and dihydrogen phosphate in acetonitrile calculated from the changes in fluorescence intensity (Figure 3.11b).[11]

(a) (b)

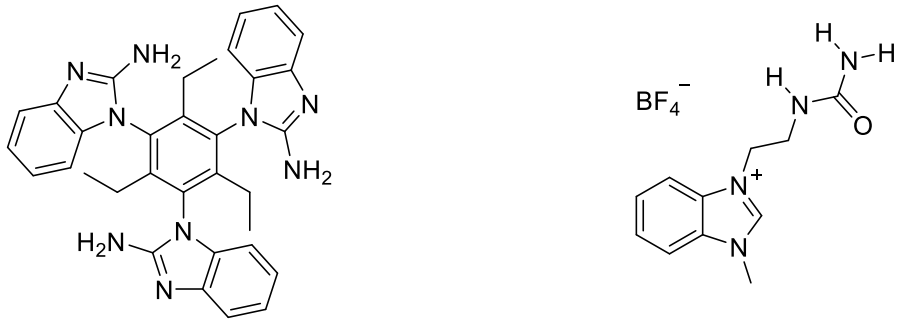
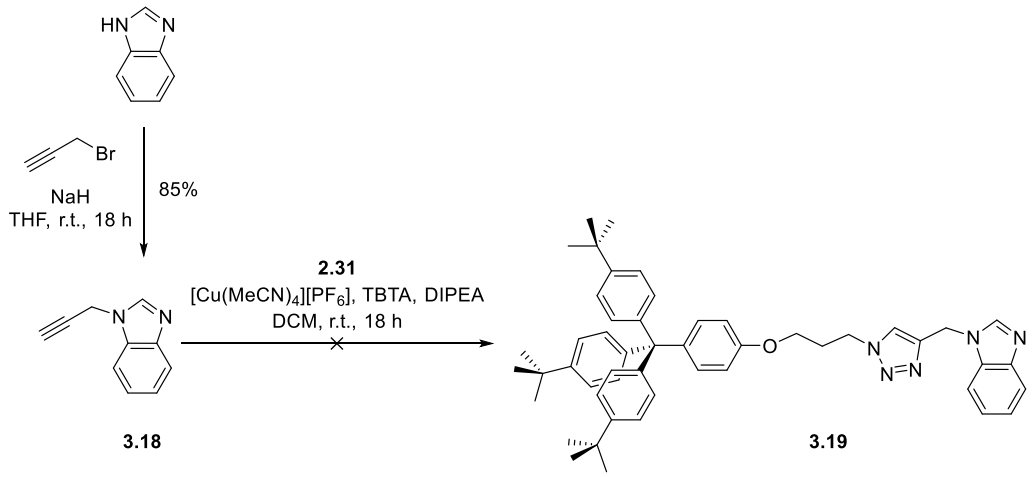


Figure 3.11: *(a) Jang's 2-aminobenzimidazole containing tripod,[9] and (b) Gao's benzimidazolium-urea receptor[10]*

The incorporation of benzimidazolium into interlocked host frameworks as the axle component, analogous to the bis(triazole)– and bis(iodotriazole)–imidazolium rotaxanes outlined in Section 3.3.4 was targeted. It was envisaged that the photophysical properties of the benzimidazolium moiety could be exploited for anion sensing applications. Many routes to the desired interlocked structures were attempted and all proved synthetically challenging, as outlined below.

3.5.1 Synthesis of benzimidazolium axle

Initially, a bis(triazole)–benzimidazolium containing axle was targeted. *N*-alkylation of benzimidazole at the N^1-position with propargyl bromide produced benzimidazole–alkyne **3.18** in 85% yield. A CuAAC 'click' reaction between **3.18** and stopper azide **2.31** was attempted, under the standard conditions (Scheme 3.9). However, evidence for triazole **3.19** was not observed by ESI mass spectrometry of the crude reaction mixture and only starting materials were isolated after silica gel column chromatography. Whilst carrying out the reaction, it was found that upon addition of $[Cu(MeCN)_4][PF_6]$ a precipitate formed; further investigation showed the formation of a precipitate when $[Cu(MeCN)_4][PF_6]$ was added to a solution of benzimidazole–alkyne **3.18** in DCM. It was postulated that an insoluble copper–acetylide complex was being formed, which hindered the progress of the reaction. In an attempt to circumvent this, several reaction conditions were tested (Table 3.2); in all cases no formation of product **3.19** was observed. The corresponding 'one-pot iodo-click' reaction was also attempted and failed to give the iodotriazole product.

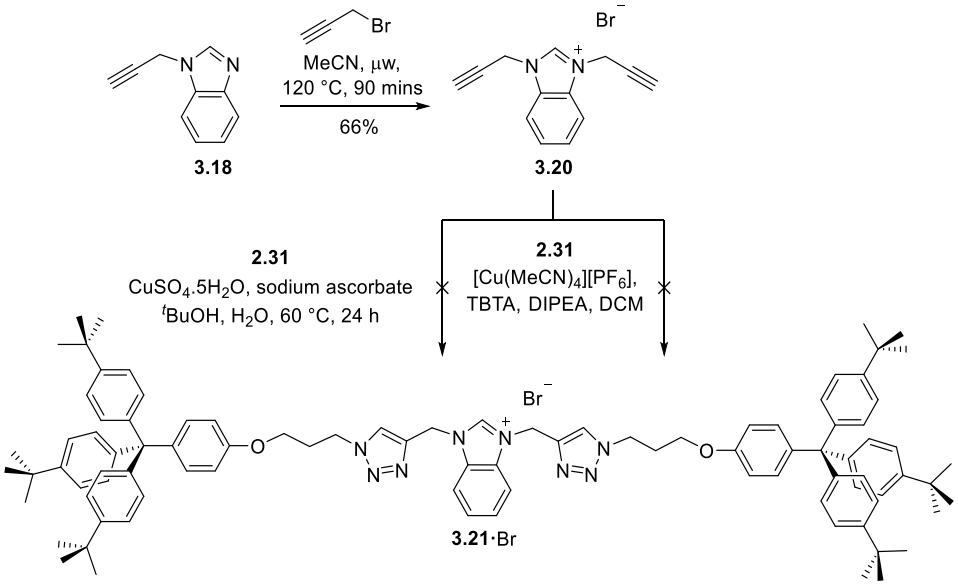


Scheme 3.9: *Attempted synthesis of stopper benzimidazole-triazole* ***3.19***

Table 3.2: *Reaction conditions for the attempted CuAAC 'click' reaction to form benzimidazole–triazole* ***3.19***

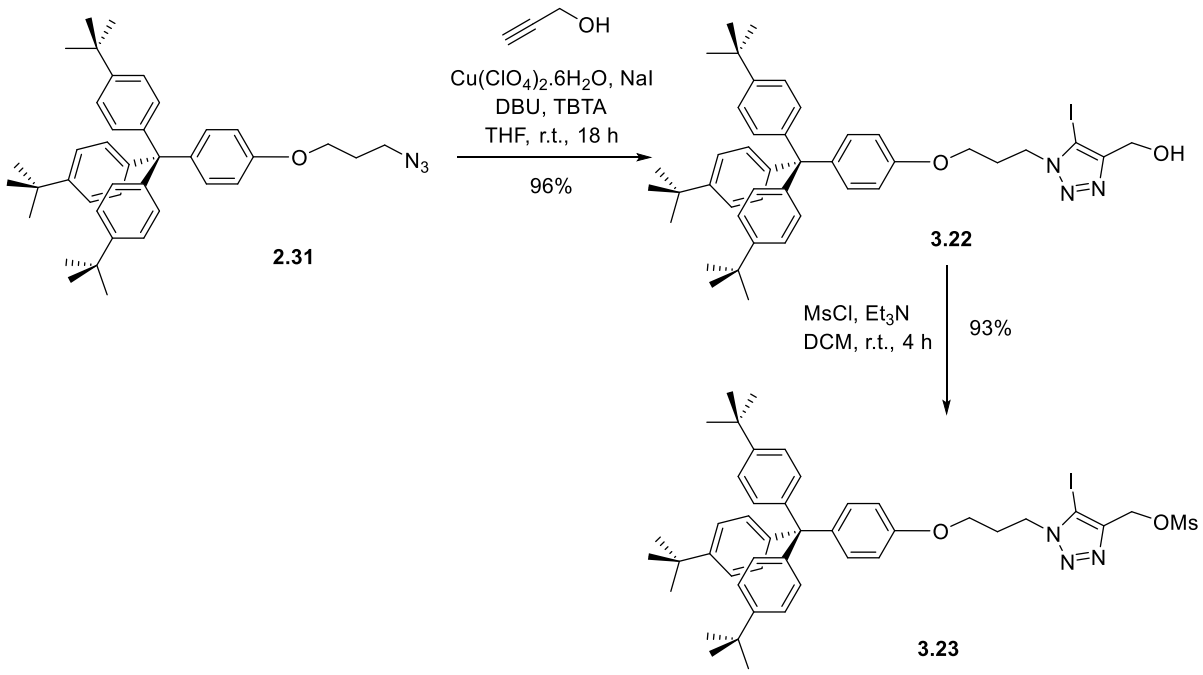
Source of copper (I)	Temperature (°C)	Solvent
Solution of TBTA and $[Cu(MeCN)_4][PF_6]$	50	DCM
Solution of TBTA and $[Cu(MeCN)_4][PF_6]$	50	THF
$[Cu(MeCN)_4][PF_6]$	60	MeCN
$[Cu(MeCN)_4][PF_6]$	60 (μw, 15 mins)	MeCN
$[Cu(MeCN)_4][PF_6]$	60	DMSO

Attention turned to an alternative route, carrying out a bis-'click' reaction on a benzimidazolium– bis-alkyne species. Further *N*-alkylation of benzimidazole–alkyne **3.18** at the N^3-position with propargyl bromide under microwave irradiation produced benzimidazolium–bis-alkyne **3.20** in 66% yield (Scheme 3.10). Bis-alkyne **3.20** was then reacted with two equivalents of stopper azide **2.31**, in the presence of copper sulfate and sodium ascorbate following a modified literature procedure.[12] Stopper azide **2.31** proved insoluble in the solvent mixture of ^{t}BuOH/H_2O required and only starting materials were isolated. Additionally, the bis-'click' reaction was attempted with two equivalents of stopper azide **2.31** in the presence of $[Cu(MeCN)_4][PF_6]$, TBTA and DIPEA; however, no product formation was observed, potentially due to the cationic charge in close proximity to the bis-alkyne.



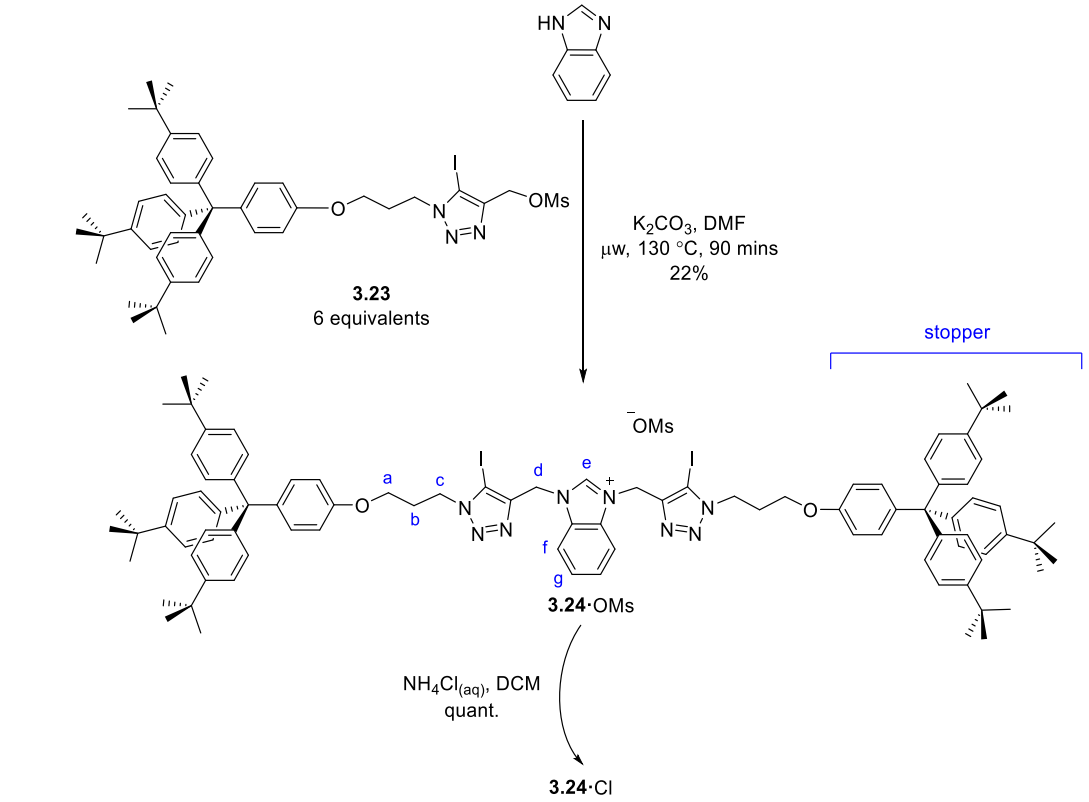
Scheme 3.10: *Attempted synthesis of benzimidazolium-triazole axle* ***3.21****·Br via a bis-'click' reaction*

After multiple attempts at utilising a CuAAC 'click' reaction for the formation of benzimidazolium axle **3.21**, a new strategy was employed whereby benzimidazole underwent a bis-alkylation reaction with a stopper triazole species to produce the targeted axle. For the synthesis of the stopper triazole mesylate, firstly, stopper azide **2.31** and propargyl alcohol were reacted under 'one-pot iodo-click' conditions to form stopper triazole alcohol **3.22** in 96% yield, which was then converted to stopper triazole mesylate **3.23** in 93% yield (Scheme 3.11).



Scheme 3.11: *Synthetic route to stopper triazole mesylate* ***3.23***

N-alkylation of benzimidazole at the N^1- and N^3-position with a large excess of stopper iodotriazole mesylate **3.23** (six equivalents) was carried out in the presence of K_2CO_3, under microwave irradiation (Scheme 3.12). After purification *via* preparative TLC and anion exchange to the chloride salt, bis(iodotriazole)–benzimidazolium axle **3.24**·Cl was isolated in 22% yield. The ^{1}H NMR spectrum of the isolated axle showed the successful formation of benzimidazolium axle with a characteristic chemical shift of 11.4 ppm for the benzimidazolium C^2-proton and the presence of a peak corresponding to the methylene protons at 5.9 ppm (Figure 3.12).



Scheme 3.12: *Synthesis of bis(iodotriazole)–benzimidazolium axle* ***3.24***·*Cl*

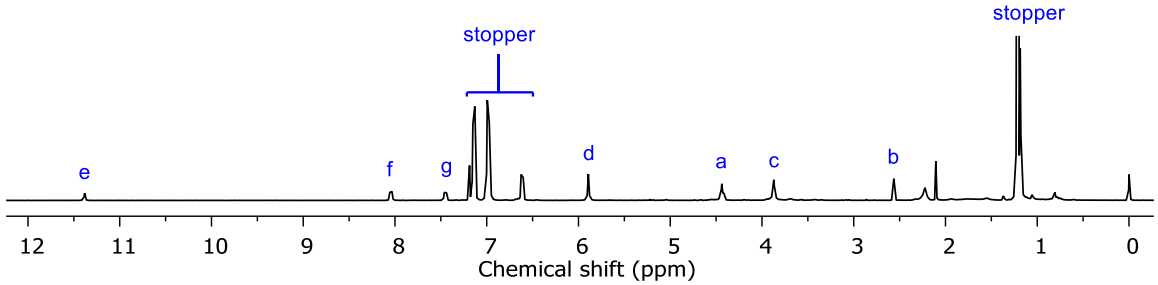
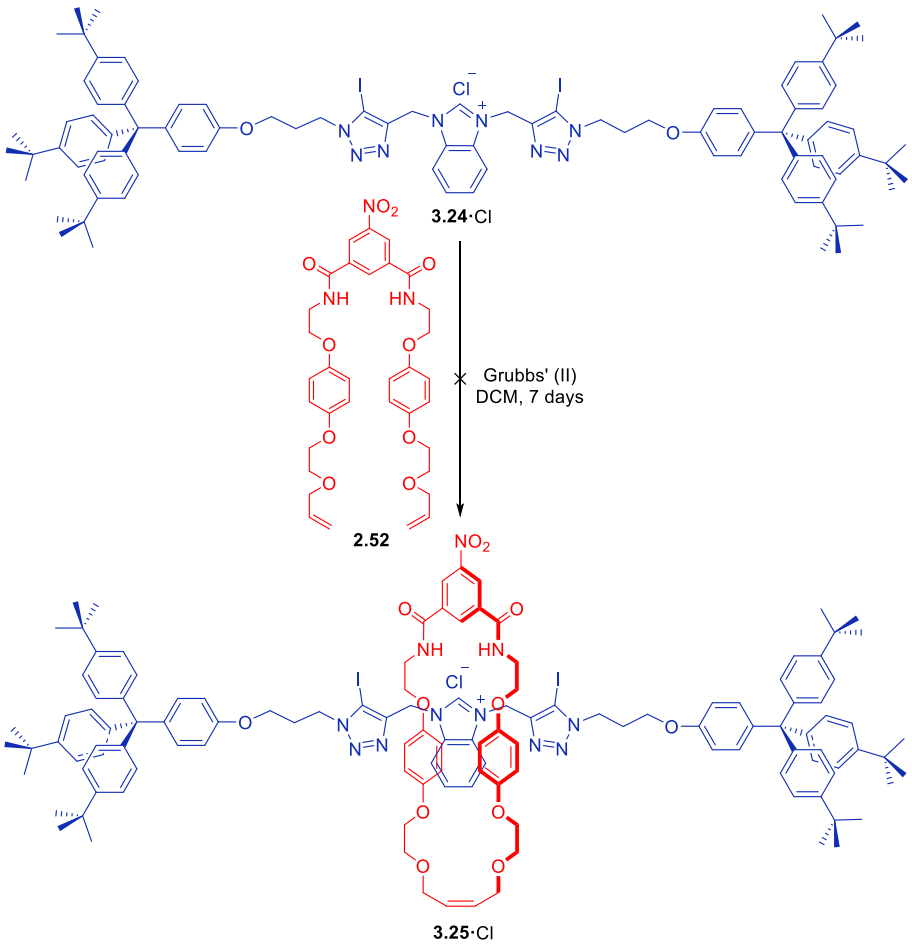


Figure 3.12: *^{1}H NMR spectrum (400 MHz, $CDCl_3$, 298 K) of bis(iodotriazole)–benzimidazolium axle* ***3.24***·*Cl*

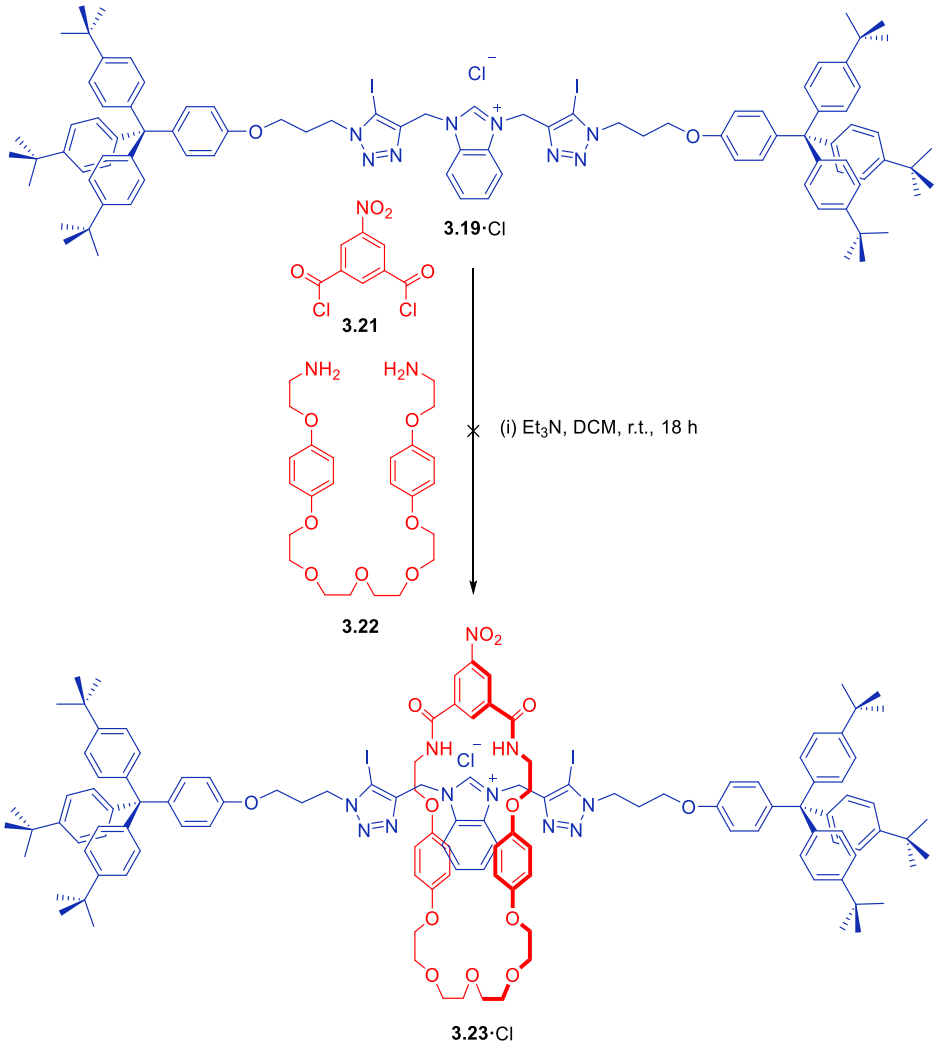
3.5.2 Towards the incorporation of bis(iodotriazole)–benzimidazolium axle into a [2]rotaxane

The attempted synthesis of a [2]rotaxane using the isolated bis(iodotriazole)–benzimidazolium axle **3.24**·Cl *via* chloride–template assembly with bis-vinyl appended macrocycle precursor **2.52** and subsequent Grubbs' II catalysed RCM reaction was carried out (Scheme 3.13). The reaction was monitored *via* TLC and ESI mass spectrometry. After seven days, no evidence of rotaxane or macrocycle formation was observed in the ESI mass spectrum and purification by preparative TLC resulted in the isolation of only axle. The lack of reactivity for this system was attributed to the ability of the benzimidazolium moiety to coordinate to the ruthenium present in the Grubbs' (II) catalyst, thus inhibiting its reactivity.



Scheme 3.13: *Attempted synthesis of (bis-iodotriazole)–benzimidazolium rotaxane* ***3.25***·*Cl via Grubbs' II ring-closing metathesis reaction with vinyl appended macrocycle precursor* ***2.52***

An alternative approach to form the [2]rotaxane employed an acid chloride and amine condensation chloride-template 'clipping' reaction,[13] between a bis-amine macrocycle precursor and 5-nitroisophthaloyl dichloride in the presence of the benzimidazolium axle. Bis(iodotriazole)–benzimidazolium axle **3.19**·Cl, acid chloride **3.21** and bis-amine **3.22** (provided by Dr Thanthapatra Bunchuay) were reacted in the presence of Et_3N in DCM (Scheme 3.14). No evidence of rotaxane formation was observed after 18 hours *via* ESI mass spectrometry, and only the formed macrocycle could be isolated. Unfortunately, the unsuccessful formation of a benzimidazolium containing [2]rotaxane rendered further investigations into the anion binding properties of such systems unattainable.



Scheme 3.14: *Attempted synthesis of bis(iodotriazole)–benzimidazolium rotaxane* ***3.23***·*Cl via acid chloride condensation*

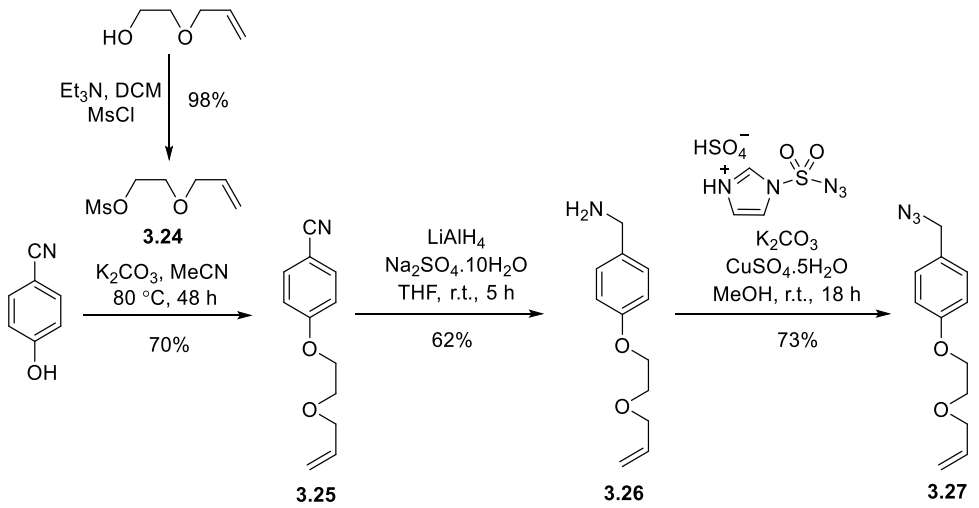
3.6 Incorporation of bis(triazole)–imidazolium motif into the macrocycle component of interlocked structures

N-Heterocyclic carbene-copper (Cu-NHC) complexes have been proven to be effective catalysts in the CuAAC 'click' reaction.[12,14] As outlined in Section 3.3.1, when carrying out the synthesis of axles **3.10**·Cl and **3.11**·Cl, the corresponding Cu-NHC axles were isolated serendipitously.

It was envisioned that through the incorporation of the bis(triazole)–imidazolium motif into a macrocycle, the corresponding Cu-NHC could be formed. Employing this Cu-NHC macrocycle, a new avenue for the synthesis of interlocked structures could be investigated. This would be the first example of an interlocked structure synthesised *via* the active–metal template methodology utilising a Cu-NHC.

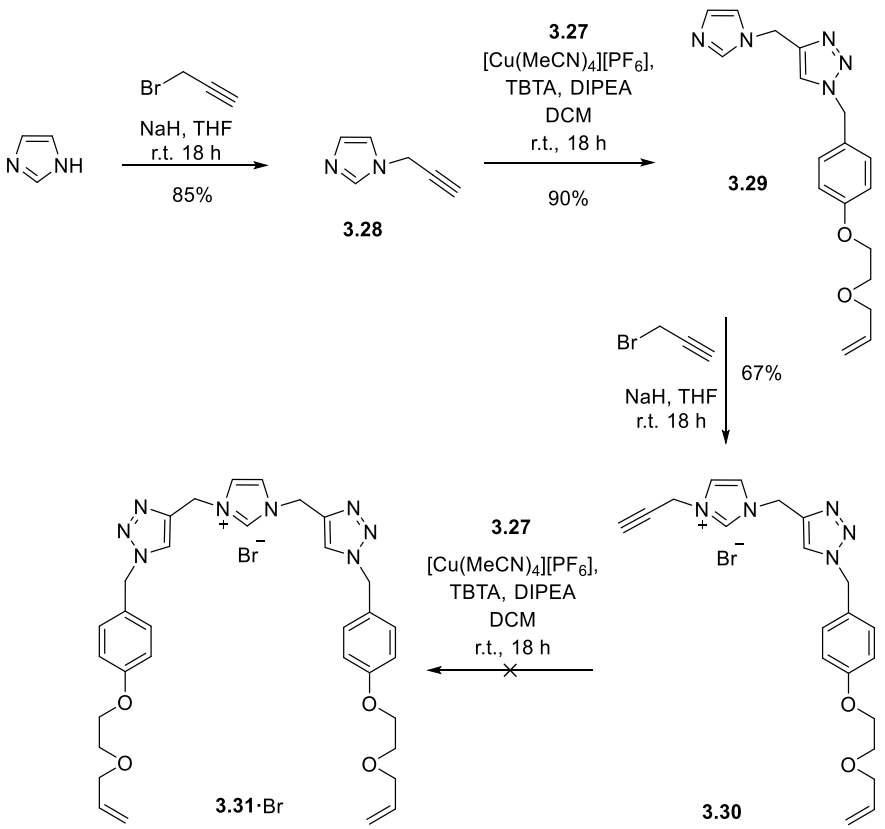
3.6.1 Attempted synthesis of macrocycle

A bis(triazole)–imidazolium containing bis(vinyl) appended macrocycle precursor was targeted. Initially, a stepwise synthetic approach was attempted, with alkylation of imidazole and subsequent CuAAC 'click' reaction. A vinyl-appended azide was prepared by mesylation of commercially available allyloxyethanol to form allyloxyethyl mesylate **3.24**, which was coupled with 4-cyanophenol to afford the vinyl-appended nitrile **3.25** in 70% yield. Reduction of the nitrile with $LiAlH_4$ afforded the amine **3.26** which on reaction with azide transfer reagent (1-(azidosulfonyl)-1*H*-imidazol-3-ium hydrogen sulfate) gave azide **3.27** in 73% yield (Scheme 3.15).



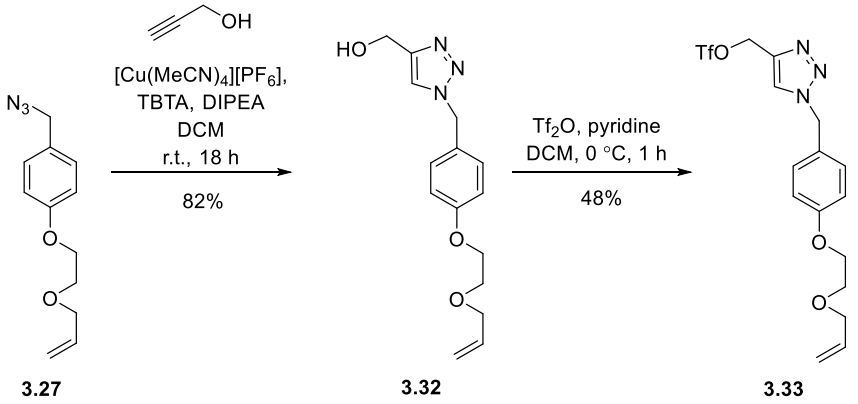
Scheme 3.15: *Synthetic route to azide* ***3.27***

Imidazole was alkylated with propargyl bromide at the N^1-position to form imidazole–alkyne **3.28** in 85% yield, which subsequently was reacted with azide **3.27** in a CuAAC 'click' reaction to form imidazole–triazole species **3.29** in 90% yield (Scheme 3.16). Further alkylation of **3.29** at the N^3-position produced alkyne **3.30** in a crude yield of 67%. Purification was problematic due to the instability of the alkyne on silica and it was therefore carried forward without purification. An attempted CuAAC 'click' reaction between the crude alkyne **3.30** and azide **3.27** proved unsuccessful, with no sign of product formation in ESI mass spectrometry and only starting materials were isolated after silica gel column chromatography.

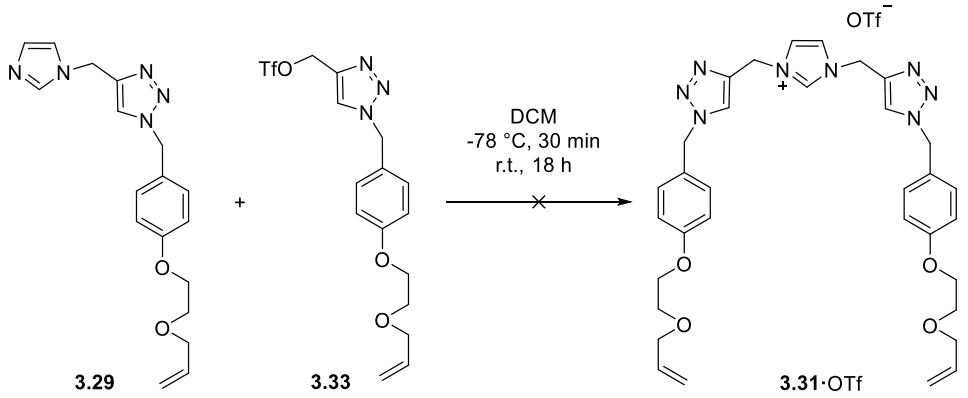


Scheme 3.16: *Attempted synthesis of imidazolium macrocycle precursor* ***3.31·****Br via a stepwise 'click' approach*

An alternative route was carried out, proceeding *via* the synthesis of a vinyl-appended triazole triflate. Azide **3.27** and propargyl alcohol were reaction in a CuAAC 'click' reaction to afford triazole alcohol **3.32** in 82% yield, which was then reacted with triflic anhydride in the presence of pyridine, to form triazole triflate **3.33** in 48% yield (Scheme 3.17). Alkylation of imidazole–triazole species **3.29** with triflate **3.33** was attempted (Scheme 3.18). Encouragingly, the ESI mass spectrum showed the correct m/z ratio for the desired product **3.31·**Br (m/z = 611.7); however, analysis of the ^{1}H NMR spectrum also revealed the presence of an unsymmetric product corresponding to alkylation at the triazole N^{3}-position rather than the anticipated imidazole N^{3}-position.

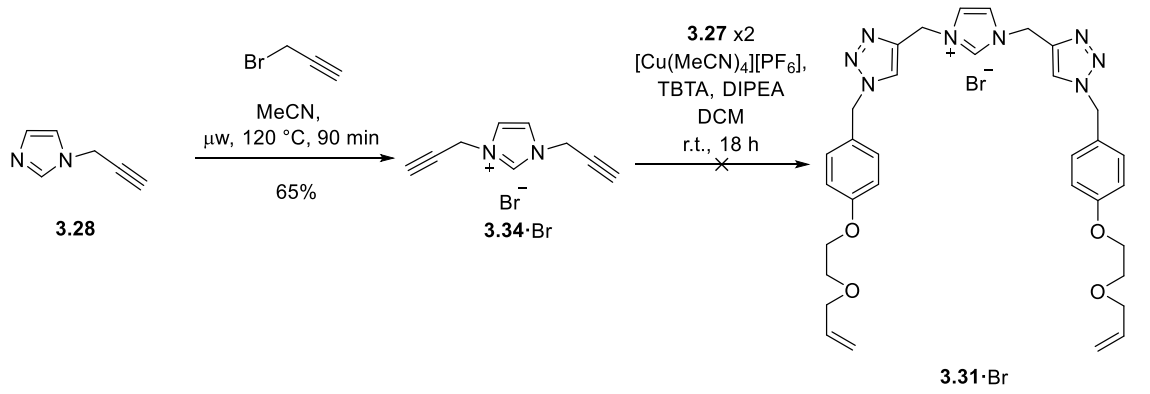


Scheme 3.17: *Synthesis of triflate* ***3.33***



Scheme 3.18: *Attempted synthesis of macrocycle precursor 3.31·OTf via alkylation*

Finally, a bis-'click' route was employed, whereby an additional alkylation was carried out on imidazole–alkyne **3.28** at the N^3-position with propargyl bromide to give imidazolium–(bis-alkyne) **3.34**·Br in 65% yield (Scheme 3.19). A CuAAC bis-'click' reaction was performed with two equivalents of vinyl appended azide **3.27**. Unfortunately, the reaction was unsuccessful, with no macrocycle precursor **3.31**·Br observed in ESI mass spectroscopy or TLC of the crude reaction mixture.



Scheme 3.19: *Attempted synthesis of imidazolium macrocycle precursor **3.31**·Br via a bis-'click' route*

3.7 Conclusions

The bis(triazole)–imidazolium and bis(iodotriazole)–imidazolium motifs have been successfully incorporated into [2]rotaxane host systems and their anion recognition properties investigated. Both the HB rotaxane **3.14**·PF_6 and XB rotaxane **3.15**·PF_6 exhibited strong halide and sulfate binding in the competitive aqueous–organic solvent mixture $CDCl_3/CD_3OD/D_2O$ (45:45:10). In particular, XB rotaxane **3.15**·PF_6 displayed preference for the relatively smaller anions $Cl^- = Br^- > SO_4^{2-} > I^-$, whereas HB rotaxane **3.14**·PF_6 showed no pronounced selectivity between Cl^-, I^- and SO_4^{2-}. It can be concluded that the strong but unselective binding suggests a dominance of charge–driven interactions.

In an attempt to exploit the inherent flexibility of the system, a hetero[3]rotaxane was ambitiously targeted, through carrying out an active-metal template rotaxanation reaction on a chloride-template assembly. Tentative evidence of the hetero[3]rotaxane was observed in the ESI mass spectrum of the crude reaction mixture and provided promising proof-of-principle results.

Further work investigated the incorporation of the bis(iodotriazole)–benzimidazolium motif into an axle. Unfortunately, attempts at the synthesis of a rotaxane *via* RCM reaction and acid chloride condensation were unsuccessful. Finally, various synthetic

routes to a bis(triazole)–imidazolium macrocycle were investigated; however, problems were encountered with all routes attempted and the target macrocycle could not be produced.

3.8 Future Work

The work presented in this chapter could be expanded by exploring the incorporation of halogen bond donors to the C^{2}-position of the imidazolium moiety and ascertaining the effect this has on anion binding strength and selectivity.

To circumvent the issues encountered with the synthesis of a bis(triazole)–imidazolium containing macrocycle, the incorporation of just the imidazolium moiety could be targeted. This would allow initial tests to be carried out to confirm the ability of novel Cu-NHC containing macrocycles to be used in the active–metal template synthesis of an interlocked structure. Attention could then turn to the integration of HB/XB donors. Ultimately, an analogous system utilising the benzimidazolium motif could also be developed, to allow for its use as a fluorescent anion sensor.

3.9 References

1 S. Tsuzuki, H. Tokuda and M. Mikami, *Phys. Chem. Chem. Phys.*, 2007, **9**, 4780–4784.

2 G. T. Spence, C. J. Serpell, J. Sardinha, P. J. Costa, V. Félix and P. D. Beer, *Chem. Eur. J.*, 2011, **17**, 12955–12966.

3 S. W. Robinson, C. L. Mustoe, N. G. White, A. Brown, A. L. Thompson, P. Kennepohl and P. D. Beer, *J. Am. Chem. Soc.,* 2015, **137**, 499–507.

4 W. S. Brotherton, R. J. Clark and L. Zhu, *J. Org. Chem.*, 2012, **77**, 6443–6455.

5 J. Y. C. Lim, T. Bunchuay and P. D. Beer, *Chem. Eur. J.*, 2017, **23**, 4700–4707.

6 M. J. Hynes, *J. Chem. Soc. Dalton Trans.*, 1993, **0**, 311–312.

7 Y. Bai, B.-G. Zhang, J. Xu, C.-Y. Duan, D.-B. Dang, D.-J. Liu and Q.-J. Meng, *New J. Chem.*, 2005, **29**, 777–779.

8 V. K. Khatri, M. Chahar, K. Pavani and P. S. Pandey, *J. Org. Chem.,* 2007, **72**, 10224–10226.

9 N. Singh and D. O. Jang, *Org. Lett.,* 2007, **9**, 1991–1994.

10 D. Y. Lee, N. Singh, M. J. Kim and D. O. Jang, *Org. Lett.*, 2011, **13**, 3024–3027.

11 Z. Dong and G. Gao, *Chinese Sci. Bull.*, 2012, **57**, 1266–1274.

12 N. Touj, I. Özdemir, S. Yaşar and N. Hamdi, *Inorganica Chim. Acta*, 2017, **467**, 21–32.

13 L. M. Hancock and P. D. Beer, *Chem. Eur. J.*, 2009, **15**, 42–44.

14 J.-M. Collinson, J. D. E. T. Wilton-Ely and S. Díez-González, *Chem. Commun.*, 2013, **49**, 11358–11360.

Chapter Four

Halogen bonding supramolecular architectures utilising Ugi multicomponent macrocyclisations

4.1 Introduction

Using strategies adopted by biotic host structures, such as preorganisation in a well-defined three-dimensional binding cavity and the macrocyclic effect, synthetic supramolecular architectures, such as cryptands, are effective anion receptors, as outlined in Chapter 1.[1–5] The synthetic challenge of constructing cyclic and macrobicyclic halogen bonding (XB) hosts remains onerous however, with no literature precedence for a XB cryptand structure.

This chapter will introduce the area of multicomponent reactions and focuses on the exploitation of the Ugi-four-component-reaction for the construction of novel halogen bonding macrocycles and cryptand-like structures for anion recognition applications.

4.1.1 Multicomponent reactions

Multicomponent reactions (MCRs) are defined as processes in which three or more separate components react convergently to form one major product. The first documented MCR was by Strecker in 1850, who reported the formation of α-amino cyanides from the condensation of three components: ammonia, an aldehyde and hydrogen cyanide (Figure 4.1a).[6] Importantly, the α–amino cyanides could be easily hydrolysed to form the corresponding amino acids. Since this seminal report, many different MCRs have been developed; the best know is the Mannich three-component condensation reaction (M-3CR), consisting of the formation of a Schiff base (imine) from the reaction of an amine with formaldehyde, which subsequently reacts with an α-acidic reagent to form a β-amino carbonyl compound (Figure 4.1b).[7] The first developed isocyanide based MCR was the Passerini reaction, which consisted of a three component condensation between a carboxylic acid, a carbonyl compound and an isocyanide to form an α–hydroxy carboxamide (Figure 4.1c).[8] Isocyanide based MCRs have received deserved attention, due to the unique reactivity of this functional group. Isocyanides are the only class of stable organic compounds with a formally divalent carbon and, importantly, they can undergo both nucleophilic and electrophilic addition at the same carbon centre to form an α-adduct.[9]

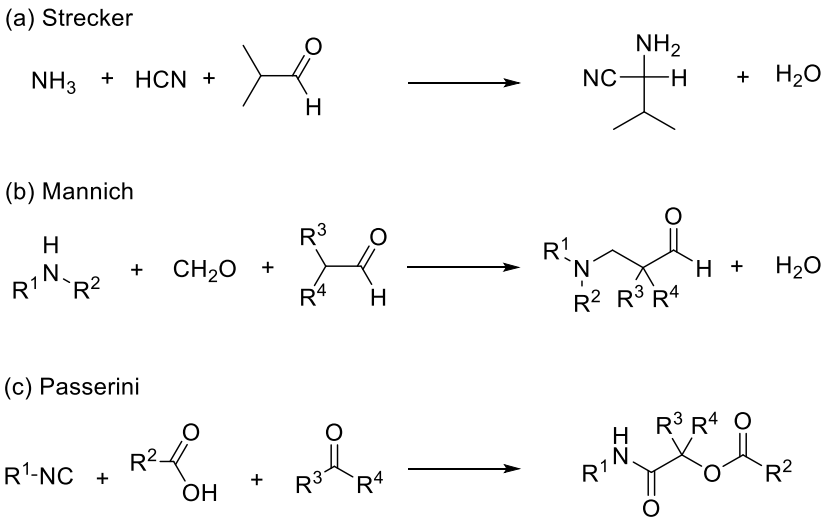
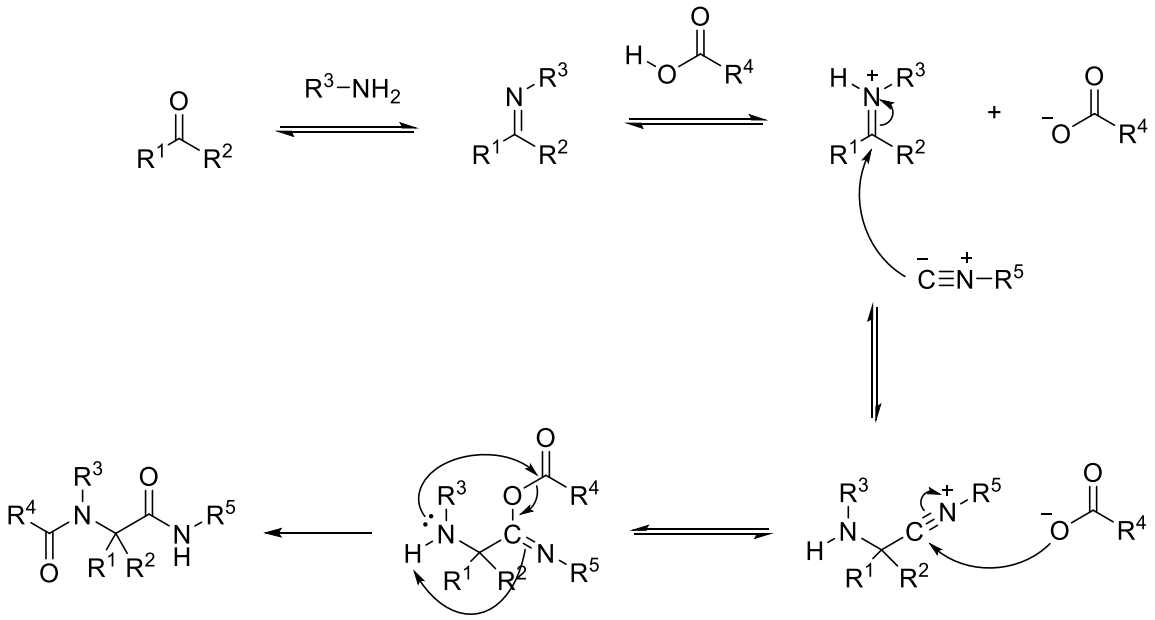


Figure 4.1: *Notable examples of multicomponent reactions*[6–8]

4.1.2 Ugi-four-component reaction

Named after Karl Ugi, who first reported the reaction in 1959, the Ugi-four-component reaction (Ugi-4CR) between an amine, carbonyl compound, isocyanide and carboxylic acid is an extension of the Passerini reaction.[10] The resulting product of the Ugi-4CR is a peptoid moiety and the reaction is therefore used extensively in the formation of peptidomimetics.[11] Advantageously, the reaction allows for the target compound to be obtained in one-pot, with high atom economy.

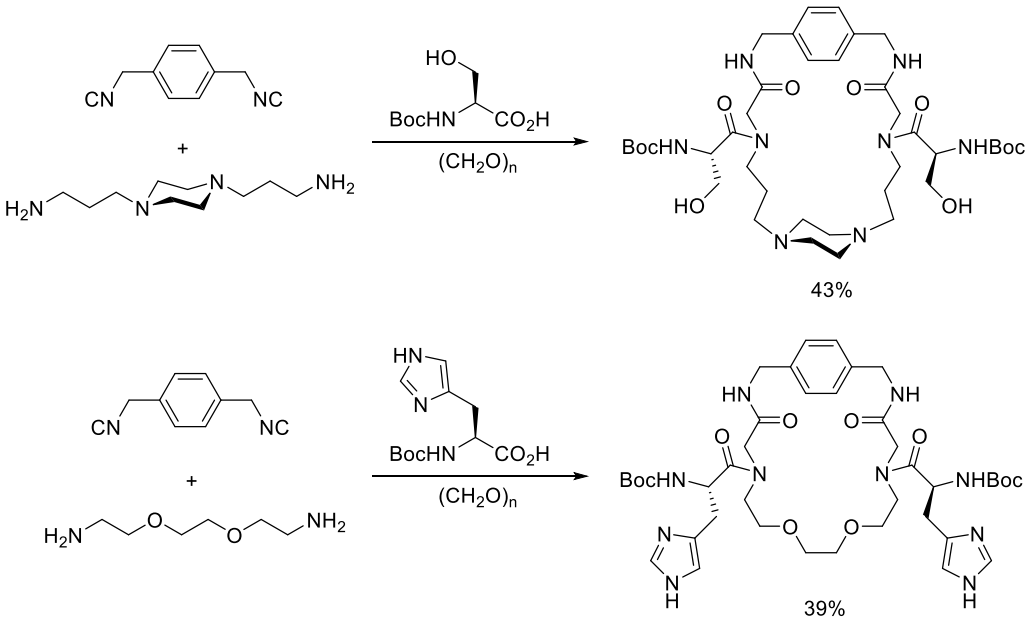
A postulated and simplified reaction mechanism for Ugi-4CRs is shown in Scheme 4.1. The first step consists of the formation of an imine, from the condensation of the carbonyl component with an amine. The electrophilic iminium ion and the nucleophilic conjugate base then add to the isocyanide carbon atom, forming an α-adduct. Finally, this undergoes a Mumm-like rearrangement[12] to form the stable Ugi peptoid product.[9] Importantly, all the elementary steps of this reaction form a network of equilibria, which all flow into a final irreversible step. The driving force for the overall reaction is the oxidation of the isocyanide divalent carbon to the amide tetravalent carbon.[9]



Scheme 4.1: *Postulated mechanism for the Ugi-4CR*[9]

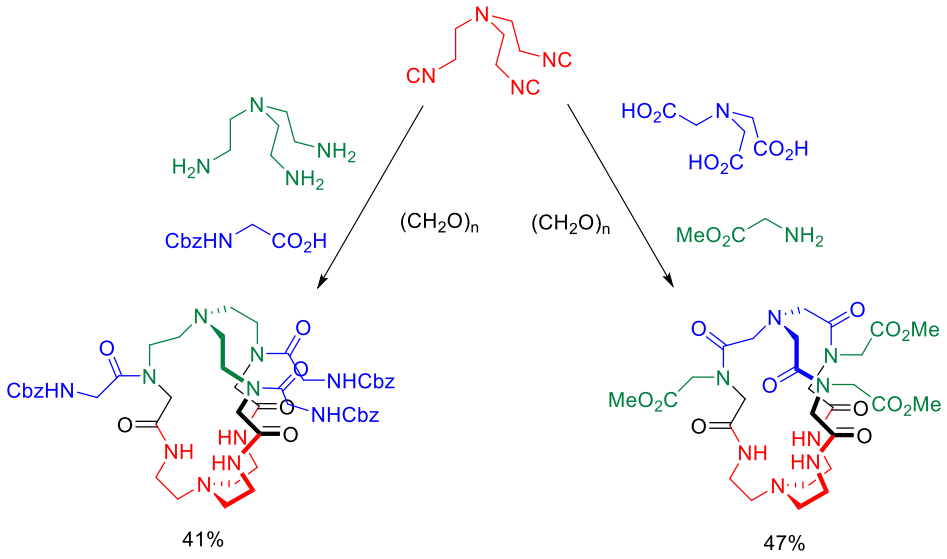
4.1.3 Ugi-4CR for the construction of macrocycles and cages

The Ugi-4CR is a highly efficient process to generate molecular complexity and diversity and has gained interest in the rapid creation of macrocyclic compounds with diverse topologies. By utilising bifunctional building blocks of a bis-isocyanide and a bis-amine Wessjohann *et al.* constructed a small library of peptoid macrocycles with natural-product-like side chains such as those shown in Scheme 4.2.[13] By modifying the acid component, different functionalities were appended outside of the macrocycle.



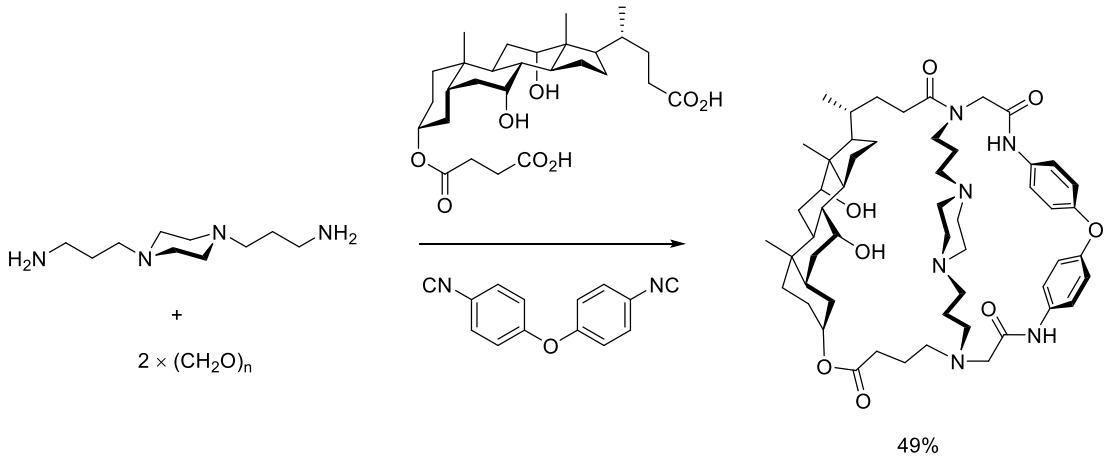
Scheme 4.2: *Wessjohann's natural-product-like macrocycles with appended α-amino acids synthesised via Ugi-4CR*[13]

To further develop the complexity of the molecular architecture Wessjohann *et al.* reported the efficient and straightforward one-pot assembly of cryptands by employing a trifunctional isocyanide and carboxylic acid with an amine and paraformaldehyde in a 3-fold Ugi-4CR-based macrocyclisation reaction (Scheme 4.3).[11] Impressively, 12 bonds were formed between eight components in one-pot, with yields as high as 47%, under pseudo-high dilution conditions, achieved by slow addition of one component to a stirred mixture of the others. A key feature of this strategy was the rapid generation of diversity and complexity by modifying the building blocks employed in the macrocyclisation reaction (Scheme 4.3).



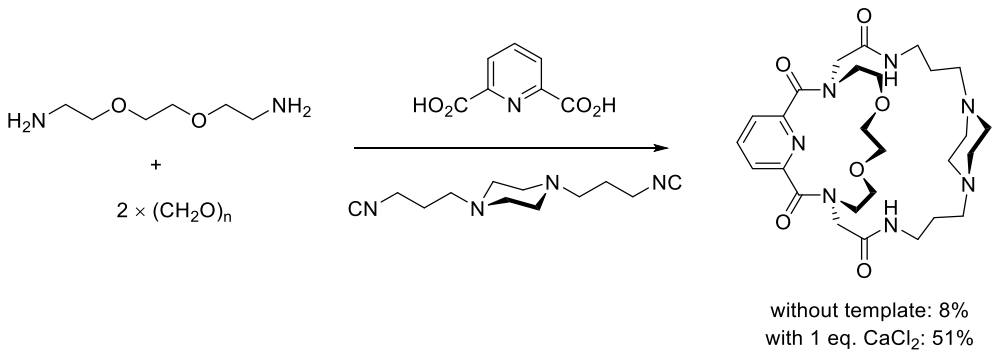
Scheme 4.3: *Peptoid-based cryptands via 3-fold Ugi-4CR macrocyclisations*[11]

More recently, synthetic strategies have advanced and a one-pot double Ugi-4CR has facilitated the assembly of macromulticycles with either three or four different tethers linked by *N*-substituted amino acid bridgeheads (Scheme 4.4).[14] Through construction at the bridgehead, at least three distinct bifunctional building blocks can be brought together in one step to create a hybrid macromulticycle cavity, under both pseudo-high dilution and metal-template macrocyclisation conditions. Rivera *et al.* utilised a double Ugi-4CR and employed a bis-amine, bis-acid and a bis-isocyanide in the presence of a carbonyl component (commonly paraformaldehyde) under pseudo-high dilution conditions, by slow addition of the bis-acid and bis-isocyanide. Impressively, cryptands with complex topologies were formed in one-pot in yields of up to 50% (Scheme 4.4).



Scheme 4.4: *Rivera's pseudo-high dilution Ugi-4CR multicomponent macrocyclisation for the formation of non-symmetric cages*[14]

An alternative template-driven macrocyclisation reaction was also developed, whereby all the bifunctional components could be added at once. The design of building blocks incorporated pyridine and polyether moieties, know to coordinate metal ions. Pyridine-2,6-dicarboxylic acid, a polyether bis-amine and a piperazine based bis-isocyanide were added to one-pot with two equivalents of paraformaldehyde at a relatively high concentration (20 mM) (Scheme 4.5). When one equivalent of calcium chloride was present the yield increased significantly from 8% to 51%. In the absence of high-dilution conditions, the success of cyclisation depended on the templating effect of the metal to direct the process towards ring closure.[14]



Scheme 4.5: *Rivera's template-driven multiple multicomponent macrocyclisations for the formation of non-symmetric cage*[14]

4.2 Chapter aims

The efficacy of the Ugi-4CR has been demonstrated; however, to date, it has not been utilised for the construction of complex host architectures for anion recognition. Furthermore, whilst the ability of cryptand-like structures to achieve strong and selective anion binding is well documented the incorporation of halogen bonds (XB) into such structures is unprecedented. This chapter aims to combine the two unexplored areas by investigating the formation of XB systems for anion recognition employing the Ugi-4CR. This is achieved by incorporating the previously reported 1,3-bis(iodotriazole)benzene motif[15] into one or more components of the reaction. Initially, the formation of an acyclic system is discussed before the syntheses of more complex macrocycle and macrobicycle architectures are outlined. Impressively, the synthetic strategy is employed for the synthesis of an XB cryptand, unprecedented in the literature, comprising six iodotriazole XB donors. Preliminary anion binding studies are then undertaken *via* fluorescence spectroscopy.

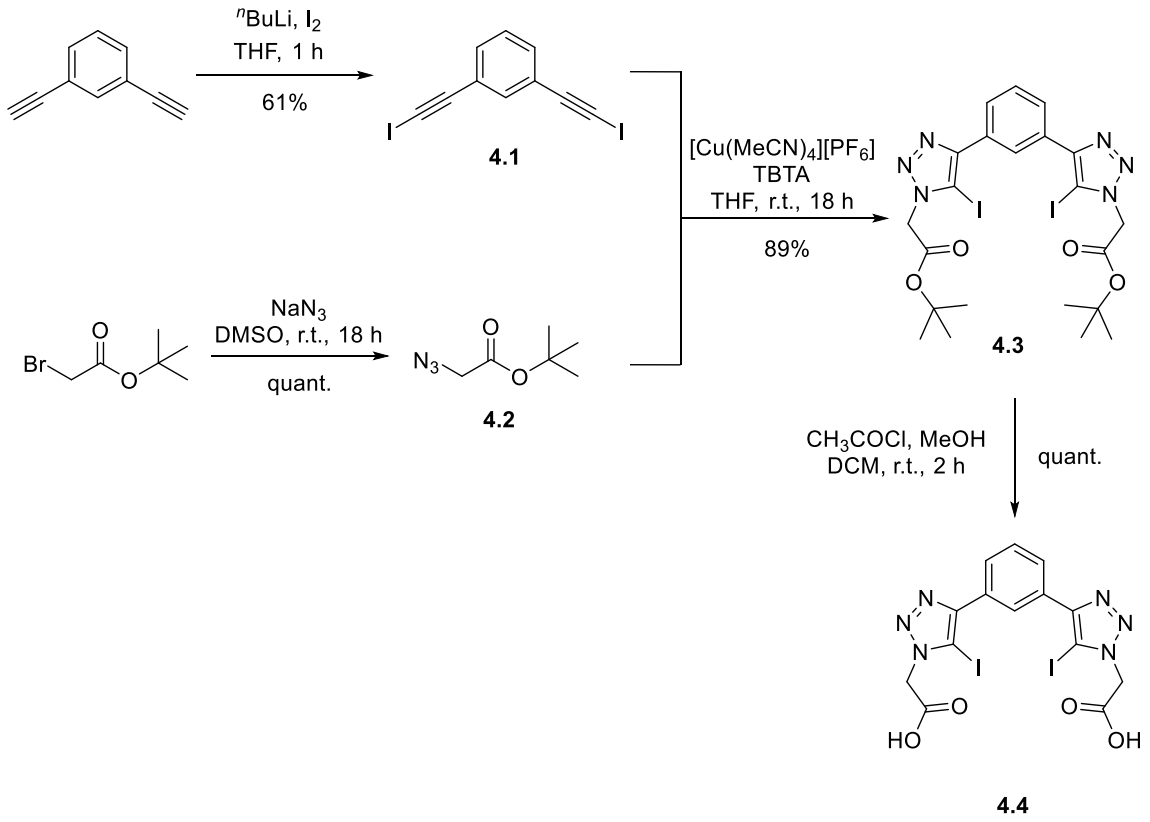
4.3 Preliminary Ugi reactions

Initial test reactions were carried out to determine the feasibility of the Ugi-4CR towards building architectures containing XB donors. Specifically, a simple acyclic system was targeted that incorporated the 1,3-bis(iodotriazole)benzene motif into a bis-acid structure, to allow for subsequent reaction with a variety of amines and isocyanides to yield a range of XB structures.

4.3.1 XB Acyclic test system

The first synthetic target was XB bis-acid **4.4**. 1,3-Diethynylbenzene was converted to the corresponding iodo-alkyne **4.1** in 61% yield, by reaction with iodine and a solution of *n*-butyllithium.[15] *tert*-Butyl bromoacetate was reacted with NaN_3 to form acid-protected azide **4.2** in quantitative yield.[16] A CuAAC 'click' reaction was carried out between bis(iodoalkyne) **4.1** and two equivalents of azide **4.2** to form bis(iodotriazole) containing

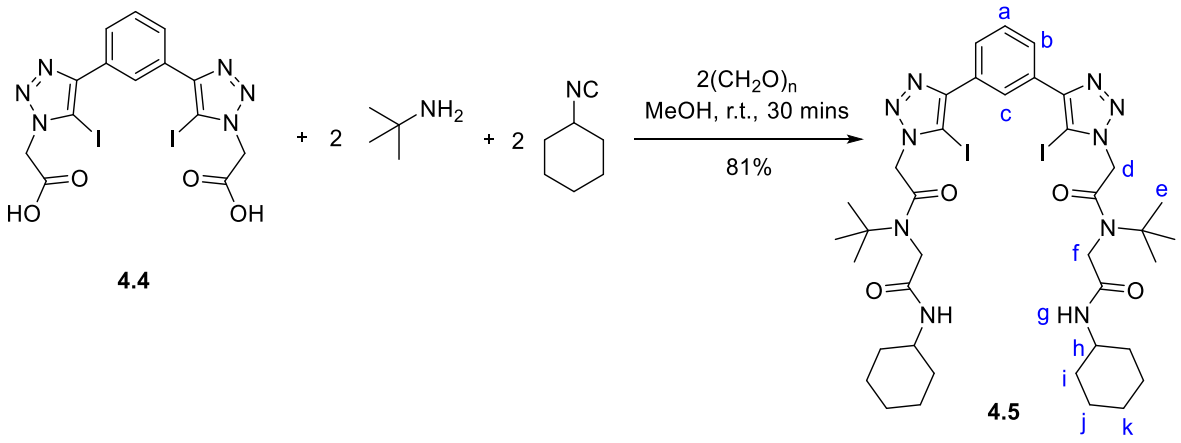
compound **4.3** in 89% yield. Finally, deprotection of the *tert*-butyl ester using trifluoroacetic acid in DCM produced bis-acid **4.4** in quantitative yield (Scheme 4.6).



Scheme 4.6: *Synthetic route to XB bis-acid* ***4.4***

A double Ugi-4CR was carried out with bis-acid **4.4**. Paraformaldehyde was chosen as the carbonyl component to avoid the formation of diastereoisomers. Cyclohexyl isocyanide and *tert*-butyl amine were used because of their commercial availability. Specifically, to a solution of two equivalents of paraformaldehyde in methanol was added two equivalents of *tert*-butyl amine and the solution was stirred for 15 minutes to allow for the formation of the corresponding imine. To this was added bis-acid **4.4** followed by two equivalents of cyclohexyl isocyanide (Scheme 4.7). After 30 minutes, a precipitate formed, the isolation of which produced the target XB containing system **4.5** in 81% yield. The ^{1}H NMR spectrum of the crude product indicated no further purification was necessary and confirmed the formation of the Ugi product with peaks observed for cyclohexyl protons

(*i, j, k*), *tert*-butyl protons (*e*) and, indicative of the reaction's success, the methylene spacer protons (*f*) (Figure 4.2).



Scheme 4.7: *Synthesis of XB acyclic system* ***4.5*** *via double Ugi-4CR*

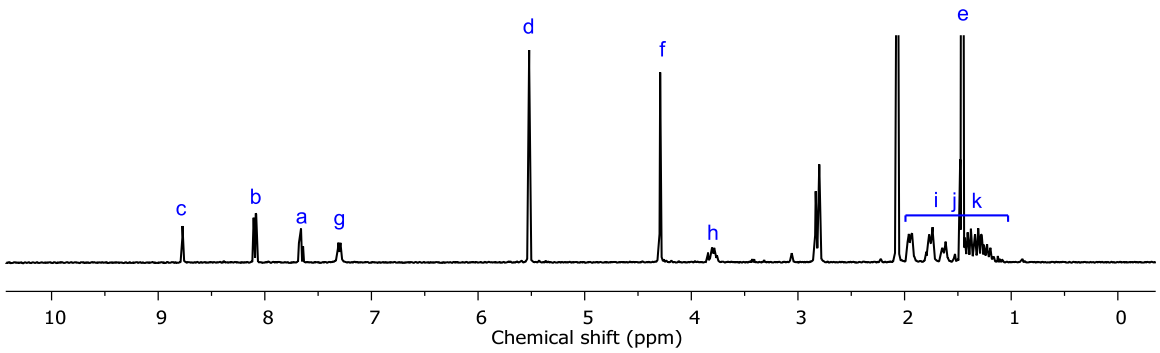


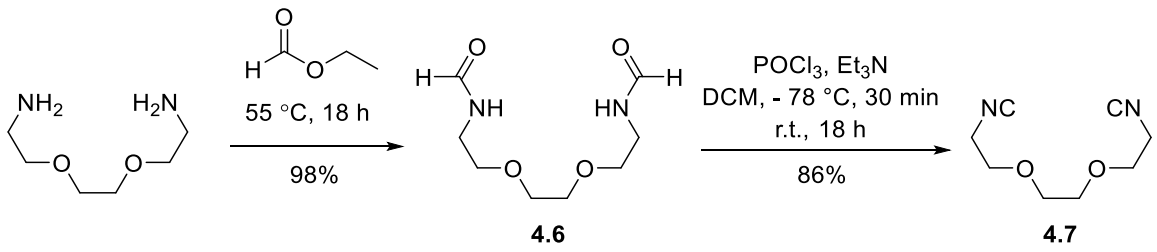
Figure 4.2: *^{1}H NMR spectrum of* ***4.5*** *(acetone-d_6, 298 K, 400 MHz)*

4.3.2 XB Macrocycle synthesis *via* Ugi-4CR

Following the successful formation of acyclic system **4.5** *via* a double Ugi-4CR, attention turned to implement the same methodology in the formation of a macrocycle. By employing a suitable bis-isocyanide component with the already synthesised bis-acid **4.4**, the corresponding Ugi-4CR with *tert*-butyl amine and paraformaldehyde was expected to result in a cyclic structure.

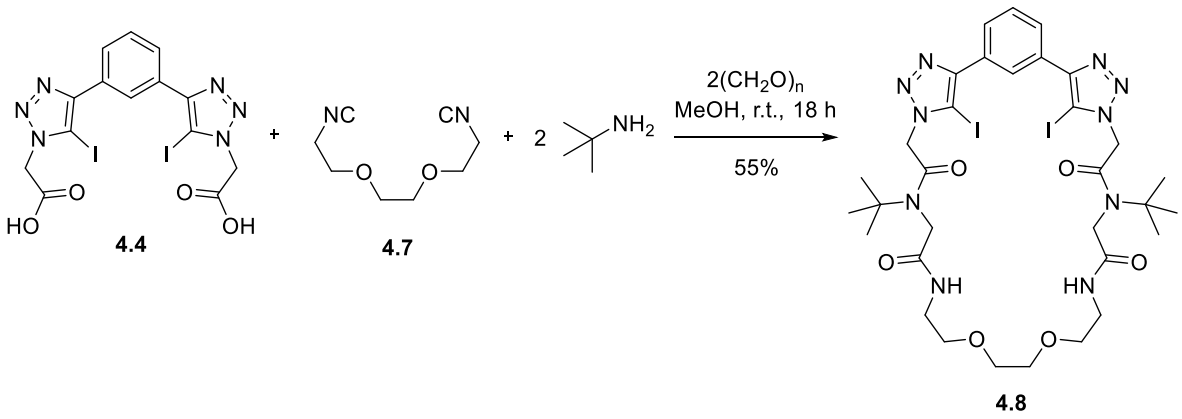
Bis-isocyanide **4.7** was synthesised in two steps from 1,2-bis(2-aminoethoxy)ethane: formamide **4.6** was formed by reaction with ethyl formate and dehydrated using

phosphoryl chloride in the presence of triethylamine to form bis-isocyanide **4.7** in an overall 62% yield (Scheme 4.8).



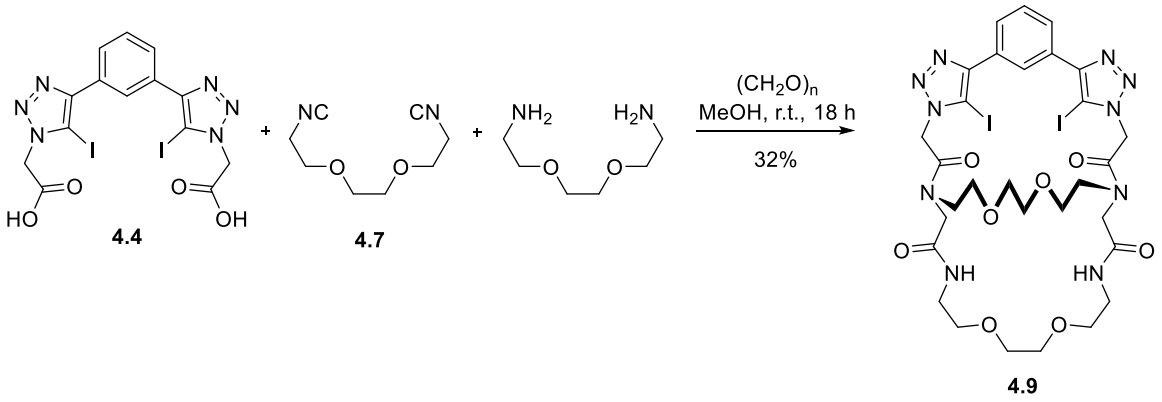
Scheme 4.8: *Synthetic route to bis-isocyanide* ***4.7***

A double Ugi-4CR was employed in a multicomponent macrocyclisation reaction in one-pot, combining bis-acid **4.4**, bis-isocyanide **4.7** and two equivalents of both *tert*-butyl amine and paraformaldehyde (Scheme 4.9). The Ugi reaction is favoured by high concentration of the reactants, however, in a macrocyclisation reaction, this would be expected to lead to the formation of oligomeric acyclic and macrocyclic products. To circumvent this, pseudo-high-dilution conditions were used, achieved through slow addition of the bis-isocyanide component into the reaction mixture. A solution of *tert*-butyl amine and paraformaldehyde in methanol was stirred for two hours at room temperature, allowing for the formation of the imine, before bis-acid **4.4** was added. Bis-isocyanide **4.7** in methanol was added dropwise *via* a syringe pump. The crude reaction product was purified by preparative TLC to give XB macrocycle **4.8** in 55% yield. This was impressive when considering the product combined six components and formed eight new covalent bonds.



Scheme 4.9: *Ugi-4CR multicomponent macrocyclisation reaction to form XB macrocycle* ***4.8***

The methodology was taken a step further and applied to the synthesis of a macrobicycle, achieved through the reaction of three bifunctional building blocks: bis-acid **4.4**, bis-isocyanide **4.7** and the commercially available 1,2-bis(2-aminoethoxy)ethane. To a pre-stirred solution of bis-amine and paraformaldehyde in methanol, bis-acid **4.4** and bis-isocyanide **4.7** were simultaneously added via syringe pump (Scheme 4.10). ESI mass spectrometry indicated the presence of macrobicycle **4.9** (m/z = 921.1) and after purification by preparative TLC this was isolated in 32% yield. Unfortunately, problems were encountered with the solubility of macrobicycle **4.9** and although an ^{1}H NMR spectrum was obtained in DMSO with signals corresponding to regions present in macrobicycle **4.9**, the broad nature of the peaks hindered the full assignment of the spectrum.



Scheme 4.10: *Synthesis of XB macrobicycle* ***4.9*** *via one-pot Ugi-4CR multi-macrocyclisation reaction*

4.4 Halogen bonding cryptand *via* Ugi-4CR

Initial studies confirmed that the Ugi-4CR was compatible with synthons incorporating the iodotriazole XB donor group. The potential of the methodology to form complex architectures was then demonstrated with the synthesis of XB macrocyclic and XB macrobicyclic structures in impressively high yields. With this knowledge, attention focused on the application of Ugi-4CR multicomponent macrocyclisation for the construction of a XB cryptand that contained iodotriazole XB donor groups in each of the three bridging linkages. The strategy executed was the synthesis of bifunctional acid, amine and isocyanide precursors, all incorporating the 1,3-bis(iodotriazole)benzene motif (Figure 4.3). The cryptand would then be synthesised *via* a bridgehead construction with two Ugi-4CRs forming the desired XB cryptand. Polyether chains would be appended to the precursors to incur solubility on the final product.

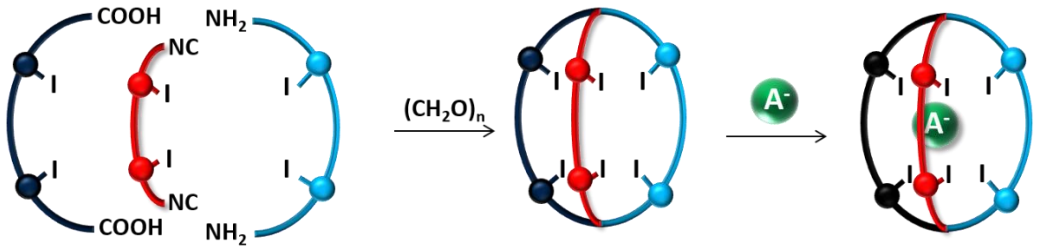
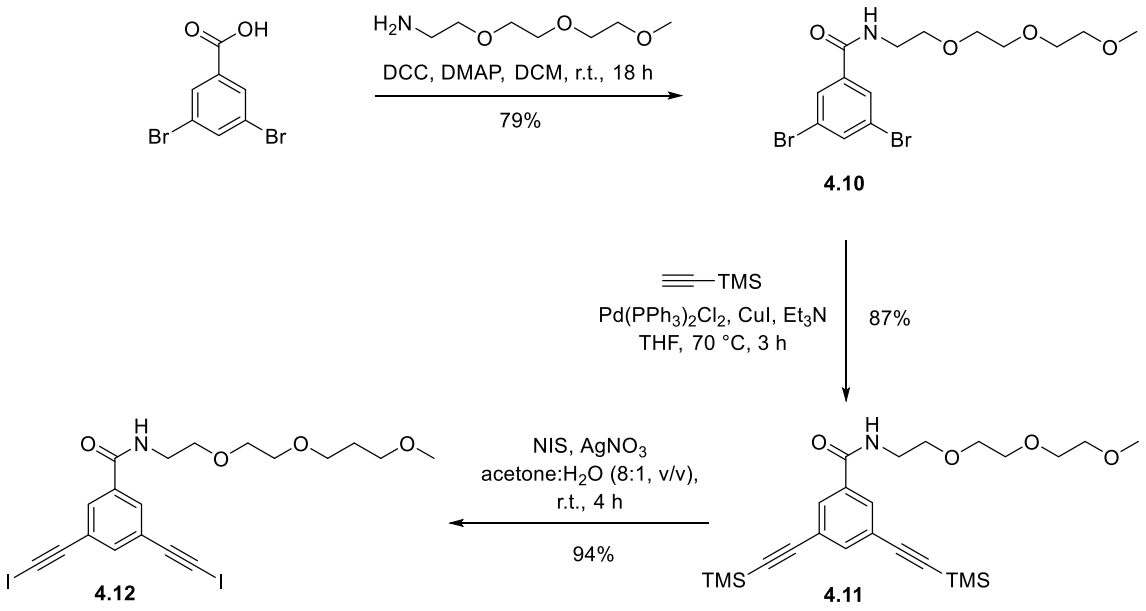


Figure 4.3: *Schematic representation of construction of XB cryptand via bridgehead construction*

4.4.1 Synthesis of XB cryptand precursors

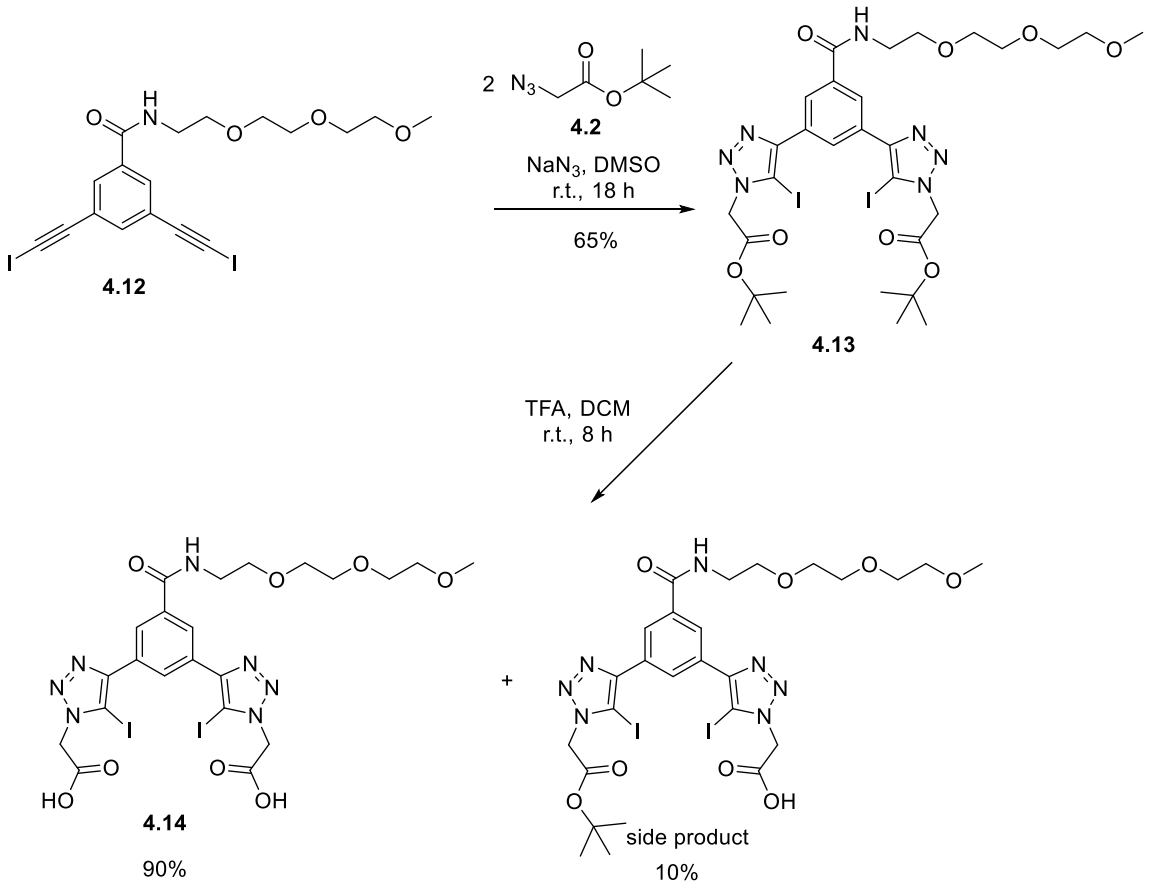
Polyether appended bis-iodoalkyne **4.12** was the initial target; this synthon could be used in a CuAAC 'click' reaction with various azides to produce bis(iodotriazole) containing precursors with the desired bis-acid, bis-amine or bis-isocyanide functionality. 3,5-Dibromobenzoic acid and polyether amine (kindly donated by Dr Thanthapatra Bunchuay) were reacted in an amide condensation reaction in the presence of DCC and DMAP to form amide **4.10** in 79% yield (Scheme 4.11). Sonogashira coupling with two equivalents of trimethylsilyl acetylene produced protected bis-alkyne **4.11** in 87% yield. Conversion to the iodoalkyne was achieved by reaction with *N*-iodosuccinimide in the

presence of silver nitrate in acetone/water (8:1) to give bis(iodoalkyne) **4.12** in 94% yield (Scheme 4.11).



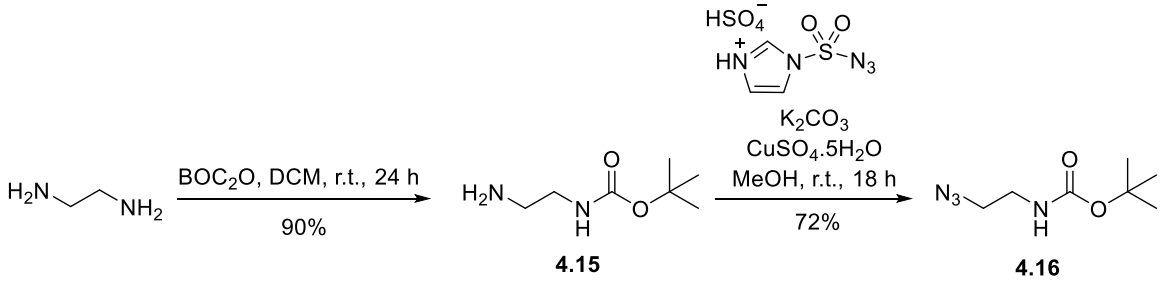
Scheme 4.11: *Synthetic route to bis-iodoalkyne* ***4.12***

A CuAAC 'click' reaction was carried out between bis(iodoalkyne) **4.12** and two equivalents of azide **4.2** to form bis(iodotriazole) containing bis-ester protected acid **4.13** in 65% yield (Scheme 4.12). Deprotection of the *tert*-butyl ester group proceeded *via* reaction with trifluoroacetic acid in DCM to produce XB bis-acid **4.14**. Unfortunately, it was found that 10% of the product was mono-protected ester-acid species, which even after reaction with neat trifluoroacetic acid at 50 °C could not be driven to completion. Purification *via* column chromatography with a range of eluents was carried out, however the mono-protected species could not be separated from the desired product **4.14**.



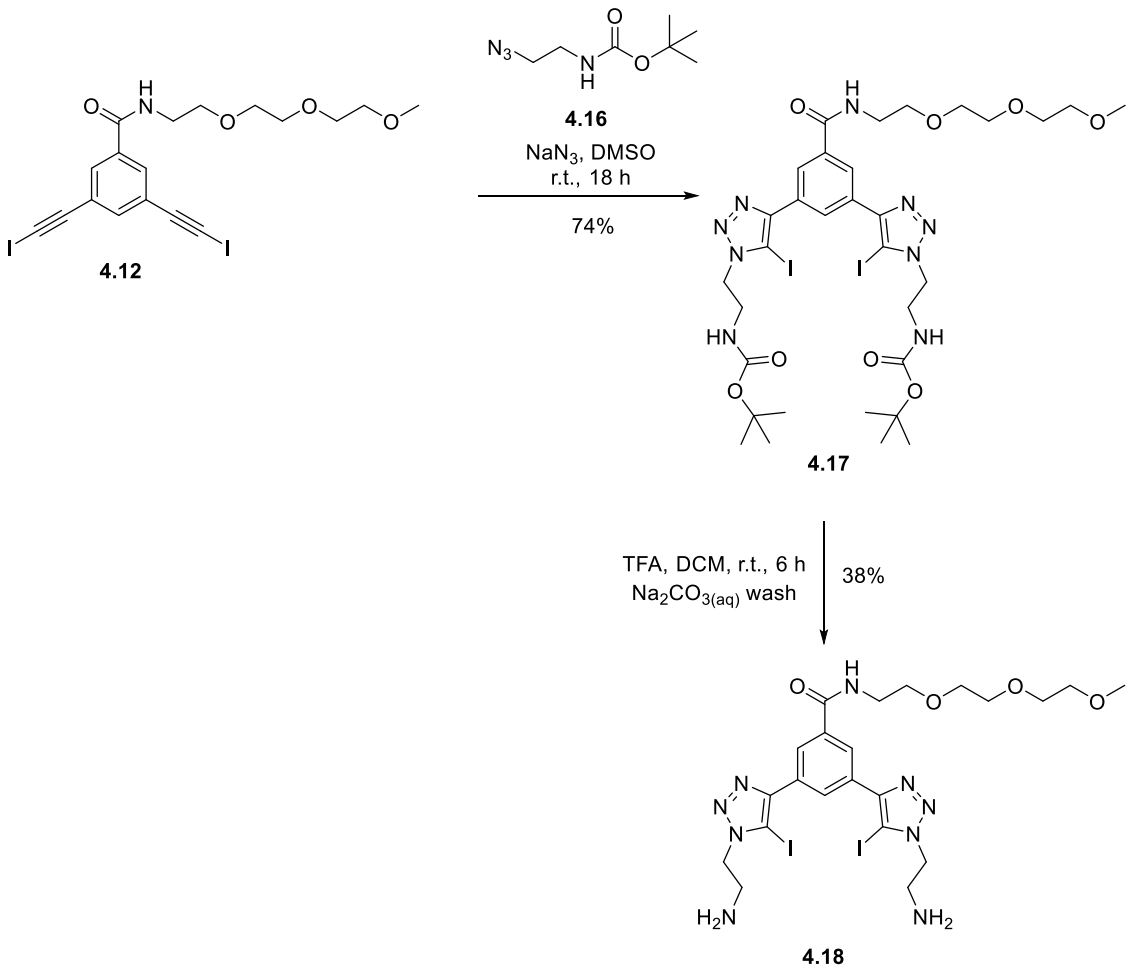
Scheme 4.12: *Synthesis of XB bis-acid* ***4.14***

Attention then turned to the synthesis of bis-amine **4.18**. Firstly, an excess of ethylenediamine was reacted with BOC anhydride in DCM to give mono-BOC-protected amine **4.15**, which on reaction with azide transfer reagent (1-(azidosulfonyl)-1*H*-imidazol-3-ium hydrogen sulfate) gave BOC-protected azide **4.16** in 65% overall yield (Scheme 4.13).



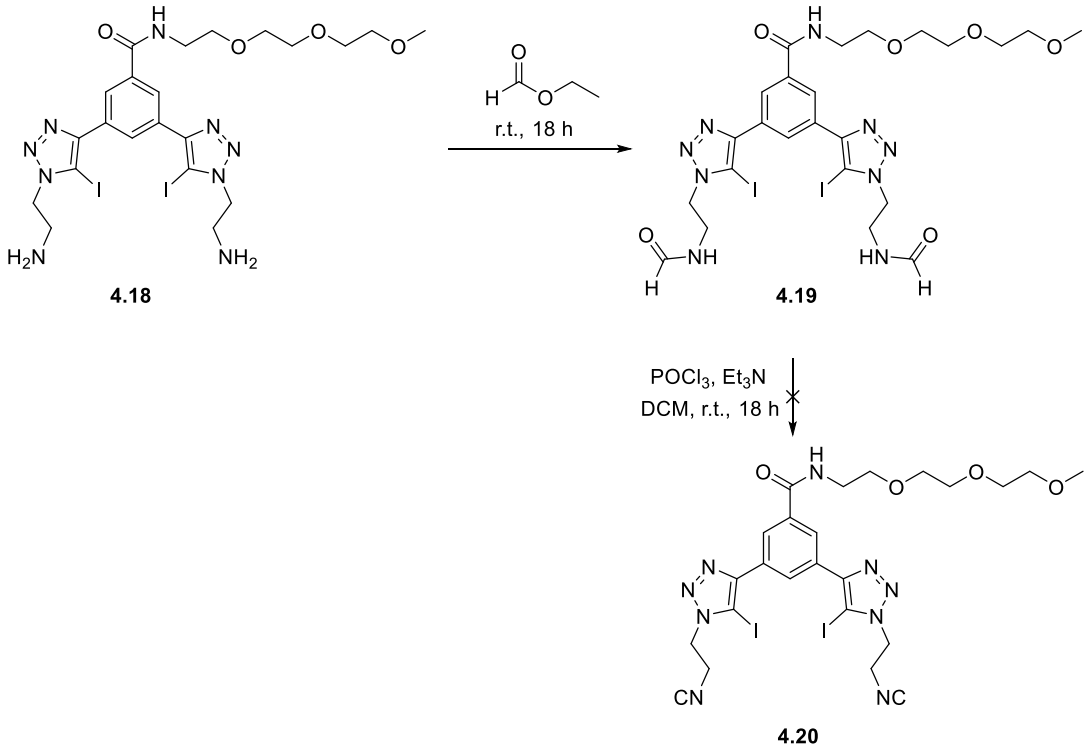
Scheme 4.13: *Synthesis of BOC-protected azide* ***4.16***

Formation of bis-BOC-protected amine **4.17** was achieved by CuAAC 'click' reaction between bis(iodoalkyne) **4.12** and two equivalents of protected azide **4.16**, in 74% yield (Scheme 4.14). Deprotection of the BOC-protecting group was carried out with trifluoroacetic acid in DCM to form the trifluoroacetate salt of the bis-amine. Isolation of the free bis-amine **4.18**, was achieved by washing with aqueous saturated $NaHCO_3$. Due to the solubility of bis-amine **4.18** in water, problems were encountered in the isolation of the product. After copious washing of the aqueous layer with various organic solvents, bis-amine was isolated in a modest 38% yield.



Scheme 4.14: *Synthetic route to XB bis-amine* ***4.18***

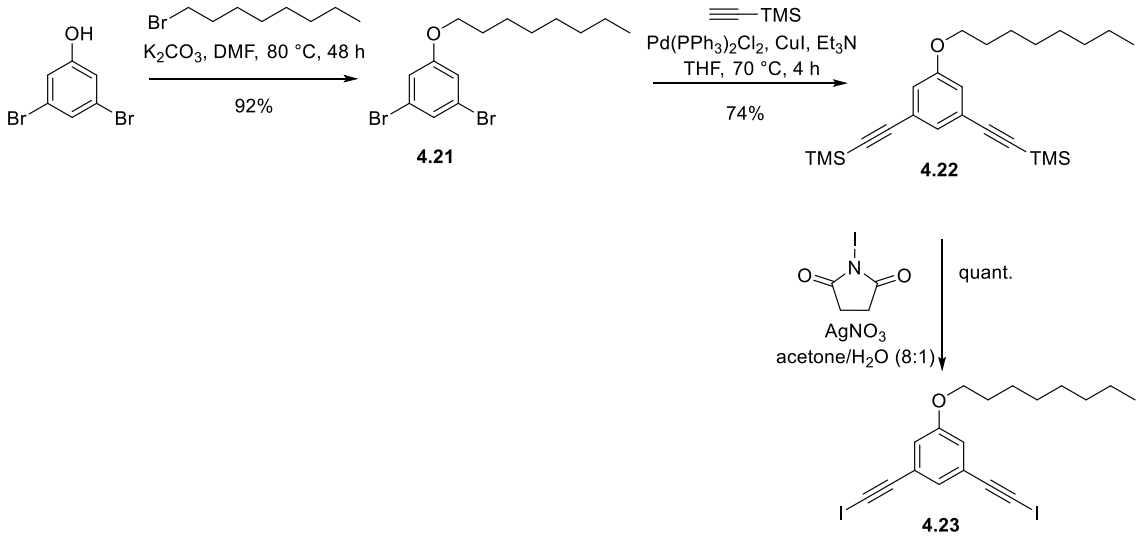
After successfully isolating bis-amine **4.18** attempts were made to produce the corresponding bis-isocyanide. Reaction of bis-amine **4.18** in neat ethyl formate produced formamide **4.19**, which immediately underwent a dehydration reaction with $POCl_3$ and Et_3N in DCM with the aim of forming bis-isocyanide **4.20** (Scheme 4.15). Unfortunately, the formation of the desired product was not observed, postulated to be from competing side reactions with the amide also present in the structure that could also undergo a dehydration reaction, with a complex mixture of products seen.



Scheme 4.15: *Attempted synthesis of XB bis-isocyanide* ***4.20***

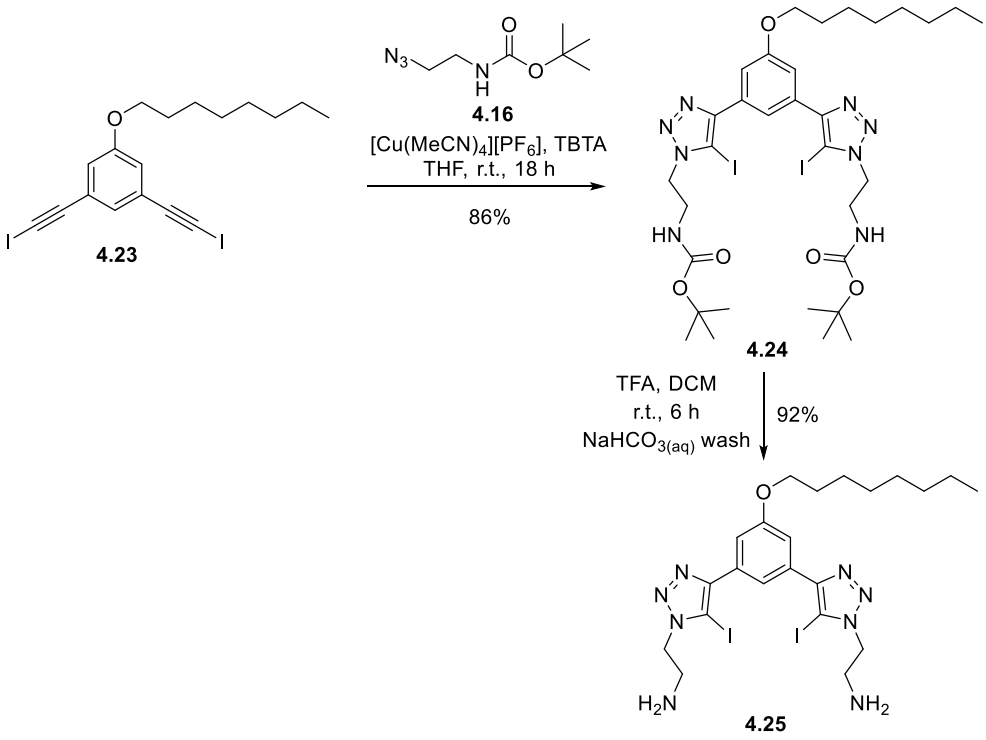
The many difficulties met in the initial route employed, stemmed from the appended amide PEG group, which imparted water solubility to the bis-amine **4.18** and competed in the synthesis of bis-isocyanide **4.20**. To circumvent these issues an analogous route was employed, replacing the appended PEG amide with a phenolic appended octyl chain, to allow for solubility in organic solvents.

An S_N2 reaction between 3,5-dibromophenol and 1-bromooctane in the presence of base formed octyl-appended species **4.21** in 92% yield (Scheme 4.16). Sonogashira coupling between **4.21** and two equivalents of trimethylsilyl acetylene afforded TMS-protected-bis-alkyne **4.22**, which was subsequently reacted with *N*-iodosuccinimide in the presence of silver nitrate to give bis(iodoalkyne) **4.23** in overall 74% yield.



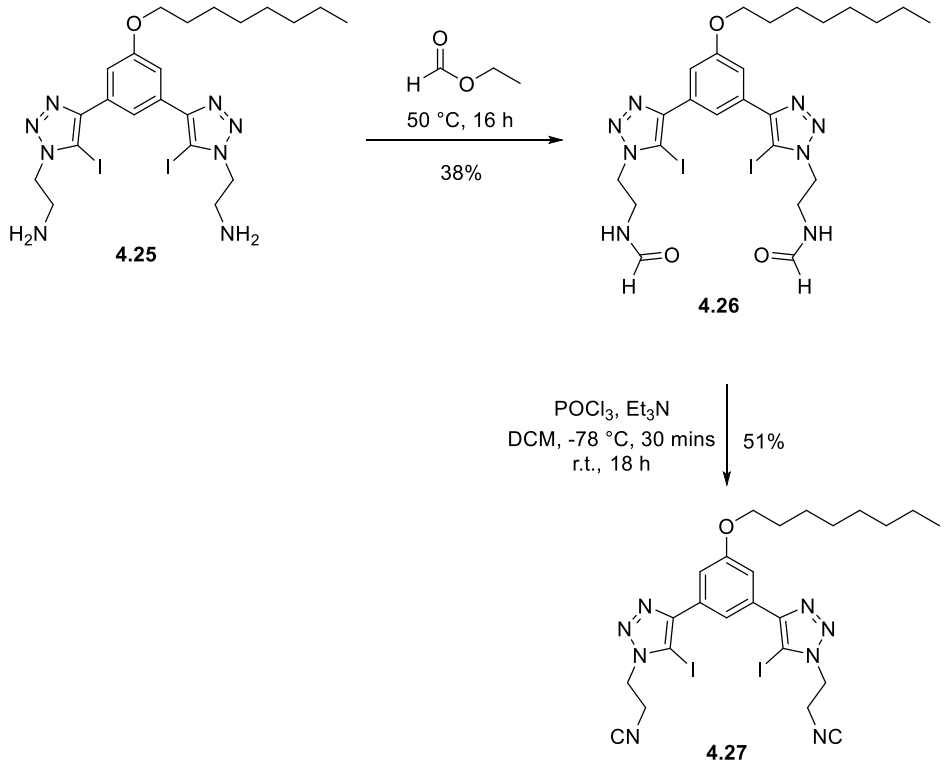
Scheme 4.16: *Synthetic route to alkyl-appended bis(iodoalkyne)* ***4.23***

For the bis-amine component, a CuAAC 'click' reaction between bis(iodoalkyne) **4.23** and two equivalents of BOC-protected azide **4.16** gave bis(iodotriazole) BOC-protected-bis-amine **4.24** in 86% yield. This was followed by deprotection of the BOC group with trifluoroacetic acid in DCM and washing with aqueous $NaHCO_3$ to give bis-amine **4.25** in 92% yield (Scheme 4.17).



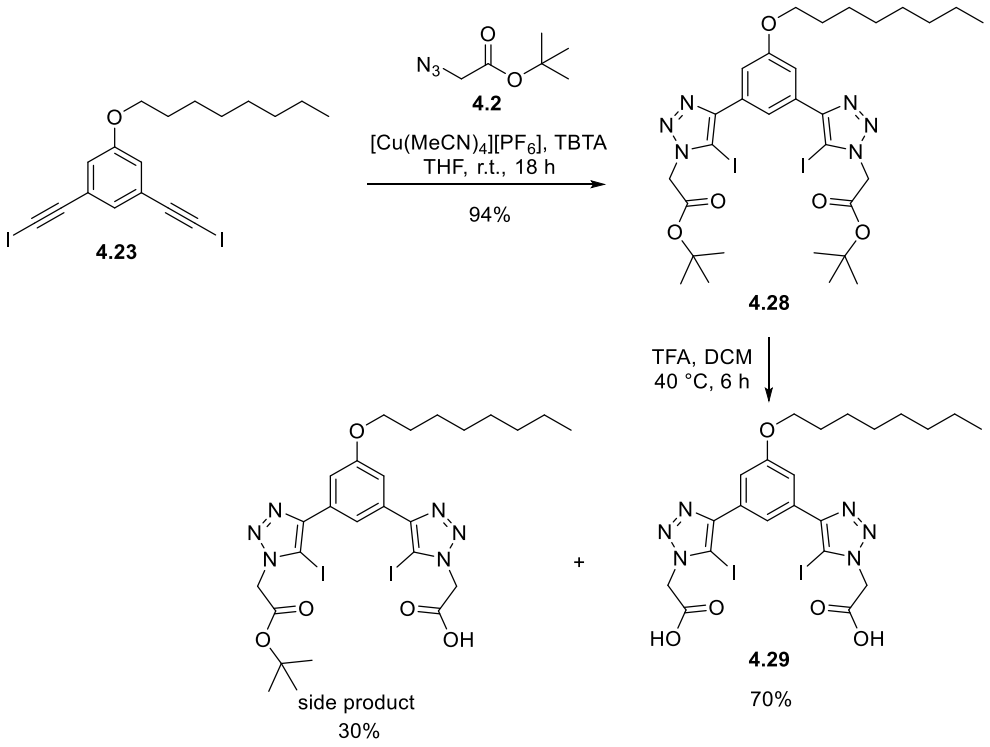
Scheme 4.17: *Synthesis of XB bis-amine* ***4.25***

For the corresponding bis-isocyanide component, bis-amine **4.25** was converted to bis-formamide **4.26** in 38% yield (Scheme 4.18). The low yield was postulated to be due to the low solubility of the bis-amine starting material in ethyl formate, used as both reactant and solvent in the reaction. In an attempt to improve the solubility, a 1:1 mixture of DCM/ ethyl formate was employed; however, minimal improvements in yields were observed. Bis-formamide **4.26** was dehydrated by reaction with $POCl_3$ and Et_3N in DCM to form bis-isocyanide **4.27** in 51% yield.



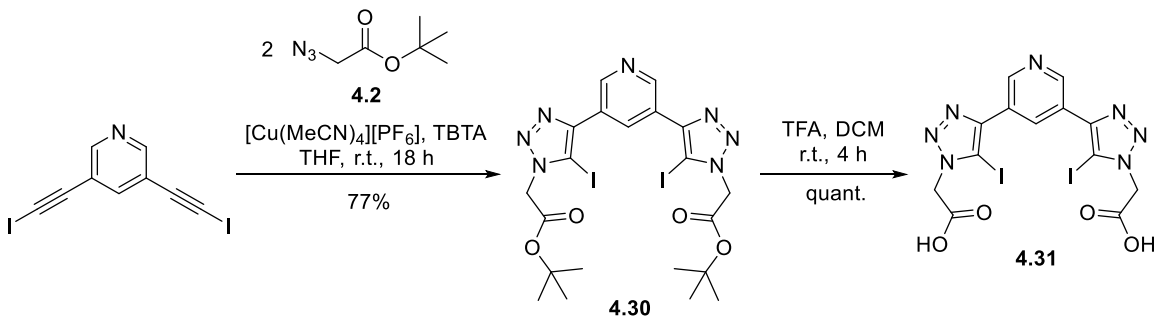
Scheme 4.18: *Synthesis of XB bis-isocyanide* ***4.27***

Attention then turned to the synthesis of the bis-acid unit. A CuAAC 'click' reaction between bis(iodoalkyne) **4.23** and *tert*-butyl ester azide **4.2** gave bis(iodotriazole)-bis-ester **4.28** in 94% yield (Scheme 4.19). Deprotection of the *tert*-butyl ester groups of **4.28** was carried out with trifluoroacetic acid in DCM to give bis-acid **4.29**; however, the corresponding mono-protected acid was again found to be also present and constituted 30% of the product, which could not be separated from the desired product.



Scheme 4.19: *Synthesis of XB bis-acid* ***4.29***

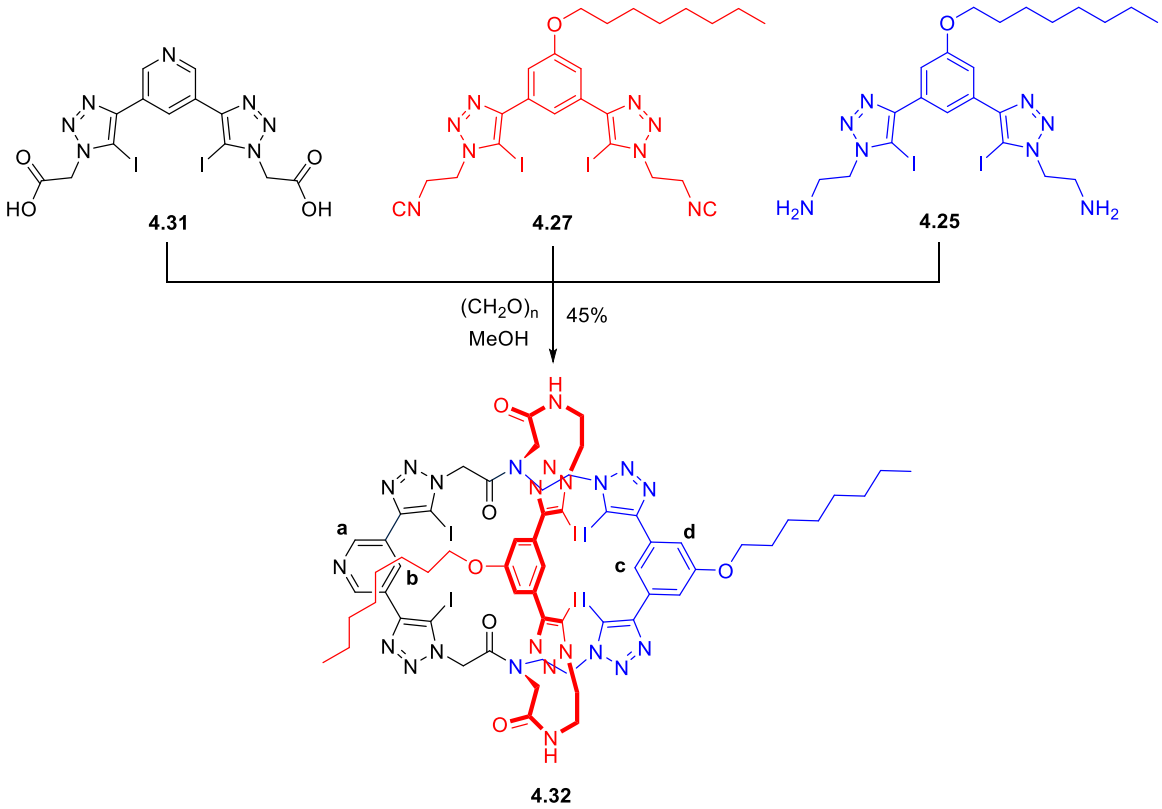
The stoichiometry in the Ugi-4CR, especially when forming complex architectures, is of the upmost importance. Bis-acid **4.29** was therefore not of sufficient purity to be utilised in such a reaction. An alternative pyridine-based bis-acid was targeted, which could also allow for alkylation of the pyridine-*N* after cryptand formation to give a cationic XB cryptand. A CuAAC 'click' reaction was carried out between 3,5-bis(iodoalkyne) pyridine and two equivalents of azide **4.2** to give bis(iodotriazole) product **4.30**. Deprotection with trifluoroacetic acid in DCM gave pure bis-acid **4.31** in quantitative yield (Scheme 4.20).



Scheme 4.20: *Synthesis of XB bis-acid* ***4.31***

4.4.2 Synthesis of XB cryptand

With the bifunctional building blocks prepared, the Ugi-4CR was carried out under pseudo-high dilution conditions to form the target XB cryptand (Scheme 4.21). Bis-amine **4.25** and two equivalents of paraformaldehyde were reacted in MeOH to allow for formation of the corresponding imine. Bis-acid **4.31** (in MeOH/DCM 1:1) and bis-isocyanide **4.27** (in MeOH/DMSO 9:1) were then added by slow addition *via* syringe pump over the course of 12 hours. After three days XB cryptand **4.32** precipitated from solution and the precipitate was washed with MeOH, H_2O and DCM to give pure product in 45% yield.



Scheme 4.21: *Synthesis of XB cryptand* ***4.32*** *via UGI-4CR multimacrocyclisation reaction*

The XB cryptand **4.32** was characterised by high resolution ESI mass spectrometry (Figure 4.4) and despite the very poor solubility in a range of organic solvents the ^{1}H NMR spectrum was obtained in DMSO-d_6 (Figure 4.5). The aromatic region could be assigned, and peaks were observed in the expected regions; however, broadening of the

signals resulted in full assignment not being possible. In an attempt to circumvent these issues, variable-temperature (VT) NMR experiments were carried out, heating XB cryptand **4.32** to 80 °C in DMSO-d_6. However, no appreciable decrease in the broadening of the ^{1}H NMR spectrum at this higher temperature was observed.

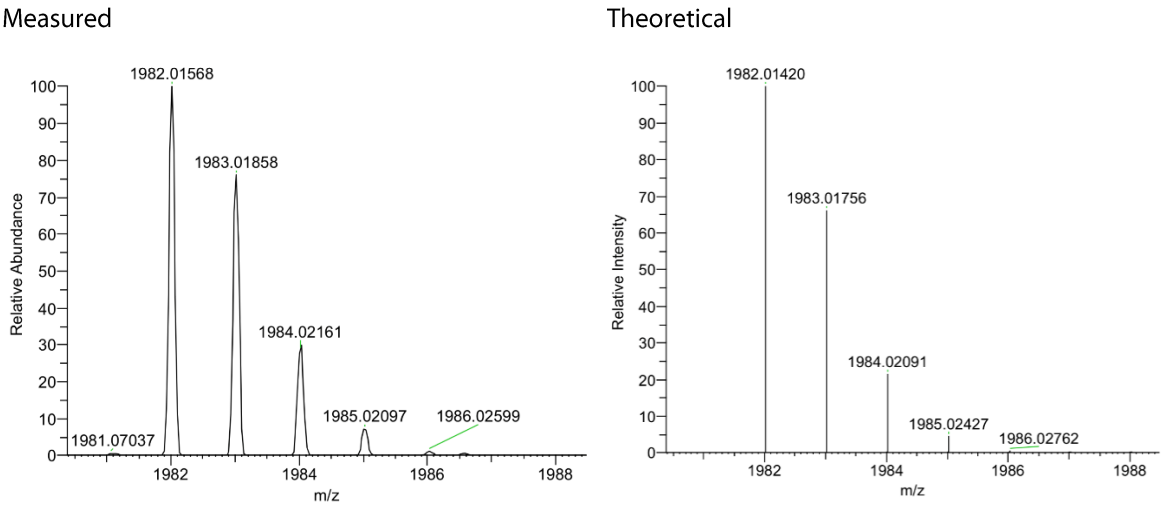


Figure 4.4: *Measured and theoretical high resolution ESI mass spectra of XB cryptand **4.32** corresponding to m/z [M+H]$^+$ calc. 1982.01420, found 1982.01568*

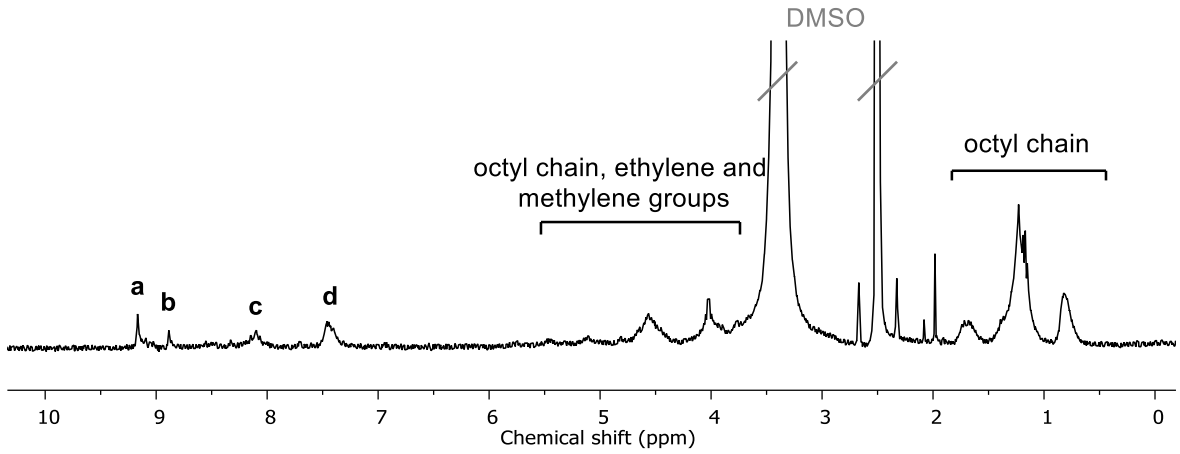


Figure 4.5: *^{1}H NMR spectrum of XB cryptand **4.32** (400 MHz, 298 K, DMSO)*

4.4.3 Fluorescence spectroscopy anion titration studies

The poor solubility of XB cryptand **4.32** in organic solvent media negated ^{1}H NMR anion titration investigations being undertaken. Instead, attention turned to preliminary

photophysical studies to ascertain anion binding behaviour. Initially, the UV–vis absorption and fluorescence spectroscopic properties of XB cryptand **4.32** were investigated in DMSO/$CHCl_3$ 9:1, to determine whether anion titration studies were feasible. The UV–vis spectrum of **4.32** revealed an absorption band at λ_{max} = 300 nm, which corresponded to the π–π^* transition of the substituted phenyl ring.[17] Photoexcitation of the cryptand at 300 nm, resulted in a broad fluorescence spectrum with an emission maxima at ~ 330 nm (Figure 4.6), displaying a Stokes shift of 30 nm, comparable to literature values of substituted phenyl systems.[17]

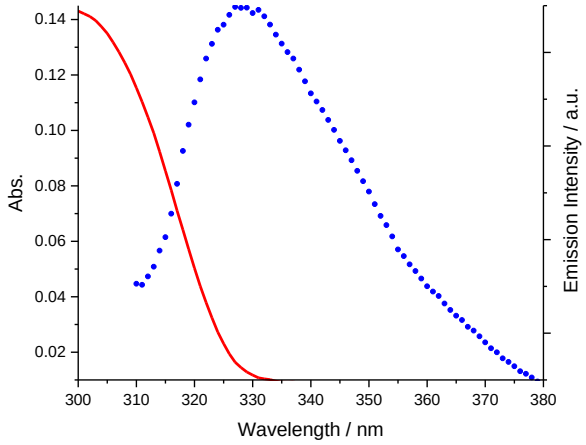


Figure 4.6: *Excitation (red) and emission (blue) spectra of XB cryptand* ***4.32*** *(λ_{ex} = 300 nm, λ_{em} = 330 nm, [5 x 10^{-5} M], 9:1 DMSO/$CHCl_3$)*

Qualitative fluorescence spectroscopic anion titration experiments were carried out with XB cryptand **4.32** by addition of 500 equivalents of TBA halide salts and the change in emission intensity was monitored. Upon addition of chloride, an enhancement in emission intensity was observed possibly due to chloride binding leading to rigidification of the XB cryptand disfavouring nonradiative decay processes. By contrast, iodide induced a quenching of the emission, attributed to the heavy atom effect (Figure 4.7).[18] Interestingly, upon addition of fluoride a complete disappearance of any emissive behaviour was observed, postulated to be due to deprotonation of the system.

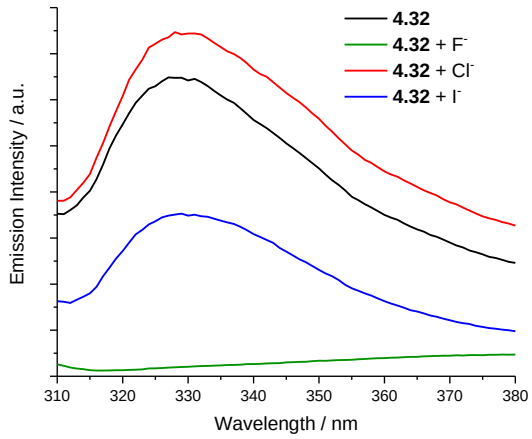


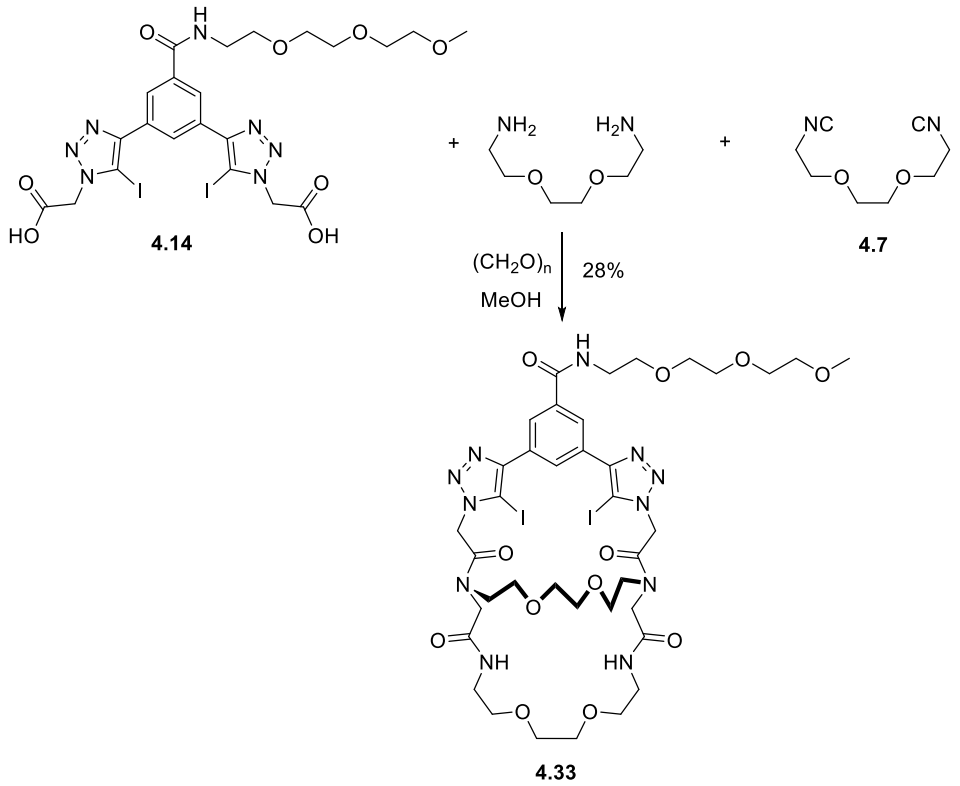
Figure 4.7: *Changes in luminescence emission intensity upon addition of 500 equivalents of halide anions (added as their TBA salts) to XB cryptand* ***4.32*** *(9:1 DMSO/$CHCl_3$, [5 x 10^{-5}], λ_{ex} = 300 nm)*

4.5 Towards the synthesis of soluble XB cryptands

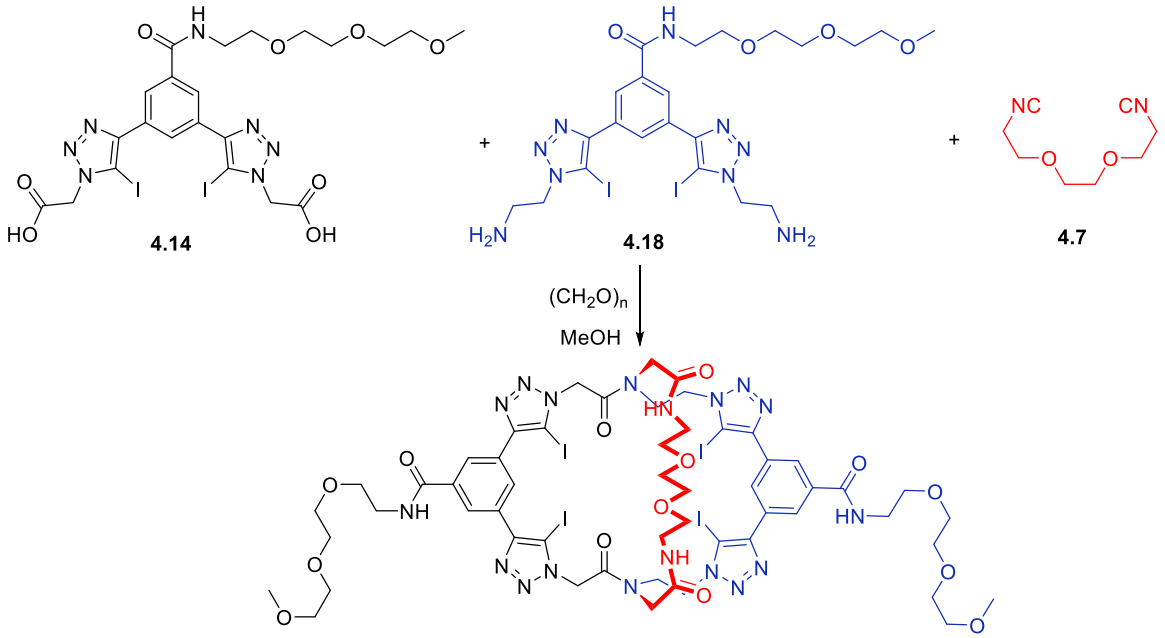
The ability of the Ugi-4CR to construct XB complex architectures in relatively high yield has been demonstrated (Section 4.4). To extend this work and obtain quantitative anion binding data, methods towards improving the solubility of the XB cryptands formed, both in organic and ultimately aqueous media, were investigated. Preliminary investigations into the influence of polyether groups on the solubility of cryptands were performed, by utilising already prepared synthons. PEG amide appended bis-acid **4.14** could not be separated from the mono-protected ester-acid side product. However, small scale test reactions were carried out to gain preliminary trends in solubility behaviour.

Macrobicycle **4.33** was synthesised *via* an Ugi-4CR between the crude PEG amide appended bis-acid **4.14** (90% pure), bis-isocyanide **4.7** and 1,2-bis(2-aminoethoxy)ethane with two equivalents of paraformaldehyde in MeOH, under pseudo-high dilution conditions (Scheme 4.22). The product was purified from this crude mixture *via* preparative TLC. Characterisation by ^{1}H NMR spectroscopy revealed a significant improvement in solubility in organic solvents from macrobicycle **4.9** (only soluble in DMSO) through to macrobicycle **4.33** (MeOH) due to the lipophilic PEG amide group

appended to the bidentate XB bis-acid component. Consequently, these findings could be applied to the synthesis of a soluble tetradentate XB host in which PEG motifs are appended to both XB donor components, as outlined in Scheme 4.23.



Scheme 4.22: *Synthesis of XB macrobicycle* ***4.33***



Scheme 4.23: *Envisaged synthesis of tetradentate XB macrobicycle*

4.6 Conclusions

The Ugi-4CR has successfully been applied to the formation of XB host systems for anion recognition. Firstly, test reactions were carried out to determine the feasibility of the Ugi-4CR towards the building of host architectures containing XB donors. Specifically, a simple acyclic system was targeted that incorporated the 1,3-bis(iodotriazole)benzene motif into a bis-acid structure, which, when reacted with two equivalents of cyclohexyl isocyanide, *tert*-butyl amine and paraformaldehyde, gave XB acyclic system **4.5** in 81% yield.

The scope of the reaction was then extended to the formation of a macrocycle, utilising bifunctional acid and isocyanide components to give XB macrocycle **4.8** in an impressive 55% yield in which six components were reacted to form eight new covalent bonds. Importantly, pseudo-high dilution conditions were implemented to minimise oligomeric products being formed. A macrobicycle was targeted, by employing bifunctional acid, isocyanide and amine components, again under pseudo-high dilution conditions to give macrobicycle **4.9** in 32% yield.

Ambitiously, the application of Ugi-4CR for the construction of an XB cryptand was investigated. The strategy employed was to implement bifunctional acid, amine and isocyanide components, all incorporating the 1,3-bis(iodotriazole)benzene motif. Initially, amide PEG groups were appended to each component to impart solubility. Problems were encountered with the synthetic routes employed, including the inability to isolate PEG amide appended bis-acid **4.14** and competing side reactions in the synthesis of bis-isocyanide **4.20**. A modified route, appending an octyl chain *via* a phenolic linkage to the Ugi-4CR components proved more straightforward, with the successful isolation of bis-amine **4.25** and bis-isocyanide **4.27**. Full deprotection to form bis-acid **4.29** could not be achieved and therefore pyridine-based bis-acid **4.31** was synthesised to circumvent this issue.

A Ugi-4CR multi-macrocyclisation reaction was carried out between bis-amine **4.25**, bis-isocyanide **4.27**, bis-acid **4.31** and paraformaldehyde, under pseudo-high dilution conditions. Impressively, a cryptand **4.32** containing six iodotriazole XB donors was isolated in 45% yield, characterised *via* high resolution ESI mass spectrometry and ^{1}H NMR spectroscopy.

Preliminary qualitative fluorescence anion titration experiments were carried out on XB cryptand **4.32** with TBA halide salts. In all cases, a change in emission intensity was observed, suggesting a successful binding event. For addition of chloride, an enhancement in emission intensity was observed, whereas iodide displayed quenching and fluoride exhibited a complete disappearance of the emission band.

In conclusion, the Ugi-4CR has been utilised for the first time in the construction of complex architectures incorporating XB donors with the aim of binding anions. Most impressively, the synthesis of XB cryptand **4.32** combined five components and formed eight new covalent bonds in one-pot and yielded a structure incorporating six iodotriazole XB donor groups. The synthesis of cryptand-like structure incorporating XB

donors is unprecedented in the literature, highlighting the originality of the work presented in this chapter.

4.7 Future work

Efforts should now focus on extending the initial results toward improving solubility outlined in Section 4.5. Firstly, to impart solubility in organic solvents, an increased number of solubilising groups could be incorporated into the structure, by employing, for example, tris-octyl appended bis-acid and bis-amine components (Figure 4.8).

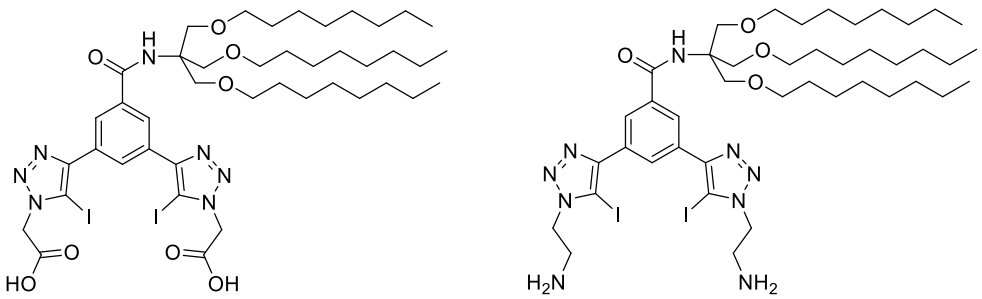
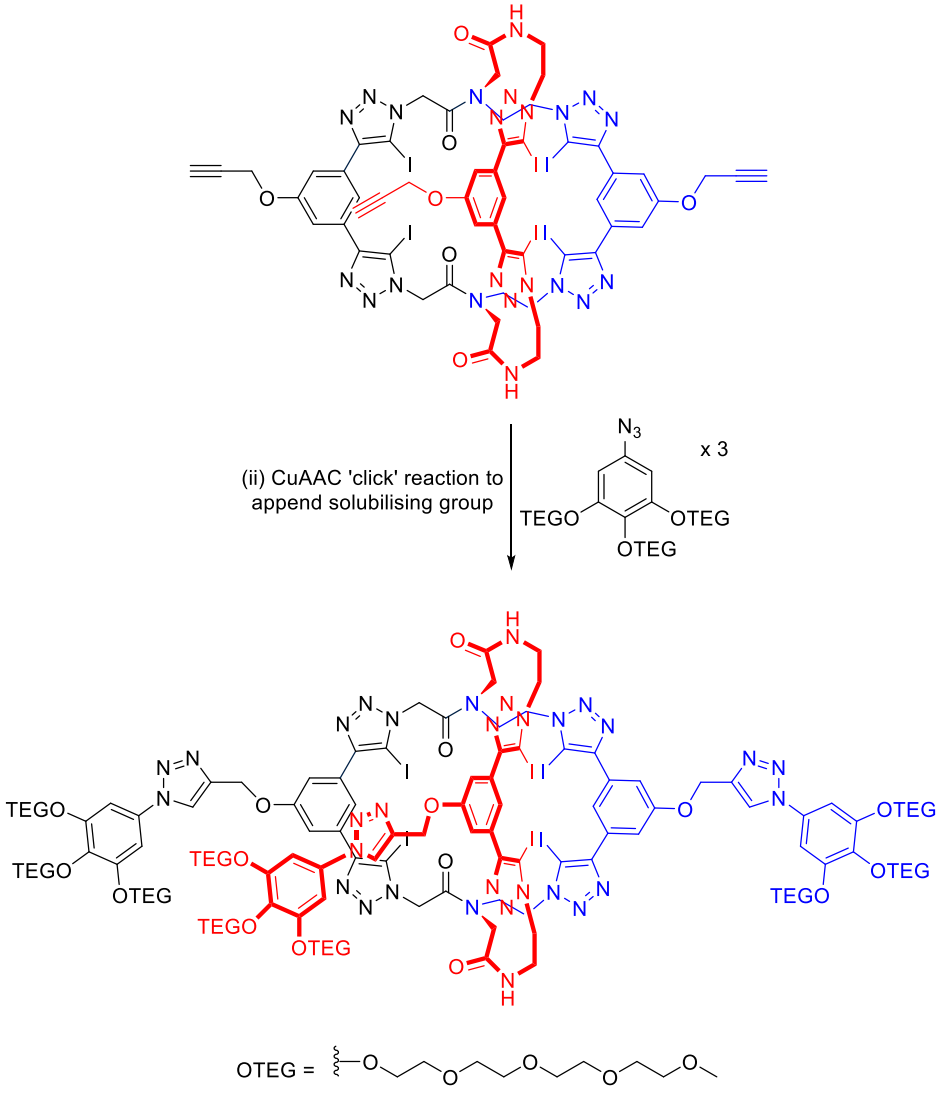


Figure 4.8: *Proposed structures with appended tris-octyl groups to impart solubility in organic solvents*

An alternative strategy is to first form the cryptand and subsequently append solubilising groups. This is particularly advantageous toward the formation of a water soluble cryptand. By first forming the cryptand without solubilising groups, the inherent insolubility of the product will result in its precipitation from solution, with no further purification necessary. Post-synthetic modification could then be carried out, to yield a water soluble XB cryptand (Scheme 4.24).



Scheme 4.24: *Proposed post-synthetic modification of an XB cryptand to impart solubility in aqueous media*

4.8 References

1 J. M. Lehn, E. Sonveaux and A. K. Willard, *J. Am. Chem. Soc.*, 1978, **100**, 4914–4916.

2 B. Dietrich, J.-M. Lehn, J. Guilhem and C. Pascard, *Tetrahedron Lett.*, 1989, **30**, 4125–4128.

3 S. D. Reilly, G. R. K. Khalsa, D. K. Ford, J. R. Brainard, B. P. Hay and P. H. Smith, *Inorg. Chem.*, 1995, **34**, 569–575.

4 S. O. Kang, J. M. Llinares, D. Powell, D. VanderVelde and K. Bowman-James, *J. Am. Chem. Soc.*, 2003, **125**, 10152–10153.

5 S. O. Kang, D. VanderVelde, D. Powell and K. Bowman-James, *J. Am. Chem. Soc.*, 2004, **126**, 12272–12273.

6 A. Strecker, *Ann. der Chemie und Pharm.*, 1850, **75**, 27–45.

7 C. Mannich and W. Krösche, *Arch. Pharm.*, 1912, **250**, 647–667.

8 L. Banfi and R. Riva, in *Organic Reactions*, John Wiley & Sons, Inc., Hoboken, NJ, USA, 2005, pp. 1–140.

9 A. Dömling and I. Ugi, *Angew. Chem.*, 2000, **39**, 3168–3210.

10 I. Ugi, *Angew. Chem.*, 1959, **71**, 373–388.

11 D. G. Rivera and L. A. Wessjohann, *J. Am. Chem. Soc.*, 2006, **128**, 7122–7123.

12 O. Mumm, H. Hesse and H. Volquartz, *Berichte der Dtsch. Chem. Gesellschaft*, 1915, **48**, 379–391.

13 D. G. Rivera, O. E. Vercillo and L. A. Wessjohann, *Org. Biomol. Chem.*, 2008, **6**, 1787–1795.

14 L. A. Wessjohann, O. Kreye and D. G. Rivera, *Angew. Chem. Int. Ed.*, 2017, **56**, 3501–3505.

15 J. Y. C. Lim, T. Bunchuay and P. D. Beer, *Chem. Eur. J.*, 2017, **23**, 4700–4707.

16 D. Dou, G. He, Y. Li, Z. Lai, L. Wei, K. R. Alliston, G. H. Lushington, D. M. Eichhorn and W. C. Groutas, *Bioorg. Med. Chem.*, 2010, **18**, 1093–1102.

17 D. Ghosh, S. Rhodes, K. Hawkins, D. Winder, A. Atkinson, W. Ming, C. Padgett, J. Orvis, K. Aiken and S. Landge, *New J. Chem.*, 2015, **39**, 295–303.

18 A. Chmyrov, T. Sandén and J. Widengren, *J. Phys. Chem. B*, 2010, **114**, 11282–11291.

Chapter Five

Conclusions

5 Conclusions

The work described in this thesis was focused on the incorporation of halogen bond donor groups into interlocked host systems and complex architectures for anion recognition. Chapter Two introduced the novel imidazolium–iodotriazole and corresponding –triazole motifs and initially they were incorporated into acyclic systems. The XB receptor demonstrated a modest increase in the chloride anion association constant compared to the HB analogue in competitive aqueous–organic solvent. Axles containing the motifs were then prepared for utilisation of a chloride-template 'clipping' methodology for rotaxane formation. The HB [2]rotaxane was successfully isolated; however, the analogous XB system proved to be unstable. The interlocked HB system displayed a moderate degree of selectivity between the halides following anion basicity trends ($Cl^- > Br^- > I^-$). Of most importance, comparison of the XB and HB acyclic systems and HB [2]rotaxane demonstrated analogous magnitudes of the chloride anion association constant, with little influence imparted from the formation of the interlocked cavity, which suggested a dominance of favourable electrostatic–driven binding with this motif. In all cases, a 1:2 (host/guest) binding stoichiometry was observed, postulated to be due to the first binding event K_1 occurring at the most acidic imidazolium C^2-proton dominated by electrostatically–driven hydrogen bonding and the second binding event, corresponding to the much weaker K_2, from binding utilising the HB/XB donors. This hypothesis was confirmed by the anion binding properties of an analogous HB 2-methylimidazolium–triazole receptor, designed to block the electrostatically–driven binding at the imidazolium C^2-position. Interestingly, a substantial 60-fold decrease in the chloride association constant was observed upon incorporation of the methyl group. It has therefore been established that the anion binding properties of the imidazolium–triazole motif should be considered to be dominated by charge–driven hydrogen bonding interactions at the imidazolium C^2-position, with small contributions from the HB or XB triazole donor groups (Figure 5.1).

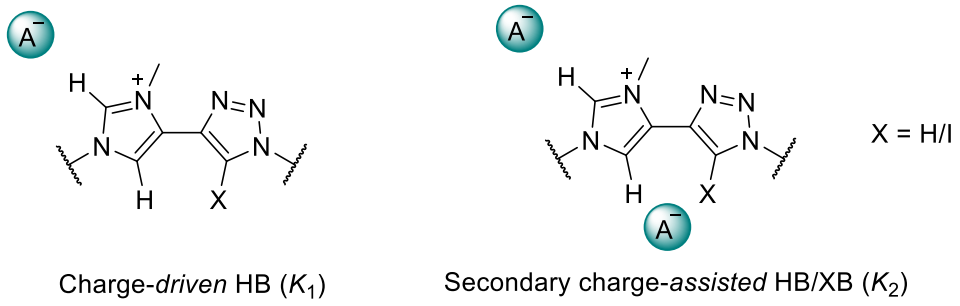


Figure 5.1: *Two binding events of the imidazolium-triazole motif determined from the results of Chapter 2*

Building on these findings, Chapter Three utilised the charge–driven hydrogen bonding at the imidazolium C^2-position in a convergent manner with appended HB and XB triazole donors. Specifically, the bis(iodotriazole)–imidazolium and corresponding HB analogue were incorporated into the axle component of [2]rotaxanes (Figure 5.2). Both HB and XB rotaxanes exhibited strong halide and sulfate binding in competitive aqueous–organic solvent. In particular, the XB rotaxane displayed preference for the relatively smaller anions Cl^- = Br^- > SO_4^{2-} > I^-, whereas HB rotaxane showed no pronounced selectivity between Cl^-, I^- and SO_4^{2-}. These results demonstrated the potency of these systems for anion recognition in competitive media and the ability of XB donors to enhance selectivity between anions. A hetero[3]rotaxane was then ambitiously targeted, achieved through the combination of an active-metal template rotaxanation reaction on a chloride-template assembly. Evidence of the successful formation of hetero[3]rotaxane was observed in the ESI mass spectrum and provided promising proof-of-principle results.

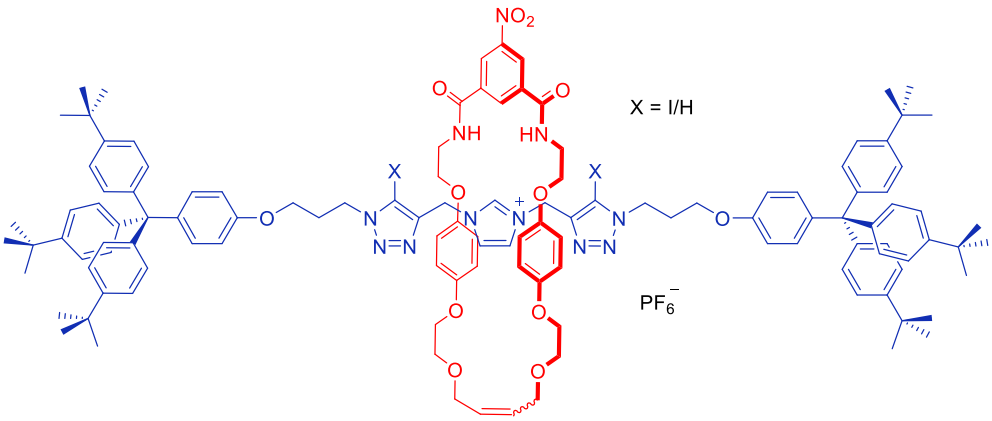


Figure 5.2: *XB and HB imidazolium-based [2]rotaxanes reported in Chapter Three*

Chapter Four presents the first example of the Ugi-4CR being employed for the construction of complex host architectures integrating XB donors for anion recognition. The 1,3-bis(iodotriazole)benzene motif was incorporated into acyclic, macrocyclic and macrobicyclic structures *via* the Ugi-4CR in impressively high yields. Most remarkable, a XB cryptand whose structure contained six iodotriazole XB donor groups was synthesised in 45% yield from five individual components, where eight new covalent bonds were formed in one-pot (Figure 5.3). Qualitative fluorescence anion titration experiments were carried out and upon addition of halides a change in emission intensity was observed; for chloride, an enhancement was observed, whereas iodide displayed quenching and fluoride exhibited a complete disappearance of emission. Promisingly, these results suggested a successful binding event was occurring. The synthesis of a cryptand-like structure incorporating XB donors is unprecedented in the literature; this work demonstrates the successful synthesis of such a system and provides an exciting avenue of exploration for the construction of multidentate XB host systems in the future.

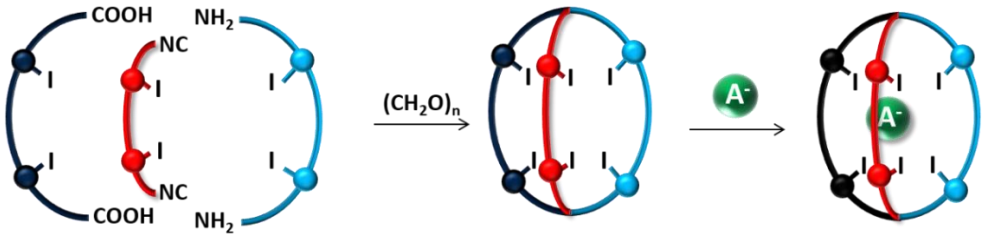


Figure 5.3: *Schematic representation of the construction of a XB cryptand via the Ugi-4CR outlined in Chapter Four*

In summary, the results in this thesis demonstrate the efficacy of three-dimensional preorganised halogen bonding host systems in overcoming the challenges of anion recognition. Still in its infancy, halogen bonding has been shown to be an attractive and competitive alternative to traditional non-covalent interactions and will no doubt be exploited extensively in the future. Ultimately, this work paves the way towards the realisation of strong and selective binding of negatively charged species and, taking inspiration from the ingenuity of Nature, further innovation of synthetic host systems will continue.

Chapter Six

Experimental

6.1 General considerations

6.1.1 Solvents and reagents

All solvents and reagents were used from commercial suppliers and used as received, unless otherwise stated. All deuterated solvents used were purchased from chemical suppliers. Anhydrous solvents were obtained by purging with $N_{2(g)}$ and dried by passing through an MBraun MPSP-800 column. Water was micro-filtered and de-ionised using a Milli-Q® Millipore machine. Triethylamine was distilled and stored over KOH pellets. Tetrabutylammonium (TBA) salts, Grubbs' II catalyst and $[Cu(MeCN)_4][PF_6]$ were stored in a vacuum desiccator containing phosphorus pentoxide prior to use. Where mixtures of solvents were used, ratios are reported by volume. Brine refers to a saturated aqueous solution of NaCl, aqueous ammonia refers to a 10% solution of NH_3 in water. Chromatography was undertaken using silica gel (particle size: 40-63 μm) or preparative TLC plates (20 x 20 cm, 1 mm silica thickness). Literature procedures were used to prepare known compounds, as referenced in the text. TBTA was prepared by Dr Thanthaptra Bunchuay.[1]

6.1.2 Characterisation and instrumentation

^{1}H, ^{13}C and ^{19}F NMR spectra were recorded using Bruker AVIII 400 and Bruker AVIII 500 spectrometers at 298 K. ^{1}H–^{1}H coupling constants are reported as 3-bond (^{3}J) unless otherwise indicated and assignments were aided by the use of two-dimensional ROESY and COSY NMR spectroscopies. Low resolution ESI mass spectra were recorded on a Walters LCT premier spectrometer. High resolution ESI mass spectra were recorded on a Bruker μTOF instrument. A Biotage Initiator 2.0 microwave was used to perform dielectric microwave heating. UV-vis spectroscopy was carried out on a T60U (PG Instruments Ltd) spectrophotometer and fluorescence spectra were recorded on a Horiba Fluorolog 3 using a quartz cuvette with a path length of 1 cm.

6.1.3 Titration protocols

Spectra for ^{1}H NMR titrations were performed on the Bruker AVIII 500 spectrometers at 298 K. In a typical titration experiment, the initial sample volume was 0.50 mL and concentrations were either 1.0 or 2.0 mM of host. Solutions of anions as their tetrabutylammonium salts were added in aliquots, the samples thoroughly shaken and spectra recorded at 0, 0.2, 0.4, 0.6, 0.8, 1.0, 1.2, 1.4, 1.6, 1.8, 2.0, 2.5, 3.0, 4.0, 5.0, 7.0, 10.0 and 15.0 equivalents of anion (0.2 eq = 0.2 μL). The chemical shift of the appropriate proton environments was monitored. The spectra were referenced to the residual solvent peak. In all cases where association constants were calculated, bound and unbound species were found to be in fast exchange on the NMR timescale.

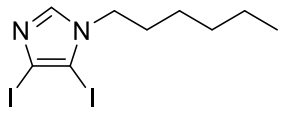
The chemical shift at each guest concentration were entered into the WinEQNMR2[2] computer program for every titration point and estimates for the binding constant and limiting chemical shifts were made. The parameters were refined by non-linear least-squares analysis using either a host-guest 1:1 or 1:2 stoichiometric binding model to obtain the best-fit between the observed and calculated chemical shifts, until convergence was reached. WinEQNMR2[2] provides an estimate of the standard error of the measurement. These errors account for the fitting of the binding isotherm to the titration data but do not account for systematic errors, such as incorrect addition of titrant solution.

Fluorescence spectroscopy titrations were performed using Horiba Fluorolog 3 and the data were processed using OriginPro software. The anion of interest was dissolved in the same receptor solution as that being studied to maintain the same receptor concentration during titrations. An aliquot of anion solution was added to the receptor solution and the fluorescence spectrum recorded.

6.2 Synthetic procedures

6.2.1 Synthesis of novel compounds from Chapter 2

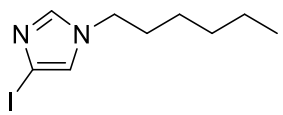
1-Hexyl-4,5-diiodoimidazole 2.2



4,5-Diiodoimidazole **2.1** (2.24 g, 7.0 mmol) was dissolved in anhydrous THF (20 mL) and cooled to 0 °C. NaH (168 mg, 7.0 mmol) was added portionwise under N_2 and left to stir for 1 hour at room temperature. Iodohexane (0.742 g, 3.50 mmol) was added portionwise at 0 °C, then the mixture was allowed to warm to room temperature and stirred under N_2 for 18 hours at 60 °C. The reaction was quenched by addition of H_2O. THF was removed *in vacuo* and the residue re-dissolved in $CHCl_3$ (50 mL). The organics were washed with aqueous HCl (25 mL), sat. $Na_2S_2O_{3(aq)}$ (25 mL), H_2O (25 mL) and brine (25 mL) and dried over anhydrous $MgSO_4$. The crude product was purified *via* silica gel column chromatography (EtOAc/Hex 1:3) to afford 1-hexyl-4,5-diiodoimidazole **2.2** as a yellow oil (0.920 g, 65%).

^{1}**H NMR** (400 MHz; $CDCl_3$) δ (ppm): 7.59 (1H, s, NC*H*N), 3.95 (2H, t, *J*= 7.4 Hz, CH_2), 1.74 (2H, quint, *J*=7.1 Hz, CH_2), 1.32-1.27 (6H, m, CH_2), 0.96–0.83 (3H, m, CH_3); ^{13}**C NMR** (101 MHz; $CDCl_3$) δ (ppm): 140.99, 95.90, 50.02, 31.31, 30.65, 26.14, 22.59, 14.09 (one peak missed, presumed overlapped); **HRESI-MS** (pos) $C_9H_{15}N_2I_2$ *m/z*: $[M+H]^+$ *calc.* 404.93191, *found* 404.93184.

1-Hexyl-4-iodoimidazole 2.3

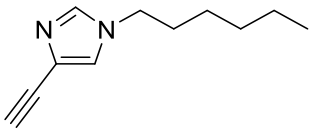


1-Hexyl-4,5-diiodoimidazole **2.2** (0.330 g, 0.82 mmol) was dissolved in anhydrous THF (3 mL) and cooled to 0 °C. EtMgBr (3 M in Et_2O, 0.3 mL) was added dropwise under N_2 and the reaction mixture was stirred for 1 hour. H_2O (0.01 mL) was added to quench the

reaction and stirred for 10 mins. Sat. $NH_4Cl_{(aq)}$ (10 mL) was added and the product extracted into DCM (3 × 25 mL). The combined organics were washed with sat. $NH_4Cl_{(aq)}$ (10 mL) and brine (10 mL) and dried over anhydrous $MgSO_4$. The crude product was purified *via* silica gel column chromatography (EtOAc/Hexane 2:1) to afford 1-hexyl-4-iodoimidazole **2.3** as a pale yellow oil (0.174 g, 76%).

^{1}H NMR (400 MHz; $CDCl_3$) δ (ppm): 7.35 (1H, d, *J*=1.3 Hz, NC*H*N), 6.98 (1H, d, *J*=1.3 Hz, CIC*H*N), 3.90 (2H, t, *J*=7.2 Hz, CH_2), 1.74 (2H, quint, *J*=7.1 Hz, CH_2), 1.32-1.27 (6H, m, CH_2), 0.95–0.80 (3H, m, CH_3); **^{13}C NMR** (101 MHz; $CDCl_3$) δ (ppm): 138.75, 124.55, 81.76, 47.60, 31.31, 31.01, 26.27, 22.57, 14.09; **HRESI-MS** (pos) $C_9H_{16}N_2I$ *m/z*: **[M+H]$^+$** *calc.* 279.03527, *found* 279.03523.

Imidazole-alkyne derivative 2.5

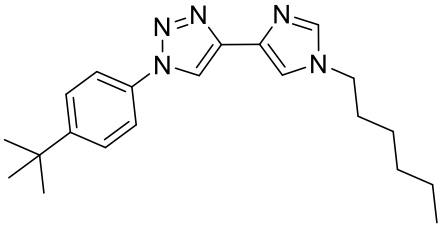


1-Hexyl-4-iodoimidazole **2.3** (0.200 g, 0.72 mmol) was dissolved in anhydrous DMF (7 mL). CuI (0.023 g, 0.12 mmol), $Pd(PPh_3)_2Cl_2$ (0.071 g, 0.10 mmol) and Et_3N (0.5 mL) were added and the reaction mixture degassed with argon for 10 mins. Thereafter, trimethylsilyl acetylene (0.34 mL, 2.38 mmol) was added and the mixture heated under microwave irradiation at 80 °C for 30 mins. The solvent was removed *in vacuo* and the residue re-dissolved in ethyl acetate and filtered through Celite. The filtrate was concentrated *in vacuo*. Purification *via* silica gel column chromatography (EtOAc/Hexane 1:1) yielded the TMS protected alkyne. Deprotection was carried out immediately; the protected alkyne was dissolved in MeOH (5 mL) and K_2CO_3 (5 eq) added. The reaction mixture was stirred for 4 hours at room temperature and the progress of the reaction was monitored by TLC. Upon completion, the solvent was removed *in vacuo* and the reaction mixture was re-dissolved in DCM (30 mL) and washed with H_2O (3 × 20 mL) and brine

(20 mL). The solvent was removed *in vacuo* to yield imidazole-alkyne derivative **2.5** as a yellow oil (0.076 g, 60%). No further purification was necessary.

^{1}**H NMR** (400 MHz; $CDCl_3$) δ (ppm): 7.38 (1H, s, NC*H*N), 7.12 (1H, s, NC*H*C), 3.89 (2H, t, *J*=7.0 Hz, NCH_2), 3.04 (1H, s, C*CH-alkyne)*, 1.76 (2H, quint, *J*=7.0 Hz, NCH_2CH_2), 1.32-1.27 (6H, m, CH_2), 0.95-0.80 (3H, m, CH_2CH_3); ^{13}**C NMR** (101 MHz; $CDCl_3$) δ (ppm): 186.32, 142.44, 138.67, 124.16, 77.23, 47.77, 31.12, 30.79, 26.10, 22.40, 13.92; **ESI-MS** (pos.) $C_{11}H_{17}N_2$ *m/z*: $[M+H]^+$ *calc.* 177.13, *found* 177.13.

Imidazole-triazole derivative 2.7

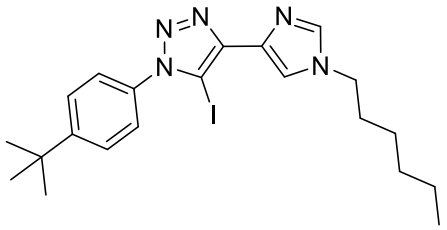


Imidazole–alkyne **2.5** (0.160 g, 0.91 mmol) and 4-*tert*-butylphenyl azide **2.6** (0.239 g, 1.37 mmol) were dissolved in dry DCM (20 mL). TBTA (0.097 g, 0.182 mmol) followed by $[Cu(MeCN)_4][PF_6]$ (0.068 g, 0.18 mmol) and DIPEA (0.376 g, 2.91 mmol) were added and the reaction mixture was stirred at room temperature for 18 hours. The reaction mixture was diluted with DCM (20 mL) and washed with $NH_4OH_{(aq)}$ (3 × 20 mL) and brine (2 × 15 mL) and dried over anhydrous $MgSO_4$. The solvent was removed *in vacuo* and the reaction mixture was purified *via* silica gel column chromatography (DCM/MeOH 97:3) to afford imidazole–triazole derivative **2.7** as a white solid (0.258 g, 84%).

^{1}**H NMR** (400 MHz; $CDCl_3$) δ (ppm): 8.29 (1H, s, NC*H*N-*imidazole*), 7.73-7.68 (2H, m, Ar*H*), 7.57-7.51 (2H, m, Ar*H*), 7.54 (1H, s, NC*H*C-*imidazole*), 7.50 (1H, s, C*H-triazole)*, 3.99 (2H, t, *J*=7.0 Hz, NCH_2), 1.83 (2H, quint, *J*=7.0 Hz, NCH_2CH_2), 1.37 (9H, s, *tert*-CH_3), 1.33-1.26 (6H, m, CH_2), 0.97-0.79 (3H, m, CH_2CH_3); ^{13}**C NMR** (126 MHz; $CDCl_3$) δ (ppm): 151.98, 137.32, 134.92, 133.97, 126.77, 120.18, 117.34, 116.33, 115.56, 47.58, 34.98,

31.43, 31.39, 31.07, 26.36, 22.62, 14.12; **HRESI-MS (pos.):** $C_{21}H_{30}N_5$ *m/z*: $[M+H]^+$ *calc.* 352.24957, *found* 352.24933.

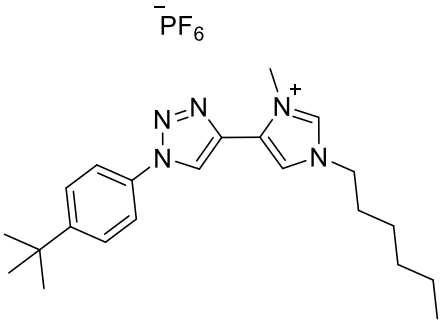
Imidazole-iodotriazole derivative 2.8



4-*tert*-Butylphenyl azide **2.6** (0.109 g, 0.62 mmol), $Cu(ClO_4)_2.6H_2O$ (0.419 g, 1.13 mmol) and NaI (0.340 g, 2.27 mmol) were dissolved in dry THF (3 mL), covered with foil and stirred for 5 minutes at room temperature. TBTA (0.030 g, 0.057 mmol) was added the reaction allowed to stir for a further 5 minutes. A solution of DBU (0.086 g, 0.58 mmol) in THF (0.5 mL) was added, followed by imidazole–alkyne **2.5** (0.100 g, 0.57 mmol). This was left to stir overnight at room temperature and then diluted with DCM (100 mL) before being washed with $NH_4OH_{(aq)}$ (3 × 20 mL) and brine (2 × 20 mL). The organics were collected and dried over anhydrous $MgSO_4$ and the solvent removed *in vacuo*. The reaction mixture was purified *via* silica gel column chromatography (EtOAc/Hexane 3:2) to afford imidazole–iodotriazole species **2.8** as a white solid (0.196 g, 72%).

^{1}**H NMR** (400 MHz; $CDCl_3$) δ (ppm): 8.31 (1H, s, NC*H*N-*imidazole*), 7.58 (1H, s, NC*H*C-*imidazole*), 7.57-7.53 (2H, m, Ar*H*), 7.49-7.44 (2H, m, Ar*H*), 3.99 (2H, t, J = 7.1 Hz, NCH_2), 1.83 (2H, quint, J = 7.1 Hz, NCH_2CH_2), 1.39 (9H, s, *tert*-CH_3), 1.33-1.26 (6H, m, CH_2), 1.02-0.78 (3H, m, CH_2CH_3); **ESI-MS** (pos.) $C_{21}H_{29}IN_5$ *m/z*: $[M+H]^+$ *calc.* 478.14, *found* 478.13.

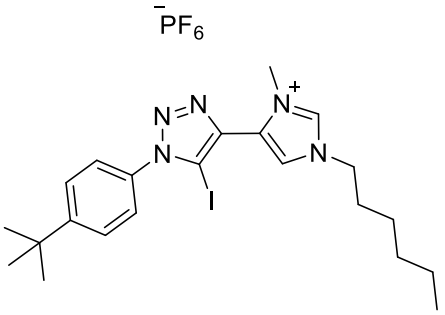
Imidazolium-triazole derivative 2.9·PF_6



Imidazole–triazole species **2.7** (0.020 g, 0.057 mmol) was dissolved in DCM (5 mL). MeI (0.17 mL, 1.14 mmol) was added and the mixture stirred at room temperature. The progress of the reaction was monitored *via* TLC. Upon completion, the reaction mixture was concentrated *in vacuo* and dried under high vacuum to yield imidazolium–triazole species **2.9**·I. The product was subsequently dissolved in DCM (20 mL) and washed with $NH_4PF_{6(aq)}$ (0.1 M, 8 × 30 mL) and H_2O (2 × 30 mL). The solvent was removed *in vacuo* to yield **2.9**·PF_6 (0.027 g, 96%).

^{1}**H NMR** (400 MHz; $CDCl_3$) δ (ppm): 8.59 (1H, s, NC*H*N-*imidazole*), 8.50 (1H, s, NC*H*C-*imidazole*), 7.73 (2H, d, *J* = 8.3 Hz, Ar*H*), 7.65 (1H, s, C*H-triazole*), 7.58 (2H, d, *J* = 8.3 Hz, Ar*H*), 4.21 (2H, t, *J* = 7.6 Hz, NCH_2), 4.15 (3H, s, N^+CH_3), 1.94 (2H, quint, *J* = 7.6 Hz, NCH_2CH_2), 1.37 (9H, s, *tert*-CH_3), 1.35-1.30 (6H, m, CH_2), 0.92-0.86 (3H, m, CH_2CH_3); ^{13}**C NMR** (126 MHz; $CDCl_3$) δ (ppm): 153.17, 136.50, 134.40, 133.89, 127.07, 126.97, 122.17, 120.45, 120.40, 50.64, 36.27, 35.02, 31.37, 31.10, 29.86, 25.99, 22.46, 14.02.; **HRESI-MS** (pos.) $C_{22}H_{32}N_5^+$ *m/z:* $[M\text{-}PF_6]^+$ *calc.* 366.26522, *found* 366.26536.

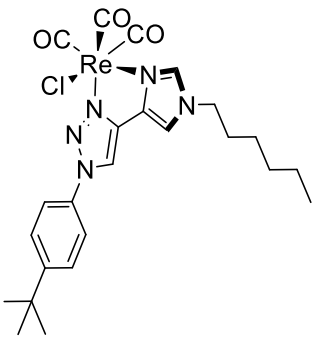
Imidazolium-iodotriazole derivative 2.10·PF_6



Imidazole–triazole species **2.8** (0.020 g, 0.042 mmol) was dissolved in DCM (5 mL). MeI (0.13 mL, 0.84 mmol) was added and the mixture stirred at room temperature. The progress of the reaction was monitored *via* TLC. Upon completion, the reaction mixture was concentrated *in vacuo* and dried under high vacuum to yield imidazolium–triazole species **2.10**·I. The product was subsequently dissolved in DCM (20 mL) and washed with NH_4PF_6 (0.1 M, 8 × 30 mL) and H_2O (2 × 30 mL). The solvent was removed *in vacuo* to yield **2.10**·PF_6 (0.025 g, 94%).

^{1}**H NMR** (400 MHz; $CDCl_3$) δ (ppm): 10.39 (1H, s, NC*H*N-*imidazole*), 7.70 (1H, s, NC*H*C-*imidazole*), 7.62 (2H, d, J = 8.5 Hz, Ar*H*), 7.46 (2H, d, J = 8.3 Hz, Ar*H*), 4.44 (2H, t, J = 7.4 Hz, NCH_2), 4.24 (3H, s, N^+CH_3), 2.02 (2H, quint, J = 7.4 Hz, NCH_2CH_2), 1.41 (9H, s, *tert*-CH_3), 1.39-1.29 (6H, m, CH_2), 0.92-0.87 (3H, m, CH_2CH_3); **ESI-MS** (pos.) $C_{22}H_{31}IN_5^+$ *m/z*: $[M\text{-}PF_6]^+$ *calc.* 492.16, *found* 492.17.

Rhenium(I) complex 2.11

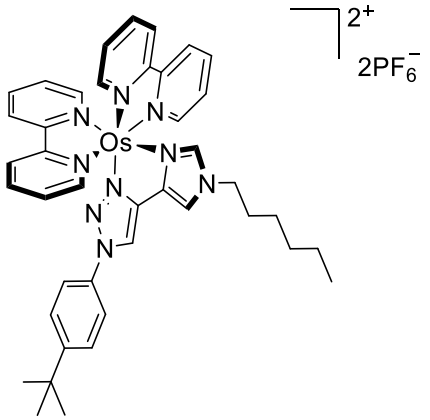


Imidazole–triazole species **2.8** (0.015 g, 0.057 mmol) was dissolved in DCM (3 mL), then $Re(CO)_3(MeCN)_2Cl$ was added the reaction mixture stirred at room temperature for 18

hours. The crude reaction mixture was purified *via* preparative TLC (DCM/MeOH 98:2) to yield rhenium(I) complex **2.11** (0.025 g, 67%).

^{1}**H NMR** (400 MHz; $CDCl_3$) δ (ppm): 8.20 (1H, s, NC*H*N-*imidazole*), 7.92 (1H, s, NC*H*C-*imidazole*), 7.70 (2H, d, *J* = 8.8 Hz, Ar*H*), 7.58 (2H, d, *J* = 8.8 Hz, Ar*H*), 7.28 (1H, s, C*H*-*triazole*), 3.96 (2H, t, *J* = 7.7 Hz, NCH_2), 1.87 (2H, quint, *J* = 7.7 Hz, NCH_2CH_2), 1.39 (9H, s, *tert*-CH_3), 1.36-1.32 (6H, m, CH_2), 1.00-0.73 (3H, m, CH_2CH_3); ^{13}**C NMR** (126 MHz; $CDCl_3$) δ (ppm): 153.94, 143.59, 139.05, 133.65, 133.47, 127.08, 120.31, 117.10, 116.25, 48.91, 35.14, 31.38, 31.23, 30.60, 26.30, 22.52, 14.07; **ESI-MS** (pos.) not observed.

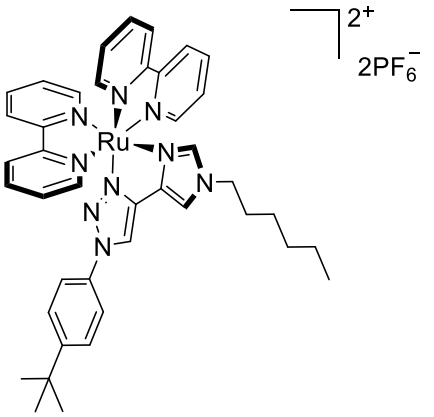
Osmium(II) complex 2.12·$(PF_6)_2$



Imidazole–triazole species **2.8** (0.020 g, 0.057 mmol) was dissolved in EtOH/H_2O (9:1, 10 mL), then $Os(bipy)_2Cl_2$ (0.052 g, 0.091 mmol) was added and the reaction mixture stirred at 90 °C for 72 hours. The ethanol was removed *in vacuo* and the reaction mixture washed with DCM (3 x 30 mL). The organics were collected and dried over anhydrous $MgSO_4$ and the solvent removed *in vacuo.* The reaction mixture was purified *via* preparative TLC (DCM/MeOH 95:5). The pure product was subsequently dissolved in DCM (20 mL) and washed with $NH_4PF_{6(aq)}$ (0.1 M, 8 × 30 mL) and H_2O (2 × 30 mL). The solvent was removed *in vacuo* to yield osmium(II) complex **2.12·**$(PF_6)_2$ as a dark green solid (0.013 g, 26%).

^{1}H NMR (400 MHz; $CDCl_3$) δ (ppm): 10.43 (1H, s, NC*H*N-*imidazole)*, 8.70-8.66 (2H, m, Ar*H-bipy*), 8.52 (1H, s, NC*H*C-*imidazole*), 8.37-8.30 (2H, m, Ar*H-bipy*), 8.03 (1H, s, C*H-triazole*), 7.88-7.63 (8H, m, Ar*H-bipy*), 7.62-7.58 (2H, m, Ar*H*), 7.40-7.36 (2H, m, Ar*H*), 7.35-7.08 (4H, m, Ar*H-bipy*), 4.03 (2H t, J = 7.5 Hz, NCH_2), 1.73 (2H, quint, J = 7.5 Hz, NCH_2CH_2), 1.22 (9H, s, *tert*-CH_3), 1.18-1.14 (6H, m, CH_2), 0.77-0.74 (3H, m, CH_2CH_3).; **HRESI-MS** (pos.): $C_{41}H_{45}N_9Os$ *m/z:* $[M]^{2+}$ *calc.* 427.67009, *found* 427.67006.

Ruthenium(II) complex 2.13·$(PF_6)_2$

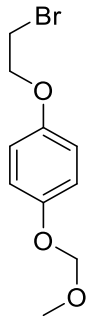


Imidazole–triazole species **2.8** (0.020 g, 0.057 mmol) was dissolved in EtOH/H_2O (9:1, 10 mL), then $Ru(bipy)_2Cl_2$ (0.044 g, 0.091 mmol) was added and the reaction mixture stirred at 90 °C for 72 hours. The ethanol was removed *in vacuo* and the reaction mixture washed with DCM (3 x 30 mL). The organics were collected and dried over anhydrous $MgSO_4$ and the solvent removed *in vacuo*. The reaction mixture was purified *via* preparative TLC (DCM/MeOH 95:5). The pure product was subsequently dissolved in DCM (20 mL) and washed with $NH_4PF_{6(aq)}$ (0.1 M, 8 × 30 mL) and H_2O (2 × 30 mL). The solvent was removed *in vacuo* to yield ruthenium(II) complex **2.13·**$(PF_6)_2$ as an orange solid (0.018 g, 40%).

^{1}H NMR (400 MHz; $CDCl_3$) δ (ppm): 10.28 (1H, s, NC*H*N-*imidazole)*, 8.89 (1H, s, NC*H*C-*imidazole*), 8.67-8.56 (4H, m, Ar*H-bipy*), 8.15-7.88 (8H, m, Ar*H-bipy*), 7.83 (1H, s, C*H-triazole*), 7.77-7.27 (8H, m, Ar*H-bipy* and Ar*H*), 4.05 (2H, t, J = 7.4 Hz, NCH_2), 1.82-1.68 (2H, quint, J = 7.4 Hz, NCH_2CH_2), 1.26 (9H, s, *tert*-CH_3), 1.22-1.16 (6H, m, CH_2),

0.85-0.69 (3H, m, CH_2CH_3); ^{13}**C NMR** (126 MHz; $CDCl_3$) δ (ppm): 158.06, 157.20, 157.12, 157.07, 153.45, 152.00, 151.83, 151.39, 143.89, 138.90, 137.57, 137.23, 136.92, 133.47, 132.41, 127.66, 127.37, 127.27, 126.78, 126.56, 123.65, 123.31, 123.15, 119.75, 118.73, 34.73, 30.91, 30.82, 30.12, 25.78, 22.23, 13.62; **HRESI-MS** (pos.): $C_{41}H_{45}N_9Ru$ *m/z*: $[M]^{2+}$ *calc.* 382.64152, *found* 382.64143.

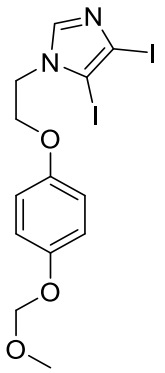
Mono-functionalised hydroquinone derivative 2.17



Mono-functionalised hydroquinone species **2.14** (1.00 g, 4.61 mmol) was dissolved in dry DCM (5 mL) and cooled to 0 °C. DIPEA (0.96 mL, 5.53 mmol) was added dropwise over 5 mins, then the reaction was allowed to stir for 10 mins. Chloromethyl methylether (0.445 g, 5.53 mmol) was added dropwise, then the reaction was warmed to room temperature and stirred for 18 hours. H_2O was added to quench the reaction, then the organics were washed with H_2O (10 mL), sat. $NaHCO_{3(aq)}$ (10 mL) and brine (10 mL) and dried over anhydrous $MgSO_4$ and filtered. The solvent was removed *in vacuo* and the reaction mixture purified *via* silica gel column chromatography (DCM) to afford mono-functionalised hydroquinone derivative **2.17** (0.360 g, 30%).

^{1}**H NMR** (400 MHz; $CDCl_3$) δ (ppm): 6.98 (2H, d, J = 8.0 Hz, Ar*H*), 6.85 (2H, d, J = 8.0 Hz, Ar*H*), 5.11 (2H, s, OCH_2O), 4.19 (2H, t, J = 5.9 Hz, OCH_2CH_2), 3.79 (2H, t, J = 5.9 Hz, CH_2Br), 3.48 (3H, s, CH_3); ^{13}**C NMR** (126 MHz; $CDCl_3$) δ (ppm): 153.30, 152.03, 117.76, 116.07, 95.34, 68.78, 56.03, 29.41; **ESI-MS** (pos.): not observed.

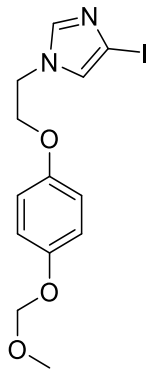
4,5-Diiodoimidazole mono-functionalised hydroquinone derivative 2.18



4,5-Diiodoimidazole **2.1** (3.06 g, 9.58 mmol) was dissolved in anhydrous THF (20 mL) and cooled to 0 °C. NaH (0.383 g, 9.58 mmol) was added portionwise under N_2 and left to stir for 1 hour at room temperature. Hydroquinone species **2.17** (0.50 g, 1.92 mmol) was added portionwise at 0 °C, then the mixture was allowed to warm to room temperature and stirred under N_2 for 18 hours at 60 °C. The reaction was quenched by addition of H_2O. THF was removed *in vacuo* and the residue re-dissolved in $CHCl_3$ (50 mL). The organics were washed with $HCl_{(aq)}$ (25 mL), sat. $Na_2S_2O_{3(Aq)}$ (25 mL), H_2O (25 mL) and brine (25 mL) and dried over anhydrous $MgSO_4$. The crude product was purified *via* silica gel column chromatography (DCM/MeOH 98:2) to afford the product **2.18 (**0.816 g, 85%).

^{1}**H NMR** (400 MHz; $CDCl_3$) δ (ppm): 7.81 (1H, s, NC*H*N-*imidazole)*, 6.96 (2H, d, J = 8.0 Hz, Ar*H*), 6.77 (2H, d, J = 8.0 Hz, Ar*H*), 5.10 (2H, s, OCH_2O), 4.37 (2H, t, J = 5.1 Hz, CH_2N), 4.15 (2H, t, J = 5.1 Hz, OCH_2CH_2), 3.47 (3H, s, CH_3); **HRESI-MS** (pos.) $C_{13}H_{15}O_3N_2I_2$ *m/z*: $[M+H]^+$ *calc.* 500.91665, *found* 500.91653.

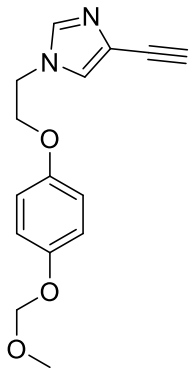
5-Iodoimidazole mono-functionalised hydroquinone derivative 2.19



4,5-Diiodoimidazole species **2.18** (0.420 g, 0.84 mmol) was dissolved in anhydrous THF (3 mL) and cooled to 0 °C. EtMgBr (3 M in Et_2O, 0.31 mL) was added dropwise under N_2 and stirred for 1 hour. H_2O (0.01 mL) was added to quench the reaction and stirred for 10 mins. Sat. $NH_4Cl_{(aq)}$ (10 mL) was added and the product extracted into DCM (3 × 25 mL). The combined organics were washed with sat. $NH_4Cl_{(aq)}$ (10 mL) and brine (10 mL) and dried over anhydrous $MgSO_4$. The crude product was purified *via* silica gel column chromatography (DCM/MeOH 98:2) to afford product **2.19** (0.299 g, 95%).

^{1}**H NMR** (400 MHz; $CDCl_3$) δ (ppm): 7.45 (1H, s, NC*H*N-*imidazole)*, 7.10 (1H, s, NC*H*C-*imidazole*), 6.98 (2H, d, J = 7.8 Hz, Ar*H*), 6.76 (2H, d, J = 7.8 Hz, Ar*H*), 5.08 (2H, s, OCH_2O), 4.25 (2H, t, J = 5.1 Hz, CH_2N), 4.12 (2H, t, J = 5.1 Hz, OCH_2CH$_2$), 3.45 (3H, s, CH_3); ^{13}**C NMR** (101 MHz; $CDCl_3$) δ (ppm): 152.77, 151.65, 139.15, 125.27, 117.45, 115.25, 94.91, 79.89, 67.26, 55.47, 46.83; **HRESI-MS** (pos.) $C_{13}H_{16}O_3N_2I$ *m/z*: $[M+H]^+$ *calc.* 375.02001, *found* 375.01986.

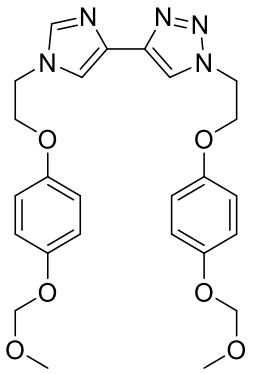
Imidazole–alkyne derivative 2.21



4-Iodoimidazole species **2.19** (0.675 g, 1.80 mmol) was dissolved in anhydrous DMF (10 mL). CuI (0.034 g, 0.18 mmol), $Pd(PPh_3)_2Cl_2$ (0.063 g, 0.09 mmol) and Et_3N (5 mL) were added and the reaction degassed with Argon for 10 mins. Thereafter, trimethylsilylacetylene (0.64 mL, 4.50 mmol) was added and the mixture heated under microwave irradiation at 80 °C for 30 mins. The solvent was removed *in vacuo* and the residue re-dissolved in ethyl acetate and filtered through Celite. The filtrate was concentrated *in vacuo*. Purification *via* silica gel column chromatography (EtOAc/Hexane 1:1) yielded the TMS protected alkyne. Deprotection was carried out immediately; the protected alkyne was dissolved in MeOH (5 mL) and K_2CO_3 (5 eq) added. The reaction mixture was stirred for 4 hours at room temperature and the progress of the reaction was monitored by TLC. Upon completion, the solvent was removed *in vacuo* and the reaction mixture was re-dissolved in DCM (30 mL) and washed with H_2O (3 × 20 mL) and brine (20 mL). The solvent was removed *in vacuo* to yield imidazole–alkyne **2.21** (0.220 g, 45%). No further purification was necessary.

^{1}H NMR (400 MHz; $CDCl_3$) δ (ppm): 7.33 (1H, s, NC*H*N-*imidazole)*, 7.08 (1H, s, NC*H*C-*imidazole*), 6.78 (2H, d, J = 7.8 Hz, Ar*H*), 6.60 (2H, d, J = 7.8 Hz, Ar*H*), 4.91 (2H, s, OCH_2O), 4.08 (2H, t, J = 5.0 Hz, CH_2N), 3.97 (2H, t, J = 5.0 Hz, OCH_2CH$_2$), 3.28 (3H, s, OCH_3), 2.86 (1H, s, CC*H-alkyne);* **^{13}C NMR** (126 MHz; $CDCl_3$) δ (ppm): 152.98, 152.18, 137.65, 124.26, 123.83, 117.79, 95.28, 77.38, 67.72, 56.02, 47.00; **HRESI-MS** (pos.) $C_{15}H_{17}O_3N_2$ *m/z*: $[M+H]^+$ *calc.* 273.12337, *found* 273.12320.

Imidazole–triazole derivative 2.22

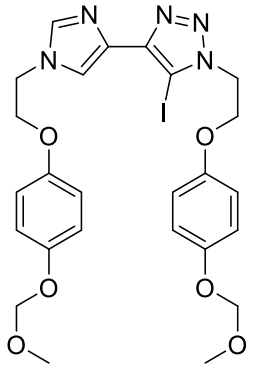


Imidazole–alkyne **2.21** (0.030 g, 0.134 mmol) and azide **2.16** (0.054 g, 0.20 mmol) were dissolved in dry DCM (3 mL). TBTA (0.014 g, 0.027 mmol) followed by $[Cu(MeCN)_4][PF_6]$ (0.010 g, 0.027 mmol) and DIPEA (0.056 g, 0.43 mmol) were added and the reaction mixture was stirred at room temperature for 18 hours. The reaction was diluted with DCM (10 mL) and washed with $NH_4OH_{(aq)}$ (3 × 20 mL) and brine (2 × 15 mL) and dried over anhydrous $MgSO_4$. The solvent was removed *in vacuo* and the reaction mixture was purified *via* silica gel column chromatography (DCM/MeOH 98:2) to afford imidazole–triazole **2.22** as a white solid (0.056 g, 87%).

^{1}H NMR (400 MHz; $CDCl_3$) δ (ppm): 8.00 (1H, s, NC*H*N-*imidazole*), 7.59-7.45 (2H, m, NC*H*C-*imidazole* and C*H-triazole*), 6.92-6.83 (4H, m, Ar*H*), 6.76-6.69 (4H, m, Ar*H*), 5.02 (2H, s, OCH_2O), 4.68 (2H, t, J = 5.1 Hz, CH_2N-*imidazole*), 4.29-4.22 (4H, m, OCH_2CH$_2$-*imidazole* and CH_2N-*triazole*), 4.13 (2H, t, J = 5.0 Hz, OCH_2CH$_2$-*triazole*), 3.38 (6H, s, OCH_3); **^{13}C NMR** (126 MHz; $CDCl_3$) δ (ppm): 159.65, 153.14, 152.02, 134.87, 129.51, 117.73, 117.49, 115.66, 95.25, 78.20, 68.00, 55.95, 48.89, 46.64 (missing peaks presumed

overlapped); **HRESI-MS** (pos.) $C_{25}H_{30}N_5O_6$ *m/z*: $[M+H]^+$ *calc.* 496.21906, *found* 496.23928.

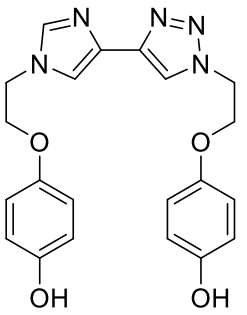
Imidazole–iodotriazole derivative 2.23



Azide **2.16** (0.090 g, 0.40 mmol), $Cu(ClO_4)_2.6H_2O$ (0.272 g, 0.73 mmol) and NaI (0.220 g, 1.47 mmol) were dissolved in dry THF (3 mL), covered with foil and stirred for 5 minutes at room temperature. TBTA (0.012 g, 0.037 mmol) was added and the reaction allowed to stir for a further 5 minutes. A solution of DBU (0.056 g, 0.37 mmol) in THF (0.5 mL) was added, followed by imidazole–alkyne **2.5** (0.100 g, 0.37 mmol). This was left to stir overnight at room temperature and then diluted with DCM (100 mL) before being washed with $NH_4OH_{(aq)}$ (3 × 20 mL) and brine (2 × 20 mL). The organics were collected and dried over anhydrous $MgSO_4$ and the solvent removed *in vacuo*. The reaction mixture was purified *via* silica gel column chromatography (DCM/MeOH 95:5) to afford imidazole–iodotriazole species **2.23** as a white solid (0.142 g, 62%).

^{1}**H NMR** (400 MHz; $CDCl_3$) δ (ppm): 7.82 (1H, s, NC*H*N-*imidazole)*, 7.76 (1H, s, NC*H*C-*imidazole*), 7.13-7.04 (4H, m, Ar*H*), 6.92 (4H, m, Ar*H*), 5.21 (4H, s, OCH_2O), 4.92 (2H, t, *J* = 5.9 Hz, CH_2N-*imidazole*), 4.52 (2H, t, *J* = 5.9 Hz, OCH_2CH_2N-*imidazole*), 4.47 (2H, t, *J* = 5.1 Hz, CH_2N-*triazole)*, 4.34 (2H, t, *J* = 5.1 Hz, OCH_2CH_2N-*triazole)*, 3.58 (6H, s, OCH_3); ^{13}**C NMR** (101 MHz; $CDCl_3$) δ (ppm): 162.76, 151.97, 132.05, 128.56, 117.64, 117.57, 115.61, 115.58, 95.18, 77.22, 66.71, 55.88, 49.45, 46.91(missing peaks presumed overlapped); **HRESI-MS** (pos.) $C_{25}H_{29}O_6N_5I$ *m/z*: $[M+H]^+$ *calc.* 622.11570, *found* 622.11536.

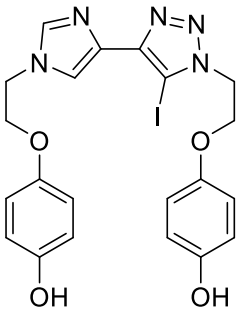
Imidazole–triazole bis-phenol 2.24



Acetyl chloride (0.11 mL, 1.52 mmol) was added to MeOH (2 mL) at 0 °C and stirred for 5 mins, before warming to room temperature and stirring for a further 15 mins. Imidazole–triazole species **2.22** (0.028 g, 0.051 mmol) was dissolved in DCM (2 mL) and added portionwise. The reaction mixture was stirred for 2 hours, then the solvent was removed *in vacuo* and the product dried under high vacuum to afford product **2.24** (0.025 g, quant.).

^{1}H NMR (400 MHz; CD_3OD) δ (ppm): 9.32 (1H, s, NC*H*N-*imidazole*), 8.32 (1H, s, NC*H*C-*imidazole*), 7.54 (1H, s, C*H*-*triazole*), 7.04-6.56 (8H, m, Ar*H*), 4.64 (2H, t, J = 5.1 Hz, CH_2N-*imidazole*), 4.24 (2H, t, J = 5.0 Hz, CH_2N-*triazole)*, 4.18 (2H, t, J = 5.1 Hz, OCH_2CH$_2$N-*imidazole*), 4.12 (2H, t, J = 5.0 Hz, OCH_2CH$_2$N-*triazole*).

Imidazole–iodotriazole bis-phenol 2.25

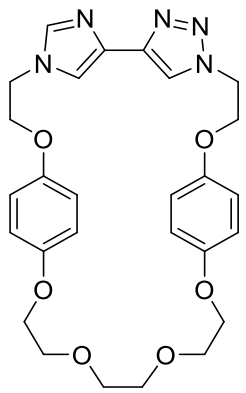


Acetyl chloride (0.69 mL, 9.66 mmol) was added to MeOH (4 mL) at 0 °C and stirred for 5 mins, before warming to room temperature and stirring for a further 15 mins. Imidazole–iodotriazole species **2.23** (0.200 g, 0.322 mmol) was dissolved in DCM (2 mL) and added portionwise. The reaction mixture was stirred for 2 hours, then the solvent was

removed *in vacuo* and the product dried under high vacuum to afford product **2.25** (0.172 g, quant.).

^{1}H NMR (400 MHz; CD_3OD) δ (ppm): 9.47 (1H, s, NC*H*N-*imidazole)*, 8.47 (1H, s, NC*H*C-*imidazole*), 7.00-6.62 (8H, m, Ar*H*), 4.97 (2H, t, J = 5.2 Hz, CH_2N-*imidazole*), 4.78 (2H, t, J = 4.9, CH_2N-*triazole*), 4.52 (2H, t, J = 5.1 Hz, OCH_2CH_2N-*imidazole*), 4.46 (2H, t, J = 5.0 Hz, OCH_2CH_2N-*triazole*); **^{13}C NMR** (126 MHz; DMSO-d_6) δ (ppm): 151.94, 150.68, 130.41, 129.04, 119.06, 118.49, 116.03, 115.80, 48.82, 37.35 (missing peaks presumed overlapped); **HRESI-MS** (pos.) $C_{21}H_{21}O_4N_5I$ *m/z*: $[M+H]^+$ *calc.* 534.06327, *found* 534.06360.

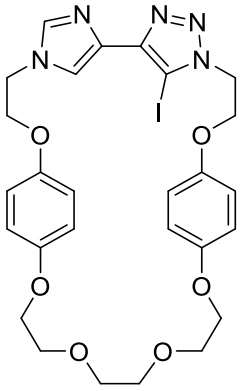
Imidazole–triazole macrocycle 2.26



Triethylene glycol bis-tosylate (0.023 g, 0.05 mmol) and bis-phenol **2.24** (0.025 g, 0.05 mmol) were dissolved in anhydrous degassed DMF (9 mL). Caesium carbonate (0.065 g, 0.25 mmol) was added and the vigorously-stirred suspension was allowed to stir for 16 hours at 70 °C under N_2. The solvent was removed *in vacuo* and the resulting solid stirred in a mixture of $CHCl_3$ (30 mL) and H_2O (30 mL). The organic layer was separated, and the aqueous layer extracted into $CHCl_3$ (4 × 30 mL). The combined organics were washed with brine (3 x×20 mL) and dried over anhydrous $MgSO_4$, filtered and the solvent removed *in vacuo.* The reaction mixture was purified *via* preparative TLC (DCM/MeOH 96:4) to afford the target macrocycle **2.26** as a white solid (0.010 g, 36%).

^{1}H NMR (400 MHz; $CDCl_3$) δ (ppm): 7.97 (1H, s, NC*H*N-*imidazole)*, 7.57 (1H, s, NC*H*C-*imidazole*), 7.48 (1H, s, C*H-triazole*), 6.76-6.59 (8H, m, Ar*H*), 4.74 (2H, t, *J* = 4.6 Hz, CH_2N-*imidazole*), 4.32-4.23 (4H, m, OCH_2CH_2N-*imidazole* and CH_2N-*triazole)*, 4.15 (2H, t, *J* = 5.2 Hz, OCH_2CH_2N-*triazole*), 4.02-3.97 (4H, m, ArOCH_2*)*, 3.80-3.69 (4H, m, OCH_2CH_2O), 3.62 (4H, s, OCH_2CH_2O); **HRESI-MS** (pos.) $C_{27}H_{32}O_6N_5$ *m/z*: $[M+H]^+$ *calc.* 522.23471, *found* 522.23509.

Imidazole–iodotriazole macrocycle 2.27

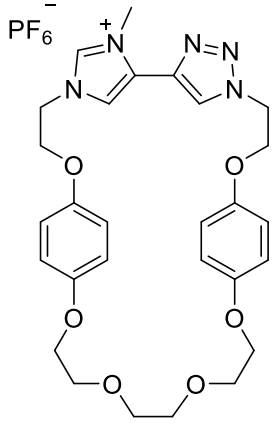


Triethylene glycol bis-tosylate (0.103 g, 0.225 mmol) and bis-phenol **2.25** (0.120 g, 0.225 mmol) were dissolved in anhydrous degassed DMF (40 mL). Caesium carbonate (0.293 g, 0.90 mmol) was added and the vigorously-stirred suspension was allowed to stir for 16 hours at 70 °C under N_2. The solvent was removed *in vacuo* and the resulting solid stirred in a mixture of $CHCl_3$ (50 mL) and H_2O (50 mL). The organic layer was separated, and the aqueous layer extracted into $CHCl_3$ (4 × 30 mL). The combined organics were washed with brine (3 × 20 mL) and dried over anhydrous $MgSO_4$, filtered and the solvent removed *in vacuo*. The reaction mixture was purified *via* preparative TLC (DCM/MeOH 98:2) to afford the target macrocycle **2.27** as a white solid (0.146 g, 25%).

^{1}H NMR (400 MHz; $CDCl_3$) δ (ppm): 7.69 (1H, s, NC*H*N-*imidazole)*, 7.62 (1H, s, NC*H*C-*imidazole*), 6.89-6.54 (8H, m, Ar*H*), 4.82 (2H, t, *J* = 4.7 Hz, CH_2N-*imidazole*), 4.41-4.30 (4H, m, OCH_2CH_2N-*imidazole* and CH_2N-*iodotriazole)*, 4.16 (2H, t, *J* = 4.5 Hz,

O*CH*$_2$CH$_2$N-*iodotriazole*), 4.05-3.95 (4H, m, ArOC*H*$_2$), 3.79-3.70 (4H, m, OC*H*$_2$C*H*$_2$O), 3.64 (4H, s, OC*H*$_2$C*H*$_2$O); **^{13}C NMR** (126 MHz; $CDCl_3$) δ (ppm): 153.62, 152.39, 137.81, 134.87, 129.21, 128.12, 123.88, 118.04, 71.53, 70.94, 70.51, 70.04, 67.90, 66.92, 61.95, 54.24, 47.24, 42.88 (missing peaks presumed overlapped); **HRESI-MS** (pos.) $C_{27}H_{31}O_6N_5I$ *m/z*: $[M+H]^+$ *calc.* 648.13135, *found* 648.13155.

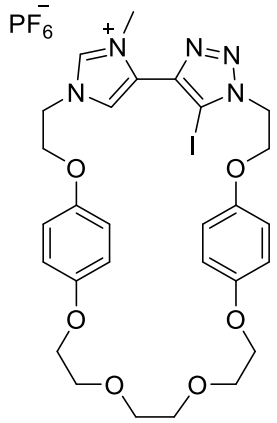
Imidazolium–triazole macrocycle 2.35·PF$_6$



Imidazolium–triazole macrocycle **2.26** (0.010 g, 0.02 mmol) was dissolved in DCM (2 mL) and MeI (0.5 mL) was added. The reaction mixture was left to stir for 6 hours. The solvent and excess MeI was removed *in vacuo*. The product was subsequently dissolved in DCM (10 mL) and washed with $NH_4PF_{6(aq)}$ (0.1 M, 8 × 5 mL) and H_2O (2 × 5 mL). The solvent was removed *in vacuo* to yield imidazolium–triazole macrocycle **2.35**·PF_6 (0.013 g, quant.).

^{1}H NMR (400 MHz, $CDCl_3$) δ/ppm: 9.01 (1H, s, NC*H*N-*imidazolium*), 8.25 (1H, s, NC*H*C-*imidazolium*), 6.92-6.59 (8H, m, Ar*H*), 4.97-4.89 (2H, m, C*H*$_2$N-*imidazolium*), 4.78-4.66 (2H, m, C*H*$_2$N-*triazole*), 4.47-4.53 (4H, m, OC*H*$_2$CH$_2$N-*imidazolium* and OC*H*$_2$CH$_2$N-*triazole*), 4.16 (3H, s, C*H*$_3$), 4.11-3.97 (4H, m, OC*H*$_2$C*H*$_2$O), 3.89-3.72 (4H, m, OC*H*$_2$C*H*$_2$O), 3.71 (4H, s, OC*H*$_2$C*H*$_2$O).

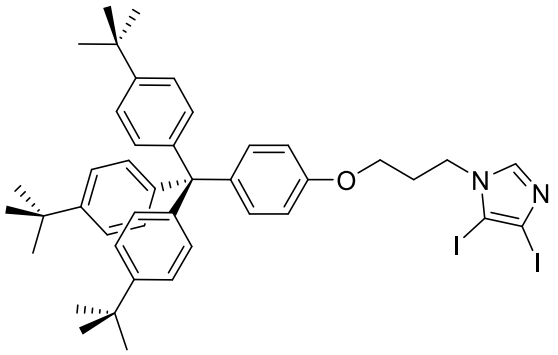
Imidazolium–iodotriazole macrocycle 2.36·PF_6



Imidazolium–iodotriazole macrocycle **2.27** (0.050 g, 0.08 mmol) was dissolved in DCM (5 mL) and MeI (2 mL) was added. The reaction mixture was left to stir for 6 hours. The solvent and excess MeI was removed *in vacuo*. The product was subsequently dissolved in DCM (20 mL) and washed with $NH_4PF_{6(aq)}$ (0.1 M, 8 × 10 mL) and H_2O (2 × 10 mL). The solvent was removed *in vacuo* to yield imidazolium–triazole macrocycle **2.36**·PF_6 (0.062 g, quant.).

^{1}H NMR (400 MHz, $CDCl_3$) δ/ppm: 8.97 (1H, s, NC*H*N-*imidazolium)*, 8.03 (1H, s, NC*H*C-*imidazolium*), 6.90-6.61 (8H, m, Ar*H*), 4.95-4.84 (2H, m, CH_2N-*imidazolium*), 4.75-4.62 (2H, m, CH_2N-*triazole)*, 4.44-4.31 (4H, m, OCH_2CH_2N-*imidazolium* and OCH_2CH_2N-*iodotriazole*), 4.14 (3H, s, CH_3), 4.09-3.96 (4H, m, OCH_2CH_2O), 3.89-3.73 (4H, m, OCH_2CH_2O), 3.69 (4H, s, OCH_2CH_2O); **^{13}C NMR** (126 MHz; CD_3OD) δ (ppm): 159.29, 146.55, 137.94, 131.81, 122.44, 116.15, 115.44, 115.31, 115.27, 70.85, 70.84, 67.16, 66.68, 49.76, 30.95 (missing peaks presumed overlapped); **HRESI-MS** (pos.) $C_{28}H_{33}O_6N_5I^+$ *m/z*: $[M+H]^+$ *calc.* 662.14700, *found* 662.14716.

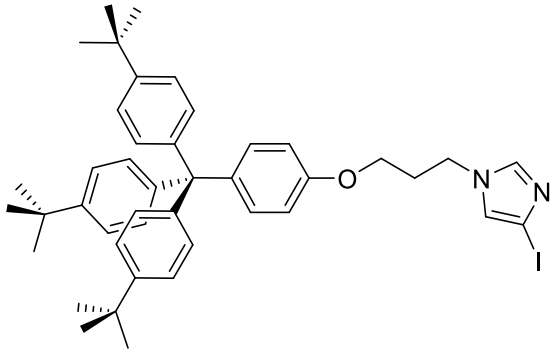
Stopper-4,5-diiodoimidazole derivative 2.38



4,5-Diiodoimidazole **2.1** (1.54 g, 4.80 mmol) was dissolved in anhydrous THF (80 mL) at 0 °C. NaH (60% in mineral oil) (0.192 g, 4.80 mmol) was added portion-wise and the reaction was warmed to room temperature and stirred under N_2 for 1 h. After cooling to 0 °C stopper bromide **2.30** (600 mg, 0.960 mmol) was added portion-wise and allowed to warm to room temperature. The reaction mixture was stirred at 60°C for 18 h, after which the reaction was quenched by addition of H_2O (5 mL). The solvent was removed *in vacuo* and the residue was re-dissolved in chloroform and washed with 1 M $HCl_{(aq)}$ (30 mL), $Na_2SO_{3(aq)}$ (30 mL), H_2O (30 mL), and brine (30 mL). The resulting residue was purified *via* silica gel column chromatography (silica, 98:2 DCM/MeOH) to give stopper-diiodoimidazole derivative **2.38** as an off-white solid in 62% yield (0.505 g, 62%).

^{1}H NMR (400 MHz, $CDCl_3$) δ/ppm: 7.60 (1H, s, NC*H*N-*imidazole*), 7.16-7.26 (6H, m, Ar*H*), 7.02-7.14 (8H, m, Ar*H*), 6.74 (2H, d, *J* = 8.8 Hz, OAr*H*), 4.23 (2H, t, *J* = 6.8 Hz, NCH_2), 3.89 (2H, t, *J* = 5.5 Hz, OCH_2), 2.16-2.22 (2H, m, CH_2), 1.30 (27H, s, CH_3); **^{13}C NMR** (101 MHz, $CDCl_3$) δ/ppm: 156.2, 148.5, 144.2, 141.6, 140.4, 132.5, 130.8, 124.2, 113.1, 96.2, 82.0, 63.2, 63.2, 46.5, 34.4, 31.5, 30.1; **HRESI-MS** (pos.) $C_{43}H_{50}I_2N_2O$ *m/z*: $[M+H]^+$ *calc.* 865.2085, *found* 865.2084.

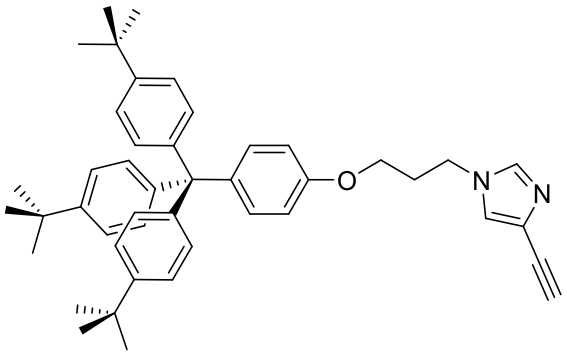
Stopper-5-iodoimidazole derivative 2.39



Stopper-4,5-diiodoimidazole **2.38** (0.370 g, 0.435 mmol) was dissolved in anhydrous THF (10 mL), and the mixture was degassed with N_2 for 10 mins at 0 °C. EtMgBr (0.172 mL, 0.516 mmol) was added dropwise and the reaction mixture was stirred for 2 h at 0 °C. H_2O (0.01 mL) was added and the reaction was stirred for 10 mins at room temperature. The reaction mixture was extracted into DCM and the combined organics washed with sat. $NH_4Cl_{(aq)}$ (10 mL), dried over anhydrous $MgSO_4$, filtered, and the solvent removed *in vacuo*. The residue was purified *via* silica gel column chromatography (DCM/MeOH 98:2) to give stopper-5-iodoimidazole derivative **2.39** as a white solid (0.30 g, 92%).

^{1}H NMR (400 MHz, $CDCl_3$) δ/ppm: 7.38 (1H, s, NC*H*N-*imidazole*), 7.19-7.25 (6H, m, Ar*H*), 7.06-7.10 (8H, m, Ar*H*), 7.01 (1H, s, NC*H*C-*imidazole*), 6.73 (2H, d, *J* = 8.8 Hz OAr*H*), 4.17 (2H, t, *J* = 6.8 Hz, NCH_2), 3.89 (2H, t, *J* = 5.6 Hz, OCH_2), 2.09-2.26 (2H, m, CH_2), 1.30 (27H, s, CH_3); **^{13}C NMR** (101 MHz, $CDCl_3$) δ/ppm: 156.2, 148.5, 144.2, 140.4, 139.1, 132.5, 130.8, 124.7, 124.2, 113.0, 82.1, 63.5, 63.2, 44.1, 34.5, 31.5, 30.8; **HRESI-MS** (pos.) $C_{43}H_{51}IN_2O$ *m/z*: $[M+H]^+$ *calc.* 739.3119, *found* 739.3115.

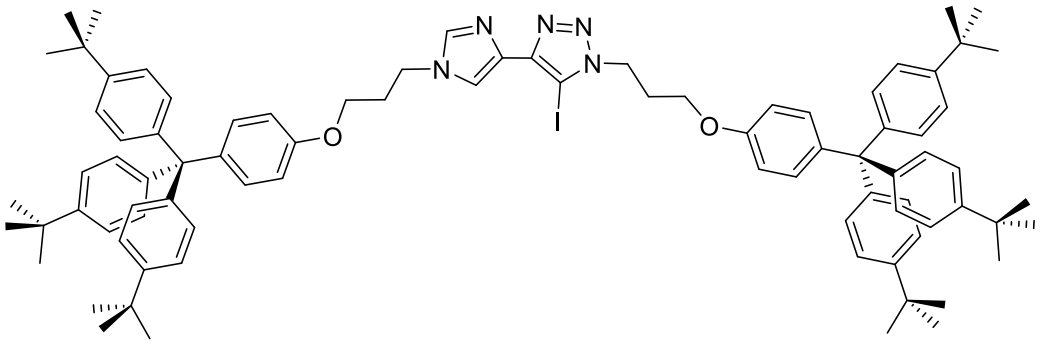
Stopper-imidazole–alkyne derivative 2.40



Stopper-5-iodoimidazole **2.39** (0.300 g, 0.407 mmol) was dissolved in anhydrous DMF (5.5 mL), to which CuI (0.012 g, 0.061 mmol), $Pd(PPh_3)_4$ (0.033 mg, 0.028 mmol) and Et_3N (1.5 mL) were added. The mixture was degassed under Ar for 10 mins. Trimethylsilylacetylene (0.114 mL, 0.813 mmol) was added and the reaction was heated under microwave irradiation for 30 mins at 80 °C. The mixture was extracted into Et_2O (40 mL) and washed with H_2O (3 × 20 mL). The organic phase was dried over anhydrous $MgSO_4$, filtered and the solvent removed *in vacuo*. The protected alkyne was purified *via* silica gel column chromatography (EtOAc/Hexane 1:1). The resulting product was dissolved in methanol (20 mL), K_2CO_3 (0.281 g, 2.04 mmol) added and the reaction stirred for 1 hour. The solvent was removed *in vacuo* and the residue was re-dissolved in DCM (30 mL) and washed with H_2O (2 × 20 mL) and brine (2 × 20 mL). The organic layer was dried over anhydrous $MgSO_4$, filtered and the solvent was removed *in vacuo* to give stopper-imidazole–alkyne derivative **2.40** in 63% yield (0.164 g, 63%).

^{1}H NMR (400 MHz, $CDCl_3$) δ/ppm: 7.41 (1H, s, NC*H*N-*imidazole*), 7.25-7.19 (6H m, Ar*H*), 7.15 (1H, s, NC*H*C-*imidazole*), 7.06-7.12 (8H, m, Ar*H*), 6.74 (2H, d, *J* = 8.9 Hz, Ar*H*), 4.15 (2H t, *J* = 6.8 Hz, NCH_2), 3.89 (2H, t, *J* = 5.6 Hz, OCH_2), 3.04 (1H, s, C*H*-*alkyne*), 2.19 (2H, m, CH_2), 1.30 (s, 27H, CH_3); **^{13}C NMR** (101 MHz, $CDCl_3$) δ/ppm: 156.2, 148.5, 144.2, 140.4, 137.5, 132.5, 130.8, 124.2, 123.9, 123.8, 113.0, 77.3, 63.4, 63.2, 44.0, 34.4, 31.5, 30.0; **HRESI-MS** (pos) $C_{45}H_{52}N_2O$ *m/z*: $[M+H]^+$ *calc.* 637.4152, *found* 637.4149.

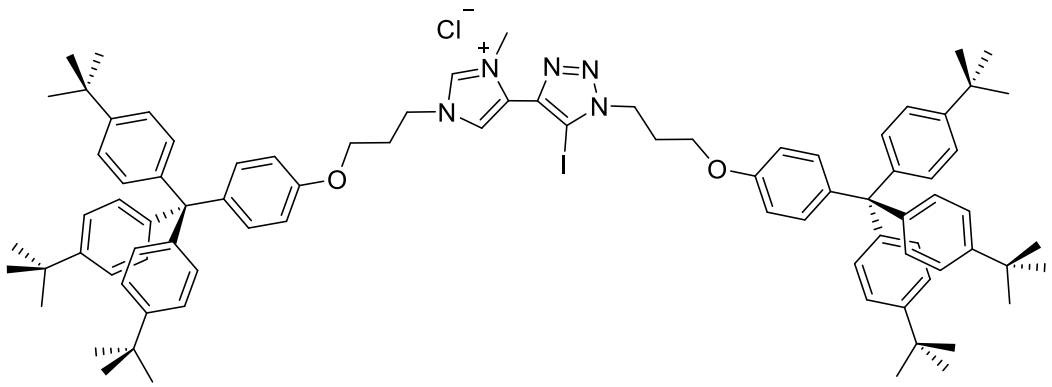
Imidazole–iodotriazole axle 2.41



Stopper azide **2.31** (0.069 g, 0.117 mmol), $Cu(ClO_4)_2{\cdot}6H_2O$ (0.079 g, 0.214 mmol) and NaI (0.064 g, 0.428 mmol) were dissolved in anhydrous THF (1 mL) and stirred in the dark for 5 mins. TBTA (0.006 g, 0.011 mmol) was added and the mixture was stirred for another 5 mins. DBU (0.016 g, 0.107 mmol) was added, followed by stopper-imidazole-alkyne derivative **2.40** (0.068 g, 0.107 mmol) and the mixture was left to stir for 18 hours in the dark at room temperature. The reaction mixture was diluted with DCM (50 mL) and washed with NH_4OH (3 × 30 mL), H_2O (2 × 30 mL), and brine (2 × 30 mL). The organics were dried over anhydrous $MgSO_4$, filtered and the solvent was removed *in vacuo*. The residue was purified *via* preparative TLC (MeOH/DCM 97:3) to give XB axle **2.41** as an off-white solid (0.085 g, 59%).

^{1}H NMR (400 MHz, $CDCl_3$) δ/ppm: 7.98 (1H, s, NC*H*N-*imidazole*), 7.56 (1H, s, NC*H*C-*imidazole*), 7.26–6.98 (28H, m, Ar*H*), 6.79–6.71 (4H, m, Ar*H*), 4.64 (2H, t, *J* = 7.1 Hz, NC*H*$_2$-*imidazole*), 4.24 (2H, t, *J* = 6.7 Hz, NC*H*$_2$-*triazole*), 4.01 (2H, t, *J* = 5.7 Hz, OC*H*$_2$), 3.92 (2H, t, *J* = 5.6 Hz, OC*H*$_2$), 2.49–2.31 (2H, m, C*H*$_2$), 2.31–2.18 (2H, m, C*H*$_2$), 1.30 (54H, s, *tert*-C*H*$_3$); **HRESI-MS** (pos.) $C_{85}H_{101}N_5O_2$ *m/z*: $[M+H]^+$ *calc.*1350.6995, *found* 1350.6964.

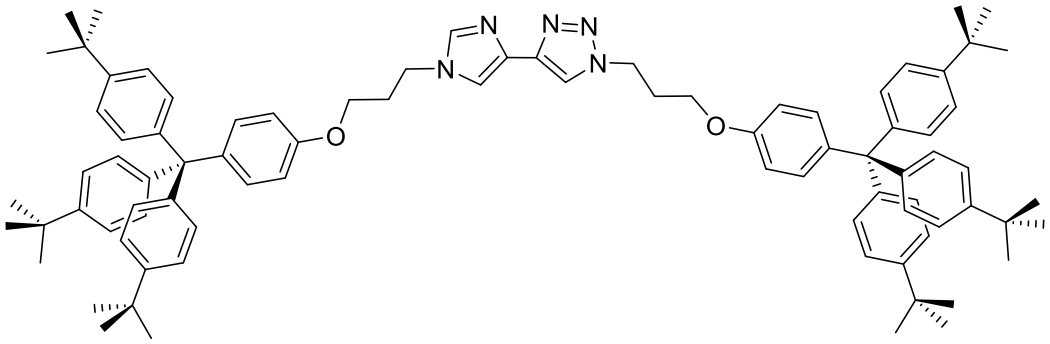
Imidazolium–iodotriazole axle 2.42·Cl



MeI (0.3 mL) was added portion-wise to compound **19** (36 mg, 0.027 mmol) in anhydrous DCM (1 mL). The reaction mixture was stirred in the dark at room temperature for 18 hours, and then concentrated to dryness under vacuum. The residue was purified by preparative TLC (DCM/MeOH 97:3). The product was subsequently dissolved in DCM (20 mL) and washed with $NH_4Cl_{(aq)}$ (0.1 M, 8 × 10 mL) and H_2O (2 × 10 mL). The solvent was removed *in vacuo* to yield imidazolium–triazole axle **2.42**·Cl (0.011 g, 32%).

^{1}H NMR (400 MHz, $CDCl_3$) δ/ppm: 10.93 (1H, s, NC*H*N-*imidazolium*), 7.64 (1H, s, NC*H*C-*imidazolium*), 7.24–7.06 (28H, m, Ar*H*), 6.75–6.69 (4H, m, Ar*H*), 4.72-4.59 (4H, m, NCH_2-*imidazolium* and NCH_2-*triazole*), 4.13 (3H, s, CH_3-*imidazolium*), 4.10-3.99 (4H, m, OCH_2), 2.50 (2H, m, CH_2), 2.57-2.38 (2H, m, CH_2), 1.29 (54H, s, *tert*-CH_3); **^{13}C NMR** (101 MHz, $CDCl_3$) δ/ppm: 156.2, 148.6, 148.5, 144.2, 144.1, 132.6, 132.5, 130.8, 130.8, 124.3, 124.2, 121.0, 113.1, 64.0, 63.2, 48.8, 37.1, 34.4, 31.5, 29.9, 29.6 (missing peaks presumed overlapped); **HRESI-MS** (pos) $C_{86}H_{103}IN_5O_2^+$ *m/z*: $[M-Cl]^+$ *calc.* 1364.7151, *found* 1364.7084.

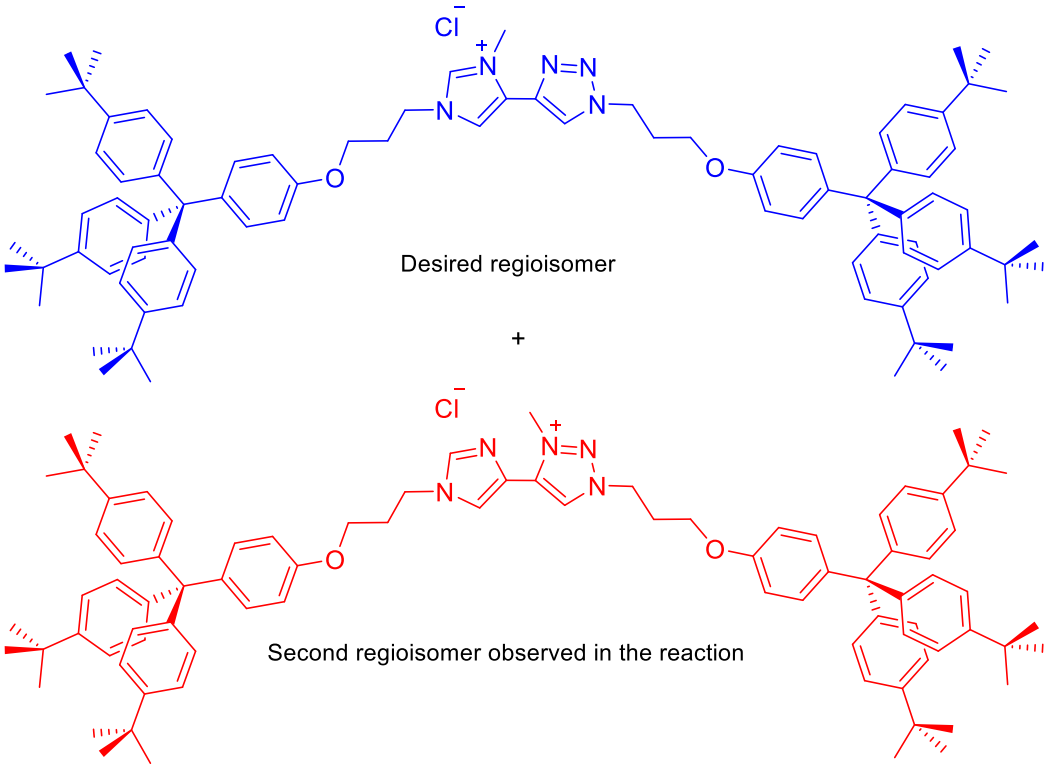
Imidazole–triazole axle 2.43



Stopper azide **2.31** (0.081 g, 0.138 mmol) and stopper imidazole–alkyne **2.40** (0.080 g, 0.126 mmol) were dissolved in anhydrous DCM (3 mL). $[Cu(MeCN)_4][PF_6]$ (0.009 g, 0.025 mmol), TBTA (0.013 g, 0.025 mmol), and DIPEA (0.024 g, 0.188 mmol) were added and the reaction mixture stirred at room temperature for 18 hours. The reaction was diluted with DCM and washed with NH_4OH (3 × 20 mL) and sat. $NaCl_{(aq)}$ (2 × 15 mL). The organic layer was dried over anhydrous $MgSO_4$, filtered and the solvent removed *in vacuo*. The residue was purified by silica gel column chromatography (EtOAc/Hexane 4:1) to afford imidazole–triazole axle **2.43** as a yellow solid (0.143 g, 85%).

^{1}H NMR (400 MHz, $CDCl_3$) δ/ppm: 7.88 (1H, s, NC*H*N-*imidazole*), 7.67 (1H, s, NC*H*C-*imidazole*), 7.45 (1H, s, NC*H*C-*triazole*), 7.25–7.03 (28H, m, Ar*H*), 6.77–6.68 (4H, m, OAr*H*), 4.61 (2H, t, *J* = 6.9 Hz, NCH_2-*imidazole*), 4.22 (2H, t, *J* = 6.7 Hz, NCH_2-*triazole*), 3.98 (2H, t, *J* = 5.7 Hz, OCH_2), 3.92 (2H, t, *J* = 5.6 Hz, OCH_2), 2.46–2.32 (2H, m, CH_2), 2.32–2.21 (2H, m, CH_2), 1.30 (54H, s, *tert*-CH_3); **ESI-MS** (pos.) $C_{85}H_{101}N_5O$ *m/z*: $[M+H]^+$ *calc.* 1224.79, *found* 1224.74.

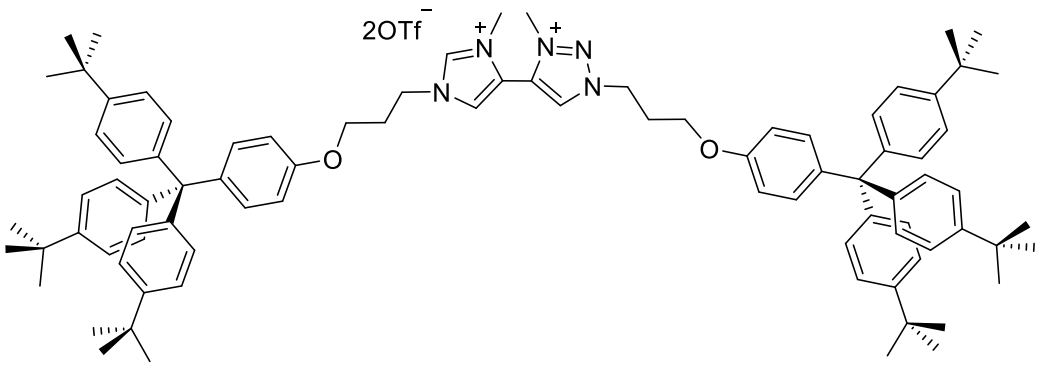
Regioisomeric HB axle 2.44·Cl



MeI (1 mL) was added dropwise to imidazole–triazole axle **2.43** (0.032 g, 0.026 mmol) in anhydrous DCM (2 mL). The reaction mixture was stirred in the dark at room temperature until completion, and then dried under vacuum. The product was subsequently dissolved in DCM (20 mL) and washed with $NH_4Cl_{(aq)}$ (0.1 M, 8 × 10 mL) and H_2O (2 × 10 mL). The solvent was removed *in vacuo* to yield regioisomeric HB axle **2.44**·Cl (0.025 g, 78%).

^{1}H NMR (400 MHz, $CDCl_3$) δ/ppm: 9.73 (1H, s, NC*H*N-*imidazolium*), 8.29 (1H, s, NC*H*C-*imidazolium*), 7.79 (1H, s, NC*H*C-*triazole*), 7.18–6.93 (28H, m, Ar*H*), 6.72-6.68 (4H, m, OAr*H*), 4.59 (2H, t, *J* = 7.0 Hz, NC*H*$_2$-*imidazolium*), 4.52 (2H, t, *J* = 6.8 Hz, NC*H*$_2$-*triazole*), 4.00 (2H, t, *J* = 5.5 Hz, OC*H*$_2$), 3.92 (2H, t, *J* = 5.6 Hz, OC*H*$_2$), 2.55–2.41 (2H, m, C*H*$_2$), 2.38 (2H, m, C*H*$_2$), 1.22 (54H, m, *tert*-C*H*$_3$); **^{13}C NMR** (101 MHz, $CDCl_3$) δ/ppm: 156.07, 148.42, 148.38, 144.02, 143.94, 132.47, 132.35, 130.70, 130.66, 124.14, 124.07, 113.00, 63.84, 63.05, 48.69, 36.99, 34.31, 31.39, 29.73 (missing peaks presumed overlapped); **ESI-MS** (pos.) $C_{86}H_{104}N_2OI$ *m/z*: $[M\text{-}I]^+$ *calc.* 1238.82, *found* 1238.77.

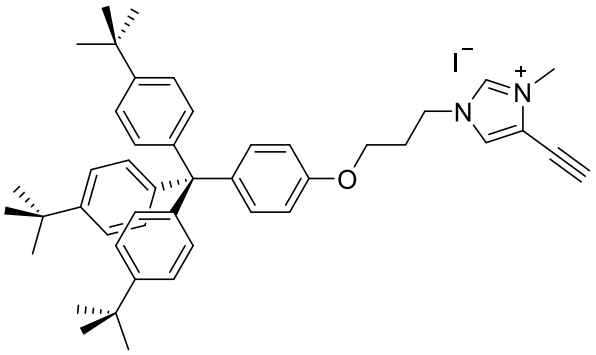
Imidazolium–triazolium axle 2.45·(OTf)$_2$



Regioisomeric HB axle **2.44**·Cl (0.110 g, 0.089 mmol) was dissolved in anhydrous DCM (2mL). MeOTf (1 drop) was added and the reaction mixture was left to stir at room temperature for 18 hours and then the solvent removed *in vacuo*. The residue was purified by preparative TLC (DCM/MeOH 95:5) to give imidazolium–triazolium axle **2.45**·(OTf)$_2$ as a white solid (0.078 g, 71%).

^{1}H NMR (400 MHz, $CDCl_3$) δ/ppm: 9.12 (s, 1H, NC*H*N-*imidazolium*), 8.95 (1H, s, NC*H*C-*imidazolium*), 7.94 (1H, s, NC*H*C-*triazolium*), 7.24–6.94 (28H, m, Ar*H*), 6.68 (4H, m, OAr*H*), 4.83 (2H, m, NCH_2-*imidazolium*), 4.46 (2H, m, NCH_2-*triazolium*), 4.06 (3H, s, NCH_3), 4.03 (2H, m, OCH_2), 3.98 (2H, m, OCH_2), 3.86 (3H, s, 3H, NCH_3), 2.49 (2H, m, C-H_2), 2.33 (2H, m, CH_2), 1.27 (54H, s, *tert*-CH_3); **^{13}C NMR** (101 MHz, (1:1) $CDCl_3$/CD_3OD) δ/ppm: 148.0, 143.8, 132.0, 130.3, 130.3, 123.7, 123.7, 112.6, 49.0, 48.8, 48.5, 48.3, 48.1, 47.9, 47.7, 47.5, 33.8, 30.8, 30.0, 29.3, 22.2, 13.4 (missing peaks presumed overlapped); **HRESI-MS** (pos.) $C_{46}H_{55}N_2O^+$ *m/z*: $[M-A]^+$ *calc.* 1252.8341, *found* 1252.8364.

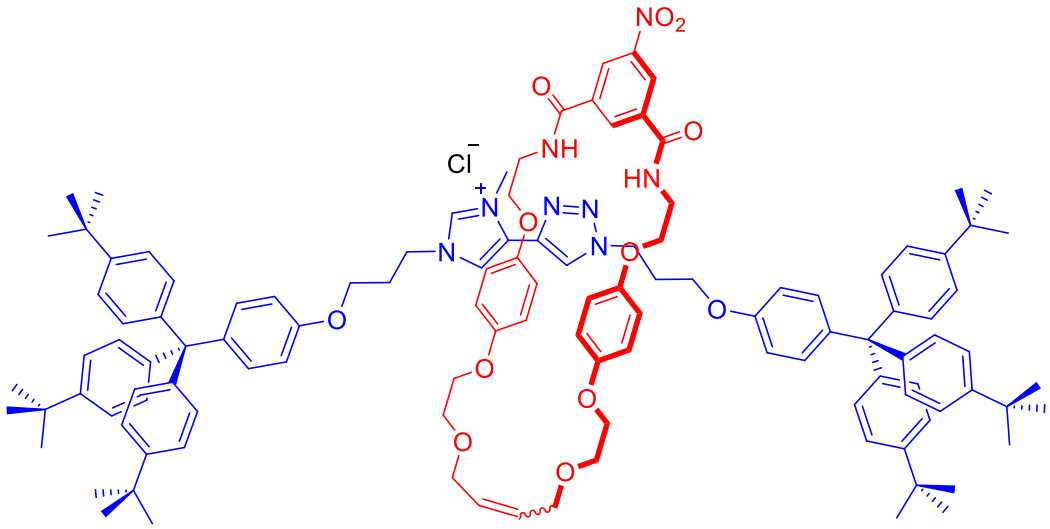
Imidazolium–alkyne 2.46·I



MeI (0.5 mL) was added portion-wise to imidazole–alkyne **2.40** (0.068 g, 0.107 mmol) in anhydrous DCM (2 mL). The reaction mixture was stirred at room temperature for 18 hours, and then the solvent removed *in vacuo*. The residue was purified by preparative TLC (DCM/MeOH 97:3) to afford imidazolium–alkyne **2.46**·I as a yellow solid (0.049 g, 70%).

^{1}H NMR (400 MHz, $CDCl_3$) δ/ppm: 10.43 (1H, s, NC*H*N-*imidazolium*), 7.46 (1H, s, NC*H*C-*imidazolium*) 7.25–7.03 (14H, m, Ar*H*), 6.72–6.66 (2H, m, Ar*H*), 4.62 (2H, t, *J* = 6.9 Hz, NCH_2-*imidazolium*), 4.06 (2H, t, *J* = 5.5 Hz, OCH_2), 3.96 (3H, s, NCH_3), 3.63 (1H, s, CC*H*-*alkyne*), 2.47 (2H, m, CH_2), 1.29 (27H, s, *tert*-CH_3); **^{13}C NMR** (101 MHz, $CDCl_3$) δ/ppm: 155.8, 148.5, 144.1, 140.6, 138.3, 132.5, 130.8, 125.8, 124.2, 117.9, 113.0, 89.4, 67.1, 64.0, 63.2, 48.3, 35.3, 34.4, 31.5, 29.8; **HRESI-MS** (pos.) $C_{46}H_{55}N_2O^+$ *m/z*: $[M–I]^+$ *calc.* 651.4309, *found* 651.4303.

Regioisomeric HB rotaxane 2.53·Cl



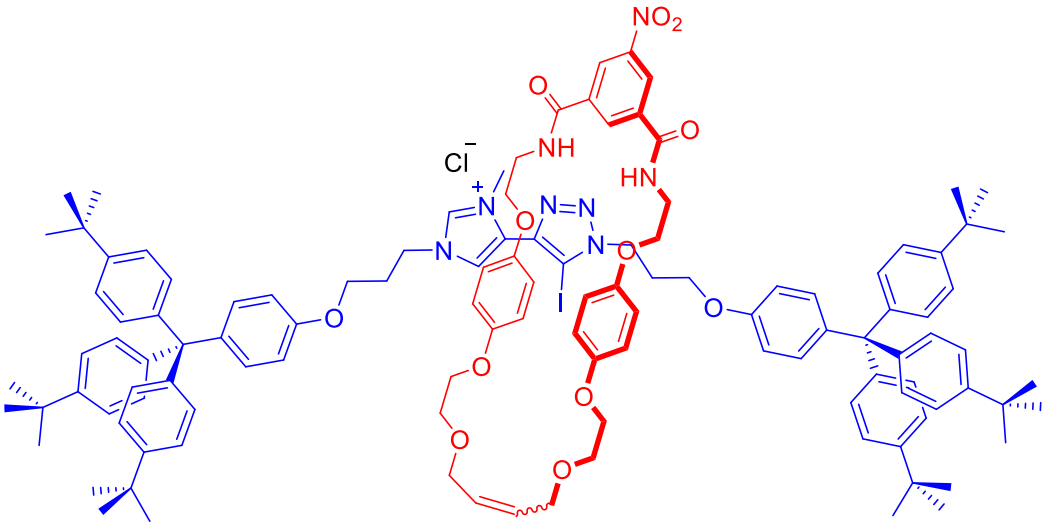
+ the corresponding triazolium-imidazole species

Regioisomeric HB axle **2.44**·Cl (0.024 g, 18.8 μmol) macrocycle precursor **2.52** (0.018 g, 28.2 μmol) were dissolved in anhydrous DCM (12 mL) and stirred for 30 mins before adding Grubbs' catalyst (2nd generation) (2.4 mg, 10% by weight). The reaction mixture was stirred at room temperature in the dark for 7 days. The solvent was removed *in vacuo* and the residue was purified by preparative TLC (EtOAc/MeOH 95:5, followed by DCM/MeOH 95:5) to yield regioisomeric mixture HB rotaxane **2.53**·Cl (0.004 g, 10%).

^{1}H NMR (400 MHz, $CDCl_3$) δ/ppm: 9.87 (1H, s, NC*H*N-*imidazolium*), 9.30 (2H, br, s, N*H-macro.*), 9.06 (2H, s, Ar*H-macro.*), 9.02 (1H, s, Ar*H-macro*), 8.49 (1H, s, NC*H*C-*imidazolium*), 7.42 (1H, s, NC*H*C-*triazole*), 7.25-7.02 (28H, m, Ar*H-axle*), 6.80-6.70 (4H, m, Ar*H-axle*), 6.51-6.21 (8H, m, Ar*H-macro.*), 5.82-5.66 (2H, m, C*H-alkene macro.*), 4.60 (2H, t, *J* = 6.9 Hz, NCH_2-*imidazolium*), 4.34-3.43 (26H, m, CH_2-*axle and macro.* and NCH_3-*axle*), 2.50-2.32 (2H, m, OCH_2-*axle*), 2.04-1.96 (2H, m, OCH_2-*axle*), 1.29 (54H, s, *tert*-CH_3). This assignment is for imidazolium–triazole regioisomer, which constitutes the 75% of the product.); **^{13}C NMR** (101 MHz, (1:1) $CDCl_3$/CD_3OD) δ/ppm: 167.92, 147.98, 143.76, 131.88, 131.83, 130.78, 130.22, 131.21, 129.15, 128.37, 123.71, 114.70, 112.62, 67.84, 53.05, 38.39, 37.51, 33.76, 30.68, 29.97, 29.20, 28.52, 23.33, 22.49, 13.29, 10.27

(missing peaks presumed overlapped); **HRESI-MS** (pos.) $C_{118}H_{139}N_8O_{12}^+$ *m/z*: $[M+H]^+$ *calc.* 1860.0507, *found* 1860.0446.

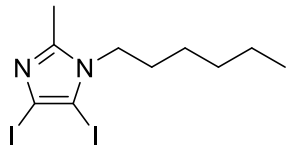
XB rotaxane 2.54·Cl



XB axle **2.41** (0.011 g, 0.0079 mmol) and macrocycle precursor **2.52** (0.008 g, 0.012 mmol) were dissolved in anhydrous DCM (1.5 mL) and stirred for 30 mins. Grubbs' catalyst (2nd generation) (1.1 mg, 10% by weight) was added and the mixture was stirred in the dark for 7 days. The solvent was removed *in vacuo* and the residue was purified by preparative TLC (EtOAc/MeOH 95:5, followed DCM/MeOH 97:3). Product could not be isolated from the corresponding proto-triazole rotaxane, a side product observed in the reaction.

^{1}H NMR (400 MHz, $CDCl_3$) δ/ppm: could not be assigned due to inseparable mixture of products; **HRESI-MS** (pos) $C_{118}H_{138}IN_8O_{12}^+$ *m/z*: **[M]$^+$** *calc.* 1985.9473, *found* 1985.9400.

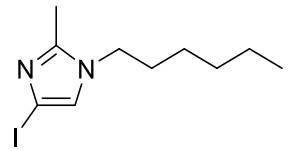
4,5-diiodo-1-hexyl-2-methylimidazole 2.56



4,5-Diiodo-2-methylimidazole **2.55** (2.00 g, 6.0 mmol) was dissolved in anhydrous THF (20 mL) and cooled to 0 °C. NaH (0.240 g, 6.0 mmol) was added portionwise under N_2 and left to stir for 1 hour at room temperature. Iodohexane (0.177 mL, 1.2 mmol) was added portionwise at 0 °C, then the mixture was allowed to warm to room temperature and stirred under N_2 for 18 hours at 60 °C. The reaction was quenched by addition of H_2O. THF was removed *in vacuo* and the residue re-dissolved in $CHCl_3$ (50 mL). The organics were washed with $HCl_{(aq)}$ (25 mL), sat. $Na_2S_2O_{3(aq)}$ (25 mL), H_2O (25 mL) and brine (25 mL) and dried over anhydrous $MgSO_4$. The crude product was purified *via* silica gel column chromatography (EtOAc/Hexane 1:3) to afford product **2.56** (0.376 g, 75%).

^{1}**H NMR** (400 MHz; $CDCl_3$) δ (ppm): 4.04-3.68 (2H, m, NC*H*$_2$), 2.47 (3H, s, C*H*$_3$-*imidazole*), 1.70-1.58 (2H, m, NCH$_2$C*H*$_2$), 1.44-1.24 (6H, m, C*H*$_2$), 0.93-0.87 (3H, m, CH$_2$C*H*$_3$); ^{13}**C NMR** (126 MHz; $CDCl_3$) δ (ppm): 149.08, 93.85, 80.79, 48.82, 31.41, 30.34, 26.34, 24.62, 14.52, 14.09; **HRESI-MS** (pos.) $C_{10}H_{17}N_2I_2$ *m/z:* $[M+H]^+$ *calc.* 418.94756, *found* 418.94823.

1-hexyl-5-iodo-2-methylimidazole 2.57

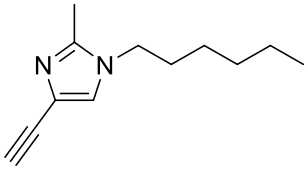


4,5-Diiodo-1-hexyl-2-methylimidazole **2.56** (0.350 g, 0.84 mmol) was dissolved in anhydrous THF (3 mL) and cooled to 0 °C. EtMgBr (1 M in THF, 0.92 mL) was added dropwise under N_2 and stirred for 1 hour. H_2O (0.01 mL) was added to quench the reaction and stirred for 10 mins. Sat. $NH_4Cl_{(aq)}$ (10 mL) was added and extracted into DCM (3 × 40 mL). The combined organics were washed with sat.$NH_4Cl_{(aq)}$ (20 mL) and

brine (20 mL) and dried over anhydrous $MgSO_4$. The crude product was purified *via* silica gel column chromatography (EtOAc/Hexane 2:1) to afford the pure product **2.57** (0.218 g, 89%).

^{1}H NMR (400 MHz; $CDCl_3$) δ (ppm): 6.84 (1H, s, NC*H*C-*imidazole*), 3.75 (2H, t, J = 7.3 Hz, NCH_2), 2.32 (3H, s, CH_3-*imidazole*), 1.64 (2H, quint, J = 7.4 Hz, NCH_2CH_2), 1.30-1.22 (6H, m, CH_2), 0.91-0.70 (3H, m, CH_2CH_3); **^{13}C NMR** (101 MHz; $CDCl_3$) δ (ppm): 146.72, 124.70, 79.22, 46.46, 31.40, 30.72, 26.33, 24.64 14.10, 13.09; **HRESI-MS (pos)** $C_{10}H_{18}N_2I$ *m/z*: $[M+H]^+$ *calc.* 293.05092, *found* 293.05050.

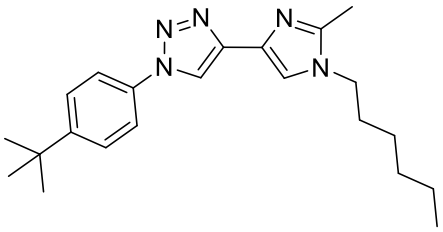
Imidazole–alkyne derivative 2.59



1-Hexyl-5-iodo-2-methylimidazole **2.57** (0.200 g, 0.72 mmol) was dissolved in anhydrous DMF (7 mL). CuI (0.013 g, 0.071 mmol), $Pd(PPh_3)_2Cl_2$ (0.025 g, 0.04 mmol) and Et_3N (2.5 mL) were added and degassed with argon for 10 mins. Thereafter, trimethylsilyl acetylene (0.20 mL, 1.41 mmol) was added and the mixture heated under microwave irradiation at 80 °C for 30 mins. The solvent was removed *in vacuo* and the residue re-dissolved in ethyl acetate and filtered through Celite and the filtrate concentrated *in vacuo.* Purification *via* silica gel column chromatography (EtOAc/Hexane 1:1) yielded the TMS protected alkyne **2.58**. Deprotection was carried out immediately; the protected alkyne **2.58** was dissolved in MeOH (5 mL) and K_2CO_3 (5 eq) added. The reaction mixture was stirred for 4 hours at room temperature and the progress of the reaction was monitored by TLC. Upon completion, the solvent was removed *in vacuo* and the reaction mixture was re-dissolved in DCM (30 mL) and washed with H_2O (3 × 20 mL) and brine (20 mL). The solvent was removed *in vacuo* to yield alkyne **2.59** (0.090 g, 66%). No further purification was necessary.

^{1}H NMR (400 MHz; $CDCl_3$) δ (ppm): 7.02 (1H, s, NC*H*C-*imidazole*), 3.77 (2H, t, J = 7.3 Hz, NCH_2), 3.01 (1H, s, C*H-alkyne*), 2.33 (3H, s, CH_3-*imidazole*), 1.68 (2H, quint, J = 7.1 Hz, NCH_2CH_2), 1.27 (6H, m, CH_2), 0.91-0.81 (3H, m, CH_2CH_3); **^{13}C NMR** (126 MHz; $CDCl_3$) δ (ppm): 144.92, 124.03, 121.15, 77.86, 77.03, 46.44, 31.37, 30.65, 26.27, 22.55, 14.05, 13.10; **ESI-MS** (pos.) $C_{12}H_{19}N_2$ *m/z*: $[M+H]^+$ *calc.* 191.15, *found* 191.16.

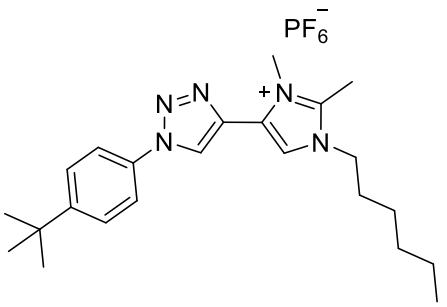
2-Methylimidazole–triazole derivative 2.60



2-Methylimidazole–alkyne **2.59** (0.045 g, 0.24 mmol) and 4-*tert*-butylphenyl azide (0.062 g, 0.36 mmol) were dissolved in dry DCM (3 mL). TBTA (0.025 g, 0.048 mmol) followed by $[Cu(MeCN)_4][PF_6]$ (0.018 g, 0.048 mmol) and DIPEA (0.031 g, 0.24 mmol) were added and the reaction mixture was stirred at room temperature for 18 hours. The reaction was diluted with DCM (20 mL) and washed with $NH_4OH_{(aq)}$ (3 × 20 mL) and brine (2 × 15 mL) and dried over anhydrous $MgSO_4$. The solvent was removed *in vacuo* and the reaction mixture was purified *via* silica gel column chromatography (DCM/MeOH 97:3) to afford 2-methylimidazole–triazole **2.60** as a white solid (0.078 g, 89%).

^{1}H NMR (400 MHz; $CDCl_3$) δ (ppm): 8.27 (1H, s, NC*H*C-*imidazole*), 7.86 (2H, d, J = 8.8 Hz, Ar*H*), 7.51 (2H, d, J = 8.8 Hz, Ar*H*), 7.43 (1H, s, C*H-triazole)*, 3.86 (2H, t, J = 7.2 Hz, NCH_2), 2.41 (3H, s, CH_3-*imidazole*), 1.76 (2H, quint, J = 7.2 Hz, NCH_2CH_2), 1.34 (9H, s, *tert*-CH_3), 1.33-1.27 (6H, m, CH_2), 0.93-0.80 (3H, m, CH_2CH_3); **^{13}C NMR** (126 MHz; $CDCl_3$) δ (ppm): 151.79, 144.89, 144.54, 134.89, 131.45, 126.69, 119.98, 116.87, 116.50, 46.48, 34.85, 31.43, 31.37, 30.72, 26.36, 22.58, 14.08, 13.13; **HRESI-MS** (pos.) $C_{22}H_{32}N_5$ *m/z*: $[M+H]^+$ *calc.* 366.26522, *found* 366.26493.

2-Methylimidazolium–triazole derivative 2.61·PF_6

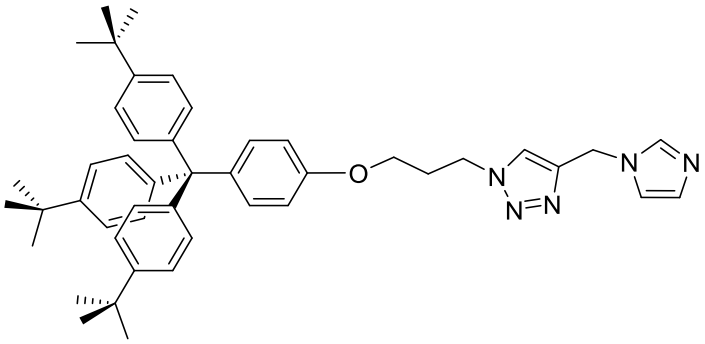


2-Methylimidazole–triazole derivative **2.60** (0.020 g, 0.055 mmol) was dissolved in DCM (5 mL). MeI (0.17 mL, 1.09 mmol) was added and the mixture stirred at room temperature and the progress of the reaction was monitored *via* TLC. Upon completion, the reaction mixture was concentrated *in vacuo* and dried under high vacuum to yield 2-methylimidazolium–triazole derivative **2.61**·I. The product was subsequently dissolved in DCM (20 mL) and washed with NH_4PF_6 (0.1 M, 8 × 30 mL) and H_2O (2 × 30 mL). The solvent was removed *in vacuo* to yield **2.61**·PF_6 (0.020 g, 96%).

^{1}**H NMR** (400 MHz; $CDCl_3$) δ (ppm): 8.27 (1H, s, NC*H*C-*imidazolium*), 7.86 (2H, d, J = 8.8 Hz, Ar*H*), 7.51 (2H, d, J = 8.8 Hz, Ar*H*), 7.43 (1H, s, C*H-triazole)*, 3.86 (2H, t, J = 7.2 Hz, NCH_2), 2.41 (3H, s, CH_3-*imidazolium*), 1.76 (2H, quint, J = 7.2 Hz, NCH_2CH_2), 1.34 (9H, s, *tert*-CH_3), 1.33-1.27 (6H, m, CH_2), 0.93-0.80 (3H, m, CH_2CH_3); ^{13}**C NMR** (126 MHz; $CDCl_3$) δ (ppm): 152.78, 144.12, 134.89, 126.90, 125.32, 123.70, 120.79, 120.73, 120.30, 49.56, 35.26, 34.93, 31.32, 31.22, 29.78, 26.19, 22.49, 14.04, 12.07; **HRESI-MS** (pos.): $C_{23}H_{34}N_5^+$ *m/z*: $[M\text{-}PF_6]^+$ *calc.* 380.28087, *found* 380.28023.

6.2.2 Synthesis of novel compounds from Chapter 3

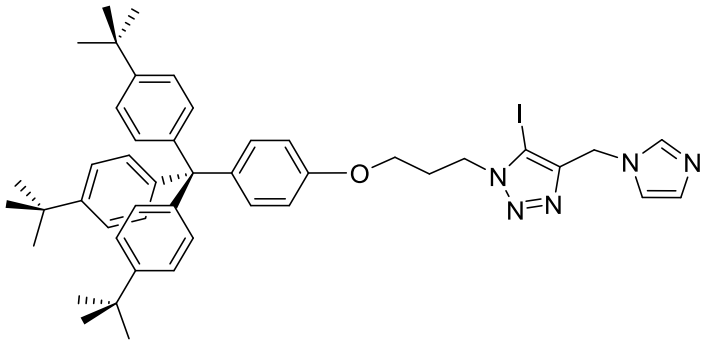
Stopper imidazole–triazole derivative 3.2



Stopper azide **2.31** (0.660 g, 1.12 mmol), $[Cu(MeCN)_4][PF_6]$ (0.070 g, 0.188 mmol) and TBTA (cat. amount) were dissolved in dry degassed DCM (10 mL). Imidazole–alkyne **3.1** (0.100 g, 0.942 mmol) and DIPEA (cat. amount) were added. The mixture was stirred at room temperature under N_2 for 18 hours, after which, the reaction mixture was diluted with DCM (80 mL). The organics were washed with $NH_4OH_{(aq)}$ (3 × 40 mL), H_2O (40 mL) and brine (2 × 40 mL) and dried over $MgSO_4$. The solvent was removed *in vacuo*. Purification *via* silica gel column chromatography (DCM/MeOH 98:2) yielded **3.2** as a white powder (0.600 g, 92%).

^{1}**H NMR** (400 MHz; $CDCl_3$) δ (ppm): 7.56 (1H, s, NC*H*N-*imidazole*), 7.38 (1H, s, C*H*-*triazole*), 7.20-7.25 (6H, m, Ar*H*), 7.06-7.14 (8H, m, Ar*H*), 7.05 (1H, br. s, NC*H*-*imidazole*), 6.96 (1H, s, NC*H*-*imidazole*), 6.70-6.76 (2H, m, Ar*H*), 5.21 (2H, s, NCH_2-*methylene*), 4.54 (2H, t, J = 6.9 Hz, NCH_2), 3.91 (2H, t, J = 5.7 Hz, OCH_2), 2.32-2.38 (2H, m, OCH_2CH_2), 1.30 (27H, s, *tert*-CH_3); ^{13}**C NMR** (126 MHz; $CDCl_3$) δ (ppm): 156.24, 148.54, 144.16, 143.66, 140.42, 132.52, 130.83, 130.19, 128.36, 124.22, 122.60, 113.04, 80.71, 63.88, 63.20, 47.56, 42.50, 34.45, 31.53, 30.03; **HRESI-MS** (pos) $C_{46}H_{56}ON_5$ *m/z*: $[M+H]^+$ *calc.* 694.44794, *found* 694.44748.

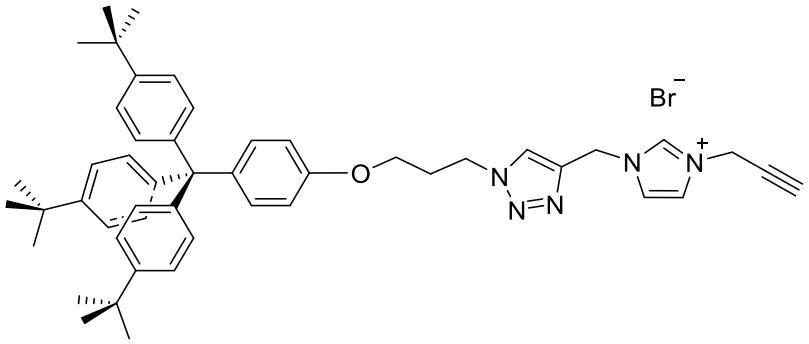
Stopper imidazole–iodotrizaole derivative 3.3



Stopper azide **2.31** (0.304 g, 0.517 mmol) was dissolved in dry degassed THF (2 mL) and the reaction vessel covered with foil. $Cu(ClO_4)_2.6H_2O$ (0.349 g, 0.940 mmol) and NaI (0.282 g, 1.88 mmol) were added and stirred under N_2 for 5 mins. TBTA (0.025 g, 0.047 mmol) was added and stirred under N_2 for 5 mins. DBU (0.071 g, 0.466 mmol) and imidazole–alkyne **3.1** (0.050 g, 0.466 mmol) were added in order and the mixture was stirred at room temperature for 18 hours, after which, the reaction mixture was diluted with DCM (50 mL). The organics were washed with $NH_4OH_{(aq)}$ (3 × 30 mL), H_2O (30 mL) and brine (2 × 30 mL) and dried over $MgSO_4$. The solvent was removed *in vacuo*. Purification *via* silica gel column chromatography (DCM/MeOH 98:2) yielded **3.3** as a white powder (0.350 g, 91%).

^{1}**H NMR** (500 MHz; $CDCl_3$) δ (ppm): 7.63 (1H, s, NC*H*N-*imidazole*), 7.20-7.26 (6H, m, Ar*H*), 7.06-7.10 (8H, m, Ar*H*), 7.05-6.99 (2H, m, NC*H*-*imidazole*), 6.70-6.76 (2H, m, Ar*H*), 5.17 (2H, s, NCH_2-*methylene*), 4.57 (2H, t, J = 7.0 Hz, NCH_2), 3.99 (2H, t, J = 5.7 Hz, OCH_2), 2.36-2.41 (2H, m, OCH_2CH_2), 1.30 (27H, s, *tert*-CH_3); ^{13}**C NMR** (126 MHz; $CDCl_3$) δ (ppm): 156.19, 148.46, 146.67, 144.16, 140.25, 132.43, 130.81, 129.98, 128.10, 124.18, 119.13, 113.15, 80.30, 63.90, 63.17, 48.18, 42.35, 34.41, 31.50, 29.67; **HRESI-MS** (pos) $C_{46}H_{55}ON_5I$ *m/z*: $[M+H]^+$ *calc.* 820.34458 , *found* 820.34387.

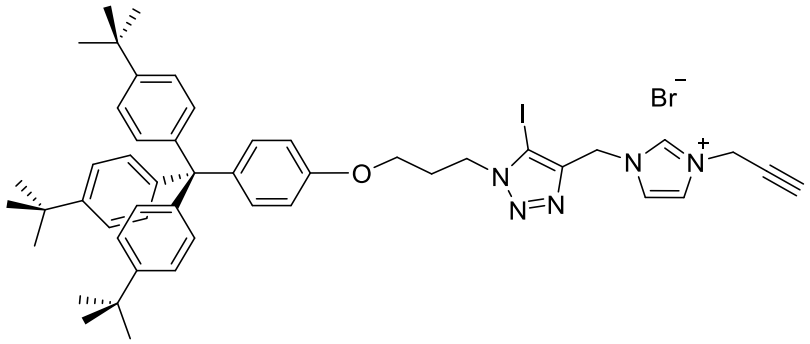
Imidazolium–alkyne derivative 3.4·Br



Stopper imidazole–triazole species **3.2** (0.350 g, 0.50 mmol) was suspended in acetone (10 mL) and propargyl bromide (0.28 mL, 2.50 mmol) added. The reaction mixture was heated under microwave irradiation at 140 °C for 75 mins and the resulting precipitate filtered to produce imidazolium–alkyne **3.4**·Br (0.345 g, 85%). No further purification was necessary.

^{1}**H NMR** (400 MHz; $CDCl_3$) δ (ppm): 10.68 (1H, t, ^{4}J = 1.7 Hz, NC*H*N-*imidazole*), 8.54 (1H, s, C*H-triazole*), 7.68 (1H, t, ^{4}J = 1.8 Hz, NC*H-imidazole*), 7.35 (1H, t, ^{4}J = 1.8 Hz, NC*H-imidazole*), 7.25-7.17 (6H, m, Ar*H*), 7.12-6.99 (8H, m, Ar*H*), 6.78-6.59 (2H, m, OAr*H*), 5.84 (2H, s, *imidazolium*-CH_2-*triazole*) 5.16 (2H, d, ^{4}J = 2.6 Hz, CH_2-*alkyne*), 4.58 (2H, t, J = 7.2 Hz, NCH_2CH_2), 3.97 (2H, t, J = 5.7 Hz, OCH_2), 2.68 (1H, t, ^{4}J = 2.6 Hz, C*H-alkyne*), 2.46-2.29 (2H, m, OCH$_2$CH_2), 1.29 (27H, s, *tert*-CH_3); ^{13}**C NMR** (126 MHz; $CDCl_3$) δ (ppm): 156.34, 148.46, 144.19, 140.21, 139.96, 137.23, 132.42, 130.83, 125.84, 124.20, 122.88, 121.19, 113.08, 78.54, 73.42, 64.22, 63.18, 47.98, 44.78, 40.05, 34.43, 31.52, 30.10.; **HRESI-MS** (pos) $C_{49}H_{58}ON_5^+$ *m/z*: [M-Br]$^+$ *calc.* 732.46359, *found* 732.46270.

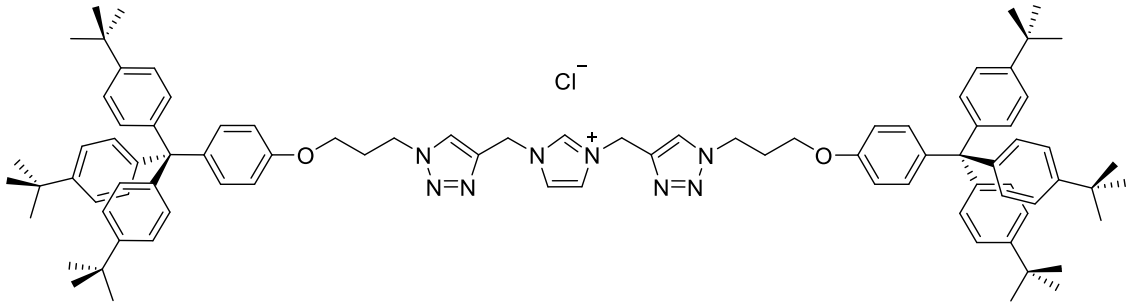
Imidazolium–alkyne derivative 3.5·Br



Stopper imidazole–iodotriazole species **3.3** (0.200 g, 0.244 mmol) was suspended in acetone (10 mL) and propargyl bromide (0.11 mL, 1.22 mmol) added. The reaction mixture was heated under microwave irradiation at 140 °C for 75 mins and the resulting precipitate filtered to produce imidazolium–alkyne **3.5**·Br (0.149 g, 65%). No further purification was necessary.

^{1}**H NMR** (400 MHz; $CDCl_3$) δ (ppm): 10.78 (1H, s, NC*H*N-*imidazolium*), 7.48 (1H, t, J = 1.8 Hz, NC*H*-*imidazole*), 7.43 (1H, t, J = 1.8 Hz, NC*H*-*imidazole*), 7.19-7.25 (6H, m, Ar*H*), 7.05-7.10 (8H, m, Ar*H*), 6.70-6.73 (2H, m, OAr*H*), 5.65 (2H, s, *imidazolium*-CH_2-*triazole*), 5.38 (2H, d, ^{4}J = 2.6 Hz, CH_2-*alkyne*), 4.59 (2H, t, J = 7.0 Hz, NCH_2), 3.98 (2H, t, J = 5.6 Hz, OCH_2), 2.65 (1H, t, ^{4}J = 2.6 Hz, C*H*-*alkyne*), 2.42-2.36 (2H, m, OCH_2CH_2), 1.29 (27H, s, CH_3); ^{13}**C NMR** (126 MHz; $CDCl_3$) δ (ppm): 156.16, 148.36, 144.05, 143.59, 140.14, 137.28, 132.31, 130.69, 124.08, 122.21, 121.73, 113.01, 85.62, 78.16, 73.73, 63.99, 63.05, 48.40, 45.47, 40.18, 34.31, 31.39, 29.52; **HRESI-MS** (pos.) $C_{49}H_{57}ON_5I^+$ *m/z*: $[M\text{-}Br]^+$ *calc.* 858.36023, *found* 858.35943.

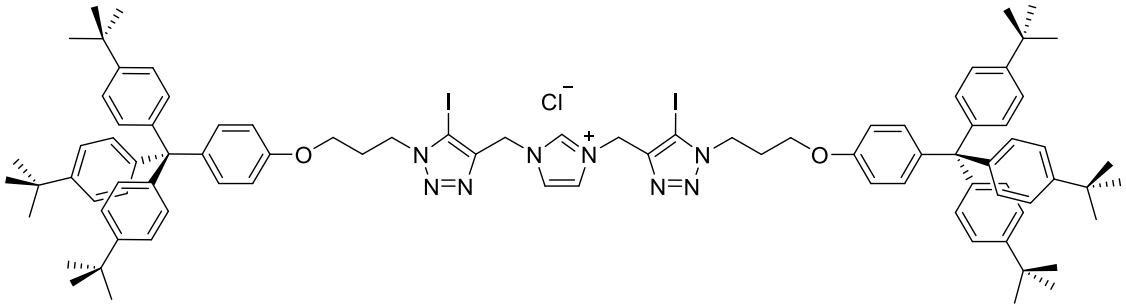
HB imidazolium–bis(triazole) axle 3.10·Cl



Imidazolium–alkyne species **3.5**·Br (0.100 g, 0.14 mmol) and stopper azide **2.31** (0.096 g, 0.16 mmol) were dissolved in dry DCM (4 mL). TBTA (0.014 g, 0.027 mmol) followed by $[Cu(MeCN)_4][PF_6]$ (0.011 g, 0.027 mmol) and DIPEA (0.026 g, 0.20 mmol) were added and the reaction mixture was stirred at room temperature for 18 hours. The reaction was diluted with DCM (20 mL) and washed with $NH_4OH_{(aq)}$ (3 × 20 mL) and brine (2 × 15 mL) and dried over anhydrous $MgSO_4$ and filtered. To the crude reaction mixture TFA (0.5 mL) was added and stirred for 30 mins. The solvent and excess TFA were removed *in vacuo* and the reaction mixture was purified *via* silica gel column chromatography (DCM/MeOH 95:5). The product was subsequently dissolved in DCM (15 mL) and washed with $NH_4Cl_{(aq)}$ (0.1 M, 8 x 30 mL) and H_2O (2 x 30 mL). The solvent was removed *in vacuo* to afford HB imidazolium–bis(triazole) axle **3.10**·Cl (0.086 g, 42%).

^{1}**H NMR** (400 MHz; $CDCl_3/CD_3OD$ 1:1) δ (ppm): 8.95 (1H, s, NC*H*N-*imidazolium*), 8.02 (2H, s, NC*H*-*imidazolium*), 7.50 (2H, s, C*H*-*triazole*), 7.27-7.12 (12H, m, Ar*H*), 7.03 (16H, m, Ar*H*), 6.70-6.65 (4H, m, OAr*H*), 5.43 (4H, s, NCH_2-*methylene*), 4.56 (2H, t, J = 7.2 Hz, NCH_2CH$_2$), 3.93 (4H, t, J = 5.7 Hz, OCH_2), 2.41-2.27 (4H, m, OCH$_2$CH_2), 1.25 (54H, s, *tert*-CH_3); ^{13}**C NMR** (126 MHz; $CDCl_3$) δ (ppm): 156.29, 148.89, 148.46, 144.18, 140.32, 140.22, 132.48, 130.84, 124.21, 113.06, 110.90, 104.79, 64.06, 63.19, 47.71, 34.44, 31.52, 30.03, 29.85; **HRESI-MS** (pos) $C_{89}H_{107}O_2N_8^+$ *m/z*: [M-Cl]$^+$ *calc.* 1320.85451, *found* 1320.85507.

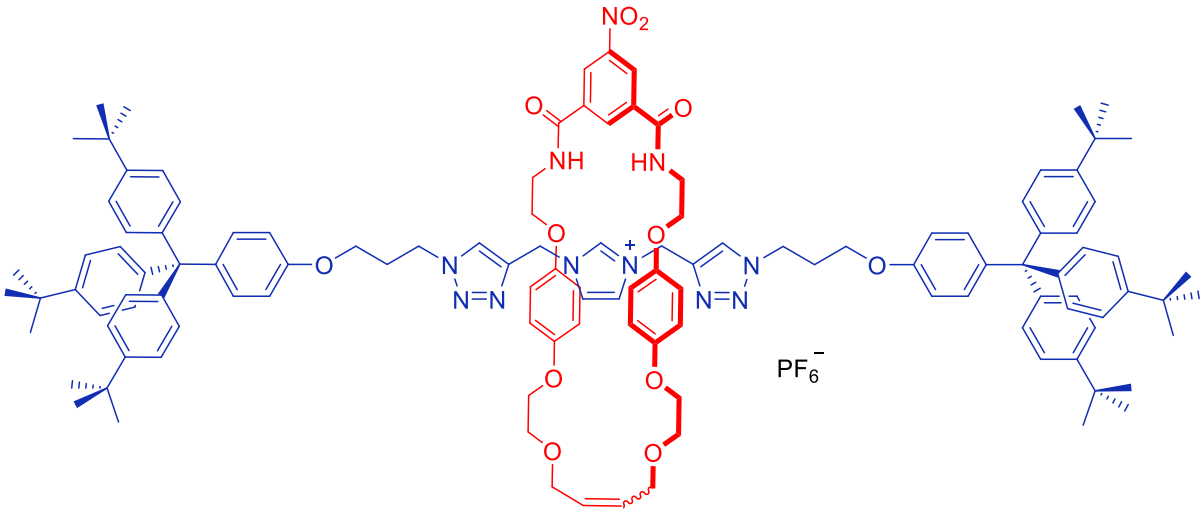
XB imidazolium–bis(iodotriazole) axle 3.11·Cl



Stopper azide **2.31** (0.069 g, 0.117 mmol) was dissolved in dry degassed THF (2 mL) and the reaction vessel covered with foil. $Cu(ClO_4)_2.6H_2O$ (0.079 g, 0.107 mmol) and NaI (0.064 g, 0.426 mmol) were added and stirred under N_2 for 5 mins. TBTA (0.006 g, 0.011 mmol) was added and stirred under N_2 for 5 mins. DBU (0.016 g, 0.107 mmol) and imidazolium–alkyne **3.1** (0.100 g, 0.107 mmol) were added in order and the mixture was stirred at room temperature for 18 hours, after which, the reaction mixture was diluted with DCM (50 mL). The organics were washed with $NH_4OH_{(aq)}$ (3 × 30 mL), H_2O (30 mL) and brine (2 × 30 mL) and dried over $MgSO_4$ and filtered. To the crude reaction mixture TFA (0.5 mL) was added and stirred for 30 mins. The solvent and excess TFA were removed *in vacuo* and the reaction mixture was purified *via* silica gel column chromatography (DCM/MeOH 95:5). The product was subsequently dissolved in DCM (15 mL) and washed with $NH_4Cl_{(aq)}$ (0.1 M, 8 x 30 mL) and H_2O (2 x 30 mL). The solvent was removed *in vacuo* to afford XB imidazolium–bis(iodotriazole) axle **3.11·**Cl (0.059 g, 35%).

^{1}**H NMR** (400 MHz; $CDCl_3$) δ (ppm): 11.02 (1H, s, NC*H*N-*imidazolium*), 7.25-7.19 (12H, m, Ar*H*), 7.18 (2H, s, NC*H-imidazolium*), 7.09-7.03 (16H, m, Ar*H*), 6.74-6.68 (4H, m, OAr*H*), 5.68 (4H, s, NCH_2-*methylene*), 4.54 (4H, t, J = 7.3 Hz, NCH_2CH$_2$), 3.96 (4H, t, J = 5.6 Hz, OCH_2), 2.49-2.22 (4H, m, OCH$_2$CH_2), 1.29 (54H, s, *tert*-CH_3); ^{13}**C NMR** (126 MHz; $CDCl_3$/CD_3OD 1:1) δ (ppm): 155.82, 147.94, 143.76, 143.66, 139.70, 131.82, 130.28, 123.63, 122.57, 112.60, 83.73, 77.35, 63.57, 62.64, 47.96, 44.49, 33.73, 30.67, 29.00; **HRESI-MS** (pos) $C_{89}H_{105}O_2N_8I_2^+$ [M-Cl$^-$]$^+$ *calc.* 1571.6444, *found* 1571.64021.

HB rotaxane 3.14·PF_6

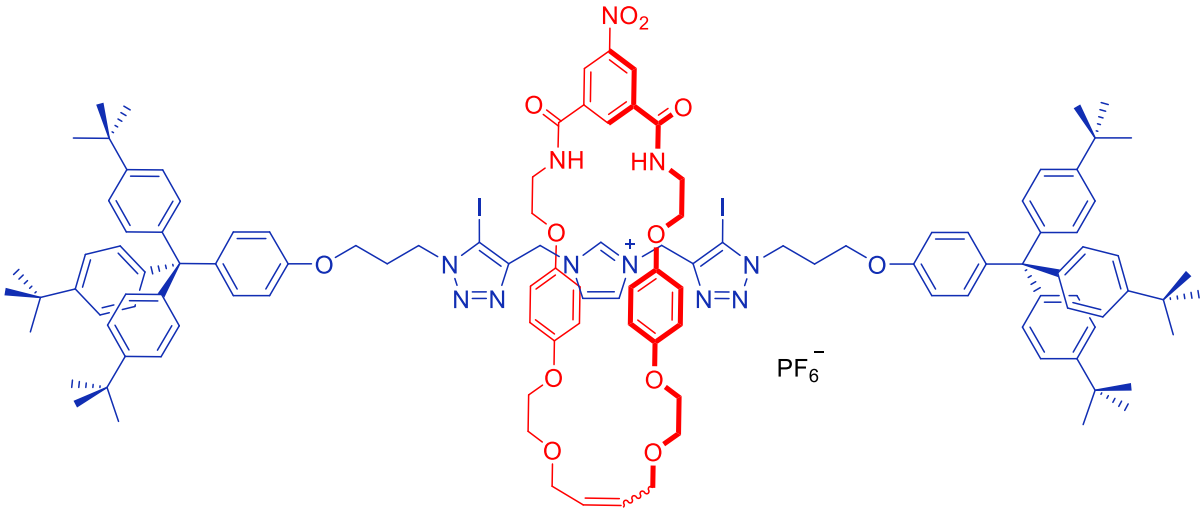


Imidazolium–bis(triazole) axle **3.10**·Cl (0.015 g, 0.011 mmol) and bis-vinyl macrocycle precursor **2.52** (0.011 g, 0.016 mmol) were dissolved in anhydrous DCM (6 mL) and stirred at room temperature for 30 mins. Grubbs' second generation catalyst (1.1 mg, 10% by weight) was added and the mixture was stirred for 48 hours, after which another portion of catalyst was added (1.1 mg) followed by stirring for a further 48 hours. The solvent was removed *in vacuo* and the crude reaction mixture purified *via* preparative TLC (EtOAc/MeOH 95:5 followed by DCM/MeOH 97:3). The product was dissolved in DCM (10 mL) and washed with $NH_4PF_{6(aq)}$ (0.1 M, 8 × 20 mL) and H_2O (2 × 20 mL). The organics were dried over $MgSO_4$, filtered and the solvent removed *in vacuo* to yield HB rotaxane **3.14**·PF_6 as an off white solid (0.008 g, 35%).

^{1}H NMR (500 MHz; $CDCl_3$/CD_3OD/D_2O 45:45:10) δ (ppm): 8.80 (2H, s, Ar*H-ext. macro.*), 8.60 (1H, s, Ar*H-int. macro.*), 7.78 (2H, s, C*H-triazole axle*), 7.29 (2H, s, NC*H-imidazolium axle*), 7.26-7.19 (12H, m, Ar*H-axle*), 7.12-7.06 (16H, m, Ar*H-axle*), 6.68-6.65 (4H, m, OAr*H-axle*), 6.50 (4H, d, J = 9.0 Hz, Ar*H-macro.*), 6.36 (4H, d, J = 9.0 Hz, Ar*H-macro*), 5.78-5.73 (2H, m, C*H-alkene macro.*), 5.20 (4H, s, NCH_2-*methylene axle*), 4.32 (4H, t, J = 6.9 Hz, NCH_2CH_2-*axle*), 3.99 (4H, t, J = 4.9 Hz, CH_2-*macro.*), 3.93-3.91 (4H, m, CH_2-*macro.*), 3.83-3.80 (4H, m, CH_2-*macro.*), 3.79-3.73 (8H, m, CH_2-*macro.*, OCH_2-*axle*), 3.67-3.64 (4H, m, , CH_2-*macro.*), 2.13-2.09 (4H, m, OCH$_2$CH_2-*axle*), 1.29 (54H, s, *tert-*

CH_3); ^{13}**C NMR** (126 MHz; $CDCl_3$) δ (ppm): 164.73, 156.30, 152.94, 152.21, 149.07, 148.48, 144.17, 140.35, 135.95, 132.46, 130.84, 130.81, 129.62, 126.51, 125.13, 124.21, 121.96, 114.96, 114.48, 113.04, 71.12, 69.52, 67.83, 66.24, 63.97, 63.18, 47.83, 40.64, 34.44, 31.52, 30.08, 29.85, 22.85 (one peak missing, presumed overlapped); **HRESI-MS** (pos) $C_{121}H_{142}O_{12}N_{11}$ *m/z*: $[M\text{-}A]^+$ *calc.* 1941.08340, *found* 1941.08375.

XB rotaxane 3.15·PF_6

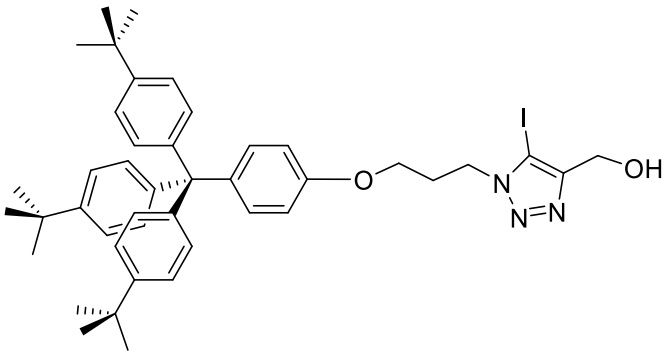


Imidazolium–bis(triazole) axle **3.11**·Cl (0.040 g, 0.025 mmol) and bis-vinyl macrocycle precursor **2.52** (0.024 g, 0.037 mmol) were dissolved in anhydrous DCM (15 mL) and stirred at room temperature for 30 mins. Grubbs' second generation catalyst (2.4 mg, 10% by weight) was added and the mixture was stirred for 48 hours, after which another portion of catalyst was added (2.4 mg) followed by stirring for a further 48 hours. The solvent was removed *in vacuo* and the crude reaction mixture purified *via* preparative TLC (EtOAc/MeOH 95:5 followed by DCM/MeOH 97:3). The product was dissolved in DCM (10 mL) and washed with $NH_4PF_{6(aq)}$ (0.1 M, 8 × 20 mL) and H_2O (2 × 20 mL). The organics were dried over $MgSO_4$, filtered and the solvent removed *in vacuo* to yield XB rotaxane **3.15**·PF_6 as an off white solid (0.014 g, 24%).

^{1}**H NMR** (500 MHz; $CDCl_3/CD_3OD/D_2O$ 45:45:10) δ (ppm): 8.82 (2H, s, Ar*H-ext. macro.*), 8.75 (1H, s, Ar*H-int. macro.*), 7.43 (2H, s, NC*H-imidazolium axle*), 7.30-7.18

(12H, m, Ar*H-axle*), 7.11-7.05 (16H, m, Ar*H-axle*), 6.69-6.64 (4H, m, OAr*H-axle*), 6.43 (4H, d, *J* = 9.1 Hz, Ar*H-macro*), 6.35 (4H, d, *J* = 9.0 Hz, Ar*H-macro*), 5.87-5.82 (2H, m, C*H-alkene macro.*), 5.17 (4H, s, NCH_2*-methylene axle*), 4.26 (4H, t, *J* = 6.9 Hz, NCH_2CH_2*-axle*), 4.03-3.94 (8H, m, CH_2*-macro.*), 3.88-3.82 (4H, m, CH_2*-macro.*), 3.80-3.72 (8H, m, CH_2*-macro.*, OCH_2*-axle*), 3.71-3.66 (4H, m, CH_2*-macro.*), 2.09 (4H, t, *J* = 6.7 Hz, OCH$_2$CH_2*-axle*), 1.29 (54H, s, *tert*-CH_3); **^{13}C NMR** (126 MHz; $CDCl_3$) δ (ppm): 164.98, 156.26, 153.12, 152.35, 148.87, 148.51, 144.17, 143.82, 140.36, 136.67, 135.56, 132.46, 130.82, 129.99, 126.21, 124.22, 122.60, 115.61, 114.66, 113.12, 71.27, 69.66, 67.67, 66.56, 63.85, 63.19, 48.82, 44.60, 40.23, 34.45, 31.53, 22.85 (two peaks missing, presumed overlapped); **HRESI-MS** (pos) $C_{121}H_{140}O_{12}N_{11}I_2$ *m/z*: $[M\text{-}A]^+$ *calc.* 2192.87668, *found* 2192.87577.

Stopper iodotriazole–alcohol 3.22

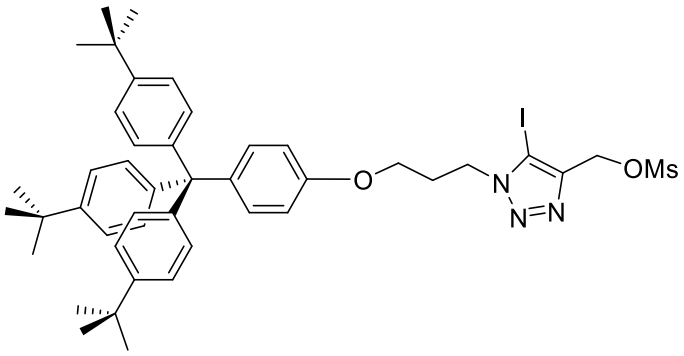


Stopper azide **2.31** (0.200 g, 0.34 mmol) was dissolved in dry degassed THF (4 mL) and the reaction vessel covered with foil. $Cu(ClO_4)_2.6H_2O$ (0.230 g, 0.62 mmol) and NaI (0.186 g, 1.24 mmol) were added and stirred under N_2 for 5 mins. TBTA (0.018 g, 0.032 mmol) was added and stirred under N_2 for 5 mins. DBU (0.048 g, 0.32 mmol) and propargyl alcohol (0.050 mL, 0.32 mmol) were added in order and the mixture was stirred at room temperature for 18 hours, after which, the reaction mixture was diluted with DCM (50 mL). The organics were washed with $NH_4OH_{(aq)}$ (3 × 30 mL), H_2O (30 mL) and brine (2 × 30 mL) and dried over $MgSO_4$. The solvent was removed *in vacuo*. Purification *via* silica

gel column chromatography (DCM/MeOH 98:2) afforded **3.22** as a white solid (0.230 g, 96%).

^{1}**H NMR** (500 MHz; $CDCl_3$) δ (ppm): 7.26.-7.20 (6H, m, Ar*H*), 7.12-7.05 (8H, m, Ar*H*), 6.78-6.71 (2H, m, OAr*H*), 4.72 (2H, d, J = 6.2 Hz, CH_2OH), 4.57 (2H, t, J = 7.0 Hz, NCH_2CH_2), 4.00 (2H, t, J = 5.8 Hz, OCH_2CH_2), 2.41 (2H, quint, J = 6.4 Hz, OCH_2CH_2), 2.03 (1H, t, J = 6.3 Hz, CH_2OH), 1.30 (27H, s, *tert*-CH_3); ^{13}**C NMR** (101 MHz; $CDCl_3$) δ (ppm): 156.16, 148.37, 144.10, 132.29, 130.69, 124.06, 113.06, 63.90, 63.06, 55.69, 47.91, 34.28, 31.33, 29.63; **HRESI-MS** (pos) $C_{43}H_{52}IN_3O_2$ *m/z*: $[M+H]^+$ *calc.* 770.31770, *found* 770.31764.

Stopper iodotriazole–mesylate 3.23

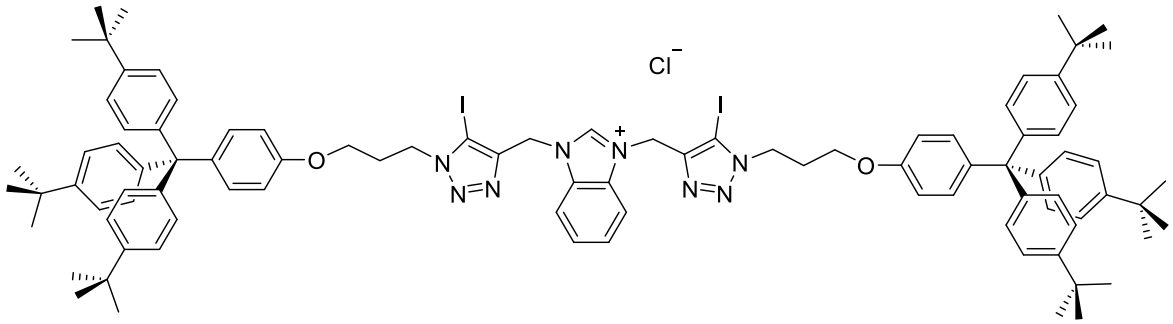


Alcohol **3.22** (0.230 g, 0.30 mmol) and Et_3N (0.083 mL, 0.60 mmol) were added to dry DCM (5 mL) and stirred for 5 mins under N_2 at 0 °C. MsCl (0.028 mL, 0.36 mmol) was dissolved in dry DCM (5 mL) and added dropwise and the reaction mixture stirred for 4 hours at room temperature. The organics were diluted with DCM (20 mL) and washed with H_2O (2 × 20 mL), $HCl_{(aq)}$ (1 M, 2 × 20 mL) and brine (20 mL), dried over anhydrous $MgSO_4$. The solvent was removed *in vacuo* to afford mesylate **3.23** as a yellow oil (0.236 g, 93%).

^{1}**H NMR** (400 MHz; $CDCl_3$) δ (ppm): 7.26-7.21 (6H, m, Ar*H*), 7.13-6.98 (8H, m, Ar*H*), 6.78-6.72 (2H, m, OAr*H*), 5.31 (2H, s, CH_2OMs), 4.62 (2H, t, J = 7.0 Hz, NCH_2CH_2), 4.00

(2H, t, *J* = 5.6 Hz, OC*H*$_2$CH$_2$), 3.67 (3H, s, C*H*$_3$-*mesylate*), 2.41 (2H, quint, *J* = 6.4 Hz, OCH$_2$C*H*$_2$), 1.30 (27H, s, *tert*-C*H*$_3$).

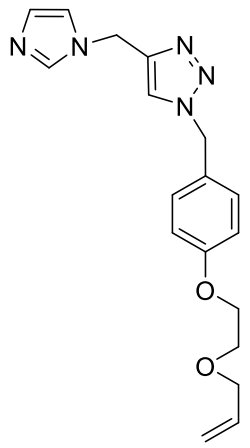
XB benzimidazolium axle 3.24·Cl



Mesylate **3.23** (0.230 g, 0.27 mmol) and benzimidazole (0.005 g, 0.045 mmol) were dissolved in dry DMF (10 mL), to which K_2CO_3 (0.037 g, 0.27 mmol) was added. The reaction was heating under microwave irradiation at 120 °C for 90 mins. The solvent was removed *in vacuo* and the crude reaction mixture dissolved in DCM (50 mL) and washed with H_2O (3 × 30 mL) and brine (2 × 30 mL), dried over anhydrous $MgSO_4$, filtered and the solvent removed *in vacuo.* Purification *via* silica gel column chromatography (DCM/MeOH 95:5) afforded XB benzimidazolium axle **3.24**·OMs. The product was dissolved in DCM (10 mL) and washed with $NH_4Cl_{(aq)}$ (0.1 M, 8 × 20 mL) and H_2O (2 × 20 mL). The organics were dried over $MgSO_4$, filtered and the solvent removed *in vacuo* to yield XB benzimidazolium axle **3.24**·Cl as a white solid (0.016 g, 22%).

^{1}**H NMR** (400 MHz; $CDCl_3$) δ (ppm): 11.28 (1H, s, NC*H*N-*benzimidazolium*), 8.14-8.05 (2H, m, Ar*H*-*benzimidazolium*), 7.54-7.48 (2H, m, Ar*H*-*benzimidazolium*), 7.22-7.15 (12H, m, Ar*H*), 7.08-6.99 (16H, m, Ar*H*), 6.68-6.52 (4H, m, OAr*H*), 5.92 (4H, s, NC*H*$_2$-*methylene*), 4.48 (4H, t, *J* = 7.2 Hz, NC*H*$_2$CH$_2$), 3.91 (4H, t, *J* = 5.8 Hz, OC*H*$_2$), 2.23 (4H, quint, *J* = 6.7 Hz, OCH$_2$C*H*$_2$), 1.26 (54H, s, *tert*-C*H*$_3$); **HRESI-MS** (pos) $C_{39}H_{107}O_2N_8I_2$ *m/z*: $[M\text{-}Cl]^+$ *calc.* 1622.66344, *found* 1622.65971.

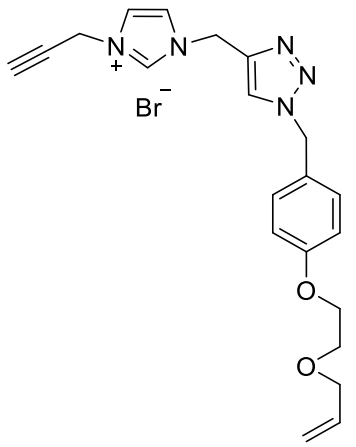
Imidazole–triazole derivative 3.29



Azide **3.27** (0.484 g, 2.08 mmol), $[Cu(MeCN)_4][PF_6]$ (0.141 g, 0.379 mmol) and TBTA (cat. amount) were dissolved in dry degassed DCM (5 mL). Imidazole–alkyne **3.28** (0.200 g, 1.89 mmol) and DIPEA (cat. amount) were added. The mixture was stirred at room temperature under N_2 for 18 hours, after which, the reaction mixture was diluted with DCM (80 mL). The organics were washed with $NH_4OH_{(aq)}$ (3 × 40 mL), H_2O (40 mL) and brine (2 × 40 mL) and dried over $MgSO_4$. The solvent was removed *in vacuo*. Purification by silica gel column chromatography (DCM/MeOH 99:1) yielded **3.29** as a white powder (0.578 g, 90%).

^{1}**H NMR** (400 MHz; $CDCl_3$) δ (ppm): 7.53 (1H, s, NC*H*N-*imidazole*), 7.22 (1H, s, NC*H*-*triazole*), 7.21-7.16 (2H, m, Ar*H*), 7.05 (1H, s, NC*H*-*imidazole*), 6.96 (1H, s, NC*H*-*imidazole*), 6.94-6.85 (2H, m, Ar*H*), 5.99-5.87 (2H, m, C*H*-*alkene*), 5.42 (2H, s, ArCH_2), 5.33-5.25 (2H, m, CH_2-*alkene*), 5.20 (2H, s, *imidazole*-CH_2-*triazole*), 4.18-4.01 (4H, m, OCH_2), 3.83-3.77 (2H, m, OCH_2); **HRESI-MS** (pos) $C_{18}H_{22}O_2N_5$ *m/z*: $[M+H]^+$ *calc.* 340.17680, *found* 340.17661.

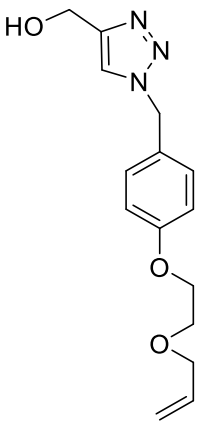
Imidazolium–alkyne derivative 3.30·Br



Imidazole–triazole species **3.29** (0.100 g, 0.27 mmol) was dissolved in acetone (2 mL), to which propargyl bromide (0.12 mL, 1.35 mmol) was added. The reaction mixture was heated under microwave radiation at 150 °C for 75 mins. The precipitate was filtered and washed with acetone (3 × 20 mL) and diethyl ether (3 × 20 mL) to afford imidazolium–alkyne derivative **3.30**·Br as a brown solid (0.083 g, 67%).

^{1}**H NMR** (400 MHz; $CDCl_3$) δ (ppm): 10.63 (1H, s, NC*H*N-*imidazolium*), 8.34 (1H, s, NC*H*-*imidazolium*), 7.69 (1H, s, NC*H*-*imidazolium*), 7.42 (NC*H*-*triazole*), 7.33-7.20 (2H, m, Ar*H*), 6.93-6.82 (2H, m, Ar*H*), 5.97-5.86 (1H, m, C*H*-*alkene*), 5.80 (2H, s, CH_2-*alkyne*), 5.44 (2H, s, *imidazolium*-CH_2-*triazole*), 5.34-5.16 (4H, m, CH_2-*alkene* and ArCH_2), 4.15-4.04 (4H, m, OCH_2), 3.83-3.74 (2H, m, OCH_2).

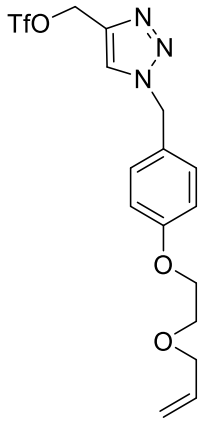
Triazole-alcohol derivative 3.32



Azide **3.27** (0.100 g, 0.43 mmol), $[Cu(MeCN)_4][PF_6]$ (0.027 g, 0.072 mmol) and TBTA (cat. amount) were dissolved in dry degassed DCM (5 mL). Propargyl alcohol (0.02 mL, 0.36 mmol) and DIPEA (cat. amount) were added. The mixture was stirred at room temperature under N_2 for 18 hours, after which, the reaction mixture was diluted with DCM (20 mL). The organics were washed with $NH_4OH_{(aq)}$ (3 × 20 mL), H_2O (20 mL) and brine (2 × 20 mL) and dried over $MgSO_4$. The solvent was removed *in vacuo*. Purification by silica gel column chromatography (DCM/MeOH 98:2) yielded **3.32** (0.085 g, 82%).

^{1}H NMR (400 MHz; $CDCl_3$) δ (ppm): 7.34 (1H, s, C*H-triazole*), 7.11 (2H, dd, J = 8.5, 2.2 Hz, Ar*H*), 6.82 (2H, dd, J = 8.5, 2.2 Hz, Ar*H*), 5.90-5.79 (1H, m, C*H-alkene*), 5.33 (2H, s, ArCH_2), 5.27-5.09 (2H, m, CH_2*-alkene*), 4.63 (2H, s, CH_2OH), 4.07-3.97 (4H, m, OCH_2), 3.74-3.66 (2H, m, OCH_2), 3.60 (1H, s, O*H*).

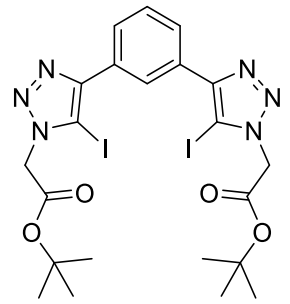
Triazole–triflate derivative 3.33



Triflic anhydride (0.031 mL, 0.29 mmol) was dissolved in dry DCM (2 mL) at 0 °C. A solution of triazole–alcohol species **3.32** (0.050 g, 0.175 mmol) and pyridine (0.028 mL, 0.175 mmol) in DCM (0.5 mL) was added dropwise. The reaction mixture was stirred at 0 °C for 1 hour, after which, the reaction was diluted with DCM (20 mL) and washed with H_2O (3 × 15 mL). The organic layer was dried over anhydrous $MgSO_4$ filtered and the solvent removed *in vacuo* to yield triazole–triflate derivative **3.33** (0.035 g, 48%). The purity of the reaction was confirmed by TLC and the product used immediately in the subsequent step. **ESI-MS** (pos) not observed.

6.2.3 Synthesis of novel compounds from Chapter 4

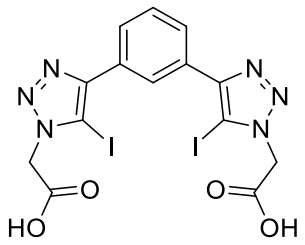
XB bis-ester 4.3



$[Cu(MeCN)_4][PF_6]$ (0.189 g, 0.50 mmol) and TBTA (0.269 g, 0.50 mmol) were dissolved in dry degassed THF (30 mL). Azide **4.2** (0.837 g, 5.323 mmol) and iodoalkyne **4.1** (0.958 g, 2.54 mmol) were added. The reaction mixture was covered with foil and stirred at room temperature under N_2 for 18 hours. The reaction was diluted with DCM (20 mL) and the organics were washed with $NH_4OH_{(aq)}$ (3 × 20 mL), H_2O (20 mL) and brine (2 × 20 mL) and dried over $MgSO_4$. The solvent was removed *in vacuo*. Purification *via* silica gel column chromatography (DCM/MeOH 98:2) afforded d bis-ester **4.3** (1.75 g, 89%).

^{1}**H NMR** (500 MHz; $CDCl_3$) δ (ppm): 8.45 (1H, s, Ar*H*), 8.10-7.77 (2H, m, Ar*H*), 7.54 (1H, dd, *J* = 9.3, 6.5 Hz, Ar*H*), 5.13 (4H, s, NC*H*$_2$-*methylene*), 1.44 (18 H, s, *tert*-C*H*$_3$); ^{13}**C NMR** (126 MHz; $CDCl_3$) δ (ppm): 164.67, 149.90, 130.41, 129.13, 127.88, 126.12, 84.25, 52.42, 27.92.; **HRESI-MS** (pos) $C_{22}H_{27}O_4N_6I_2$ *m/z*: $[M+H]^+$ *calc.* 693.01777, *found* 693.01764.

XB Bis-acid 4.4

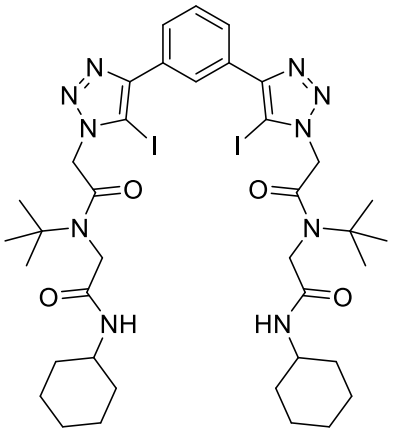


XB bis-ester **4.3** (0.500 g, 0.72 mmol) was dissolved in DCM (10 mL) and TFA (1 mL) was added. The reaction was stirred at room temperature and monitored by TLC. Upon

completion, the solvent was removed *in vacuo* and residuals removed by high vacuum to afford bis-acid **4.4** (0.417 g, quant.).

^{1}H NMR (400 MHz; CD_3OD) δ (ppm): 8.50 (1H, s, Ar*H*), 7.99 (2H, d, J = 7.8 Hz, Ar*H*), 7.64 (2H, t, J = 7.8 Hz, Ar*H*), 5.39 (4H, s, C*H*$_2$COOH); **^{13}C NMR** (126 MHz; CD_3OD) δ (ppm): 169.14, 150.88, 132.14, 130.18, 128.82, 127.28, 81.73, 52.69; **HRESI-MS** (pos) $C_{14}H_{11}O_4N_6I_2$ *m/z*: $[M+H]^+$ *calc.* 580.89257, *found* 580.89269.

XB acyclic species 4.5

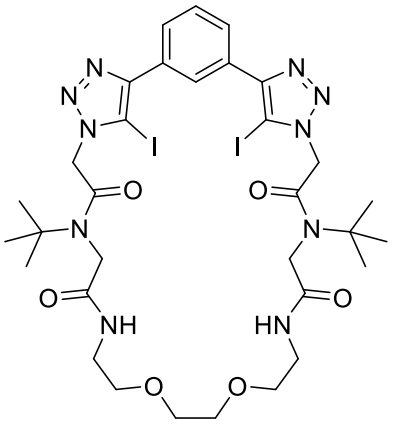


Paraformaldehyde (0.010 g, 0.34 mmol) was dissolved in MeOH (1 mL) and isopropyl amine (0.036 mL, 0.34 mmol) added. The reaction mixture was left to stir for 15 mins at room temperature, after which a precipitate corresponding to the formation of the imine was observed. Bis-acid **4.4** (0.100 g, 0.17 mmol) was added followed by cyclohexyl isocyanide (0.043 ml, 0.34 mmol) and the reaction left to stir. After 30 mins a white precipitate formed, which was filtered and washed with MeOH to afford XB acyclic species **4.5** (0.165 g, 81%). Further purification was not necessary.

^{1}H NMR (400 MHz; C_3D_6O) δ (ppm): 8.76 (1H, t, ^{4}J = 1.8 Hz, Ar*H*), 8.08 (2H, dd, J = 7.8, 1.8 Hz, Ar*H*), 7.64 (1H, t, J = 7.8 Hz, Ar*H*), 7.28 (d, J = 8.0 Hz, N*H-amide*), 5.50 (4H, s, C*H*$_2$*-iodotriazole*), 4.28 (4H, s, C*H*$_2$*-amide*), 3.86-3.70 (2H, m, C*H-cyclo-hex*), 1.96-1.86 (4H, m, C*H*$_2$*-cyclo-hex*), 1.79-1.70 (4H, m, C*H*$_2$*-cyclo-hex*), 1.65-1.57 (4H, m, C*H*$_2$*-cyclo-hex*), 1.44 (18H, s, *tert*-C*H*$_3$), 1.41-1.14 (8H, m, C*H*$_2$*-cyclo-hex*); **^{13}C NMR** could not be

obtained due to limited solubility; **HRESI-MS** (pos) $C_{38}H_{55}O_4N_{10}I_2$ *m/z*: $[M+H]^+$ *calc.* 969.24916, *found* 969.24950

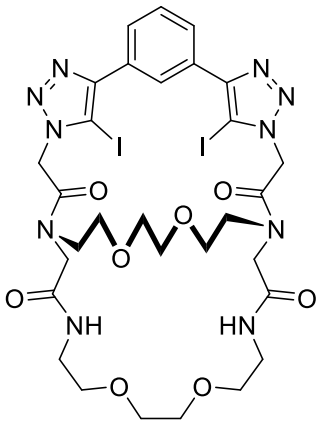
XB macrocycle 4.8



Paraformaldehyde (0.005 g, 0.172 mmol) was dissolved in MeOH (25 mL) and *tert*-butylamine (0.018 mL, 0.172 mmol) was added. The reaction mixture was left to stir for 2 hours at room temperature to allow for the formation of imine. Bis-acid **4.4** (0.050 g, 0.086 mmol) was added and the stirring continued for 30 mins. Bis-isocyanide **4.7** (0.015 g, 0.086 mmol) in MeOH (7 mL) was added to the reaction mixture using a syringe pump (flow rate 0.5 mL/h). After addition was complete, the reaction mixture was stirred for 18 hours. The solvent was removed *in vacuo*. Purification *via* preparative TLC (DCM/MeOH 93:7) afforded XB macrocycle **4.8** (0.043 g, 55%).

^{1}**H NMR** (400 MHz; $CDCl_3$) δ (ppm): 8.59 (1H, s, Ar*H*), 8.02 (2H, d, J = 7.8 Hz, Ar*H*), 7.56 (1H, t, J = 7.8 Hz, Ar*H*), 6.80 (2H, s, N*H*), 5.26 (4H, s, CH_2-*iodotriazole*), 4.09 (4H, s, CH_2-*amide*), 3.73-3.54 (8H, m, CH_2), 3.49 (4H, s, OCH_2CH_2O), 1.48 (18H, s, *tert*-CH_3); ^{13}**C NMR** (126 MHz; $CDCl_3$) δ (ppm): 173.05, 169.56, 138.27, 136.94, 135.43, 133.04, 132.91, 129.99, 73.39, 72.30, 63.23, 57.59, 56.44, 43.34, 32.04; **HRESI-MS** (pos) $C_{32}H_{45}O_6N_{10}I_2$ *m/z*: $[M+H\}^+$ *calc.* 919.16074, *found* 919.16185.

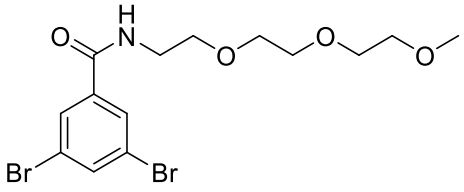
XB macrobicycle 4.9



Paraformaldehyde (0.005 g, 0.172 mmol) was dissolved in MeOH (25 mL) and 1,2-bis(2-aminoethoxy)ethane (12.7 µL, 0.086 mmol) was added. The reaction mixture was left to stir for 2 hours at room temperature to allow for the formation of imine. Bis-acid **4.4** (0.050 g, 0.086 mmol) in MeOH (3.5 mL) and bis-isocyanide **4.7** (0.016 g, 0.86 mmol) in MeOH (3.5 mL) were simultaneously added to the reaction mixture *via* syringe pump (flow rate 0.5 mL/h). After addition was complete, the reaction mixture was stirred for 18 hours. The solvent was removed *in vacuo*. Purification *via* preparative TLC (DCM/MeOH 93:7) afforded XB macrobicycle **4.9** (0.025 g, 32%).

^{1}**H NMR** (400 MHz; DMSO-d_6) δ (ppm): 8.29 (1H, s, Ar*H*), 7.78 (2H, d, J = 7.3 Hz, Ar*H*), 7.11 (1H, t, J = 7.2 Hz, Ar*H*), 4.04 (4H, s, CH_2-*iodotriazole*), 3.93 (4H, s, CH_2-*amide*), 3.76-2.98 (24H, m, CH_2); ^{13}**C NMR** could not be obtained due to limited solubility; **ESI-MS** (pos) $C_{30}H_{39}I_2N_{10}O_8$ *m/z*: $[M+H]^+$ *calc.* 921.10, *found* 921.10.

PEG amide appended bis-bromo derivative 4.10

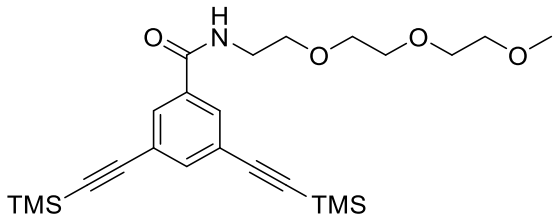


3,5-Dibromobenzoic acid (1.400 g, 5.0 mmol) was added to dry DCM (100 mL) and the solution cooled to 0 °C. DCC (1.032 g, 5.5 mmol) and DMAP (0.061 g, 0.5 mmol) were

dissolved separately in dry DCM (1 mL) and added to the reaction mixture. Polyether amine (0.898 g, 5.5 mmol) was added and the reaction was allowed to warm to room temperature and stirred for 18 hours. The reaction mixture was filtered and concentrated *in vacuo*. Purification *via* silica gel column chromatography (DCM) afford PEG amide appended bis-bromo derivative **4.10** as an off-white solid (1.68 g, 79%).

^{1}**H NMR** (400 MHz; $CDCl_3$) δ (ppm): 7.85 (2H, t, ^{4}J = 1.7 Hz, Ar*H*), 7.72 (1H, t, ^{4}J = 1.6 Hz, Ar*H*), 7.11 (1H, s, N*H-amide*), 3.68-3.54 (10H, m, OCH_2), 3.52-3.47 (2H, m, OCH_2), 3.26 (3H, s, OCH_3); ^{13}**C NMR** (126 MHz; $CDCl_3$) δ (ppm): 164.84, 138.06, 136.69, 129.27, 123.18, 72.01, 70.65, 70.55, 70.37, 69.65, 59.00, 40.20; **ESI-MS** (pos) $C_{14}H_{21}Br_2NO_4$ *m/z*: $[M+H]^+$ *calc.* 423.97, *found* 424.00.

TMS-protected bis-alkyne derivative 4.11

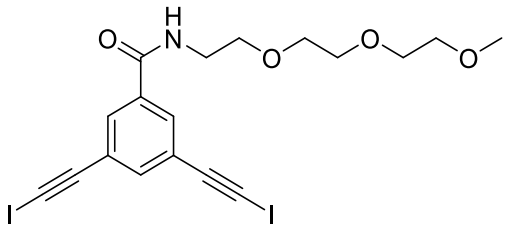


Bis-bromo species **4.10** (1.00 g, 2.35 mmol) was dissolved in dry degassed THF (10 mL) and CuI (0.022 g, 0.12 mmol), $Pd(PPh_3)_2Cl_2$ (0.083 g, 0.12 mmol) and Et_3N (2 mL) were added. The reaction mixture was degassed with argon, then trimethylsilyl acetylene (3.24 mL, 23.5 mmol) was added and the reaction heated to 70 °C for 3 hours. The crude reaction mixture was concentrated *in vacuo* and diluted with EtOAc and passed through a silica plug. The solvent was removed *in vacuo* and purification *via* silica gel column chromatography (EtOAc/Hexane 2:3) afforded TMS-protected bis-alkyne **4.11** (0.940 g, 87%).

^{1}**H NMR** (400 MHz; $CDCl_3$) δ (ppm): 7.81 (2H, t, ^{4}J = 1.4 Hz, Ar*H*), 7.66 (1H, t, ^{4}J = 1.5 Hz, Ar*H*), 6.95 (1H, s, N*H-amide*), 3.68-3.62 (10H, m, OCH_2), 3.55-3.50(2H, m, OCH_2),

3.31 (3H, s, OC*H*$_3$), 0.24 (18H, s, C*H*$_3$-*TMS*); **ESI-MS** (pos) $C_{24}H_{38}NO_4Si_2$ *m/z*: $[M+H]^+$ *calc.* 460.23, *found* 460.23.

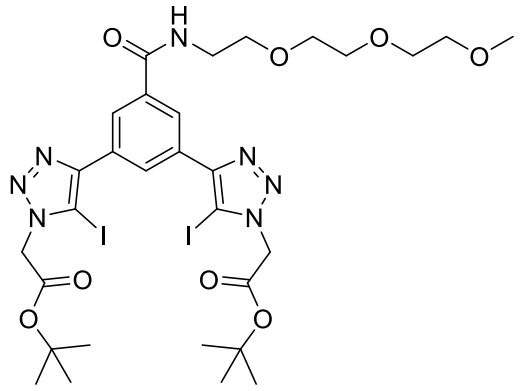
Bis-iodoalkyne derivative 4.12



TMS-protected bis-alkyne **4.11** (0.500 g, 1.09 mmol) was dissolved in acetone (8 mL). *N*-iodosuccinimide (0.563 g, 2.50 mmol) was added. $AgNO_3$ was dissolved in H_2O (1 mL) and added to the reaction mixture, which was then stirred in the dark for 4 hours. The reaction mixture was diluted with H_2O (40 mL) and extracted into DCM (5 × 30 mL). The combined organics were washed with $Na_2S_2O_3$, dried over anhydrous $MgSO_4$ and the solvent removed *in vacuo* to yield bis-iodoalkyne **4.12** (0.581 g, 94%). The product was used immediately.

^{1}**H NMR** (400 MHz; $CDCl_3$) δ (ppm): 7.78 (2H, t, ^4J = 1.5 Hz, Ar*H*), 7.55 (1H, t, ^4J = 1.5 Hz, Ar*H*), 6.95 (1H, s, N*H-amide*), 3.67-3.59 (10H, m, OC*H*$_2$), 3.55-3.49 (2H, m, OC*H*$_2$), 3.31 (3H, s, OC*H*$_3$). ^{13}**C NMR** could not be obtained due to instability of product. **ESI-MS** (pos) not observed.

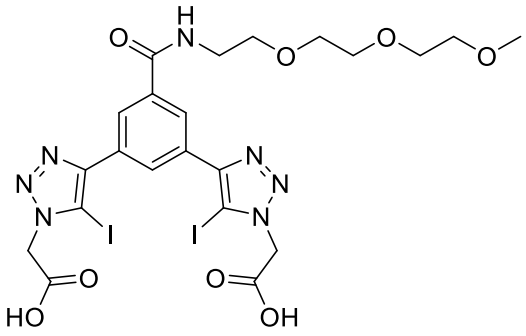
XB bis-ester derivative 4.13



$[Cu(MeCN)_4][PF_6]$ (0.063 g, 0.17 mmol) and TBTA (0.090 g, 0.17 mmol) were dissolved in dry degassed THF (12 mL). Azide **4.2** (0.274 g, 1.74 mmol) and bis-iodoalkyne **4.12** (0.470 g, 0.83 mmol) were added. The reaction mixture was covered with foil and stirred at room temperature under N_2 for 18 hours. The reaction was diluted with DCM (40 mL) and the organics were washed with $NH_4OH_{(aq)}$ (3 × 30 mL), H_2O (30 mL) and brine (2 × 30 mL) and dried over $MgSO_4$. The solvent was removed *in vacuo*. Purification *via* silica gel column chromatography (DCM/MeOH 97:3) afforded bis-ester **4.13** (0.476 g, 65%).

^{1}**H NMR** (400 MHz; $CDCl_3$) δ (ppm): 8.67 (1H, t, ^4J = 1.7 Hz, Ar*H*), 8.44 (2H, d, ^4J = 1.7 Hz, Ar*H*), 7.66 (1H, s, N*H-amide*), 5.15 (4H, s, NCH_2*-methylene*), 3.67-3.61 (8H, m, CH_2), 3.60-3.56 (2H, m, CH_2), 3.49-3.44 (2H, m, CH_2), 3.26 (3H, s, OCH_3), 1.46 (18H, s, *tert*-CH_3); ^{13}**C NMR** (126 MHz; $CDCl_3$) δ (ppm): 167.28, 164.55, 149.14, 135.60, 135.57, 130.90, 128.45, 126.30, 84.25, 78.97, 71.85, 70.57, 70.45, 70.27, 69.86, 58.92, 40.13, 27.97; **HRESI-MS** (pos) $C_{30}H_{42}O_8N_7I_2$ *m/z*: $[M+H]^+$ *calc.* 882.11787, *found* 882.11671.

XB bis-acid derivative 4.14

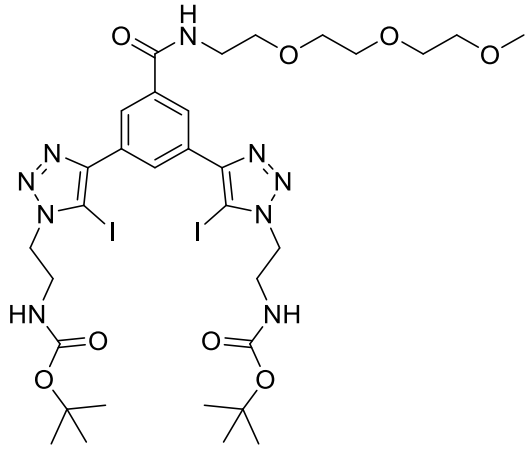


Bis-ester **4.13** (0.270 g, 0.31 mmol) was dissolved in DCM (5 mL) and TFA (2 mL) added and the reaction mixture stirred at room temperature for 8 hours. The solvent was removed *in vacuo* and the residue dried under high vacuum to afford bis-acid **4.14** as a white solid (0.238 g, 90%). The mono-protected species was also present (10%) and could not be isolated from the desired product.

^{1}**H NMR (**400 MHz; CD_3OD) δ (ppm): 8.68 (1H, t, ^4J = 1.7 Hz, Ar*H*), 8.46 (2H, d, ^4J = 1.7 Hz, Ar*H*), 5.39 (4H, s, CH_2COOH), 3.75-3.57 (10H, m, CH_2), 3.52-3.42 (2H, m, CH_2), 3.27

(3H, s, OC*H*$_3$); ^{13}**C NMR** (126 MHz; CD_3OD) δ (ppm): 169.33, 150.19, 136.98, 132.59, 129.59, 127.49, 82.10, 72.85, 71.53, 71.33, 71.31, 70.45, 59.09, 41.11 (two peaks missing, presumed overlapped); **HRESI-MS** (pos) $C_{22}H_{26}O_8N_7I_2$ *m/z*: $[M+H]^+$ *calc.* 769.99267, *found* 769.99268.

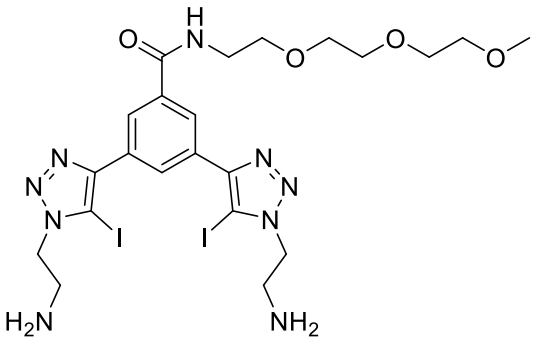
BOC-protected bis-amine derivative 4.17



$[Cu(MeCN)_4][PF_6]$ (0.063 g, 0.17 mmol) and TBTA (0.090 g, 0.17 mmol) were dissolved in dry degassed THF (12 mL). Azide **4.16** (0.331 g, 1.78 mmol) and bis-iodoalkyne **4.12** (0.480 g, 0.85 mmol) were added. The reaction mixture was covered with foil and stirred at room temperature under N_2 for 18 hours. The reaction was diluted with DCM (40 mL) and the organics were washed with $NH_4OH_{(aq)}$ (3 × 30 mL), H_2O (30 mL) and brine (2 × 30 mL) and dried over $MgSO_4$. The solvent was removed *in vacuo*. Purification *via* silica gel column chromatography (DCM/MeOH/Et_3N 96:3:1) afforded BOC-protected bis-amine **4.17** (0.591 g, 74%).

^{1}**H NMR** (400 MHz; $CDCl_3$) δ (ppm): 8.69 (1H, s, Ar*H*), 8.42 (2H, s, Ar*H*), 4.58 (4H, t, *J* = 5.6 Hz, C*H*$_2$-*iodotriazole*), 3.79-3.57 (12H, m, C*H*$_2$NH and OC*H*$_2$), 3.49 (2H, t, *J* = 5.8 Hz, OC*H*$_2$), 3.41 (2H, t, *J* = 5.8 Hz, OC*H*$_2$), 3.29 (3H, s, OC*H*$_3$), 1.44 (18H, s, *tert*-C*H*$_3$); **ESI-MS** (pos) $C_{32}H_{48}I_2N_9O_8$ $[M+H]^+$ *calc.* 940.16, *found* 940.16.

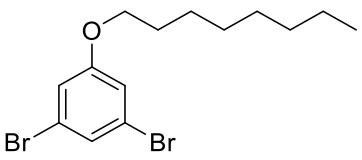
XB bis-amine derivative 4.18



BOC-protected bis-amine **4.17** (0.520 g, 0.55 mmol) was dissolved in DCM (5 mL) and TFA (2 mL) was added and the reaction mixture stirred at room temperature for 4 hours. The solvent and excess TFA were removed *in vacuo*. The crude reaction mixture was re-dissolved in EtOAc (50 mL) and washed with sat. $NaHCO_{3(aq)}$ (5 × 30 mL). The aqueous layers were washed with EtOAc (8 × 50 mL). The combined organics were dried over anhydrous $MgSO_4$ and the solvent removed *in vacuo* to afford bis-amine **4.18** (0.154 g, 38%).

^{1}**H NMR** (400 MHz; CD_3OD) δ (ppm): 8.45 (1H, s, Ar*H*), 8.27 (2H, s, Ar*H*), 4.72 (4H, t, *J* = 6.0 Hz, C*H*$_2$*-iodotriazole*), 4.01-3.99 (4H, m, C*H*$_2$NH$_2$), 3.61-3.45 (10H, m, OC*H*$_2$), 3.37-3.31 (2H, m, OC*H*$_2$), 3.14 (3H, s, OC*H*$_3$); **ESI-MS** (pos) $C_{32}H_{48}I_2N_9O_8$ *m/z*: $[M+H]^+$ *calc.* 740.01, *found* 740.00.

Octyl-appended bis-bromo derivative 4.21

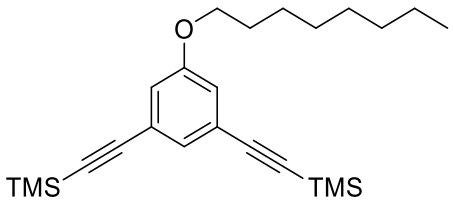


3,5-Dibromophenol (1.00 g, 3.97 mmol) was dissolved in DMF (12 mL) and 1-bromooctane (1.03 mL, 5.95 mmol) then K_2CO_3 (2.20 g, 15.9 mmol) were added. The reaction mixture was heated to 80 °C under N_2 for 48 hours. The solvent was removed *in vacuo* and the crude residue re-dissolved in DCM (50 mL) and washed with H_2O (3 × 30 mL) and brine (2 × 30 mL) and dried over anhydrous $MgSO_4$ and the solvent removed *in*

vacuo. Purification *via* silica gel column chromatography (DCM) afforded bis-bromo species **4.21** (1.33 g, 92%).

^{1}H NMR (500 MHz; $CDCl_3$) δ (ppm): 7.22 (1H, t, ^{4}J = 1.8 Hz, Ar*H*), 6.98 (2H, d, ^{4}J = 1.8 Hz, Ar*H*), 3.91 (2H, t, J = 6.5 Hz, OCH_2), 1.75 (2H, quint, J = 6.7 Hz, OCH_2CH_2), 1.47-1.39 (2H, m, CH_2), 1.37-1.23 (8H, m, CH_2), 0.89 (3H, t, J = 6.6 Hz, CH_3); **^{13}C NMR** (126 MHz; $CDCl_3$) δ (ppm): 160.52, 126.29, 123.19, 117.09, 68.80, 31.94, 29.41, 29.34, 29.14, 26.06, 22.80, 14.24; **ESI-MS** (pos) not observed.

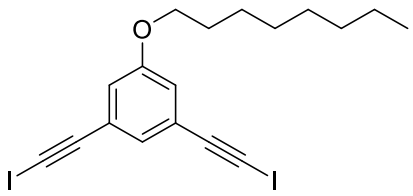
TMS-protected bis-alkyne derivative 4.22



Bis-bromo species **4.21** (1.00 g, 2.75 mmol) was dissolved in dry degassed THF (10 mL) and CuI (0.026 g, 0.14 mmol), $Pd(PPh_3)_2Cl_2$ (0.096 g, 0.14 mmol) and Et_3N (2 mL) were added. The reaction mixture was degassed with argon, then trimethylsilyl acetylene (3.80 mL, 27.5 mmol) was added and the reaction heated to 70 °C for 3 hours. The crude reaction mixture was concentrated *in vacuo* and diluted with EtOAc and passed through a silica plug. The solvent was removed *in vacuo* and purification *via* silica gel column chromatography (EtOAc/Hex 2:3) afforded TMS-protected bis-alkyne **4.22** (0.810 g, 74%).

^{1}H NMR (400 MHz; $CDCl_3$) δ (ppm): 7.35 (1H, t, ^{4}J = 1.8 Hz, Ar*H*), 7.02 (2H, d, ^{4}J = 1.8 Hz, Ar*H*), 4.01 (2H, t, J = 6.5 Hz, OCH_2), 1.84 (2H, quint, J = 6.8 Hz, OCH_2CH_2), 1.58-1.45 (2H, m, CH_2), 1.46-1.30 (8H, m, CH_2), 1.03-0.90 (3H, m, CH_3), 0.32 (18H, s, CH_3-*TMS*); **^{13}C NMR** (126 MHz; $CDCl_3$) δ (ppm): 158.74, 128.10, 124.35, 118.38, 104.32, 94.53, 68.30, 31.97, 29.44, 29.27, 26.12, 22.82, 14.26, 1.18; **ESI-MS** (pos) not observed.

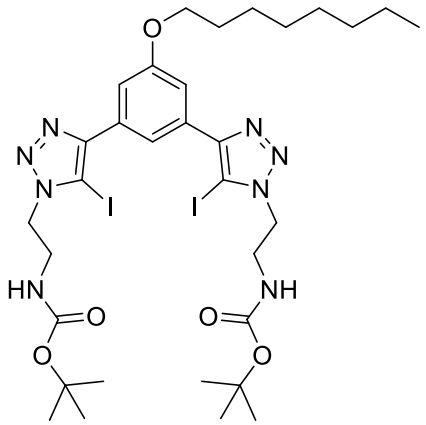
Bis-iodoalkyne derivative 4.23



TMS-protected bis-alkyne **4.22** (0.500 g, 1.25 mmol) was dissolved in acetone (8 mL). *N*-iodosuccinimide (0.649 g, 2.88 mmol) was added. $AgNO_3$ was dissolved in H_2O (1 mL) and added to the reaction mixture, which was then stirred in the dark for 4 hours. The reaction mixture was diluted with H_2O (40 mL) and extracted into DCM (5 × 30 mL). The combined organics were washed with $Na_2S_2O_3$, dried over anhydrous $MgSO_4$ and the solvent removed *in vacuo* to yield bis-iodoalkyne **4.23** (0.633 g, quant.). The product was used immediately.

^{1}**H NMR (**400 MHz; $CDCl_3$) δ (ppm): 7.07 (1H, t, ^4J = 1.4 Hz, Ar*H*), 6.91 (2H, d, ^4J = 1.4 Hz, Ar*H*), 3.90 (2H, t, J = 6.6 Hz, OCH_2), 1.75 (2H, quint, J = 6.6 Hz, OCH$_2CH_2$), 1.47-1.43 (10H, m, CH_2), 0.92-0.84 (3H, m, CH_3); ^{13}**C NMR** (126 MHz; $CDCl_3$) δ (ppm): 158.61, 128.58, 124.49, 119.19, 93.28, 68.45, 31.93, 29.41, 29.35, 29.18, 26.07, 22.80, 14.26, 7.49; **HRESI-MS** (pos) not observed.

BOC-protected bis-amine derivative 4.24

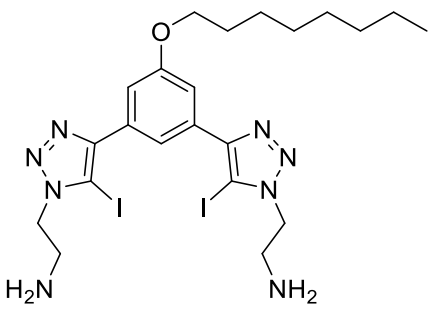


$[Cu(MeCN)_4][PF_6]$ (0.059g, 0.16 mmol) and TBTA (0.084 g, 0.16 mmol) were dissolved in dry degassed THF (12 mL). Azide **4.16** (0.309 g, 1.66 mmol) and bis-iodoalkyne **4.23**

(0.400 g, 0.79 mmol) were added. The reaction mixture was covered with foil and stirred at room temperature under N_2 for 18 hours. The reaction was diluted with DCM (40 mL) and the organics were washed with $NH_4OH_{(aq)}$ (3 × 30 mL), H_2O (30 mL) and brine (2 × 30 mL) and dried over $MgSO_4$. The solvent was removed *in vacuo*. Purification *via* silica gel column chromatography (EtOAc/Hexane 1:1) afforded BOC-protected bis-amine **4.24** (0.597 g, 86%).

^{1}H NMR (500 MHz; $CDCl_3$) δ (ppm): 8.14 (1H, t, ^4J = 1.5 Hz, Ar*H*), 7.55 (2H, d, ^4J = 1.5 Hz, Ar*H*), 4.96 (2H, t, J = 6.9 Hz, N*H*), 4.56 (4H, t, J = 5.6 Hz, CH_2-*iodotriazole*), 4.09 (2H, t, J = 6.6 Hz, OCH_2), 3.75 (4H, m, CH_2-*amide*), 1.83 (2H, quint, J = 6.8 Hz, OCH_2CH_2), 1.44 (18H, s, *tert*-CH_3), 1.39-1.18 (10H, m, CH_2), 0.93-0.74 (3H, m, CH_3); **^{13}C NMR** (126 MHz; $CDCl_3$) δ (ppm): 159.43, 155.90, 149.15, 131.57, 118.15, 113.87, 79.75, 78.10, 68.36, 50.69, 40.10, 31.82, 29.37, 29.25, 28.44, 26.07, 22.66, 14.13; **HRESI-MS** (pos) $C_{32}H_{49}O_5N_8I_2$ *m/z*: $[M+H]^+$ *calc.* 879.19098, *found* 879.19086.

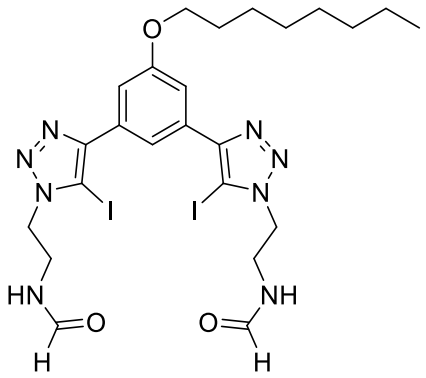
XB bis-amine derivative 4.25



BOC-protected bis-amine **4.24** (0.200 g, 0.23 mmol) was dissolved in DCM (5 mL) and TFA (2 mL) was added. The reaction was stirred at room temperature for 4 hours. The solvent and excess TFA were then removed *in vacuo*. The crude was re-dissolved in DCM (50 mL) and washed with sat. $NaHCO_{3(aq)}$ (5 x 30 mL). The aqueous layers were washed with DCM (2 × 30 mL). The combined organics were washed with brine (3 × 30 mL) and dried over anhydrous $MgSO_4$ and the solvent removed *in vacuo* to afford XB bis-amine **4.25** (0.144 g, 92%).

^{1}H NMR (400 MHz; $CDCl_3$) δ (ppm): 8.12 (1H, t, ^{4}J = 1.6 Hz, Ar*H*), 7.55 (2H, d, ^{4}J = 1.5 Hz, Ar*H*), 4.51 (2H, t, J = 6.1 Hz, CH_2-*iodotriazole*), 4.09 (2H, t, J = 6.6 Hz, OCH_2), 3.30 (4H, t, J = 6.1 Hz, CH_2-*amide*), 1.83 (2H, quint, J = 6.8 Hz, OCH_2CH_2), 1.53-1.22 (10H, m, CH_2), 0.93-0.76 (3H, m, CH_3); **^{13}C NMR** (126 MHz; CD_3OD) δ (ppm): 163.50, 160.10, 150.17, 132.20, 119.14, 114.66, 79.65, 68.91, 53.58, 41.39, 32.30, 30.14, 29.73, 26.53, 23.10, 14.28; **HRESI-MS** (pos) $C_{22}H_{33}ON_8I_2$ *m/z*: $[M+H]^+$ *calc.* 679.08612, *found* 679.08690.

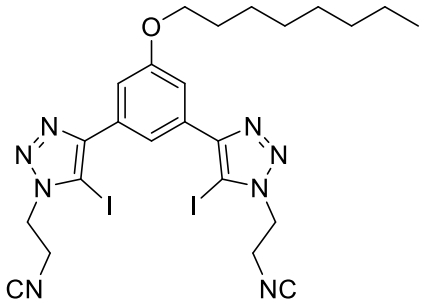
Bis-formamide derivative 4.26



Bis-amine **4.25** (0.057 g, 0.0084 mmol) was dissolved in ethyl formate (20 mL) and heated to 55 °C for 16 hours. The solvent was removed *in vacuo* and the product dried under high vacuum to afford bis-formamide derivative **4.26** (0.023 g, 38%). The product was carried forward into the next step without purification. Yield of product calculated from the ^{1}H NMR spectrum.

^{1}H NMR (400 MHz; $CDCl_3$) δ (ppm): 8.07 (2H, s, OC*H*), 7.97 (1H, s, Ar*H*), 7.46 (2H, s, Ar*H*), 4.61 (4H, t, J = 6.0 Hz, CH_2-*iodotriazole*), 4.07 (2H, t, J = 6.5 Hz, OCH_2), 3.80 (4H, t, J = 5.8 Hz, CH_2-*amide*), 1.81 (2H, quint, J = 6.9 Hz, OCH_2CH_2), 1.52-1.40 (2H, m, CH_2), 1.39-1.20 (8H, m, CH_2), 0.98-0.71 (3H, m, CH_3); **^{13}C NMR** could not be obtained due to low solubility.

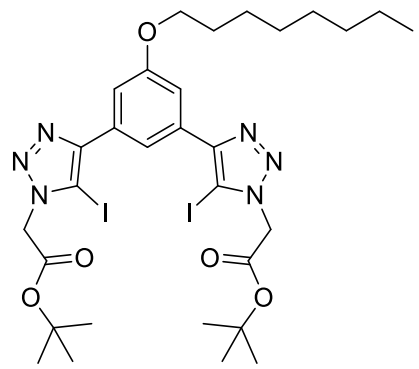
XB bis-isocyanide derivative 4.27



Bis-formamide **4.26** (0.090 g, 0.123 mmol) was dissolved in dry DCM (2 mL). Et_3N (1 mL) was added and the solution cooled to −78 °C. A solution of $POCl_3$ (0.04 mL, 0.258 mmol) in DCM (0.2 mL) was added dropwise under N_2. The reaction mixture was allowed to warm to room temperature and stirred for 16 hours, then poured into ice cold H_2O (30 mL) and extracted into DCM (3 × 30 mL). The organics were washed with sat. $NaHCO_{3(aq)}$ (2 x 20 mL) and brine (2 × 20 mL) and dried over anhydrous $MgSO_4$ and the solvent removed *in vacuo*. Purification *via* preparative TLC (DCM/MeOH 99:1) afforded bis-isocyanide **4.27** as a colourless oil (0.044 g, 51%).

^{1}**H NMR** (400 MHz; $CDCl_3$) δ (ppm): 8.11 (1H, t, ^4J = 1.5 Hz, Ar*H*), 7.56 (2H, d, ^4J = 1.5 Hz, Ar*H*), 4.76 (4H, t, J = 5.6 Hz, CH_2-*iodotriazole*), 4.10-3.96 (6H, m, OCH_2 and CH_2-*amide*), 1.83 (2H, quint, J = 6.8 Hz, OCH_2CH_2), 1.53-1.42 (2H, m, CH_2), 1.42-1.20 (8H, m, CH_2), 0.95-0.82 (3H, m, CH_3); **ESI-MS** (pos) $C_{24}H_{29}I_2N_8O$ *m/z*: $[M+H]^+$ *calc.* 699.05, *found* 699.04.

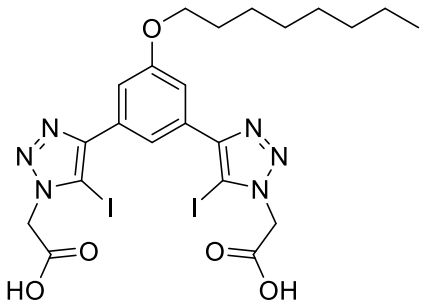
XB bis-ester derivative 4.28



$[Cu(MeCN)_4][PF_6]$ (0.030 g, 0.080 mmol) and TBTA (0.042 g, 0.080 mmol) were dissolved in dry degassed THF (6 mL). Azide **4.2** (0.131 g, 0.83 mmol) and bis-iodoalkyne **4.23** (0.200 g, 0.40 mmol) were added. The reaction mixture was covered with foil and stirred at room temperature under N_2 for 18 hours. The reaction was diluted with DCM (30 mL) and the organics were washed with $NH_4OH_{(aq)}$ (3 × 20 mL), H_2O (20 mL) and brine (2 × 20 mL) and dried over anhydrous $MgSO_4$. The solvent was removed *in vacuo*. Purification *via* silica gel column chromatography (EtOAc/Hex 40:60) afforded bis-ester **4.28** (0.305 g, 94%).

^{1}H NMR (400 MHz; $CDCl_3$): 8.12 (1H, s, Ar*H*), 7.56 (2H, s, Ar*H*), 5.19 (4H, s, C*H*$_2$-*iodotriazole*), 4.12 (2h, t, *J* = 6.5 Hz, OC*H*$_2$), 1.83 (2H, quint, *J* = 6.8 Hz, OCH$_2$C*H*$_2$), 1.45 (18H, s, *tert*-C*H*$_3$), 1.48-1.24 (10H, m, C*H*$_2$), 0.93-0.74 (3H, m, C*H*$_3$); **ESI-MS** (pos) $C_{30}H_{43}I_2N_6O_5$ *m/z*: $[M+H]^+$ *calc.* 821.14, *found* 821.13.

XB bis-acid derivative 4.29

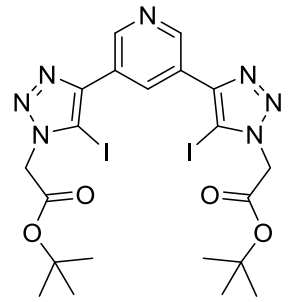


Bis-ester **4.28** (0.300 g, 0.37 mmol) was dissolved in DCM (5 mL), to which TFA (2 mL) was added. The reaction was heated to 40 °C and stirred for 6 hours. The solvent and excess TFA were removed *in vacuo* to afford bis-acid **4.29** (0.183 g, 70%). Unfortunately, monoprotected product was also present (30%) and could not be isolated from the desired product.

^{1}H NMR (400 MHz; CD_3OD δ (ppm): 8.10 (1H, s, Ar*H*), 7.53 (2H, s, Ar*H*), 5.36 (4H, s, C*H*$_2$COOH), 4.13 (2H, t, *J* = 6.4 Hz, OC*H*$_2$), 1.84 (2H, quint, *J* = 6.7 Hz, OCH$_2$C*H*$_2$), 1.57-1.45 (2H, m, C*H*$_2$), 1.43-1.26 (8H, m, C*H*$_2$), 0.93-0.85 (3H, m, C*H*$_3$); **^{13}C NMR** could not be

determined due to mixture of products; **ESI-MS** (pos) $C_{22}H_{27}I_2N_6O_5$ *m/z*: $[M+H]^+$ *calc.* 709.01, *found* 709.01.

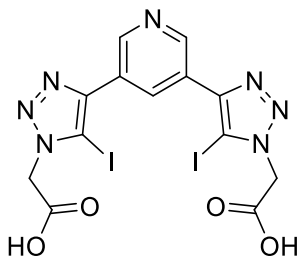
XB bis-ester derivative 4.30



$[Cu(MeCN)_4][PF_6]$ (0.010 g, 0.026 mmol) and TBTA (0.014 g, 0.026 mmol) were dissolved in dry degassed THF (3 mL). Azide **4.2** (0.044 g, 0.28 mmol) and 3,5-bis(iodoalkyne) pyridine (0.050 g, 0.13 mmol) were added. The reaction mixture was covered with foil and stirred at room temperature under N_2 for 18 hours. The reaction was diluted with DCM (20 mL) and the organics were washed with $NH_4OH_{(aq)}$ (3 × 10 mL), H_2O (10 mL) and brine (2 × 10 mL) and dried over $MgSO_4$. The solvent was removed *in vacuo*. Purification *via* silica gel column chromatography (DCM/MeOH 97:3) afforded bis-ester **4.30** (0.070 g, 77%).

^{1}**H NMR (**400 MHz; $CDCl_3$) δ (ppm): 9.27 (1H, d, ^4J = 2.2 Hz, Ar*H*), 8.88 (2H, d, ^4J = 2.1 Hz, Ar*H*), 5.19 (4H, s, CH_2), 1.51 (18H, s, *tert*-CH_3).

XB bis-acid derivative 4.31

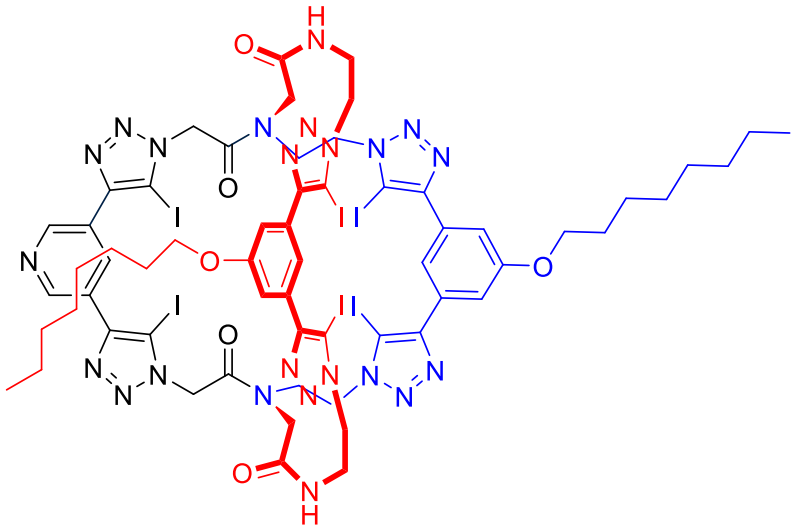


Bis-ester **4.30** (0.070 g, 0.10 mmol) was dissolved in DCM (5 mL), to which TFA (2 mL) was added. The reaction mixture was stirred at room temperature for 4 hours, or until

completion. The solvent and excess TFA were removed *in vacuo* and the product dried under high vacuum to afford XB bis-acid **4.31** (0.058 g, quant.).

^{1}H NMR (400 MHz; CD_3OD) δ (ppm): 9.54 (1H, s, Ar*H*), 9.36 (2H, s, Ar*H*), 5.42 (4H, s, CH_2COOH); **^{13}C NMR** (126 MHz; DMSO-d_6) δ (ppm): 206.52, 167.75, 146.84, 145.72, 131.06, 126.43, 84.58; **HRESI-MS** (pos) $C_{13}H_{10}O_4N_7I_2$ *m/z*: $[M+H]^+$ *calc.* 581.88781, *found* 581.88829.

XB cryptand 4.32

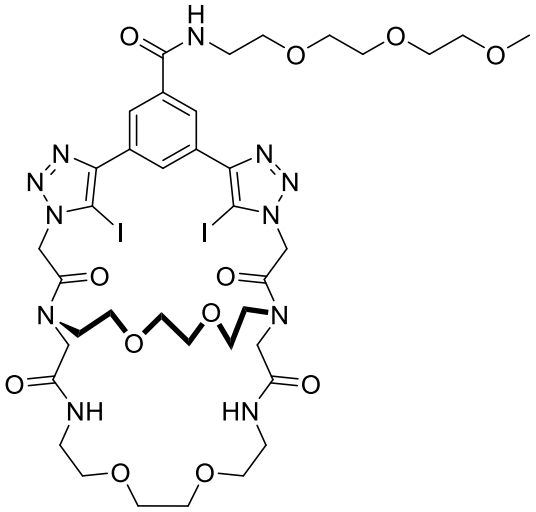


Bis-amine **4.25** (0.024 g, 0.035 mmol) and paraformaldehyde (0.002 g, 0.070 mmol) were dissolved in MeOH (16 mL) and stirred at room temperature for 2 hours, to allow for formation of imine. A solution of bis-acid **4.31** (0.020 g, 0.035 mmol) in MeOH (3 mL) and bis-isocyanide **4.27** (0.024 g, 0.035 mmol) in MeOH (3 mL) were simultaneously added *via* syringe pump (flow rate 0.5 mL/h). After addition was complete, the reaction mixture was stirred at room temperature for 72 hours. The precipitate was filtered and washed with DCM, MeOH and H_2O. The product was dried under high vacuum to afford XB cryptand **4.32** (0.031 g, 45%).

^{1}H NMR (400 MHz; DMSO-d_6) δ (ppm): 9.16 (2H, s, Ar*H-pyridine*), 8.89 (1H, s, Ar*H-pyridine*), 8.21-8.03 (2H, m, Ar*H*), 7.51-7.33 (4H, m, Ar*H*), 5.45 (4H, br. s, NCH_2), 5.08 (4H, br. s, NCH_2), 4.73-3.91 (20H, m, CH_2), 1.80-1.57 (4H, m, CH_2), 0.89-0.66 (6H, m,

C*H*$_3$). ^{13}**C NMR** could not be obtained due to low solubility; **HRESI-MS** (pos) $C_{61}H_{70}O_6N_{23}I_6$ *m/z*: **[M+H]**$^+$ *calc.*1982.01420, *found* 1982.01568.

XB macrobicycle 4.33



Paraformaldehyde (0.002 g, 0.08 mmol) was dissolved in MeOH (19 mL) and 1,2-bis(2-aminoethoxy)ethane (5.7 μL, 0.04 mmol) was added. The reaction mixture was left to stir for 2 hours at room temperature to allow for the formation of imine. Bis-acid **4.14** (0.030 g, 0.04 mmol) in MeOH (3 mL) and bis-isocyanide **4.7** (0.007 g, 0.04 mmol) in MeOH (3 mL) were simultaneously added to the reaction mixture *via* syringe pump (flow rate 0.5 mL/h). After addition was complete, the reaction mixture was stirred for 18 hours. The solvent was removed *in vacuo*. Purification *via* preparative TLC (DCM/MeOH 93:7) afforded XB macrobicycle **4.33** (0.012 g, 28%).

^{1}**H NMR (**400 MHz; CD_3OD) δ (ppm): 8.29 (2H, s, Ar*H*), 7.65 (1H, s, Ar*H*), 5.50 (4H, s, CH_2-*iodotriazole*), 4.27-3.40 (43H, m, CH_2-*amide,* OCH_2, NCH_2 and CH_3); **HRESI-MS** (pos) $C_{38}H_{54}O_{12}N_{11}I_2$ *m/z*: *calc.* 1110.20373, *found* 110.20218.

6.3 References

1 B.-Y. Lee, S. R. Park, H. B. Jeon and K. S. Kim, *Tetrahedron Lett.*, 2006, **47**, 5105–5109.

2 M. J. Hynes, *J. Chem. Soc. Dalton Trans.*, 1993, 311-312.